# SYNTHESIS AND CHARACTERISATION OF NOVEL POLYMERIC NANO-SYSTEMS FOR PHARMACEUTICAL APPLICATIONS

**SHAIMAA SHAKARGI**

A thesis submitted in partial fulfilment of the requirements of the University of Brighton for the degree of Doctor of Philosophy

School of Pharmacy & Biomolecular Sciences
University of Brighton

2018

# ABSTRACT

Polymeric nano-systems formed by self-assembling block copolymers have attracted attention due to their ability to load and deliver therapeutic agents intracellularly, and high *in-vitro* and *in-vivo* stability. Systems utilising biocompatible phosphorylcholine (PC) based copolymers have shown promise, particularly the diblock copolymer poly(2-methacryloyloxyethyl phosphorylcholine-*b*-poly(2-(diisopropylamino)ethyl methacrylate) (MPC-DPA). However, previous studies have not elucidated the relationships of ethanolic atom transfer radical polymerisation (ATRP) to MPC-DPA block length limits, MPC-DPA block length to particle size, morphology, and cell uptake, and the ability to load and delivery the anticancer drug Docetaxel (DTX) to human cancer cell lines. In this project, a series of novel block length MPC-DPA diblock copolymers were successfully synthesised at ambient temperature via ethanolic ATRP. $^{1}$H-NMR and gel permeation chromatography (GPC) revealed the copolymers to be well defined with molecular weights ($M_n$) ranging from 10 K-64 K and polydispersity ($M_w/M_n$) < 1.1. Dynamic light scattering (DLS) revealed the copolymers formed controllable, and stable, nanoparticle systems, ranging from 25 nm to 140 nm diameter, relative to polymer molecular weight. The MPC-DPA formed self-assembled nanoparticles at physiological pH, with unimer to micelle transition occurring between pH 6.0-7.0, and were stable across a wide temperature range (5-70°C). Critical micelle concentration (CMC) and DLS particle stability upon dilution data were comparable, suggesting that the MPC-DPA nano-systems were resistant to dissociation, and therefore a suitable candidate for pharmaceutical application development. DLS and scanning transmission electron microscopy (STEM) indicated that the MPC-DPA formed differing colloidal aggregates, such as micelles or vesicles, as MPC and DPA block lengths were adjusted. The toxicological profile of the MPC-DPA was assessed via clonogenic, MTT, and LDH assays, which revealed the copolymers to be of low cytotoxicity. *In-vitro* cellular uptake was studied in response to changes in the physical properties of MPC-DPA, via flow cytometry and confocal laser scanning microscopy, and demonstrated successful and rapid uptake of MPC-DPA nanoparticles in healthy and cancer cell lines. The anticancer drug DTX was successfully encapsulated into the MPC-DPA micelles via nanoprecipitation and direct dissolution. Subsequent *in-vitro* studies of DTX loaded MPC-DPA nano-systems were performed on the human cancer cell lines, MCF-7, SKOV-3, and PC3, which revealed that 42 nm diameter DTX loaded MPC-DPA micelles produced an anticancer effect in SKOV-3 ovarian cancer and PC3 prostate cancer cells. Therefore, the novel data obtained from this study suggested that MPC-DPA diblock copolymers have the potential for pharmaceutical application in the form of a DTX anticancer drug delivery system.

# CONTENTS

# LIST OF TABLES

# LIST OF FIGURES

## ❖ Introduction



## ❖ Materials and Methods

❖ **Polymer Synthesis**



❖ **Polymer Characterisation**

❖ **Bioevaluation**

# ACKNOWLEDGEMENTS

First of all, I would like to sincerely thank my supervisor, Dr Jonathan Salvage, for providing me the opportunity exploring in broad research disciplines, and for lighting my way to think as a scientist. I am especially indebted to my co-supervisors, Dr Guy Standen for his insightful advice and fruitful discussions, and Dr Dipak Sarkar for his constructive criticism and advices.

Next, I would like to express my thanks to my country, Iraq, and the Ministry of Higher Education and Scientific Research (MOHSR) for the fully-funded scholarship that provided the necessary financial support for this research. I also would like to thank the Iraqi Cultural Attaché/London for the appreciated help and support throughout my PhD study.

Moreover, I am very grateful for the help and support of all the nice and wonderful staff of the Doctoral College Department, particularly Prof Neil Ravenscroft, Alice Parkes, Sarah Longstaff, Sarah Mockler, and Ursula O'Toole. I also would like to thank all the technical staff at University of Brighton for their help and guidance.

Additionally, I would also like to thank my best friend, Safaa and I wish you all the best success.

Last but by no means the least, I must thank my husband Oday and my kids Zaid, Zainab, Olla and Obaidah for believing in me and I wish to express my deep appreciation and my love to my mother and beloved sister Shatha and her husband Ebu, without your prayers, encouragement and motivation, I would not achieve anything in my life, therefore, I owe you everything and to you all, I dedicate this thesis.

# AUTHORS DECLARATION

## Declaration

I declare that the research contained in this thesis, unless otherwise formally indicated within the text, is the original work of the author. The thesis has not been previously submitted to this or any other university for a degree, and does not incorporate any material already submitted for a degree.

Signed

Dated

# LIST OF ABBREVIATIONS

| | |
|---|---|
| $^1$H NMR | Proton nuclear magnetic resonance spectroscopy |
| ANOVA | Analysis of variance |
| ATRP | Atom transfer radical polymerization |
| bpy | bipyridine |
| CLSM | Confocal laser scanning microscopy |
| CME | Clathrin-mediated endocytosis |
| CMC | Critical micelle concentration |
| Cm-6 | Coumarin-6 |
| DL | Drug loading |
| DLS | Dynamic light scattering |
| DMSO | Dimethyl sulfoxide |
| DPA | 2- (diisopropylamino) ethyl methacrylate |
| DTX | Docetaxel |
| EE | Encapsulation efficiency |
| EtOH | Ethanol |
| EPR | Enhanced permeability and retention effect |
| FCM | Flow cytometry |
| GPC | Gel permeation chromatography |
| LDH | Lactate dehydrogenase assay |
| MEBr | 2-(4-morpholino)ethyl 2-bromosiobutyrate |
| MeOH | Methanol |
| MP-AES | Microwave plasma atomic emission spectrophotometer |
| $M_n$ | Number-average molecular weight |
| MPC | 2-methacryloyloxyethyl phosphorylcholine |
| MTT | (3-(4,5-dimethylthiazol-2-yl)-2,5-diphenyltetrozolium bromide) |
| $M_w$ | Weight average molecular weight |
| MWCO | Molecular weight cut off |
| Mwt | Molecular weight |
| PBS | Phosphate buffer saline |
| PDI | Polydispersity |
| PC | Phosphatidylcholine |
| PEG | Poly (ethylene glycol) |
| PEO | Poly (ethylene oxide) |
| PM | Polymeric micelle |
| RAFT | Reversible addition−fragmentation chain transfer |
| RES | Reticuloendothelial system |
| SDS | Sodium dodecyl sulphate |
| STEM | Scanning transmission electron microscopy |
| UV-vis | Ultraviolet-visible |

# CHAPTER ONE

# INTRODUCTION

The poor water solubility of hydrophobic drugs and the systemic drug toxicity associated with their use are leading causes for the development of new systems that can selectively deliver a drug to its target site with minimal unintended side effects. Therefore, the introduction of nanoparticle-based drug delivery systems offers a promising approach for the delivery of a wide range of drugs even if they are immiscible with water. One example of the nanoparticle-based systems are self-assembled polymeric nanoparticles, which have advanced to the clinical trials stage.

## 1.1 Nanoparticles

It was evident from reviewing current scientific literature, that the development of nanoparticle based drug delivery systems remains a major focus for research. However, it was also clear that there are many challenges remaining that must be overcome in order to successfully develop effective nanoscale drug delivery vehicles. These challenges include, achieving the controllable and consistent ability to load, carry, and deliver therapeutically relevant amounts of drugs, and in doing so overcome physiological and physicochemical barriers currently hindering the effective, and accurate delivery of drugs, whilst optimising the therapeutic efficacy of the compound as it is used to treat the target site. This approach could result not only in extending the commercial and clinical lifetime of the pre-existing drugs, but also offers the potential to improve the bioavailability of the drugs whilst reducing the side effects to normal cells and tissues. Therefore, increased attention and research have been directed towards the use of nanoparticles for drug delivery applications as an alternative to conventional drug designs (Parveen et al., 2012).

This research impetus, has resulted in the development of a range of nano-carriers as drug delivery systems, varying from biological substances, such as albumin (Koo et al., 2005), and phospholipids for liposomes (Lasic, 1998), through chemical compounds, such as polymers and solid metal-containing nanoparticles (Son et al., 2013). Additionally, nanoparticles are small particles, typically less than 200 nm in diameter (Nicolas et al., 2013; Xu et al., 2015) (Figure 1.1), and they exist in a wide variety of sizes, shapes, and compositions as indicated by the classification system suggested in Figure 1.2.

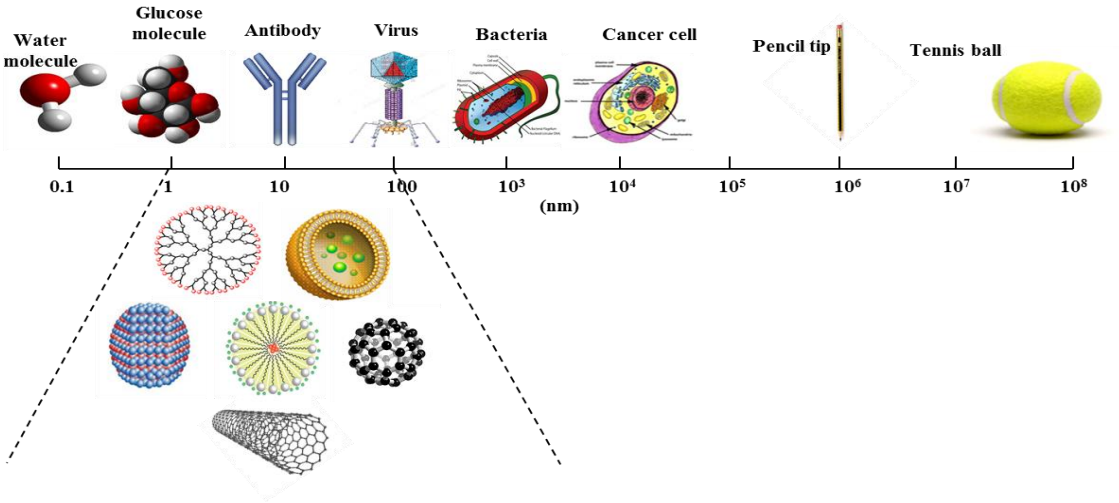


**Figure 1.1.** Size comparison of nanoparticles with various objects and biological moieties

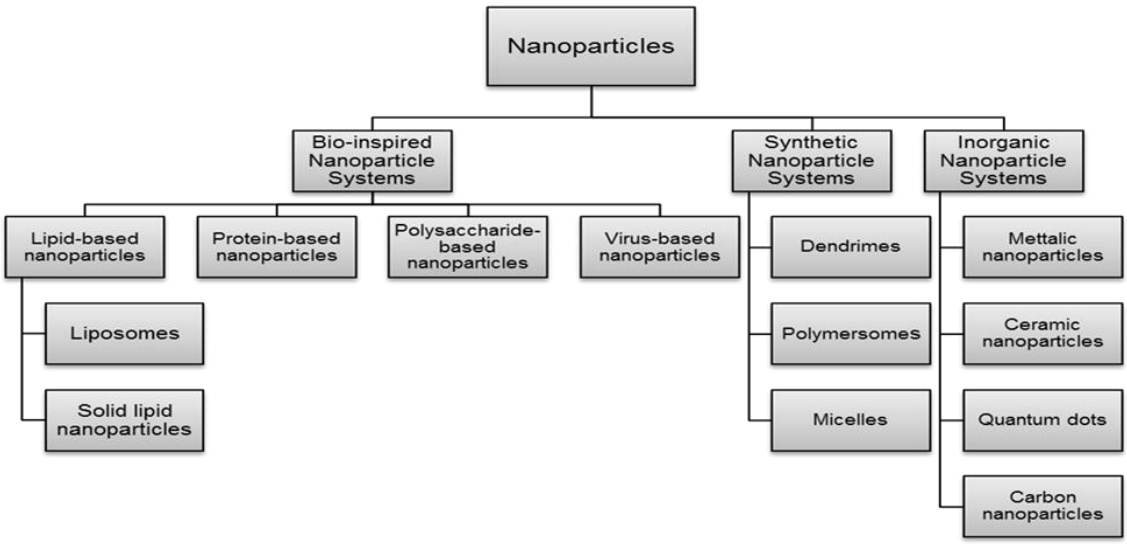


**Figure 1.2.** Nanoparticles Classification (modified from (Mishra et al., 2013)

In spite of the potential advantages offered by nanoparticles such as improved drug efficacy with reduced toxicity, enhanced biodistribution and improved patient compliance (Zhao et al., 2013), there are also limitations that must be considered, such as their small size and large surface area, which can lead to particle-particle aggregation, making physical handling of nanoparticles difficult in liquid and dry forms, in addition to limited drug loading and burst release (Dadwal et al., 2014).

## 1.2 Nanotoxicity

Although nanocarriers offer great potential for drug delivery applications, the risk of adverse effects and toxicity associated with their use are not yet fully understood (Linkov et al., 2008; Gnach et al., 2015), and studies show that different nanoparticles can damage cell membranes by various mechanisms, which eventually affects membrane integrity and stability (Elsaesser and Howard, 2012). Moreover, nanoparticles can induce structural damage to mitochondria, cause DNA mutation, and even result in cell death (Wani et al., 2011). It is noteworthy that nanotoxicity is considered a relatively new field that needs carefully designed studies and evaluation particularly as many nanotoxicological studies focus on acute toxicity or local adverse

effects rather than long-term toxicity (Aillon et al., 2009; Kunzmann et al., 2011; Li et al., 2015a). Nanomaterial toxicity is not only related to nanoparticles and their surface properties (corona), but also related to the nanomaterial environment, therefore, a complete understanding of nanomaterial physiochemical properties and their interaction with the biological surroundings in addition to the establishment of standardised and validating methods for characterisation is necessary to improve the quality and relevance of nanotoxicological studies (Fadeel et al., 2015; Hussain et al., 2015; Bahadar et al., 2016).

## 1.3 Micelles:

### 1.3.1 General considerations and properties:

Micelles are colloidal dispersions belonging to a large group of dispersed systems consisting of particulate matter or dispersed phase, distributed within a continuous phase or dispersion medium (Torchilin, 2004). At specific concentrations and temperatures, micelles are spontaneously formed by amphiphilics or surfactants (surface active agents) that possess a characteristic molecular structure consisting of two portions; a hydrophobic (non-polar) domain; usually termed the tail, and a hydrophilic (polar) domain, referred to as the head (Rosen and Kunjappu, 2012). Depending on the nature of their hydrophilic group, hydrocarbon based surfactants are classified into anionic, non-ionic, cationic and zwitterionic, all of which are capable of self-assembly into a micelle in a manner similar to that of amphiphilic block copolymers when they are placed in an aqueous environment (Alexandridis and Lindman, 2000). Unfortunately, surfactant micelles are unsuitable for drug delivery as they cause *in-vivo* cell damage arising from their ability to solubilise biological membranes (Almgren, 2000), therefore, polymeric micelles offer the potential for

developing a system that possess the self-assembly and loading properties of surfactant micelles and displaying biocompatibility and biomimetic properties at the same time. Polymeric micelles obtained by the self-assembly of amphiphilic block copolymers are macromolecular, nano-sized colloidal particles that have attracted wide attention as drug delivery systems due to their unique core-shell architecture (Figure 1.3), which is characterized by a hydrophobic core and an outer hydrophilic shell. The former has the capability to encapsulate poorly water-soluble drugs, whereas the shell protects the drugs from the aqueous environment and stabilizes the polymeric micelles against recognition *in-vivo* by the reticuloendothelial system (RES) (Torchilin, 2007a; Kedar et al., 2010; Movassaghian et al., 2015). One of the promising polymeric micelle examples is Pluronic® (also known as poloxamers), which are amphiphilic block copolymers consisting of a central poly (propylene oxide) (PPO) block with terminal poly (ethylene oxide) (PEO) blocks that self-assemble in aqueous solution to form micelles and they are available in a range of molecular weights and PPO/PEO composition ratios (Moghimi and Hunter, 2000; Sahay et al., 2008; Patel et al., 2009).

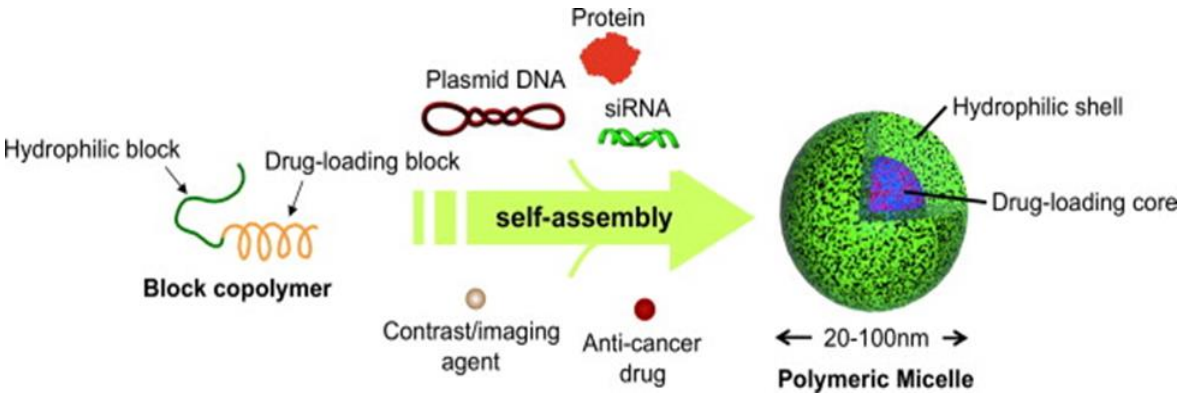


**Figure 1.3.** Polymeric micelles prepared by self-assembly of block copolymers and drugs (Miyata et al., 2011)

In general, the physicochemical properties of the outer shell determine the stability of polymeric micelles, longevity in blood stream, biocompatibility, and the pharmacokinetic and biodistribution behaviour of the incorporated drug, whilst the core is primarily responsible for the pharmacological activity via drug loading and release characteristics (Yokoyama, 2010). It has been shown that polymers with a large hydrophobic domain form micelles at lower concentrations and temperatures whilst large hydrophilic segments would lead to difficulty in micelle formation, which indicates that the hydrophobic domain is the primary factor in the micellisation process (Alexandridis and Hatton, 1995).

Polymeric micelles possess many advantages that render them a promising candidate for drug delivery systems, which include:

1- They can be designed to be either biocompatible and/or biodegradable (Giacomelli et al., 2006).

2- They are nanosized (< 100nm) and their outer hydrophilic shell can help prevent their uptake and clearance by reticuloendothelial system (RES), which in turn should prolong their circulation time in blood (Nishiyama and Kataoka, 2006; Torchilin, 2007a). Additionally, their small size allows for the passive accumulation of micelles in solid tumour sites due to the enhanced permeability and retention (EPR) effect (Maeda et al., 2000; Torchilin, 2011), which results in improved therapeutic effects of the entrapped drug whilst minimizing side effects (Movassaghian et al., 2015). Their nano size also benefits the sterilization processing of polymeric micelles, as this permits simple and inexpensive sterilization by filtration (Yokoyama, 2011).

3- Low-molecular weight drugs primarily face rapid elimination by the liver and/or kidneys; however, loading the drugs in nanoparticles has been shown to

increases their bioavailability (Matsumura, 2008). Although PEGylation has been extensively studied and utilised in nanoparticle systems to increase hydrophilicity and improve circulation half-life, the *in-vivo* immunological response and unexpected changes to the pharmacokinetic profile of PEGylated nanoparticles has been seen to affect drug bioavailability and biodistribution profiles (Chanan-Khan et al., 2003; Ishida et al., 2003; Cho et al., 2013). Therefore, polymeric micelles possessing a cell membrane like outer surface structure, namely phospholipids, offer the potential to design more effective, biomimetic, stealth drug carriers (Zhao et al., 2015).

4- Usually, hydrophobic drugs can only be administered intravenously (i.v.) after the addition of solubilising adjuvants, for example the currently available formulation for paclitaxel requires the use of either dehydrated ethanol or Cremophor EL (poly ethoxylated castor oil), which is often accompanied with toxic side effects (Weiss et al., 1990; Kloover et al., 2004), including hypersensitivity reactions, nephrotoxicity, and cardiotoxicity (Torchilin, 2007a; Kedar et al., 2010). Alternatively, the use of surfactants may result in drug precipitation upon the dilution of the solubilised drug preparations within aqueous solutions, which results in gastrointestinal tract irritation in case of oral administration and pain upon injection after parenteral administration (Lawrence, 1994; Strickley, 2004).

   However, the incorporation of these drugs within micelles avoids the use of adjuvants (Rijcken et al., 2007), and thus may help to reduce the associated unwanted side effects. Moreover, the approach of utilising liposomes and cyclodextrins is limited by the low capacity of the liposomal membrane or cyclodextrin inner cavity for water-insoluble molecules (Torchilin, 2004).

5- In comparison to liposomes, micelles have a higher drug-loading capacity and higher stability in the blood stream (Ahmad et al., 2014). Moreover, micelles have been shown to elicit a much lower immune response and exhibit compatible interactions with body fluids and organelles, unlike many other types of nanoparticle (Hasenstein et al., 2012).

6- Finally, polymeric micelles are amenable to surface modification with the targeting ligands, which can specifically recognize the receptors overexpressed on the surface of tumor cells and or, tumor endothelium, resulting in highly efficient intracellular delivery of micellar drugs (Torchilin, 2007b).

   For example, drug-loaded folic acid-functionalized micelles have been demonstrated to selectively targeting cancer cells (Licciardi et al., 2005; Hami et al., 2014; Li et al., 2015b; Liu et al., 2015).

The focused development of micelles as drug delivery systems can be traced back approximately four decades to the 1980s, as shown in Figure 1.4, from low-molecular weight surfactants that self-assemble in aqueous systems (Kwon and Kataoka, 2012), through to the progression of current micelle based drug delivery technologies, including to the co-delivery of two drugs (Aw et al., 2013). An early and pioneering example of micelles being proposed as drug carriers was made by Bader and Ringdorf who studied the application of polymerised liposomes as stable models for biomembranes (Pratten et al., 1985; Bader et al., 1985), which was followed by the Kabanov group who reported that the activity of a neuroleptic drug (haloperidol) increased when it was solubilized in surfactant micelles (Pluronic-P85) (Kabanov et al., 1989). Subsequently, the incorporation of poorly water soluble, hydrophobic, drugs into the hydrophobic core of micelles by hydrophobic interactions was reported in number of studies (Kwon and Okano, 1996; Yokoyama et al., 1996; Allen et al.,

1999; Kataoka et al., 2001), and polymeric micelles are now considered to have the potential to be effective drug carrier systems, having been successfully utilised to achieve drug targeting, particularly tumour targeting (Bae et al., 2005; Oerlemans et al., 2010; Wang et al., 2012b; Akimoto et al., 2014; Nakayama et al., 2014; Emami et al., 2015), via the EPR effect (Torchilin, 2011; Ke et al., 2014; Danhier et al., 2015; Maeda, 2015; Burris et al., 2016; Varela-Moreira et al., 2017).

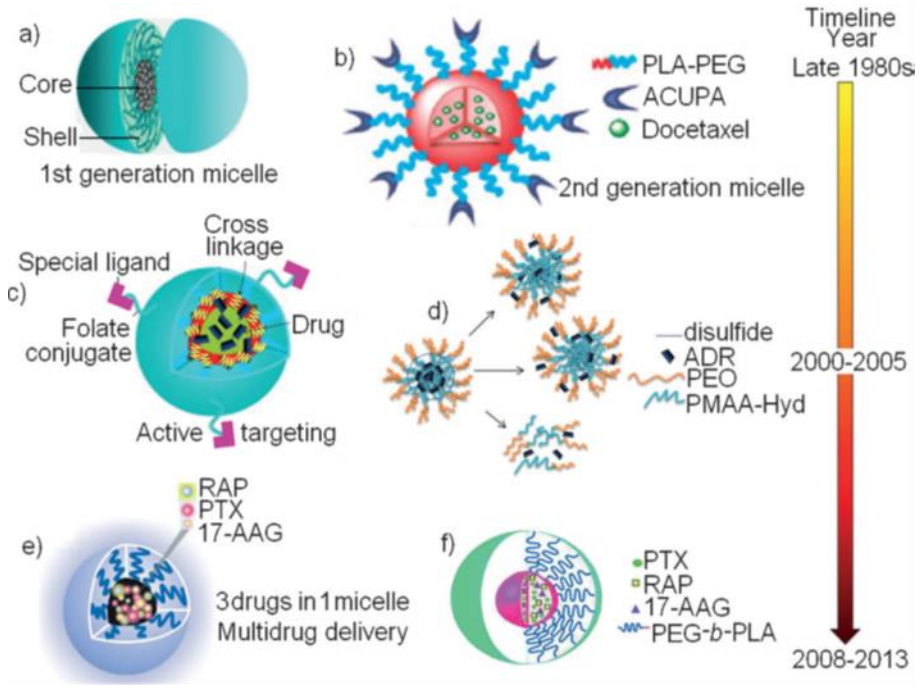


**Figure 1.4.** The development of polymeric micelles for drug delivery applications (Aw et al., 2013), a. Low-molecular weight surfactants. b. & c. Active targeting micelles equipped with functional groups, cross-linkage, or special ligands. d. Dual-stimuli responsive micelles for drug release with controllable dosage. e. & f. Multidrug delivery with 2–3 drugs in one micelle.

Micelles preparation methods are highly dependent on the solubility of micelle-forming block copolymers in aqueous medium (Letchford and Burt, 2007; Kore et al., 2014). This can be altered as the molecular weight ratios of hydrophilic and hydrophobic blocks change, therefore, when the molecular weight of the hydrophilic block exceeds that of the hydrophobic block, the copolymer is easily dispersed in water

and will self-assemble into small, relatively monodisperse micelles (Letchford and Burt, 2007). However, when the ratio of hydrophobic block approaches or exceeds that of hydrophilic block, a copolymer becomes more water insoluble and cannot self-assembly into a nanoparticle through direct dissolution or film casting methods, therefore, other methods such as dialysis, emulsification and nanoprecipitation are employed (Letchford and Burt, 2007).

### 1.3.2 Characterisations:

#### 1.3.2.1 Thermodynamic and Kinetic Stability:

The self-assembly of amphiphilic polymers into micelles occurs due to hydrophobic interactions, which lower the free energy of the system by removing the hydrophobic segments to form the core and the hydrophilic segments are submerged in the aqueous environment forming the shell micelle (Torchilin, 2005; Lu and Park, 2013). Critical micelle concentration (CMC) is a key factor in characterising the self-assembly of amphiphilic block copolymers into micelles, and is defined as the minimum concentration of polymer required in solution for micelles to form (Owen et al., 2012), therefore, CMC is used to describe the thermodynamic stability of micelle (Deng et al., 2012). At low polymer concentrations, copolymer molecules exist in aqueous solutions as individual molecules, unimers, and act as surfactants, adsorbing at the air/water interface (Owen et al., 2012; Ding et al., 2012a) . As the concentration of polymer increases, at CMC, more chains are adsorbed at the interface, and both the bulk solution and interface become saturated with polymer chains (Kedar et al., 2010; Owen et al., 2012). At high polymer concentration, the micelles are stable unless they are diluted below the CMC, then the micelles will disassemble, and free chains are again found in the bulk solution and adsorbed at the air/water interface. Thus, it is a reversible thermodynamic process (Figure 1.5) (Cho et al., 2010).

Self-assembly of both surfactant and polymeric micelles starts as the concentration of the surfactant or polymer reaches the threshold CMC (Gong et al., 2012). However, the CMC of polymeric micelles ($10^{-6}$ - $10^{-7}$ M) can be 1,000 times lower than the CMC of low-molecular-weight surfactants ($10^{-3}$ -$10^{-4}$ M), because polymer chains have more interaction points which increases the stability of micellar structure with extreme dilutions after intravenous administration to patients (Lin et al., 2009; Wang et al., 2009). It has been reported that hydrophobic block length is directly correlated to micelle stability (Adams et al., 2003), therefore an increase in the length of the hydrophobic block of a copolymer may result in a decreased CMC, whereas changes in the length of the hydrophilic block of copolymer are believed to have no significant effect on the CMC (Allen et al., 1999; Lee et al., 2003a). Micellisation is also affected by a number of factors such as size of hydrophobic moiety, addition of salt, pH, and temperature (Biswas et al., 2013). Kinetic stability describes the behaviour of micelles in an aqueous environment over time and during the disassembly period (Owen et al., 2012), and it depends on core structure, size or length of the hydrophobic block, and the hydrophilic-hydrophobic ratio. There are several methods to determine the CMC value for a given amphiphilic compound such as HPLC, particle size measurement by using small angle light scattering, and fluorescent spectroscopy, however, fluorescent spectroscopy is consider by many to be the most sensitive and precise (Torchilin et al., 2001).

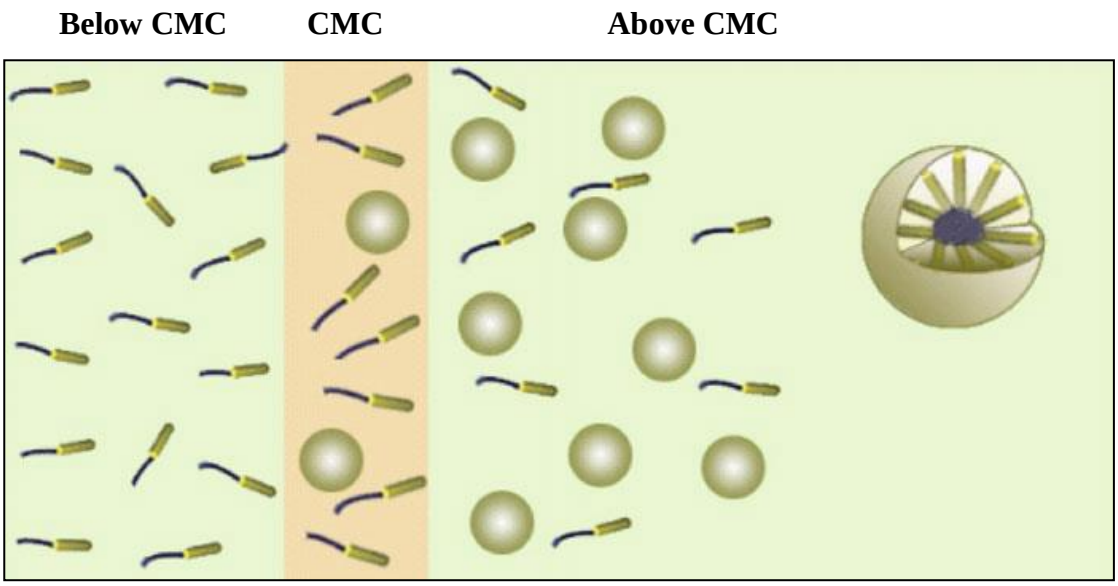


**Figure 1.5.** Schematic representation of the theory of critical micelle concentration (CMC) for solutions of block copolymers (Ding et al., 2012a)

**1.3.2.2 Size:**

The size of nanoparticles is a crucial factor for determining nanoparticle pharmacokinetic profiles and *in-vivo* fate (Mohanraj and Chen, 2007). Drug release is affected by particle size in that smaller particles can release a drug faster than larger particles because smaller particles have a larger surface area, thus most of the drug association will be at or near the small particle surface, whereas large particles have large cores, which allow greater levels of drug encapsulation and a slow release profile (Owen et al., 2012). The cell membrane is a barrier for large particles, and it is thought that particles can only passively diffuse across the membrane when they are within the size range of 10 nm-30 nm (Kettler et al., 2014). For larger particles, there is a mechanism that overcomes this barrier and allows the uptake of nanoparticles, beside proteins and other nutrients, known as "Endocytosis" (Doherty and McMahon, 2009; He et al., 2010; Duncan and Richardson, 2012; Kettler et al., 2014). Endocytosis is divided into four categories, depending on the size and surface properties of particles, (Figure 1.6) (1) phagocytosis, which is responsible for large particles uptake ( > 250

nm), and is performed in specialized mammalian cells such as macrophages, monocytes and neutrophils (Conner and Schmid, 2003). (2) pinocytosis for fluid and solute uptake that occurs in all types of cells (Sahay et al., 2010). (3) clathrin-mediated endocytosis (CME), clathrin is a cytosolic protein that spontaneously self-assembles at the cell membrane and is associated with other proteins known as adaptor proteins (AP) (Schmid, 1997), resulting in the formation of vesicles that vary in size with a maximum diameter of circa 200 nm (Cureton et al., 2009). (4) caveolae-mediated endocytosis, caveolin is also a protein that coats caveolae vesicles resulting in small vesicles (50-80 nm) (Canton and Battaglia, 2012).

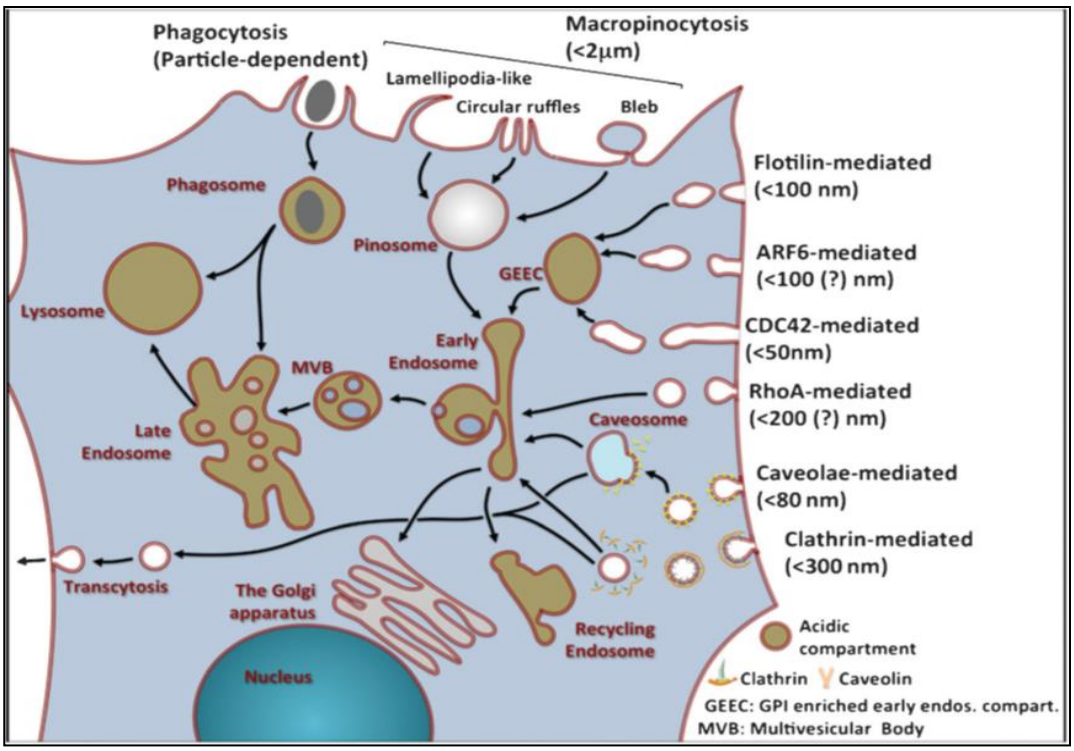


**Figure 1.6.** Mechanisms of extracellular uptake by endocytosis in a typical eukaryotic cell (Canton and Battaglia, 2012)

Polymeric micelles within the size range of 10 – 100 nm, and in particular sizes less than 50 nm, are considered suitable for effective avoidance of clearance by the kidneys and capture by the reticuloendothelial systems in the liver and spleen (Miyata et al., 2011; Yokoyama, 2014). Compared to liposomes, the preparation of polymeric micelle

particles smaller than 50 nm can be achieved without the technical problems that can occur during liposome preparation due to excess hysteresis on the lipid bilayer of a small liposome (Yokoyama, 2014), and in addition, the control of micelle size can be made via alterations in the chemical structure and material composition, as well as with the preparation process (Yokoyama, 2014). Indeed, the size of micelles can, in theory, be predicted from the chemical structure and chain lengths of block copolymers via theoretical calculation (Hamad and Qutubuddin, 1990; Xu et al., 1992). Cabral and colleagues studied the relation between the size of polymeric micelles and their targeting efficacy in highly and poorly permeable tumours in mice (Cabral et al., 2011), and the results indicated that micelles with a diameter of 30, 50, 70 and 100 nm penetrated a highly permeable tumour, and 30 nm micelles were able to penetrate poorly permeable tumours to achieve their therapeutic effect. Although, several studies demonstrated that sub-100 nm diameter particles are regarded to be important for tumour penetration, other factors such as tumour type, surface characteristics, and nanoparticle shape may also influence selection of optimal size (Gref et al., 1994).

#### 1.3.2.3 Shape and geometry:

Amphiphilic block copolymers can self-assemble to produce different morphologies such as spheres, rod-like, star-like, lamellas and vesicles (Shen et al., 2008). The major driving force behind self-association of amphiphilic polymers is the decrease in free energy of the system due to the removal of hydrophobic fragments from the aqueous surroundings via the formation of a micelle core stabilised with hydrophilic blocks exposed to the aqueous water phase (Jones and Leroux, 1999). Block copolymer composition and length ratio, both influence micelle formation and morphology (Zhang et al., 1996). Thus, the hydrophobic to hydrophilic ratio affects both nanoparticle physical state and morphology (Letchford and Burt, 2007). Typically, the

morphology of prepared amphiphilic block copolymer nanoparticles is spherical, particularly if the molecular weight of the hydrophilic block exceeds that of the hydrophobic block thus forming aggregates in which the corona is larger than the core (so-called star micelles) (Letchford and Burt, 2007). Membrane curvature is considered to be a main factor in determining block copolymer self-assemble structures, and it can be resolved by using the molecular packing parameter (p), which can be obtained from following equation (1.1) (Smart et al., 2008):

**Equation 1.1.** The molecular packing parameter equation

$$p = \frac{v}{a_0 l}$$

Where $a_0$ is the optimal interfacial area between hydrophilic and hydrophobic regions, v is the molecular volume of hydrophobic segment, and l is the length of the hydrophobic block (Nagarajan, 2002; Nagarajan, 2011). As shown in Figure 1.7, spherical micelles are formed when $p \leq 1/3$, cylindrical micelles are formed $1/3 < p \leq 1/2$ and polymer membranes $1/2 < p \leq 1$ (Smart et al., 2008).

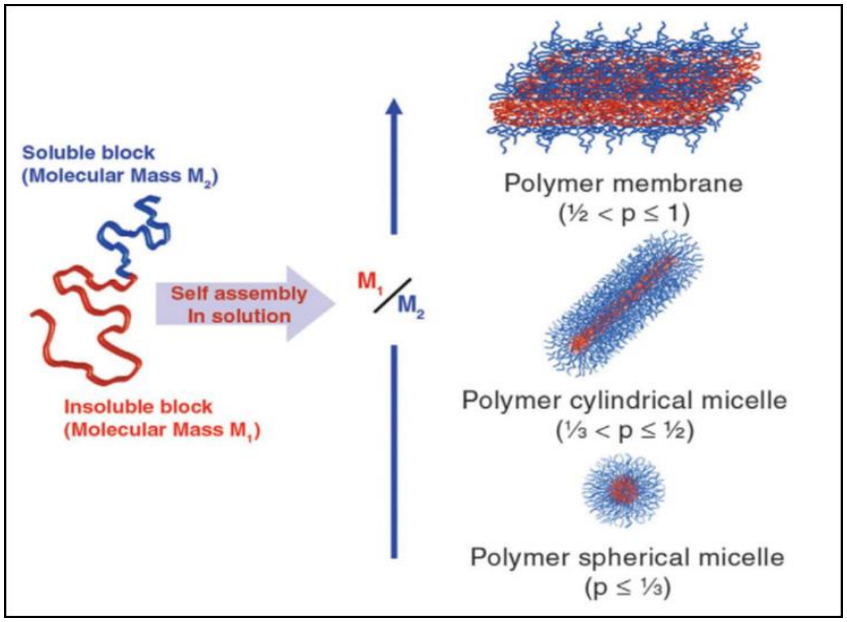


**Figure 1.7.** Different geometries formed by block copolymers in selective solvent conditions, which preferentially dissolve one part of a molecule over another (Smart et al., 2008)

### 1.3.2.4 Surface properties:

The biocompatibility of nanoparticles inside the body is mainly determined by their surface characteristics (Dobrovolskaia and McNeil, 2007), whilst nanoparticle hydrophobicity, along with particle size, are thought to affect the *in-vivo* fate of nanoparticles (Brigger et al., 2002). Surface non-modified nanoparticles are more liable to opsonisation; a process of particles becoming coated with opsonin proteins (Owens and Peppas, 2006), and cleared from the blood stream (Grislain et al., 1983). In the 1970s, Abuchowski studied the principle of introducing covalent bonding of poly (ethylene glycol) to a drug or therapeutic protein, a process which developed later to be the basis of PEGylation (Abuchowski et al., 1977) (Figure 1.8), and the production of 'stealth' nanoparticle carriers (Peracchia et al., 1999).

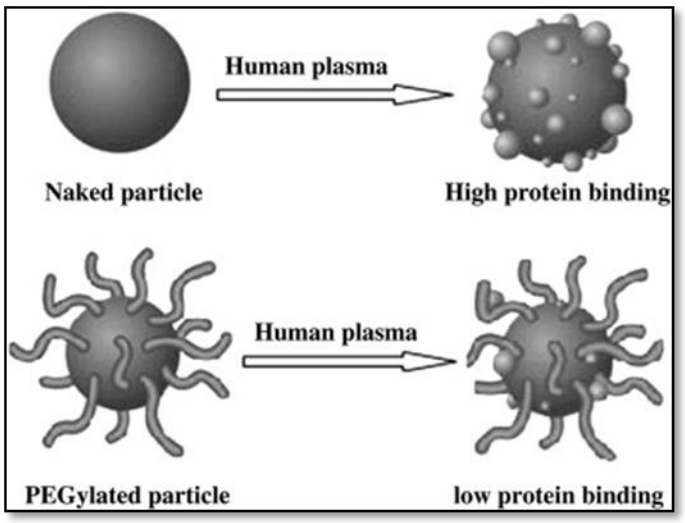


**Figure 1.8.** PEGylated nanoparticles are able to avoid clearance from the blood stream by repelling protein adsorption, thus prolonging nanoparticle circulation time within the body (Naahidi et al., 2013)

To date many long circulating drug carriers have been obtained by grafting their surface with hydrophilic polymers containing well-solvated and flexible main chains such as PEG (Torchilin and Trubetskoy, 1995). Consequently, those surface-grafted polymers will slow down the opsonisation, reducing binding of plasma proteins, of drugs and drug carriers and minimize their nonspecific uptake by the reticuloendothelial system (RES) (Thakur et al., 2015; Suk et al., 2016; Ishii et al.,

2016). Thus, PEGylation increases the stability of nanocarriers by its steric effect that acts as a barrier for aggregation (Ahl et al., 1997), and thereby increases particle circulation time, which subsequently benefits EPR-based targeting of drugs to tumour (Fang et al., 2011).

The surface charge also has an impact on nanoparticle uptake, and in many studies positive and negative surface charged particles have displayed increased nanoparticle uptake by the RES in comparison with neutral particles (He et al., 2010) Moreover, positively charged particles have been reported to undergo a faster uptake than negatively charged nanoparticles (Harush-Frenkel et al., 2007; He et al., 2010). A new strategy has been developed to prolong nanoparticle circulation time, which utilises zwitterionic polymer-based nanoparticles because they are resistant to nonspecific protein adsorption via electrostatically induced hydration (Yuan et al., 2012; Leng et al., 2015). 2-methacryloyloxyethyl phosphorylcholine (MPC) is another example of polymers that resist protein adsorption and cell adhesion, and has been utilised in implantable devices, tissue engineering, and biosensor applications (Lewis et al., 2000).

### 1.4 Polymeric micelles in clinical trials

A large volume of research utilising polymeric micelles has been published, but only limited clinical trials have been undertaken to date, primarily concerned with anticancer treatments (Lu and Park, 2013). Table 1.1 details some of the clinical trials involving therapeutic loaded polymeric micelles, and the clinical phase achieved, which further indicates the continued potential that polymeric micelle offer as drugs delivery (Oerlemans et al., 2010).

**Table 1.1.** Polymeric Micelles in Different Clinical Trials

| Polymeric Micelle Name | Block Copolymer | Drug | Diameter (nm) | Indication | Development Phase | Ref. |
|---|---|---|---|---|---|---|
| Genexol-PM | PEG-poly(D,L-lactic acid) | Paclitaxel | 20-50 | Breast, lung, ovarian cancer | Approved† Phase III | (Cabral and Kataoka, 2014) |
| NK105 | PEG-*b*-poly(α,β-aspartic acid) | Paclitaxel | 85 | Gastric cancer Recurrent breast cancer | Phase II Phase III | (Hamaguchi et al., 2007; Kato et al., 2012) |
| NK911 | PEG-*b*-poly(α,β-aspartic acid) | Doxorubicin | 40 | Solid tumors | Phase II | (Matsumura et al., 2004) |
| NK012 | PEG-*b*-poly(L-glutamic acid) | SN-38 | 20 | Breast and lung cancer | Phase II | (Hamaguchi et al., 2010) |
| NC-6300 | PEG-*b*-poly(aspartate-hydrazone) | Epirubicin | 60 | Hepatocellular carcinoma | Phase I | (Takahashi et al., 2013) |
| NC-6004 | PEG-*b*-poly(L-glutamic acid) | Cisplatin | 20 | Pancreatic cancer | Phase III | (Plummer et al., 2011) |
| NC-4016 | PEG-*b*-poly(L-glutamic acid) | Oxaliplatin | 30 | Solid tumors | Phase I | (Cabral and Kataoka, 2014) |
| SP1049C | Pluronic L61 and F127 | Doxorubicin | 22-27 | Adenocarcinoma of esophagus and gastersophageal junction | Phase III | (Valle et al., 2011) |
| siRNA micelles | PEG-b-polycations | siRNA | 40-60 | ------ | Preclinical | (Christie et al., 2012; Pittella et al., 2014) |
| CriPec | mPEG-*b*-p(HPMAm-$Lac_n$) | Docetaxel | 66 | Breast tumour | Phase I | (Hu et al., 2015b) |

† Approved in South Korea for the treatment of breast and non-small cell lung cancer

### 1.5 Targeted drug delivery:

The design and development of specific drug systems to achieve selective drug targeting was first proposed by Paul Ehrlich who suggested a system that would act as a magic bullet (Ehrlich, 1907; Strebhardt and Ullrich, 2008). The principle aim of a targeted drug delivery system is to increase the bioavailability and drug accumulation at the target site, and hence their therapeutic activity whilst minimizing systemic toxicity due to delivery to unwanted sites (Torchilin, 2007b; Agrawal et al., 2015).There are two strategies for effective targeted delivery of compounds, passive and active targeting (Movassaghian et al., 2015) (Figure 1.9).

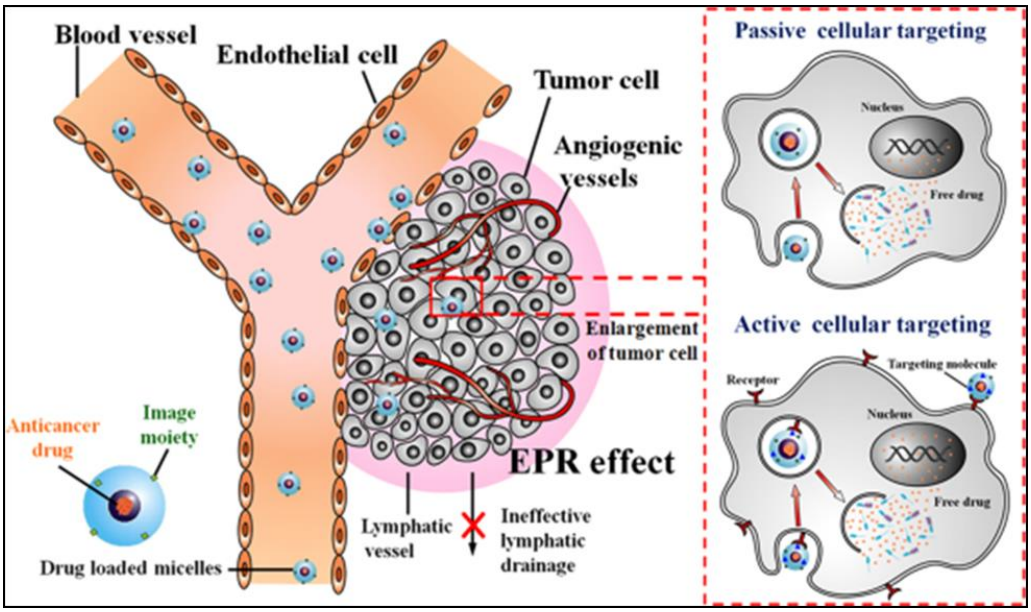


**Figure 1.9.** Schematic representation of drug loaded micelles (circles) with image moiety transport from injection site to tumor sites (Chen et al, 2013).

#### 1.5.1 Passive Targeting:

Under certain circumstances such as inflammation or hypoxia, which is typical for tumours, and other pathological conditions in the body, the endothelial lining of blood vessel walls can be impaired or compromised, with a gap of 10 nm-2 µm occurring, depending on tumour type, and thus the vessels become leaky, or more permeable than under normal physiological conditions (Movassaghian et al., 2015). Additionally,

impaired lymphatic drainage can occur, therefore, this high permeability of tumour vasculature permits nanoparticles to enter the tumour interstitial space and remain entrapped there due to the compromised lymphatic filtration, thereby delaying their clearance (Fang et al., 2011; Torchilin, 2011). This "passive targeting" resulting from the unique combination of leaky vasculature and poor lymphatic flow is known as the enhanced permeability and retention (EPR) effect and is considered to be important process when developing anticancer drug therapies (Torchilin, 2011). EPR-mediated drug delivery strategies are influenced by the physicochemical properties of nanocarriers such as hydrophilicity, hydrophobicity, surface charge, size (less than 200 nm to avoid uptake) (Wang et al., 2015b) and mass (less than 40 kDa to avoid renal filtration) (Torchilin, 2011; Movassaghian et al., 2015). Therefore, due to the small size, hydrophilic shell, and high molecular weight of polymeric micelles, they have been shown to have prolonged systemic circulatory times (Torchilin, 2011), and thus are often seen as suitable for EPR passive targeting delivery applications (Wang et al., 2015b). Small dioleoyl-N-(monomethoxy polyethyleneglycol succinyl)-phosphatidylethanolamine (PEG-PE) micelles (15-20 nm diameter) represent an example of passive EPR-based micelle delivery systems, which have demonstrated effective delivery of a model protein drug to a solid tumour in mice, in contrast to large long-circulating liposomes (100 nm diameter) which did not provide an increased level of target site accumulation in a Lewis lung carcinoma model (Weissig et al., 1998). Genexol-PM (polymeric micelle-based preparation of paclitaxel is an example of passive targeting nanomedicine that has successfully transited to clinical use (Xu et al., 2015). Although the EPR effect has become a landmark principle for anticancer drug delivery design, tumour heterogeneity limits this strategy (Fang et al., 2011). Strategies to overcome this issue have been developed, utilising either elevated blood

pressure, or application of nitric oxide (NO)-releasing agent to intensify the EPR effect in order to achieve more homogenous drug delivery to tumours (Fang et al., 2011).

### 1.5.2 Active Targeting:

Although PEGylation and the EPR effect can improve the biodistribution of therapeutic agents, most of these agents remain subject to clearance by mononuclear phagocytes and accumulation in the reticuloendothelial system (RES) organs (Albanese et al., 2012). Therefore, active targeting aims to enhance drug delivery efficacy by reducing the impact of RES clearance, and via selective and active accumulation and uptake at target sites (Kedar et al., 2010; Movassaghian et al., 2015). Two of the main approaches employed to achieve active targeting are utilisation of targeting ligands, and manipulation of the nanocarriers to specifically respond to pathological triggers that occur in disease conditions (Movassaghian et al., 2015).

It has been demonstrated that nanocarriers functionalised with targeting ligands can facilitate binding with cell-surface receptors in targeted cells and trigger the cellular uptake of drugs by endocytosis (Zhang et al, 2012). Examples of ligands used to modify nanoparticles include monoclonal antibodies (mAbs) (Torchilin, 2004; Biswas et al., 2013), folic acid (Licciardi et al., 2005; Li et al., 2014a), carbohydrate (Craparo et al., 2014), proteins (Wang et al., 2014), peptides (Wang et al., 2012a), and aptamers (Park et al, 2013). When the second approach, stimuli-responsive delivery systems, is utilised, the release of the cargo drug is in response to external stimuli such as pH, enzymatic reaction, redox process, temperature, light and ultrasound. For example, an acidic environment may facilitate the passive targeting of drug and pH-sensitive polymeric micelles that are designed to be stable at a physiological pH (7.4) but degraded in an acidic environment to release an active drug into the target tissues (Prabhu et al., 2015).

## 1.6 Phosphorylcholine discovery

Biocompatibility, particularly haemocompatibility and tissue compatibility, is a major property required for biomaterials that are intended to be utilised for biological applications (Hayward and Chapman, 1984; Williams, 2008). Unfortunately, many materials do not possess excellent biocompatibility, which is highly dependent on the surface physicochemical properties of those materials (Zhou et al., 2014). Therefore, the modification of material surfaces represents an efficient method of improving the biocompatibility of biomaterials (Durrani et al., 1986; Zhou et al., 2014). Inspired by the structure of the cell membrane, especially its main components the phospholipids, many studies have focused on the preparation of phospholipid-assembled surfaces that suppress biological responses (Hayward and Chapman, 1984; Ishihara, 2000; Lewis et al., 2000). The phospholipids in the cell membrane (Figure 1.10) are a mixture of phosphatidylcholine (PC), phosphatidylethanolamine (PE), phosphatidylserine (PS), phosphtidic acid (PA), phosphatidylinositol (PI), and sphingomyelin (SM). These components are arranged so that the negatively charged phospholipids (such as phosphatidylserine) mainly constitute the inner cytoplasmic part of membrane, whereas the outside surface is mainly zwitterionic phospholipids (such as phosphatidylcholine (PC)) that is it contains both positive and negative charges but is overall electrochemically neutral within a wide pH range (Zwaal and Schroit, 1997; Virtanen et al., 1998).

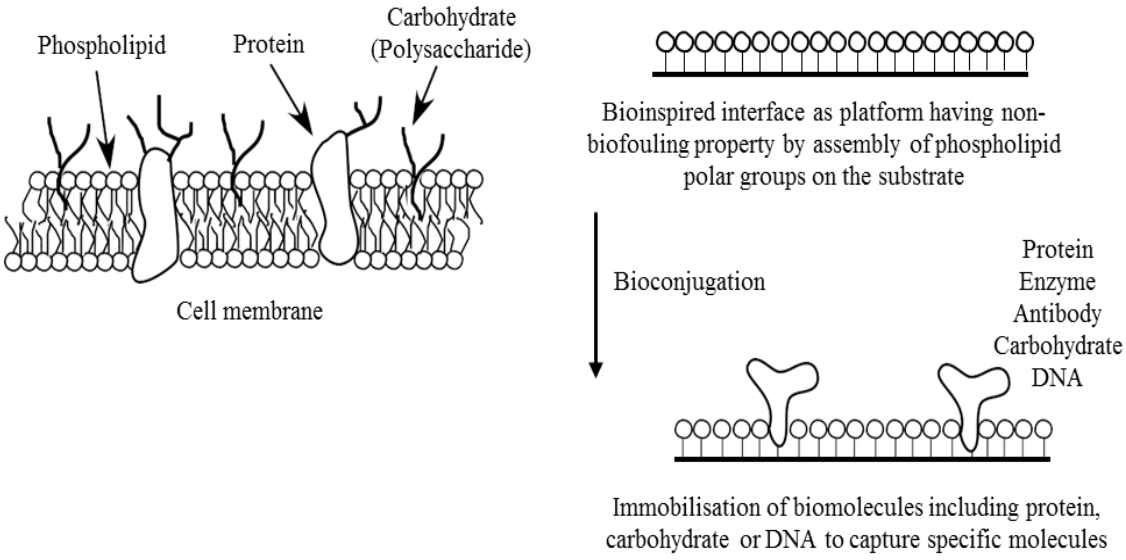


**Figure 1.10.** Schematic of a bioinspired interface based on the cell membrane structure (Ishihara and Takai, 2009)

The chemical and physical instability of phospholipid membranes is their major disadvantage because they do not covalently bond and have high mobility (Nakai et al., 1977; Hub et al., 1980). Therefore, to overcome this problem phospholipid molecules with polymerisable groups were synthesized (Hub et al., 1980; Bonté et al., 1987). In 1984, the Chapman group found that polymerisation of the diacetylenic group resulted in a regular polymer with a stable polymeric phospholipid, which was used to coat artificial surfaces to render them more biocompatible (Hayward and Chapman, 1984). Later, phosphorylcholine was covalently bound to a variety of polymer surfaces; such as surface hydroxyl groups present on glass and silica in order to retain the chemical, physical and topological properties of the materials, and to provide a surface stable to friction whilst the interfacial surfaces changed to mimic biomembranes (Hayward et al., 1986b). Upon evaluation, the deposition of phosphorylcholine on glass provided the structural integrity of the deposited group and their thermal stability at high temperatures for extended periods (Hayward et al., 1986a; Hayward et al., 1986b). Eventually, Chapman and colleagues, studied the

blood-compatibility of surfaces, for which they prepared non-thrombogenic surfaces by introducing phosphatidylcholine groups onto biomaterial surfaces, which resulted in the emergence of what is referred to today as ‘’PC technology’’(Hayward and Chapman, 1984).

### 1.6.1 Methacryloyloxyethyl phosphorylcholine (MPC) development

Many attempts have been undertaken to design blood-compatible, biocompatible, polymeric materials with cell membrane-like surfaces, which have ultimately resulted in the development of 2-methacryloyloxyethyl phosphorylcholine (MPC) (Mwt 295.27 g $mol^{-1}$) (Figure 1.11), a methacrylate monomer with a phosphorylcholine head group and side chain consisting of phosphate anion ($PO_4^{-3}$) and a quaternary ammonium cation ($NR_4^+$, R being an alkyl or an aryl group) (Kadoma, 1978).

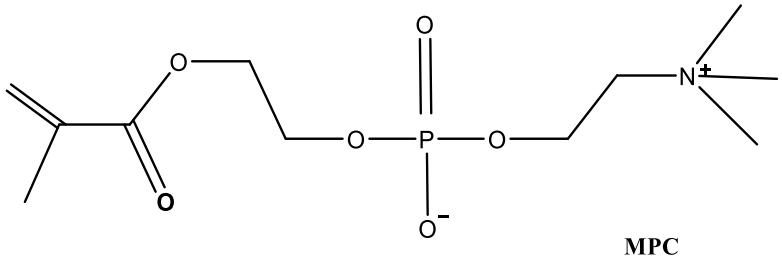


**Figure 1.11.** The chemical structure of 2-methacryloyloxyethyl phosphorylcholine (MPC)

Although MPC polymers were studied back in 1978, their properties were not fully understood and synthesis was difficult and complex (Kadoma, 1978), thus, the initial synthesis of MPC proved challenging, with insufficient amounts of pure MPC being obtained at the final yield (Ishihara et al., 1990). Consequently, Ishihara et al established an optimised process for the synthesis and purification of MPC that resulted in a sufficient quantity of MPC with excellent purity (Ishihara et al., 1990). This achievement represented a considerable step in the development of PC polymers as biomaterials and since 1990, MPC and its polymers have been produced on an

industrial scale (Ishihara and Takai, 2009). The biocompatibility of MPC is due to a high free water fraction associated with their zwitterionic PC head groups that allows proteins to interact reversibly with coatings of surface, without significant conformational change (Ueda et al., 1992; Ishihara et al., 1998), and hence results in inhibition of cellular adhesion and activation (Lewis, 2000). Moreover, MPC based polymers have a wide range of applications in biomedical fields because they possess an exceptional haemocompatibility, antithromobotic activity, and antiprotein adsorption activity (Iwasaki et al., 2008; Goda et al., 2009; Kim et al., 2014). MPC polymers have been applied to the surface of a wide variety of substrates as antifouling coating materials with copolymers of MPC with butyl methacrylate (Lewis, 2000) or PMB (Ueda et al., 1992; Chen et al., 2015; Ishihara et al., 2015) and lauryl (dodecyl) methacrylate (Clarke et al., 2000; Tang et al., 2002; Lewis et al., 2004) represents the most reported systems. Polymer blends are another method for surface modification of materials to reduce elution of MPC polymers from substrate. Blends of segmented polyurethane (SPU) (Ishihara et al., 1996; Ishihara and Iwasaki, 2000; Morimoto et al., 2002; Liu et al., 2014) and polysulfone (PSf) with MPC were prepared to improve the surface properties of blends whilst maintaining the mechanical properties of SPU and PSf (Iwasaki and Ishihara, 2012). A number of medical devices modified with MPC were polymers are used nowadays with the cardiovascular area being a pioneer for commercial application, these include angioplasty guidewires or catheters (Lewis et al., 2001; Gobeil et al., 2002), oxygenators and haemodialysis membranes (Iwasaki et al., 2003; Myers et al., 2003; Ye et al., 2005; Ueda et al., 2006; Dahe et al., 2011), vascular grafts (Yoneyama et al., 2000; Yoneyama et al., 2002; Soletti et al., 2011), and cardiovascular stents (Lewis et al., 2000; Lewis et al., 2002; Lewis et al., 2004). MPC polymers have also been used for ophthalmic devices including soft contact

lenses with low eye irritation properties known as Proclear® (Goda and Ishihara, 2006), intraocular lenses (IOLs) implants (Shigeta et al., 2006), and glaucoma drainage devices (GDDs) (Lim, 2003). MPC polymers have also been used to coat artificial joints (Moro et al., 2009; Kyomoto et al., 2012; Kyomoto et al., 2014). Additionally, MPC is considered as a promising alternative to poly ethylene glycol (PEG), therefore, MPC can be prepared as a block copolymer in combination with many polymers such as 2-(diisopropylamino) ethyl methacrylate (DPA) (Ma et al., 2003), poly(2-(dimethylamino) ethyl methacrylate) (PDMA) (Yuan et al., 2006), poly(D,L-lactide) (PLA) (Hsiue et al., 2007), and poly(2-hydroxypropyl methacrylate) (PHPMA) (Madsen et al., 2009).

### 1.7 2-(diisopropylamino) ethyl methacrylate (DPA)

2-(diisopropylamino) ethyl methacrylate (DPA) (Mwt 213.32 g $mol^{-1}$) is a tertiary amine methacrylate (Figure 1.12) and is considered to be a weak cationic polyelectrolyte with pKa of approximately 6.2 (Licciardi et al., 2005), resulting in a pH responsive property, that has been widely used in preparation of nanoparticles indicated for gene and drug delivery (Massignani et al., 2010; Faccia and Amalvy, 2013; Góis et al., 2014). DPA polymer is hydrophobic at physiological pH (i.e. pH > pKa), whilst in mildly acidic solutions it becomes hydrophilic as a result of protonation of the di-isopropyl tertiary amines (Lomas et al., 2007). Consequently, and due to its hydrophobic-hydrophilic transition induced by pH, DPA is considered a promising polymer for the development of tumor targeting drug delivery polymeric nanocarriers (Giacomelli et al., 2011; Li et al., 2014a).

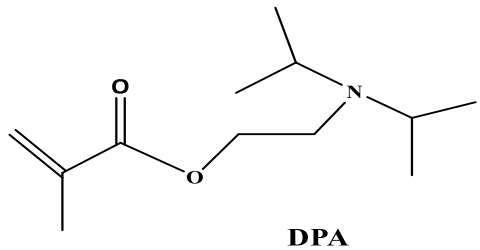


DPA

**Figure 1.12.** The chemical structure of 2- (diisopropylamino) ethyl methacrylate (DPA)

### 1.8 2-methacryloyloxyethyl phosphorylcholine-co-2 (diisopropylamino) ethyl methacrylate (MPC-DPA) diblock copolymer

Armes and co-workers pioneered the early development of the block copolymer 2-methacryloyloxyethyl phosphorylcholine-co- 2-(diisopropylamino) ethyl methacrylate (MPC-DPA), synthesised via atom transfer radical polymerisation (ATRP) (Ma et al., 2003). The MPC-DPA diblock copolymer is based on the highly hydrophilic corona-forming MPC that has a similar stealth characteristic to PEG-based nanoparticles and pH-responsive core-forming DPA, which can be dissolved in a dilute acidic solution because DPA is hydrophilic under these conditions. If the pH of the solution is then raised to pH 6-7, the DPA becomes hydrophobic and results in the formation of micelles (Scheme 1.1) (Giacomelli et al., 2006). The low levels of cytotoxicity and the intracellular uptake of MPC-DPA nanoparticles by mammalian cells; mainly via endocytic pathway, were the main factors that determined the suitability of MPC-DPA diblock copolymer as a drug delivery system. Therefore, MPC-DPA diblock copolymer represented a promising nanocarrier for several biomedical applications such as DNA, anticancer compounds, antibiotics, proteins, and antibodies as shown in Table 1.2.

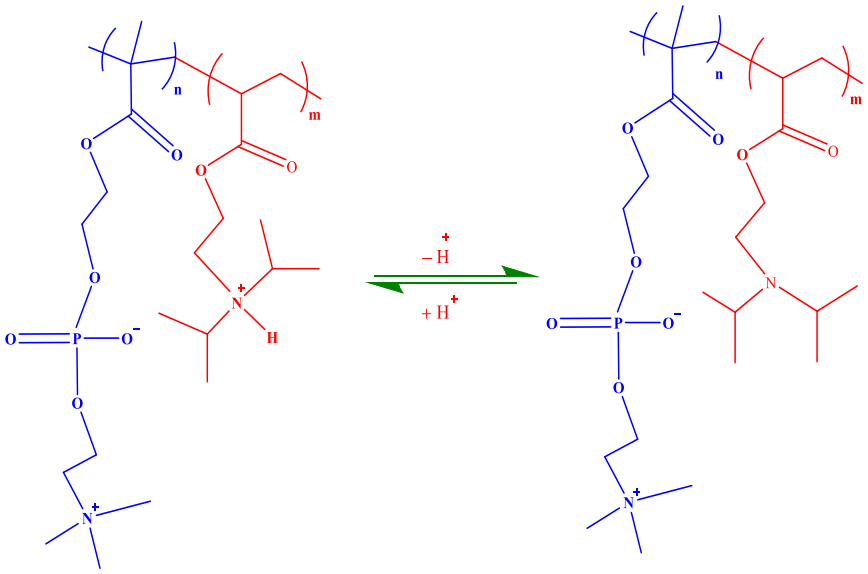


**Figure 1.13.** Schematic representation of pH dependent micellisation behavior of PMPC-b-PDPA (Giacomelli et al., 2006)

**Table 1.2.** Examples of MPC-DPA diblock copolymers synthesis and applications

| MPC | DPA | Ratio | Synthesis | Form | Diameter (nm) | Load | Ref. |
|---|---|---|---|---|---|---|---|
| 30 | 30 | 1:1 | ATRP | Micelle | ----- | -------- | (Ma et al., 2003) |
| 30 | 60 | 1:2 | | | | | |
| 100 | 100 | 1:2 | | | | | |
| 30 | 60 | 1:2 | ATRP | Micelle | 43 | Orange OT | (Salvage et al., 2005) |
| 100 | 100 | 1:1 | | | 33 | | |
| 25 | 70 | 1:2.8 | ATRP | Polymersome and Micelle | ------- | ------ | (Du et al., 2005) |
| 25 | 120 | 1:4.8 | | Polymersome | | | |
| 25 | 160 | 1:6.4 | | Polymersome | | | |
| 30 | 50 | 1:1.6 | ATRP | Micelle | 58 | Tamoxifen | (Licciardi et al., 2005; Licciardi et al., 2006) |
| 30 | 80 | 1:2.6 | | | 68 | Paclitaxel | |
| 30 | 30 | 1:1 | ATRP | Micelle | 15 | Dipyridamole | (Giacomelli et al., 2006) |
| 30 | 60 | 1:2 | | | 29 | | |
| 25 | 70 | 1:2.8 | ATRP | Polymersome | ---- | Plasmid DNA | (Lomas et al., 2007) |
| 30 | 50 | 1:1.6 | ATRP | Micelle | 71 | Tamoxifen | (Licciardi et al., 2008) |
| 30 | 80 | 1:2.6 | | | 62 | Paclitaxel | |
| 25 | 70 | 1:2.8 | ATRP | Polymersome | ----- | Rhodamine B | (Massignani et al., 2009) |
| 25 | 70 | 1:2.8 | ATRP | Polymersome | ---- | Antibodies | (Massignani et al., 2010) |
| 25 | 70 | 1:2.8 | ATRP | Polymersome | 60-400 | Plasmid DNA | (Lomas et al., 2010) |
| 25 | 90 | 1:3.6 | | | | | |
| 25 | 120 | 1:4.8 | | | | | |
| 25 | 160 | 1:6.4 | | | | | |
| 25 | 70 | 1:2.8 | ATRP | Polymersome | 130 nm | Rhodamine B | (Murdoch et al., 2010) |
| 30 | 60 | 1:2 | | | | | |
| 30 | 60 | 1:2 | ATRP | Lamellar | ------- | -------- | (Porto et al., 2011) |

| MPC | DPA | Ratio | Synthesis | Form | Diameter (nm) | Load | Ref. |
|---|---|---|---|---|---|---|---|
| 30 | 60 | 1:2 | ATRP | Polymersome | 101 | Doxorubicin | (Pegoraro et al., 2013) |
| 25 | 59 | 1:2.4 | ATRP | Polymersome | ----- | Nile blue | (Madsen et al., 2013) |
| 25 | 61 | 1:2.4 | | | | | |
| 25 | 62 | 1:2.5 | | | | | |
| 25 | 47 | 1:1.9 | RAFT | ------- | ------- | -------- | (Pearson et al., 2013) |
| 25 | 77 | 1:3 | | | | | |
| 25 | 94 | 1:3.8 | | | | | |
| 25 | 147 | 1:5.9 | | | | | |
| 25 | 90 | 1:3.6 | ATRP | Nanoparticle | ----- | siRNA | (Yu et al., 2013) |
| 25 | 70 | 1:2.8 | ATRP | Polymersome | 208 | Paclitaxel | (Colley et al., 2014) |
| | | | | | 193.6 | Doxorubicin | |
| | | | | | 224.5 | Paclitaxel + Doxorubicin | |
| 100 | 100 | 1:1 | ATRP | Micelle | 70 | Nile Red | (Salvage et al., 2015) |
| 100 | 100 | 1:1 | ATRP | Micelle | 65-70 | Coumarin-6 | (Salvage et al., 2016) |
| 25 | 72 | 1:2.88 | ATRP | Polymersome | 100-200 | Trypsin | (Messager et al., 2016) |
| 25 | 65 | 1:2.6 | RAFT | Polymersome | ------- | Ursolic Acid and Ursocholanic Acid | (Yealland et al., 2016) |

## 1.9 Atom Transfer Radical Polymerization (ATRP)

Since emergence in 1995 (Wang and Matyjaszewski, 1995), atom transfer radical polymerization (ATRP) has attracted a great deal of attention and research focus, with a large number of catalyst systems being investigated and utilised for ATRP polymer synthesis (He et al., 2013). Additionally, several types of ATRP have been developed in order to reduce catalyst levels, lower transition metal toxicity, and extend the usable monomer ranges, namely normal (NI) ATRP, reverse (SR) ATRP, activators

regenerated by electron transfer (ARGET) ATRP, and initiators for continuous activator regeneration (ICAR) ATRP (He et al., 2013). ATRP is a versatile and effective process that can be used for the efficient synthesis of copolymers with desired compositions and molecular architectures, as it enables precise control over molecular weight, molecular weight distribution (MWD), and functionality (Matyjaszewski and Xia, 2001). ATRP can be used to prepare polymers with a molecular weight range from 1000-150000 (Matyjaszewski and Xia, 2001), with polydispersities of 1.5 or less, which is determined by the ratio of consumed monomer and initiator. By utilising ATRP, a variety of polymers can be prepared with controlled topology that range from linear chains to branched structures such as star (Gao and Matyjaszewski, 2008), network (Hernández-Ortiz et al., 2014), comb-like polymers (Lee et al., 2010a), and hyperbranched dendritic system (He et al., 2013). Furthermore, ATRP can be used to control the polymer chain composition to prepare block (Ran et al., 2014), random (Xiang et al., 2014), graft (Siegwart et al., 2012), periodic (Matyjaszewski, 2012a) and gradient copolymers (Van Steenberge et al., 2012). ATRP can also be used to incorporate functional groups at various sites on the polymer such as at the end chains or at a specific site or macromolecule, and in the center or branch point (Matyjaszewski, 2012a), therefore different polymers can be produced via ATRP ranging from those that contain one functional group or two groups as in telechelics, to multifunctional polymers (Matyjaszewski and Tsarevsky, 2009; Matyjaszewski, 2012a).

The principal of normal ATRP is based upon the establishment of a dynamic equilibrium between active and dormant chain ends (Figure 1.14) (Patten et al., 1996). ATRP is a catalytic process in which the transition-metal complex, ($M_t^n$-X/L), known as the activator is used as a mediator for the intermittent generation of propagating

radicals from alkyl halide, ($M_t^n$-X/L) is oxidized to form a halogenated transition-metal complex (X-$M_t^{n+1}$-X/L); the deactivator, by transferring a halogen atom from a halogen-terminated dormant species ($P_n$-X), to form reversibly active radicals ($P_n^{\bullet}$), and it is this step which differentiates ATRP from the conventional radical polymerization (Lee et al., 2010b). Figure 1.14 shows the reaction components of ATRP, which consist of initiator, catalyst and monomer.

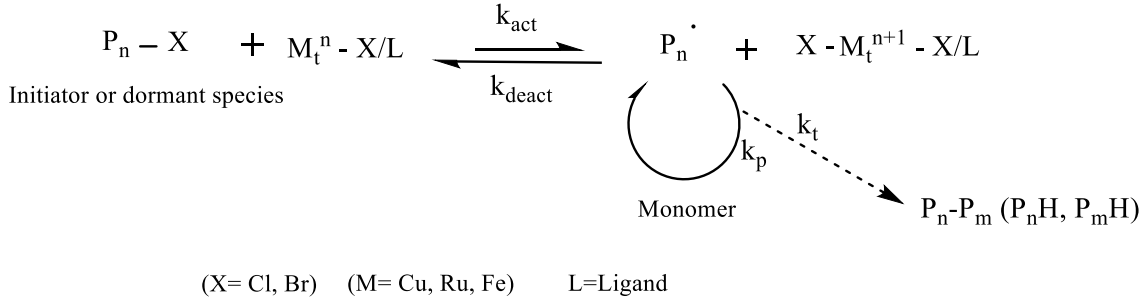


**Figure 1.14.** General ATRP mechanism (He et al., 2013)

Thermodynamically, this equilibrium must lie toward the dormant chain end side so as to maintain a sufficiently low steady-state concentration of radicals, and thereby, biomolecular termination is minimised (Patten et al., 1996; Matyjaszewski and Xia, 2001). Kinetically, the exchange between dormant and active polymer chain ends must be fast to ensure all chains grow at the same rate and polydispersity is decreased (Matyjaszewski and Xia, 2001). ATRP control largely depends on the appropriate equilibrium between the activation process (generation of radicals, $k_{act}$) and the deactivation process (formation of alkyl halides, $k_{deact}$). The rate constants and their ratio ($K_{ATRP} = k_{act}/k_{deact}$) (or $K_{eq}$) determines the concentration of radicals and, consequently, the rates of polymerization and termination as well as polydispersities (Matyjaszewski and Tsarevsky, 2014).

Moreover, factors such as catalyst, initiator and monomer structure, in addition to the type of solvent and the reaction conditions, have influence on the values of $K_{ATRP}$, $k_{act}$ and $k_{deact}$ (Matyjaszewski and Xia, 2001), i.e., $K_{ATRP}$ should be small, to maintain a low radical concentration and to minimize the termination reactions, whilst large $k_{act}$ and $k_{deact}$ are required to provide good control over the polydispersities and a reasonable polymerization rate.

### 1.9.1 ATRP components:

#### 1.9.1.1 Monomers:

A variety of monomers such as styrenes, (meth)acrylates, (meth)acryl amides, and acrylonitrile have been successfully polymerised with ATRP, yielding polymers with narrow polydispersities (Davis and Matyjaszewski, 2000; Shinoda and Matyjaszewski, 2001). It is noteworthy that each monomer has its own set of values for $K_{ATRP}$, $k_{act}$ and $k_{deact}$ and possesses its own intrinsic radical propagation rate ($k_p$) even if the same conditions and catalyst are employed (Matyjaszewski and Xia, 2001; di Lena and Matyjaszewski, 2010). However, polymerisation of acidic monomer via ATRP is a challenge as they protonate nitrogen-containing ligands result in metal complexation (Coessens and Matyjaszewski, 2010).

#### 1.9.1.2 Initiators:

The role of the ATRP initiator is to determine the number of growing polymer chains, therefore, the amount of initiator determines the final molecular weight of polymer at full monomer conversion (Matyjaszewski and Xia, 2001). In ATRP, the theoretical molecular weight or degree of polymerization (DP) increases with the initial concentration of initiator as expressed in equation (1.2).

**Equation 1.2.** Degree of polymerization (DP) equation

$$DP = [M]_0/[Initiator]_0 \times Conversion$$

Moreover, the polydispersity index ($M_w/M_n$) in ATRP, in the absence of significant chain termination and transfer, relates to the concentrations of initiator (RX) and deactivator (D), the rate constants of propagation ($k_p$) and deactivation ($k_{deact}$), and the monomer conversion (p) according to equation 1.3 (di Lena and Matyjaszewski, 2010).

**Equation 1.3.** Polydispersity index ($M_w/M_n$) equation in ATRP

$$M_w/M_n = 1 + \left( \frac{[RX]_0 k_p}{k_{deact}\,[D]} \right) \left( \frac{2}{P} - 1 \right)$$

Therefore, a catalyst that deactivates the growing chains faster will result in polymers with lower polydispersities (smaller $k_p/ k_{deact}$) (Patten et al., 1996). There are two prerequisites for a successful ATRP initiating system, first, initiation should be fast compared to propagation, and second, side reactions should kept to a minimum (Matyjaszewski and Xia, 2001). Alkyl halides (RX) are typically used as initiators and their reactivity depends on the structure of the alkyl group and transferable (pseudo) halogen (Matyjaszewski, 2012a). In order to obtain well-defined polymers with low polydispersities, the halide group (X) must rapidly and selectivity transfer between the growing polymer chain and transition-metal complex, therefore, good control of molecular weight can be achieved when X is either bromine or chlorine (Matyjaszewski and Xia, 2001). Other halides such as iodine are used for acrylate polymerization in copper-mediated ATRP (Davis and Matyjaszewski, 2000), and for styrene in rhenium-based ATRP (Kotani et al., 2000). Fluorine is not used as the C-F bond is too strong to undergo haemolytic cleavage (Matyjaszewski and Xia, 2001).

### 1.9.1.3 Catalyst System:

The catalyst is the key component in the ATRP process as it determines the position of atom transfer equilibrium and the dynamics of exchange between the dormant and active species (Matyjaszewski, 2012b). There are several requirements for the catalyst used in ATRP, first, the metal centre must have at least two readily accessible oxidation states separated by one electron and the metal centre should have reasonable affinity toward a halogen (Matyjaszewski and Xia, 2001). Secondly, the metal should complex strongly with the selected ligand (Matyjaszewski and Xia, 2001). A variety of transition-metal complexes have been used as ATRP catalysts, however, copper catalysts are widely used in ATRP because of their higher efficiency, availability and cost (Boyer et al., 2016). Other catalysts such as iron (Fe) are mainly used in the preparation of biomaterials because of their biocompatibility (He et al., 2013). The type of monomer to be polymerized dictates which other components can be used, therefore, copper-based ATRP systems have been adapted successfully for the polymerization of styrenes, acrylates, methacrylates, acrylonitrile, and other monomers (Patten et al., 1996), ruthenium/aluminum alkoxide based ATRP systems for methacrylates, styrenes, and acrylates (Kato et al., 1995), iron-based ATRP for styrenes and methacrylates, and nickel-based ATRP systems have also been shown to work with methacrylates (Patten et al., 1996). The high concentration of catalyst, typically 0.1-1 mol% relative to monomer, is a limiting factor for ATRP, as this high concentration is required to overcome radical termination reactions (Shen et al., 2004; Tsarevsky and Matyjaszewski, 2007). Various purification strategies have been developed to remove the catalyst from the final product including passing the polymer solution through silica or neutral alumina columns (Ma et al., 2002), stirring with an ion-exchange resin (Matyjaszewski et al., 2000), clay (Munirasu et al., 2008),

precipitation of polymers into a nonsolvent (Kasko et al., 1998), or the use of a heterogeneous catalyst that could be isolated after polymerization (Haddleton et al., 1999). The role of the ligand in ATRP is to aid the solubilisation of the transition-metal catalyst in organic media and to adjust the redox potential of the metal centre for appropriate equilibrium position between active and dormant moieties (Matyjaszewski, 2012b). Moreover, the catalyst activity is affected by choosing the suitable ligand that in turn influences establishment of a suitable $K_{ATRP}$ value (Nanda and Matyjaszewski, 2003; Tang et al., 2008). The most effective ligands are derivatives of 2, 2´-bipyridine (bpy) (Wang and Matyjaszewski, 1995), other π-accepting, chelating nitrogen-based ligands such as 2-iminopyridines (Haddleton et al., 1997), and some aliphatic polyamines (Xia and Matyjaszewski, 1997).

**1.9.1.4 Solvents and additives:**

In ATRP, a suitable solvent is required not only to dissolve the monomers and catalysts but also to control the polymerization rate (Davis and Matyjaszewski, 2000; He et al., 2013) as the solvent affects the ATRP equilibrium and rate constants (Matyjaszewski et al., 1998).There are several factors which may affect solvent choice such as the potential of some solvents for chain transfer that should be minimal (Matyjaszewski and Xia, 2001), and the interaction with the catalyst system such as solvolysis of halogen ligand or displacement of spectator ligands, which should be avoided (Patten and Matyjaszewski, 1998), additionally certain polymer end groups, such as polystyryl halides, can undergo solvolysis or elimination of HX in polar solvent, which should be minimized (Patten and Matyjaszewski, 1998). A broad range of solvents have to date been utilised for ATRP including water (Gaynor et al., 1998), toluene (Amin and El-Gaffar, 2008), anisole (Dong and Matyjaszewski, 2008), *N*,*N*-dimethylformamide (DMF) (Muñoz-Bonilla et al., 2012), dimethyl sulfoxide (DMSO) (Teoh et al., 2006),

methanol (Robinson et al., 2001; Bories-Azeau et al., 2004; Paterson et al., 2010) ethanol (Yu et al., 2007), isopropanol (Xia et al., 1999; McDonald and Rannard, 2001), and ethylene glycol (Oh and Matyjaszewski, 2006). Additives can have varying effects on ATRP, for example the addition of moderate concentrations of water to water-miscible solvents such as methanol (Save et al., 2002; Ma et al., 2003; Iddon et al., 2004; Mao et al., 2006), ethanol (Chatterjee et al., 2005; Abreu et al., 2012), 2-propanol (Lee et al., 2003b; Ma et al., 2003) and DMF (Masci et al., 2004), result in well-controlled and relatively fast polymerisation rates in copper-mediated ATRP. A small increase in polymerization rate was observed with the addition of phenols as radical inhibitors to xylene solution (Haddleton et al., 1997), whilst the presence of strong nucleophiles like phosphines may sometimes terminate the process (Matyjaszewski et al., 1997). Whilst polymerisation is sensitive to oxygen, ATRP can proceed even if very small amounts are present, as it can be scavenged by the catalyst, but oxidation of the catalyst reduces metal complex concentration and forms an excess of deactivator, and thus results in a reduction in the rate of polymerisation (Patten and Matyjaszewski, 1998).

#### 1.9.1.5 Temperature, Pressure and Reaction time:

The optimum temperature for each ATRP is highly dependent on monomer, catalyst, and targeted molecular weight (di Lena and Matyjaszewski, 2010). In ATRP, the rate of polymerisation increases with increasing temperature due to the increase of both the radical propagation rate constant ($k_p$) and atom transfer equilibrium constant ($K_{ATRP}$) (Coessens and Matyjaszewski, 2010). Moreover, stability of the catalytically active complexes is significantly affected by increased temperature that destabilizes catalyst oxidation states resulting in catalyst decomposition (Tsarevsky and Matyjaszewski, 2007), therefore, polymerisation temperatures can be controlled by immersing the

reaction flask into an oil bath (Ma et al., 2002). However, a high temperature (70°C-90°C) is often adopted when polymerization is performed in nonpolar solvents while low temperature (30°C-70°C) for polymerization in polar and protic solvents (He et al., 2013).

Another important factor in ATRP control is the pressure, as high pressure results in enhancing the propagation ratio and ATRP equilibrium constants (Morick et al., 2012), which enables synthesis of well-defined high molecular weight even at room temperature (Kwiatkowski et al., 2008). Further studies should be conducted to precisely reveal the effect of pressure on ATRP, as high pressure increases $K_{ATRP}$ in Cu-mediated ATRP (Morick et al., 2011), while a decrease in $K_{ATRP}$ was observed in some iron-mediated ATRP (Schroeder et al., 2012).

In ATRP, the reaction time effect is most important at high monomer conversions because whilst the prolonged reaction times may lead to nearly complete monomer conversion, it may induce loss of end groups as continued heating after complete monomer conversion may lead to this loss (Matyjaszewski and Xia, 2001).

Over recent decades, the bioinspired polymer 2-methacryloyloxyethyl phosphorylcholine (MPC) has proved to be a suitable candidate for the formation of nanoparticle hydrophilic shell blocks due to its excellent biocompatibility and antithrombogencity (Ishihara, 1997; Lewis et al., 2000; Nakabayashi and Williams, 2003). Additionally, the pH-responsive 2-(diisopropylamino)ethyl methacrylate (DPA) monomer with a low pKa (6.2) (Licciardi et al., 2005), has attracted attention due to its hydrophobic nature at physiological pH condition and hydrophilic properties at low pH due to protonation of the di-isopropyl tertiary amines (Ma et al., 2003; Licciardi et al., 2005).

## 1.10 Summary

With advances in nanotechnology, self-assembled polymeric nanoparticles formed from amphiphilic block copolymer have emerged as potential candidates for pharmaceutical applications. Their controllable and customisable composition, range and flexibility of synthesis methods, together with the possibility to be functionalised by surface moieties, offer great scope for the generation of novel polymeric materials with the potential for pharmaceutical development.

## Project Aim

The overall aim of this project was to develop novel diblock copolymer nano-systems for pharmaceutical applications, and this was to be achieved by completing the following core objectives:

**1- Polymer synthesis.** Synthesis of a series of MPC-DPA diblock copolymers at differing novel block ratio compositions via ethanolic ATRP, in order to determine the suitability of ethanol for this ATRP application, using $^{1}$H NMR and GPC.

**2- Characterisation.** Determine nanoparticle size and stability for the range of novel MPC-DPA diblock copolymers, by studying the physiochemical properties of self-assembled MPC-DPA nanoparticles via DLS, CMC, and STEM, and determine the relationship of nanoparticle size relative to MPC-DPA block ratio composition.

**3- Bioevaluation.** Determine uptake of MPC-DPA nanoparticles of different sizes via *in-vitro* cell culture, and establish the capacity for MPC-DPA nano-systems to load and deliver the anticancer drug Docetaxel *in-vitro* to relevant cancer cell models.

## Rationale

In the current project, the block ratio between MPC and DPA will be customised in order to control the size and type of the nanoparticle produced. Therefore, two novel block ratios will be synthesised and tested, the 1:1 ratio MPC-DPA diblock copolymer in an attempt to maintain a stable particle size and 1:2 ratio MPC-DPA diblock copolymer to increase the loading efficacy of the prepared nanoparticles.

## Hypothesis

The overarching hypothesis of this project was that MPC-DPA nano-systems would be suitable for DTX loading and *in-vitro* delivery to cancer cells lines, and thus suitable candidates for pharmaceutical application development.

# CHAPTER TWO

# GENERAL METHODS

This chapter describes all the materials used and the methods applied in this project.

## 2.1 Materials

**Acetic acid**, glacial, 99.8%. Sigma-Aldrich, UK. Catalogue number: 537020.

**2, 2´- Bipyridyl (Bby)** ≥ 99%. Sigma-Aldrich, UK. Catalogue number: D216305.

**Boric acid**. Sigma Aldrich, UK. Catalogue number: B6768.

**2-Bromo 2-methylpropionyl bromide** 98%. Acros Organics, UK. Catalogue number: 403091000.

**Chloroform-d-** 99.9% D. Sigma-Aldrich, UK. Catalogue number: 151831.

**Chloroform-** HPLC gradient grade. Fisher Scientific, UK. Catalogue number: 10102190.

**Citric acid monohydrate-** Sigma-Aldrich, UK. Catalogue number: C1909.

**Copper (I) bromide (CuBr)** 99.99%. Sigma-Aldrich, USA. Catalogue number: 254185.

**Copper (II) sulfate pentahydrate-** ACS reagent ≥ 98%. Sigma-Aldrich, UK. Catalogue number: 209198.

**Coumarin-6** 98%. Sigma-Aldrich, UK. Catalogue number: 442631.

**CytoTox 96® Non-Radioactive Cytotoxicity (LDH) Assay**. Promega, Southamption, UK. Catalogue number: G1780.

**Decon 90®**. Decon Laboratories Ltd, UK. Catalogue number: 215-181-3

**Deuterium oxide ($D_2O$)** 99.9%- Sigma-Aldrich, UK. Catalogue number: 151882.

**Deuterium chloride solution (DCl)** - 35wt% in $D_2O$, 99 atom %D Hydrochloric acid-d solution. Sigma-Aldrich, UK. Catalogue number: 543047.

**Dichloromethane, anhydrous** ≥ 99.8%. Sigma-Aldrich, UK. Catalogue number: 270997.

**2-(diisopropylamino)ethyl methacrylate** (DPA) 97%. Sigma-Aldrich, UK. Catalogue number: 730971.

**Dimethylsulfoxide (DMSO) Hybri-Max®**. Sigma-Aldrich, UK. Catalogue number: D2650.

**3-(4,5-dimethylthiazol-2-yl)-2,5-diphenyltetrazolium bromide, Thiazolyl blue formazan (MTT)**. Sigma-Aldrich, UK. Catalogue number: M2003.

**Double-tipped needle-** gauge 18 (L24in). Sigma-Aldrich, UK. Catalogue number: Z100889.

**Double-tipped needle-** gauge 20 (L24in). Sigma-Aldrich, UK. Catalogue number: Z101095.

**Docetaxel** 98%. Acros Organics- Fisher Scientific, UK. Catalogue number: 15345068.

**Dulbecco's Modified Eagle Medium (DMEM), high glucose, pyruvate with L-Glutamine, phenol-red (1X)**. Gibco, Fisher Scientific, UK. Catalogue number: 41966029.

**Ethanol, absolute**- Analytical reagent grade. Fisher Scientific, UK. Catalogue number: 10437341.

**Ethanol, anhydrous** ≥ 99.5%. Sigma-Aldrich, UK. Catalogue number: 459836.

**Fetal Bovine Serum (FBS)**, heat treated, EU approved. PAA Laboratories Ltd., UK. Catalogue number: A15-104, University of Brighton reserved batch number: A10408-1516.

**FisherBrand® Glass Bottle (250ml)-** round with PTFE lined 24/400 white cap attached Fisher Scientific, UK. Catalogue number: 11768949.

**FisherBrand® Glass vial (2 ml)-** glass vial sample with attached black PTFE faced rubber lined caps. Fisher Scientific, UK. Catalogue number: 11503532.

**FisherBrand® Glass vial (8 ml)-** borosilicate clear glass with black phenolic cap. Fisher Scientific, UK. Catalogue number: 11543532.

**FisherBrand® Glass vial (20 ml)-** borosilicate glass vial sample with attached black PTFE faced rubber lined caps. Fisher Scientific, UK. Catalogue number: 11513542.

**FisherBrand® turnover Rubber stopper-** Large (24 mm). Fisher Scientific, UK. Catalogue number: 11578132.

**FisherBrand® turnover Rubber stopper-** Small (19 mm). Fisher Scientific, UK. Catalogue number: 11548132.

**FisherBrand® 4.5 mL single use UV cuvette**. PMMA UV grade 10mm pathlength 12mm width x 12mm depth x 45mm height, 280nm to 800nm range, Fisher Scientific, UK. Catalogue number: 11388773.

**Formvar coated 3mm copper 200 mesh TEM grids**. Agar Scientific Ltd, UK. Catalogue number: S138.

**Glass wool**- for laboratory use. Acros Organics, UK. Catalogue number: 386062500.

**Ham's F-12K (Kaighn's) Medium, with L-Glutamine, phenol-red (1X)**. Gibco, Fisher Scientific, UK. Catalogue number: 21127022.

**Ham's F-12 Nutrient Mix, GlutaMAX™ Supplement, with L-Glutamine, phenol-red (1X)**. Gibco, Fisher Scientific, UK. Catalogue number: 31765027.

**Hexane**- HPLC grade. Fisher Scientific, UK. Catalogue number: 10101910.

**Hydrochloric acid solution** (37%). Fisher Scientific, UK. Catalogue number: 10053023.

**4-(2-Hydroxyethyl) morpholine** 99%. Sigma-Aldrich, UK. Catalogue number: H28203.

**Inhibitor removers**. Sigma-Aldrich, UK. Catalogue number: 306312.

**Magnetic flea, with pivot ring (2cm)**. Fisher Scientific, UK. Catalogue number: 11597802.

**McCoy's 5A (Modified) medium, with L-Glutamine, phenol-red (1X)**. Gibco, Fisher Scientific, UK. Catalogue number: 26600023.

**MCF7 Cell Line-** human breast adenocarcinoma-1VL. Sigma-Aldrich, UK. Catalogue number: 86012803.

**Methacryloyloxyyethyl phosphorylcholine (MPC)** - 97%. Sigma-Aldrich, UK. Catalogue number: 730114.

**Methanol-** HPLC grade. Fisher Scientific, UK. Catalogue number: 10365710.

**Methanol-** HPLC gradient grade. Fisher Scientific, UK. Catalogue number: 10499560.

**Methanol-d4-** 99.8%. Sigma-Aldrich, UK. Catalogue number: 151947.

**Minimum Essential Medium (MEM), with Earle's salts and L-Glutamine, phenol-red (1X)**. Gibco, Fisher Scientific, UK. Catalogue number: 31095029.

**MEM Non-Essential Amino Acids Solution (100X)**. Gibco, Fisher Scientific, UK. Catalogue number: 11140050.

**Nanosphere ™ size standard**- Polystyrene polymer microspheres in aqueous suspension (1% solid) (50nm). NIST™ traceable Mean Diameter, Fischer Scientific, UK. Catalogue number: 10389609.

**2-(4-morpholino)ethyl 2-bromosiobutyrate (MEBr) initiator**- In house supply.

**PC-3 Cell Line-** Human Caucasian prostate adenocarcinoma-1VL.Sigma-Aldrich, UK. Catalogue number: 90112714.

**Phosphotungstic acid (PTA) (Tungstophosphoric acid)**. Sigma-Aldrich, UK. Catalogue number: 79690.

**Phosphate buffer saline (PBS) tablets**, Oxoid, Fisher Scientific, UK. Catalogue number: BR0014G.

**Poly(ethyleneglycol) (PEG) nominal Mp 4K**. Agilent Technologies, UK. Catalogue number: PL2070-7001.

**Poly(ethyleneglycol) (PEG) nominal Mp 10K**. Agilent Technologies, UK. Catalogue number: PL2070-9001.

**Poly(ethyleneoxide) (PEO) nominal Mp 20K**. Agilent Technologies, UK. Catalogue number: PL2083-1001.

**Poly(ethyleneoxide) (PEO) nominal Mp 30K**. Agilent Technologies, UK. Catalogue number: PL2083-2001.

**Poly(ethyleneoxide) (PEO) nominal Mp 50K**. Agilent Technologies, UK. Catalogue number: PL2083-3001.

**Poly(ethyleneoxide) (PEO) nominal Mp 70K**. Agilent Technologies, UK. Catalogue number: PL2083-4001.

**Poly(ethyleneoxide) (PEO) nominal Mp 100K**. Agilent Technologies, UK. Catalogue number: PL2083-5001.

**Pyrene (py)** for fluorescence ≥ 99% GC. Sigma-Aldrich, UK. Catalogue number: 82648.

**Silica gel** for chromatography 0.060-0.2mm, nitrogen flushed. Acros Organics, UK. Catalogue number: 10730941.

**SKOV-3 Cell Line**- Human Caucasian ovary adenocarcinoma- 1VL.Sigma-Aldrich, UK. Catalogue number: 91091004.

**Sodium chloride (NaCl)**. BDH, UK. Catalogue number: 8014.

**Sodium dodecyl sulfate (SDS)**. Fischer Scientific, UK. Catalogue number: 10090490.

**Stainless steel 304 syringe needle, noncoring point, gauge 20** (L12in). Sigma-Aldrich, UK. Catalogue number: Z101133.

**Stainless steel 304 syringe needle, noncoring point, gauge 18** (L12in). Sigma-Aldrich, UK. Catalogue number: Z185221.

**Syringe (1ml, disposable**) Plastipak™. Becton Dickinson, Fisher Scientific, UK. Catalogue number: 300013.

**Syringe (2ml, disposable)** Plastipak™. Becton Dickinson, Fisher Scientific, UK. Catalogue number: 300185.

**Syringe (5ml, disposable)** Plastipak™. Becton Dickinson, Fisher Scientific, UK. Catalogue number: 302187.

**Syringe (10ml, disposable)** Plastipak™. Becton Dickinson, Fisher Scientific, UK. Catalogue number: 302188.

**Syringe glass hypodermic luer 10ml**. Samco, Fisher Scientific, UK. Catalogue number: G811/04.

**Syringe-driven filter unit (0.2µm)** Millex®-GP, polyethersulfone, 33 mm, gamma sterilised. Milipore Ltd, Fisher Scientific, UK. Catalogue number: SLGP033RS.

**Syringe-driven filter unit (0.45µm)** Medical Millex-HA, mixed cellulose esters, 33 mm, sterilized by ethylene oxide. Milipore Ltd, Fisher Scientific, UK. Catalogue number: SLHP033RS.

**T-25 Thermo Scientific Nunc™ tissue culture flask**. Fischer Scientific, UK. Catalogue number: TKT-130-050P.

**T-75 Thermo Scientific Nunc™ tissue culture flask**. Fischer Scientific, UK. Catalogue number: TKT-130-370U.

**Tertiary sodium phosphate**. Sigma-Aldrich, UK. Catalogue number: B7778.

**Thermo Scientific Nunc™ 12-well plate**. Fisher Scientific, UK. Catalogue number: 150628.

**Thermo Scientific Nunc™ 24-well plate**. Fisher Scientific, UK. Catalogue number: 142485.

**Thermo Scientific Nunc™ 96 Microwell™**. Fisher Scientific, UK. Catalogue number: TKT-180-070U.

**Thiazolyl Blue Tetrazolium Bromide**. Sigma-Aldrich, UK. Catalogue number: M5655.

**Toluene**- HPLC grade. Fischer Scientific, UK. Catalogue number: 10040500.

**Triethylamine** ≥ 99.5%. Sigma-Aldrich, UK. Catalogue number: 471283.

**Trifluroacetic acid (TFA)**- HPLC grade. Fisher Scientific, UK. Catalogue number: 10294110.

**Trypsin-EDTA** (0.25%) w/v, phenol red (1X). Gibco, Fisher Scientific, UK. Catalogue number: 25200056.

**Universal tube** (20ml). Aseptic polystyrene base/polypropylene cap. Sterilin, Fisher Scientific, UK. Catalogue number: 11339633.

## 2.2 Methods

### 2.2.1 Polymer synthesis

Atom Transfer Radical Polymerisation (ATRP) is a controlled radical polymerisation technique, which was originally developed by the Matyjaszewski research group (Wang and Matyjaszewski, 1995), and subsequently used to develop and synthesise a range of functional materials with controllable structure and composition (Matyjaszewski, 2012a; Ran et al., 2014; Boyer et al., 2015). Moreover, the route of polymer synthesis via ATRP has been proven to be an efficient and reproducible method to prepare well-defined polymers with good control over molecular weight, and thus low polydispersities (Lobb et al., 2001; Ma et al., 2003; Matyjaszewski and Tsarevsky, 2014). The polymers studied in this work were composed of 2-methacryloyloxyethyl phosphorylcholine (MPC) with 2-(diisopropylamino)ethyl methacrylate (DPA), synthesised via sequential addition using a modified version of a previously published ATRP protocol (Ma et al., 2003), to form the diblock copolymer 2-methacryloyloxyethyl phosphorylcholine–*b*-2-(diisopropylamino)ethyl methacrylate (MPC-DPA) **(**Figure 2.1). A range of 1:1 and 1:2 ratio MPC-DPA diblock copolymers were synthesised, with a target weight yield of 5 g copolymer per ATRP undertaken. The target MPC-DPA composition and monomer, ligand, initiator, and catalyst amounts used for each synthesis are detailed in Table 2.1. The following protocol used for ATRP synthesis of the polymers was adapted to each target composition as per Table 2.1. The sequential steps of ATRP polymer synthesis are summarised in Figure 2.2.

**Table 2.1.** Block copolymers target compositions and amount used for ATRP synthesis

| Target Ratios | | | Monomers | | Initiator | Ligand | Catalyst |
|---|---|---|---|---|---|---|---|
| **Ratio** | **MPC** | **DPA** | **Required MPC** | **Required DPA** | **MEBr** | **Bpy** | **CuBr** |
| **1:1** | 20 | 20 | 2.92 g (9.88 mmol) | 2.08 g (9.75 mmol) | 0.138 g (0.492 mmol) | 0.154 g (0.986 mmol) | 0.07 g (0.487 mmol) |
| | 50 | 50 | | | 0.055 g (0.196 mmol) | 0.062 g (0.396 mmol) | 0.028 g (0.195 mmol) |
| | 70 | 70 | | | 0.039 g (0.139 mmol) | 0.044 g (0.281 mmol) | 0.020 g (0.139 mmol) |
| | 90 | 90 | | | 0.030 g (0.107 mmol) | 0.034 g (0.217 mmol) | 0.015 g (0.104 mmol) |
| | 120 | 120 | | | 0.023 g (0.082 mmol) | 0.025 g (0.160 mmol) | 0.011 g (0.076 mmol) |
| **1:2** | 20 | 40 | 2.06 g (6.97 mmol) | 2.94 g (13.78 mmol) | 0.097 g (0.346 mmol) | 0.108 g (0.691 mmol) | 0.050 g (0.348 mmol) |
| | 50 | 100 | | | 0.039 g (0.139 mmol) | 0.043g (0.275mmol) | 0.020 g (0.139 mmol) |
| | 70 | 140 | | | 0.027g (0.096 mmol) | 0.031g (0.198 mmol) | 0.014 g (0.097 mmol) |
| | 90 | 180 | | | 0.021 g (0.074 mmol) | 0.024 g (0.153 mmol) | 0.011 g (0.076 mmol) |
| | 120 | 240 | | | 0.016 g (0.057 mmol) | 0.018 g (0.115 mmol) | 0.008 g (0.055 mmol) |

MPC monomer (Sigma-Aldrich, UK) was polymerised first in 8 ml of degassed anhydrous ethanol (Sigma-Aldrich, UK), using MPC:MEBr:CuBr:bpy under nitrogen atomsphere at ambient temperature. (Initiator, Cu(I)Br and bpy use different amounts depending on block ratios). [$MPC_n$]: [$DPA_m$]: [Me-Br]: [CuBr]: [bpy] = (n and m differ by different monomer length): 1:1:2. Upon addition of the Cu(I)Br and bpy, the reaction mixture immediately became dark brown and progressively more viscous as polymerisation progressed. The two neck RBF was suspended in a thermally equilibrated water bath to maintain the temperature stability for the duration of ATRP reaction.

In order to monitor the ATRP reaction, samples for $^1$H NMR analysis (Bruker, UK) were withdrawn after 3 hours (Ma et al., 2003), and transferred into glass vials (Fisher scientific, UK) containing deuterium oxide solution, $D_2O$ (Sigma-Aldrich, UK) and of copper (II) sulfate pentahydrate (Sigma-Aldrich, UK). Each MPC polymerisation had a duration of 3 hours (Ma et al., 2002), which was sufficient for MPC monomer conversion to reach 98%-99% as indicated by $^1$H NMR data. After 3 hours of MPC polymerisation, the filtered and degassed DPA (Sigma-Aldrich, UK) was transferred under nitrogen pressure to the MPC mixture in the two neck RBF, and the MPC-DPA polymerisation began.

According to previous reports (Ma et al., 2003), completion of MPC-DPA polymerisation using MeOH was expected to take 24-48 hours, therefore, the EtOH ATRP MPC-DPA reaction was run for 48 hours. The polymerisation mixture was maintained under dry nitrogen purge for the whole duration of the synthesis and upon exposure to air at 48 hours, and the addition of analytical reagent grade ethanol (Fisher Scientific, UK), the reaction mixture turned blue, indicating oxidation of the ATRP catalyst and termination of polymerisation (Ma et al., 2003).

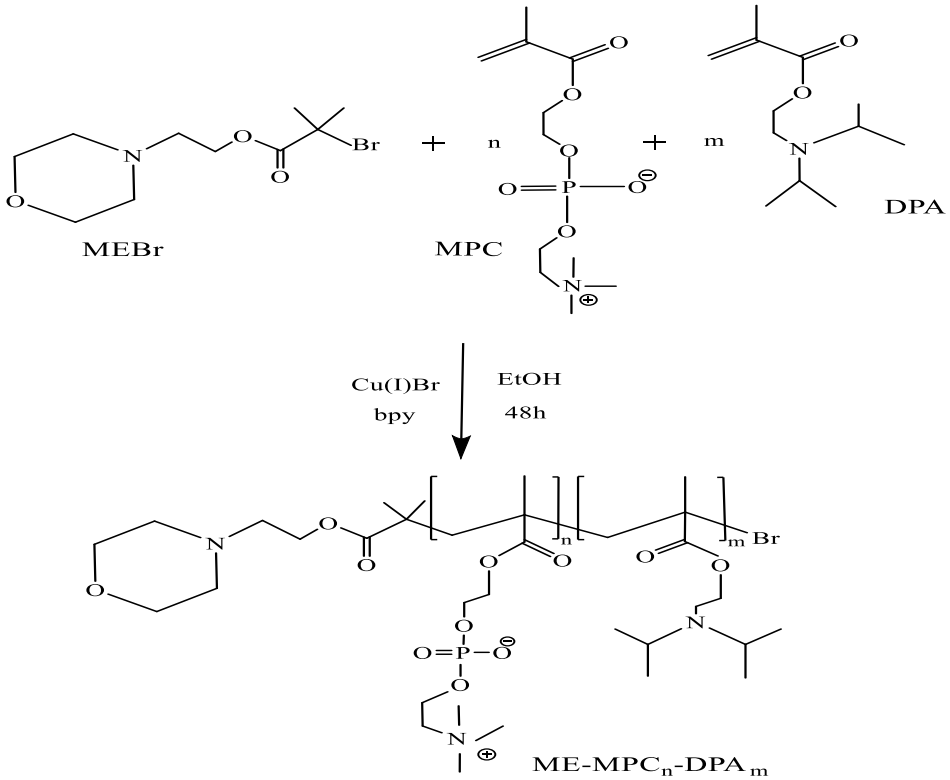


**Figure 2.1.** Schematic of the synthesis of MPC-DPA diblock copolymers via ATRP in protic media at ambient temperature (n and m differ by different monomer length)

The blue reaction mixture was transferred to the silica gel column and low nitrogen pressure applied to facilitate filtration. The filtered polymer solution elute was collected, and solvent evaporation used to remove the EtOH, and leave a sticky liquid, via rotary evaporator (Rotavapor R-114, Buchi, Switzerland) at 30°C, which was then redissolved in HPLC grade methanol (Fisher scientific, UK) and shaken, then rotary evaporated again. To remove any residual DPA monomer, HPLC grade methanol was added to the polymer, and then 100 ml hexane was added before transferring the mixture to a separation funnel (Quickfit, UK), and after 30 minutes the bottom layer was collected and rotary evaporated (30°C) to a sticky liquid.

The recovered polymer was then frozen (-80°C) (New Brunswick Scientific U725 Innova Ultra-Low Temperature Freezers, USA) for 24 hours before being freeze-dried overnight (Christ LOC-1m, SciQuip, UK) (condenser temperature -60°C and pressure

0.250 mbar) to produce a solid dry white powder polymer. The dry purified polymer was transferred to a pre-weighed 20 ml glass vial (Fisher scientific, UK) to determine the yield, then sealed after being flushing with nitrogen.

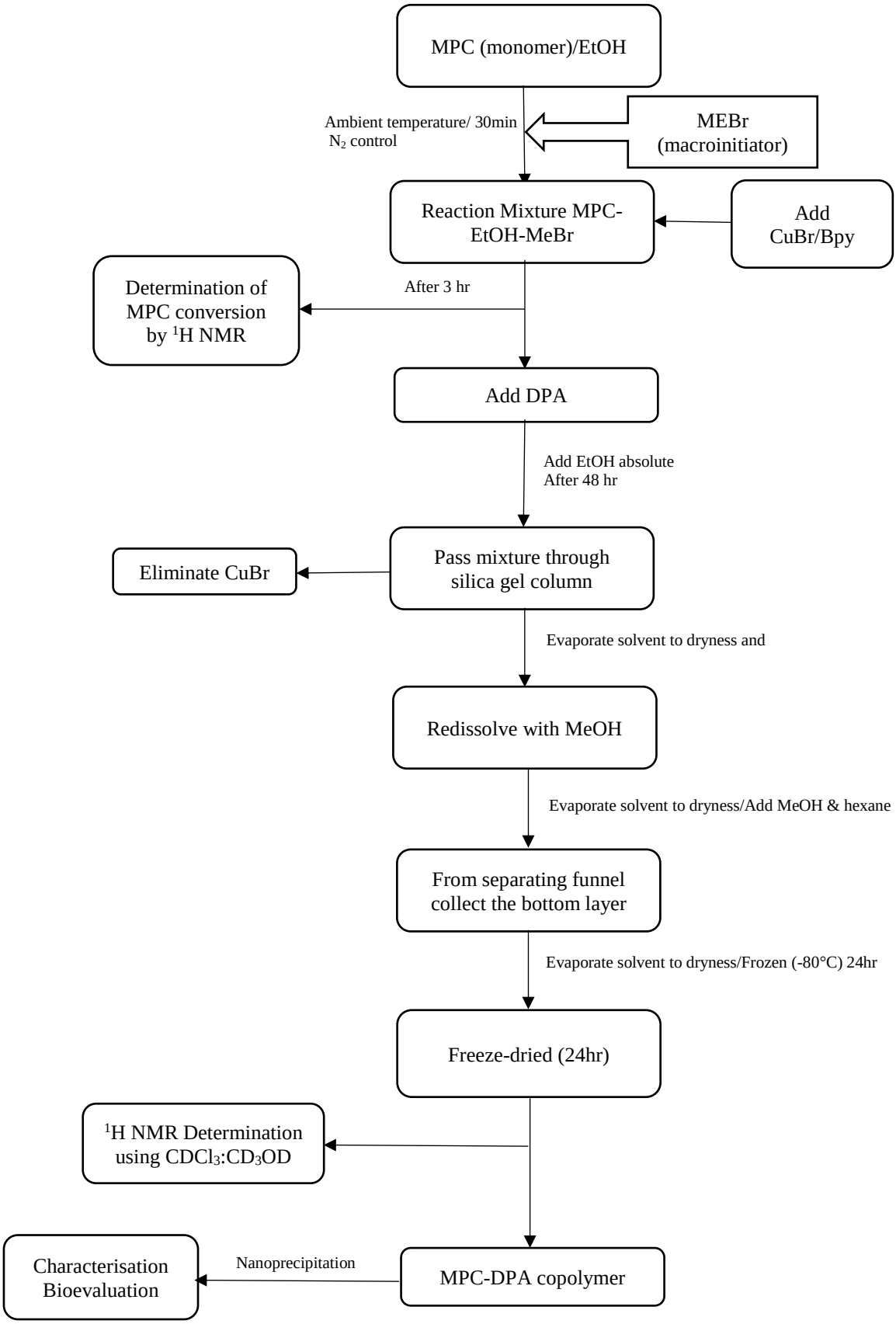


**Figure 2.2.** Schematic of ATRP synthesis of MPC-DPA diblock copolymer

#### 2.2.1.1 Equipment cleaning

To ensure a complete and effective removal of any surfactant or contaminants, all needles, and cannulas were cleaned and flushed with methanol. The used glassware was flushed with methanol before being soaked in 5% Decon 90® (Decon Laboratories Ltd, UK) for 48 hours, then rinsed 5 times with deionised water (Munirasu et al., 2008), and then soaked in 0.1M HCl (37%) (Fischer Scientific, UK) for 48 hours. Finally, the acid soaked glassware was rinsed thoroughly (5 times) with deionised water, and oven dried (Payne, UK) at 75°C prior to use. This method has been effectively used to clean glassware previously (Moore, 1997). Additionally, all needles and cannula were flushed immediately after use with methanol by pushing MeOH through using a 2 ml syringe (3 times), and wiped with clean MeOH soaked laboratory tissue.

#### 2.2.1.2 MP-AES determination of the residual ATRP catalyst level

Microwave plasma atomic emission spectrophotometer (MP-AES) is an analytical technique that is used to determine elemental compositions using atomic emission, as shown in Figure 2.3. It utilises a microwave excitation assembly to create a concentrated axial magnetic field around a conventional torch. Typically, liquid samples are nebulized prior to interaction with the microwave-induced nitrogen plasma, and the atomized sample passes through the plasma where electrons are promoted to the excited state. The light emitted electrons return to the ground state light is separated into a spectrum, and the intensity of each emission line measured at the detector, which is directly proportional to the concentration of an element (Hammer, 2008). Based on previously published methods (Ma et al., 2002; Iddon et al., 2004), the purified MPC-DPA polymers were analysed for their Cu contents using the Agilent 4100 Microwave Plasma Atomic Emission Spectrophotometer (MP-

AES). An aqueous solution of each polymer (50 mg polymer dissolved in deionised water containing 5% (v/v) "trace analysis" grade nitric acid and made up to 5 ml) was introduced into a nitrogen based plasma and the copper emission was measured at 327.396 nm compared to that found for stock solutions containing 0.10, 0.05 and 0.02 ppm Cu; with a blank solution containing 5% (v/v) nitric acid in distilled water was used as a fourth calibration solution.

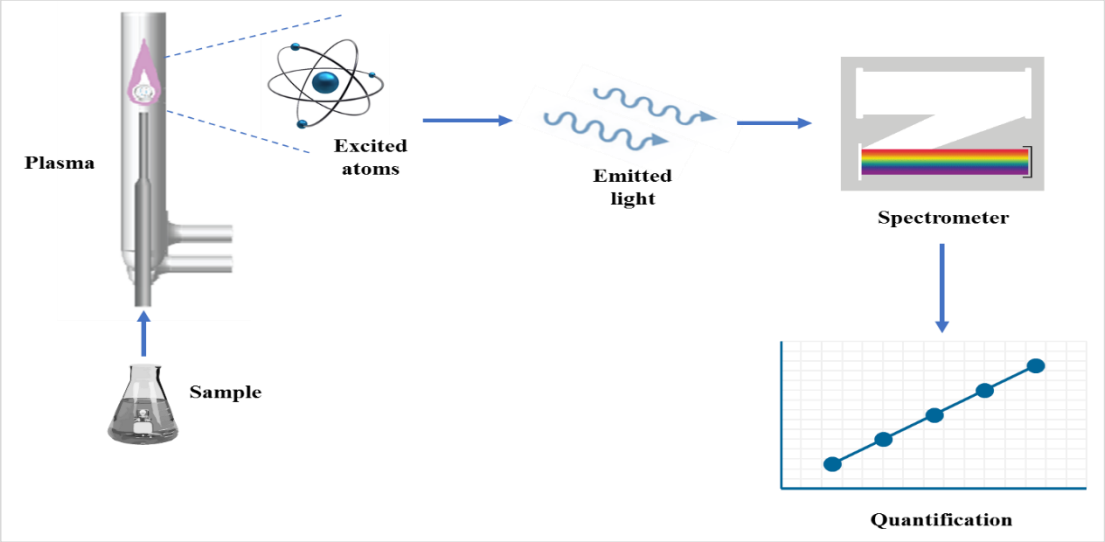


**Figure 2.3.** Schematic diagram of a microwave plasma atomic emission spectrophotometer (MP-AES) (adopted from Agilent, 2012)

### 2.2.2 Characterisation of materials

#### 2.2.2.1 Nuclear Magnetic Resonance (NMR)

NMR is a versatile tool for determining the organic structure and molecular interaction of compounds. $^{1}$H NMR was used to monitor the ATRP reaction until the monomer had been consumed (conversion from monomer to polymer), which typically occurs after 3 hours for MPC and 24 hours for DPA at ambient temperature (Ma et al., 2003), relative to target block lengths. $^{1}$H NMR spectra were recorded using a Brucker Ascend™ (UK) (400MHz) spectrometer with 16 scans at ambient temperature using either $D_2O$ or $CDCl_3$:$CD_3OD$ as solvents. During MPC-DPA synthesis, (as detailed in Section 2.2.1) samples were withdrawn into glass vials

containing 15 mg copper sulphate dissolved in 1 ml deuterium oxide ($D_2O$) for MPC (Ma et al., 2003). Final molecular weight ($M_n$) determination of the purified copolymers composition was undertaken using $^1H$ NMR, by dissolving 10 mg of purified polymer in a mixture of chloroform-d (Sigma-Aldrich, UK): methanol-$d_4$ (Sigma-Aldrich, UK) ($CDCl_3$:$CD_3OD$) (3:1) solvents (Pearson et al., 2013).

### 2.2.2.2 Gel Permeation Chromatography (GPC)

Gel permeation chromatography (GPC), is a powerful analytical tool that is used to determine the molecular weight characterisations of polymers. The number-average molecular weight ($M_n$), weight average molecular weight ($M_w$), and molecular weight distribution ($M_w/M_n$) of the synthesised MPC-DPA copolymers, were measured by organic solvent-based GPC using Phenomenex (UK) columns (Phenogel™ 5 µm, $10^4$ Å and 5 µm $10^3$ Å columns (300 mm x 7.8 mm) in series, with a Phenogel™ guard column (5 µm, 50mm x 7.8mm), all maintained at 45ºC. HPLC mobile phase, consisting of 3:1 chloroform: methanol (HPLC gradient grade - Thermo Fisher Scientific, UK) containing 0.1% acetic acid and 0.05% trifluoroacetic acid (HPLC grade - Thermo Fisher Scientific, UK) was delivered at 1ml $min^{-1}$ via a Perkin Elmer lc 200 series gradient pump (Perkin Elmer, USA). Samples (10 kD-86 kD block copolymers, 2 mg $ml^{-1}$ in mobile phase containing a toluene (Thermo Fisher Scientific, UK) flow marker (20 µl $ml^{-1}$), and standards (poly(ethyleneglycol), PEG or poly(ethyleneoxide), PEO (4 kD-130 kD, 2 mg $ml^{-1}$ in mobile phase containing a toluene (Thermo Fisher Scientific, UK) flow marker (20 µl $ml^{-1}$) were pipetted into separate 250 µl inserts within capped shell vials (Thermo Fisher Scientific, UK) and placed in a Waters (UK) 717 (plus) autosampler kept at 10ºC.

A 5µl (n=3) injection of standards and samples was made in sequence, with blanks (mobile phase including flow marker) being run at the beginning and end. Eluted materials were passed firstly through a Waters (USA) 2487 two channel UV-vis detector (set at 254 nm) and then a Polymer Labs (PL-ELS-2100 Ice) evaporative light scattering detector (ELSD, 45°C nebuliser and evaporator, 1.1 l $min^{-1}$ nitrogen gas flow). Data acquisition (dual channel) was achieved using Perkin Elmer (USA) Totalchrom software on a pc connected to a Perkin Elmer (USA) PE Nelson 900 Series Model 970A Chromatography Interface Controller.

### 2.2.2.3 Preparation of polymeric nanoparticles via nanoprecipitation

Nanopreciptation is a one step process, whereby nanoparticles are formed instantaneously without the need of extended shearing, stirring or sonication (Bilati et al., 2005). The core-shell polymeric self-assembled nanoparticles were prepared from the amphiphilic block copolymer MPC-DPA, which possessed a hydrophobic DPA core and a hydrophilic MPC shell, with preparation based on a previously described procedure (Salvage et al., 2015). Solutions of $MPC_n$-$DPA_m$ copolymers (n & m represent the different block ratios) (Table 2.1) (40 mg $ml^{-1}$) were prepared in HPLC grade methanol (MeOH) (Fischer Scientific, UK). Aliquots (500 µl) of this solution were added drop-wise; using a 1000 µl micropipette (Genex Beta, UK), to 9.5 ml of phosphate buffer saline (PBS) (prepared by dissolving one tablet in 100 mL of laboratory grade deionised water) (Oxoid, UK), pH 7.4. The prepared MPC-DPA nanoparticle solutions were characterised for particle size, polydispersity and morphology using dynamic light scattering (DLS) and scanning transmission electron microscopy (STEM).

### 2.2.2.4 Dynamic Light Scattering (DLS)

Dynamic Light Scattering (DLS) also referred to in literature as Photon Correlation Spectroscopy (PCS), is a non-invasive technique that measures the diffusion of particles moving under Brownian motion, where the velocity of this motion is defined as the translational diffusion coefficient (D), which is converted into size and size distribution using the Stokes-Einstein equation (2.1).

**Equation 2.1.** Stokes-Einstein equation

$$d_h = \frac{kT}{3\pi\eta D}$$

Where, $d_h$ is hydrodynamic diameter (reported as Z-average), k is Boltzmann's constant, T is absolute temperature, η is viscosity, and D is diffusion coefficient (Kaszuba et al., 2008). Brownian motion is a random movement of particles due to collisions caused by bombardment by the solvent molecules that surround them, and speed of the Brownian motion is influenced by particle size, sample viscosity and temperature. Large particles tend to move slowly, compared to smaller particles, and therefore the intensity of scattered light also fluctuates slowly for large particles, whilst small particles move more rapidly (Figure 2.4) (Malvern, 2011). For this study, DLS was used to determine the particle size characteristics of the prepared self-assembled nanoparticles and their polydispersity, in response to changes in pH, temperature, concentration, and time. The DLS instrument employed in this project was a Malvern Zetasizer Nano ZS90 (Malvern instruments Ltd, UK) equipped with a 4mW He-Ne laser operating at a wavelength of 633nm, with a 90° scattering angel of detection. Each DLS size measurement had a total duration of 17 minutes, consisting of 3 replicate measurements containing 12 runs of 20 seconds, each with an initial sample equilibration period of 5 minutes to ensure only Brownian motion was

measured. The average particle size and polydispersity (Cumulants analysis method) calculations were based on the intensity of scattered light (Shaw, 2014).

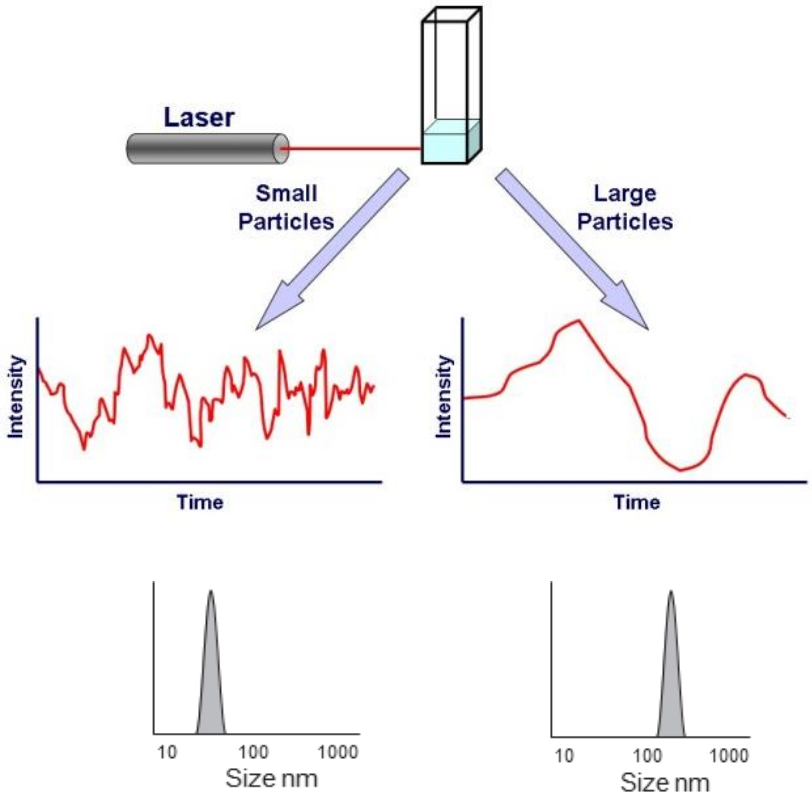


**Figure 2.4.** DLS measurements determine particle size from the pattern of intensity fluctuations in scattered light (Shaw, 2014)

### *2.2.2.4.1 Dilution*

The effect of copolymer concentration on self-assembled polymeric nanoparticle diameter and particle stability was investigated by DLS, as system dilution will induce micelle dissociation once the concentrations falls below the CMC. Resistance to dilution, is therefore a major challenge to overcome when developing micelle based pharmaceutical application and therapies intended for a systemic administration. The dilution stability of MPC-DPA self-assemble nanoparticle solutions in PBS (pH 7.4), described in the preparation Section (2.2.2.3), were assessed at 25°C by measuring signal intensity (KCps), particle diameter (ZAve), and polydispersity (PDI) in response to serial halving dilutions of the nanoparticle solution using PBS. The diluted

samples were filtered with 0.22 µm pore size syringe filters (Milipore Ltd, UK) immediately prior to measurement to ensure sample quality, and an aliquot (2 ml) of the filtered particle suspension was transferred into a clear 4-sided UV grade cuvette (Fisher Scientific, UK). DLS measurement was conducted in triplicate for each sample dilution. For method and instrument validation, serial dilutions of 50 nm polystyrene standard beads (Fischer Scientific, UK), were prepared using 10 mM sodium chloride (NaCl) (BDH, UK) (International Orgnisation for Standardisation, 1996) and measured as described earlier.

#### *2.2.2.4.2 pH*

The particle size (ZAve) and polydispersity (PDI) of the MPC-DPA self-assembled nanoparticle suspensions across a range of pH values (3-10) were measured by DLS, as pH influences the stability of MPC-DPA nanoparticles due to the pH dependent hydrophilic-hydrophobic transition characteristic of DPA (Ma et al., 2003; Salvage et al., 2005). A wide range buffer system comprising two stock solutions was prepared (Carmody, 1961), namely stock solution A (Boric acid 0.2 M and Citric acid 0.05 M) and stock solution B (Tertiary sodium phosphate 0.1 M), to produce the pH range of 3-10. Separate stock solutions were prepared by weighing out 12.36 g boric acid, 10.50 g citric acid, and 38.01 g tertiary sodium phosphate and dissolving them in 1 L deionised water in a volumetric flask. 200 ml of each buffer solution was prepared for each pH value as shown in Table 2.2. pH measurements were taken and confirmed using a Mettler Toledo Seven easy™ pH meter (Mettler Toledo Ltd, UK), and the instrument was calibrated against pH solutions of 7, 4.01 and 9.21 respectively. To determine the effect of pH on particle formation during nanoprecipitation, a series of pH buffer solutions were prepared (pH 3-10) as per Table 2.2, and 500 µl of polymer solution was add to 9.5 ml of each pH buffer. The solutions were then filtered, and

ZAve, PDI, and KCps measured using DLS at 25°C as per Section 2.2.2.4. An aliquot (2 ml) of the filtered particle suspension was transferred into a clear 4-sided UV grade cuvette, measured at 25°C, and DLS measurement repeated for each pH value. Furthermore, an additional pH range (6-7) was prepared with smaller increments in order to determine the pH of micellisation and nanoparticle self-assemble to 0.1 pH level of accuracy. The same stock solutions previously prepared were used and 200 ml of buffer solution was required to prepare the 6-7 pH range.

**Table 2.2.** Volumes of acid solution (A) and basic solution (B) required for the preparation of 200 ml of solutions in buffer series (Carmody, 1961)

| Target pH | Solution A* (ml) | Solution B** (ml) |
|---|---|---|
| 3 | 176 | 24 |
| 4 | 155 | 45 |
| 5 | 134 | 66 |
| 6 | 118 | 82 |
| 7 | 99 | 101 |
| 8 | 85 | 115 |
| 9 | 69 | 131 |
| 10 | 54 | 146 |

* Solution A: Boric acid 0.2 M and Citric acid 0.05 M
** Solution B: Tertiary sodium phosphate 0.1 M

***2.2.2.4.3 Temperature and time stability***

A product may be exposed to a range of temperatures during transport and storage before being used, therefore, the temperature stability of MPC-DPA self-assembled polymeric nanoparticle solutions was examined. Samples were prepared as described in Section 2.2.2.3, and the particle size (ZAve), PDI and KCps for each sample measured by DLS, as described in Section 2.2.2.4, across the temperature range of 5-70°C, at 5°C intervals, with 20 minutes thermal equilibration after each 5 °C temperature change before DLS measurement commenced, to ensure only Brownian

motion was measured. Moreover, a closer examination of the physiologically related temperature range was carried out by testing MPC-DPA sample solutions at temperatures ranging from 30-40°C, at 1°C intervals with 20 minutes thermal equilibration after each 1 °C temperature change. Validation of the Zetasizer, and thermal stability method, was undertaken using 50 nm monodisperse polystyrene standard particles, measuring ZAve, PDI and KCps as described in Section 2.2.2.4, across both temperature ranges, utilised 5-70°C and 30-40°C.

Long-term polymeric nanoparticle stability has an impact on the storage and transport requirements of products, and therefore, stability over time of MPC-DPA self-assembled polymeric nanoparticles were conducted via DLS for two sample sets prepared as described in Section 2.2.2.3, exploring the effect of storage at ambient room temperature, and cold storage at 4°C. DLS measurements were carried out on a monthly basis using the same condition as Section 2.2.2.4, in order to explore time and temperature effects on particle stability during transport and storage.

### 2.2.2.5 Critical micelle concentration (CMC) determination

The critical micelle concentration (CMC) is one of the most important parameters related to micellar stability, therefore the CMC of the MPC-DPA copolymers was determined by fluorescence spectroscopy using pyrene (Sigma-Aldrich, UK) as a fluorescence probe. Pyrene is a condensed aromatic hydrocarbon and the sensitivity of the pyrene fluorescence intensity to the solvent polarity is widely used for the determination of the CMC of micellar systems (Domínguez et al., 1997; Aguiar et al., 2003; Piñeiro et al., 2015). The CMC method utilised was based on a published method (Domínguez et al., 1997), a solution of pyrene was prepared by dissolving 5 mg of pyrene in 10 ml of methanol, and then diluting this solution 20 times with methanol in a volumetric flask, the resultant pyrene concentration was 0.12 mM . An

aliquot (50 µl) of methanolic pyrene was transferred into a clear 4-sided UV grade cuvette and mixed with 2.95 ml of serial halving dilutions of each copolymer solution prepared as per Section 2.2.2.3, which were filtered with 0.22 µm pore size syringe filters; to give a total final volume of 3 ml. The fluorescence emission of pyrene was measured with Cary Eclipse fluorescence spectrophotometer (UK) at 25°C, the excitation wavelength was 334 nm, and the emission was recorded at 345-480 nm, with the use of excitation and emission slit widths of 10 and 2.5 nm respectively (Domínguez et al., 1997), and with a scan rate of 30.00 nm/min, and 0.5000 nm data interval. Triplicate preparation of the polymer systems was undertaken, and each set was measured in triplicate. The instrument was zeroed with a UV grade cuvette containing 3 ml of blank (PBS) before the measurement of each samples cuvettes. Method validation was undertaken using sodium dodecyl sulfate (SDS) (Fischer scientific, UK) aqueous solutions (200 mM -0.09 mM) in triplicate and measured in the same manner to polymers.

#### 2.2.2.6 Scanning Transmission Electron Microscopy (STEM)

The particle size and morphology of MPC-DPA systems was also examined by STEM analysis using a Zeiss SIGMA field emission gun (FEG-SEM) operating in STEM mode. Formvar carbon 200 mesh coated copper grids (Agar Scientific, UK) were treated with plasma glow discharge (Polaron, Plasma Barrel Etcher, PT7150, Quorum Technologies Ltd, UK) (compressed air flow rate 0.5-1 and power adjusted to 5 watts) for 40 seconds to create a hydrophilic surface (Blanazs et al., 2012). Sample preparation was carried out in a chemical fume hood. Samples were filtered with 0.22 µm pore size syringe filters, and then 1 drop of diblock copolymer solution was placed onto a freshly plasma treated grid, via a 100 µl micropipette and allowed to adsorb for 1 min. The grid was then carefully edge blotted with filter paper to remove excess

solution, and the droplet application then repeated twice more (total three droplets). Then a droplet of 2% phosphotungstic acid (PTA) stain (pH 7.5) (Sigma-Aldrich, UK) was applied to the sample-loaded grid for 1 min, and again carefully edge blotted to remove excess stain, and allowed to air dry.

Samples were loaded into a STEM-sample holder (STEM 12x), and examined using a Zeiss SIGMA field emission gun scanning electron microscope (FEG-SEM) equipped with a Zeiss STEM detector with 20 kV accelerating voltage, 20 μm aperture, and 3 mm working distance. Particles measured were at different magnifications (100K X, 200K X, and 500 K X) at different areas of each sample.

### 2.2.3 Bioevaluation

#### 2.2.3.1 Preparation of Docetaxel (DTX)-loaded micelles

At this stage, two preparation methods; nanoprecipitation and direct dissolution, were applied to encapsulate docetaxel within MPC-DPA micelles. In the nanoprecipitation method, solutions of $MPC_{20}$-$DPA_{20}$, $MPC_{50}$-$DPA_{50}$, and $MPC_{90}$-$DPA_{90}$ copolymers (40 mg $ml^{-1}$) were prepared in HPLC grade methanol (MeOH) and ethanol (EtOH) (Fischer Scientific, UK) with the addition of 1 mg $ml^{-1}$ of the hydrophobic anticancer drug-docetaxel (Acros organics) (i.e. polymer:DTX ratio was 40:1), depending on DTX solubility in MeOH and EtOH determined from a standard calibration curve (Appendix 1.0).

Aliquots (500 μl) of this solution were added drop-wise to 9.5 ml of phosphate buffer saline (PBS) (pH 7.4). In the direct dissolution method, micelle samples were first prepared via nanoprecipitation method as mentioned above but without DTX addition, and following the completion of the addition, the micelle solutions of $MPC_{20}$-$DPA_{20}$, $MPC_{50}$-$DPA_{50}$, and $MPC_{90}$-$DPA_{90}$ copolymers were placed into separate dialysis bags (MWCO 6-8 kDa) (with stirring with 1 cm magnetic flea at 100 rpm), and dialysed

against 100 ml PBS to remove MeOH or EtOH, with changes of the dialysis medium each 24 hour period for seven days. Then, 0.5 mg docetaxel was added to each polymer solution after dialysis, and stirring gently for 24 hours. Three different batches were prepared for each copolymer from the two procedures with all of the prepared samples subsequently filtrated using 0.22 µm pore size syringe filter to remove any unloaded drug. Blank micelles were also prepared by direct dissolution according to a previously adopted protocol (Du and Armes, 2008).

#### 2.2.3.2 Determination of Docetaxel (DTX) loading and encapsulation efficiency

The determination of DTX concentration was carried out by measuring the UV absorbance of sample solutions at a recorded lambda max ($\lambda_{max}$) of 230 nm using a Lambda 25 UV-vis spectrophotometer (PerkinElmer, UK). The amount of DTX present in the samples were calculated using a standard calibration curve experimentally obtained with MeOH and EtOH solutions, constructed according to published procedure with some modifications (Sheetal, 2013) as shown in Appendix 1.0. The drug loading (DL%) and encapsulation efficiency (EE%) were calculated according to the following equations (2.2) & (2.3):

**Equation 2.2.** Drug loading (DL%) equation

$$\text{DL}\ (\%) = \frac{\text{Weight of DTX in micelle}}{\text{Weight of micelle}}\ \text{x}\ 100$$

**Equation 2.3.** Encapsulation efficiency (EE%) equation

$$\text{EE}\ (\%) = \frac{\text{Weight of DTX in micelle}}{\text{Weight of feeding DTX}}\ \text{x}\ 100$$

### 2.2.3.3 *In-vitro* Release of Docetaxel from Polymeric Micelle

The release profile of docetaxel from DTX loaded micelles was examined in PBS (pH 7.4) using the dialysis bag diffusion method. The release experiment was initiated by placing 3 ml of DTX-loaded micelles (prepared in Section 2.2.3.1) in a dialysis bag with 6-8 kDa molecular weight cutoff, then the sealed end of the bag was placed in a universal tube containing 10 ml pre-warmed PBS (pH 7.4) maintained at 37°C with 100 rpm magnetic bar stirring, to begin drug release. At predetermined time intervals (0.5, 1, 2, 3, 4, 6, 8, 10, 24, 48, 72, and 98 hours), the dialysis bags were transferred to 10 ml prewarmed fresh PBS (pH 7.4). All experiments were carried out in triplicate and the concentration of the released DTX in the sample was determined by measuring the absorbance at 230 nm via UV-vis spectrophotometer, depending on the standard calibration curve of DTX.

### 2.2.3.4 Cell culture

In this project, normal and cancer cell lines were used as listed in Table 2.3. The passage of all the utilised cell lines was carried out after cell populations reached 70-80% confluency, by standard trypsinisation (0.25% w/v trypsin/EDTA (1X) for 3-5 minutes at 37°C, 5% $CO_2$), then cell suspensions were removed from the flask and centrifuged at 500 x g for 5 minutes. Cell pellets were re-suspended in the desired volume of fresh medium and cell counting performed via a haemocytometer.

All cell lines were maintained using routine culture conditions by culturing them in T-75 surface treated polystyrene tissue culture flasks, which were incubated at 37°C in a humidified, 5% CO2 atmosphere (Sanyo-MCO715), cell culture medium was replenished every 2-3 days and cells were used up to 10-15 passages after the passage they were purchased, or until their behaviour (e.g. speed of growth) changed

**Table 2.3.** Different cell lines with their origin, culture medium in which they grow and seeding density

| | Cell Line | Origin | Cell Culture Medium Description | Seeding Density (cells/cm$^2$) |
|---|---|---|---|---|
| ***Normal*** | **3T3** | Mouse Swiss NIH embryo | ***Dulbecco's modified Eagle's Medium (DMEM) (1X)*** supplemented by the addition of 10% (v/v) heat inactivated (H.I.) fetal bovine serum (FBS), with 4.5 g/L glucose, L-glutamine, sodium pyruvate, and sodium bicarbonate | 2-5x10$^4$ |
| | **V79** | Hamster Chinese lung | | 2-4x10$^4$ |
| | **Vero** | Monkey African Green kidney | | 1-3x10$^4$ |
| | **CHO** | Hamster Chinese ovary | ***Ham's F-12 Nut Mix (1X)*** + GlutaMAX™-I supplemented by the addition of 10% (v/v) (H.I.) fetal bovine serum (FBS) with GlutaMAX™-I | 1-3x10$^4$ |
| | **MRC-5** | Human foetal lung | ***Minimum Essential Medium (MEM) (1X)*** supplemented by the addition of 10% (v/v) (H.I.) fetal bovine serum (FBS), 1% non-essential amino acids, with Earle's salts and L-glutamine | 2-4x10$^4$ |
| ***Cancer*** | **MCF-7** | Human Caucasian breast adenocarcinoma | ***Minimum Essential Medium (MEM) (1X)*** supplemented by the addition of 10% (v/v) (H.I.) fetal bovine serum (FBS), 1% non-essential amino acids, with Earle's salts and L-glutamine | 2-4x10$^4$ |
| | **PC3** | Human Caucasian prostate adenocarcinoma | ***Ham's F-12K (Kaighn's) Medium (1X)*** supplemented by the addition of 10% (v/v) (H.I.) fetal bovine serum (FBS) and L-glutamine | 2-5x10$^4$ |
| | **SKOV-3** | Human Caucasian ovary adenocarcinoma | ***McCoy's 5A (Modified) Medium (1X)*** supplemented by the addition of 15% (v/v) (H.I.) fetal bovine serum (FBS) and L-glutamine | 3-6x10$^4$ |

### 2.2.3.5 *In-vitro* cell cytotoxicity studies

#### *2.2.3.5.1 Cell Colony Formation Test*

The procedure for this test was adapted from previously reported studies that were employed to evaluate MPC-DPA micelle toxicity (Salvage et al., 2015). In this test, V79 cell fibroblasts were seeded into 24-well plates (Nunc, UK) at a seeding density of 100 cells/ well in 0.5 ml of DMEM (10% FBS) and incubated at 37°C, 5% $CO_2$ for 24 hours. After 24 hours incubation period, culture medium was removed from wells and replaced with 0.5 ml of MPC-DPA solutions that were prepared as per Section, 2.2.2.3 with a series of half dilution concentrations in DMEM (2.5% FBS) made to provide polymer concentrations from 1000-31.25 μg $ml^{-1}$. The plates were then kept in an incubator at 37°C, 5% $CO_2$ for 5 days to allow cell colony growth.

After 5 days, the cell medium was gently removed before being fixed with 3.7% w/v formaldehyde (Sigma, UK) for 30 min, and then stained with 10% Giemsa stain (Sigma, UK) for a further 30 mins. In each addition and removal step in this assay, wells were washed with 1 ml deionised water. The numbers of cell colonies in each well for each dilution of sample were counted and recorded.

#### *2.2.3.5.2 MTT cell viability assay*

MTT is a quantitative colorimetric assay that was developed by Mosmann (Mosmann, 1983), and relies on measuring the mitochondrial activity of viable cells (Berridge and Tan, 1993). MTT (3-(4,5-dimethylthiazol-2-yl)-2,5-diphenyltetrazolium bromide) is a yellow soluble compound that is reduced by metabolically active cells to form purple insoluble formazan crystals (Mosmann, 1983) as shown in Figure 2.5, a process that is dependent on the involvement of the coenzymes nicotinamide adenine dinucleotide phosphate hydrogenase (NADPH) and NADH (Berridge et al., 1996), which are exist only in healthy cells.

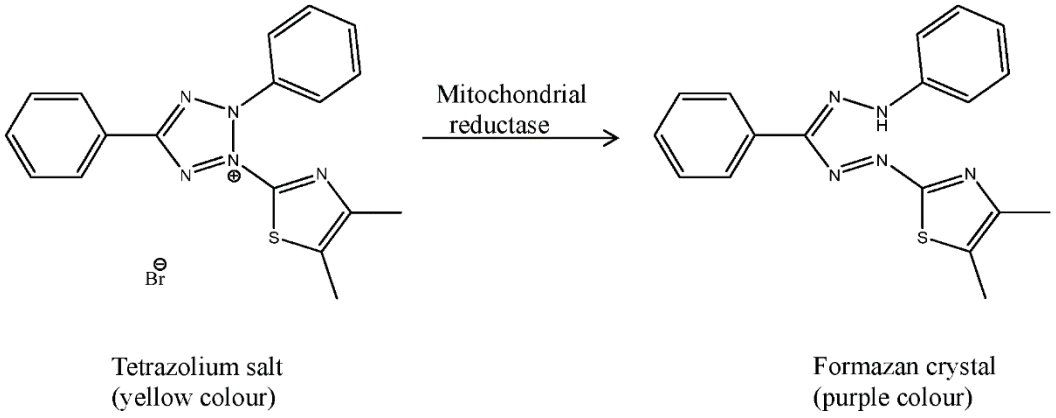


**Figure 2.5.** Mechanism of MTT assay (Barahuie et al., 2014)

Following previously published method (Salvage et al., 2016), V79 and 3T3 cell lines were seeded in 1 ml DMEM (10% FBS) in 24-well plates (Thermo Scientific Nunc™ 24 Microwell™, Fisher Scientific, UK) at a density of $10^4$ cells/well (Benoit et al., 1997), and $15x10^3$ cells/well (Lee et al., 2011) respectively, and then incubated at 37°C, in 5% $CO_2$ for 24 hour to allow cell growth. MPC-DPA nano-systems ($MPC_{20}$-$DPA_{20}$, $MPC_{50}$-$DPA_{50}$, $MPC_{70}$-$DPA_{70}$, $MPC_{90}$-$DPA_{90}$, and $MPC_{120}$-$DPA_{120}$) were prepared as described in section 2.2.2.3, then a series of halving dilutions were prepared in the growth medium to provide polymer concentrations from 1000-31.25 µg $ml^{-1}$. Following incubation, polymer samples were added to the growing cells and they were incubated for 24 hours under the same conditions. After 24 hours treatment exposure, the growth medium was removed, the cells were washed with PBS (pH 7.4), and then incubated at 37°C, 5% $CO_2$ with 1 ml freshly prepared MTT solution (0.5 mg $ml^{-1}$) for 4 hours in a dark incubator. Following incubation, the MTT medium was removed and then wells were washed with PBS (pH 7.4). 1 ml of dimethyl sulphoxide (DMSO) (Sigma, UK) was then added to each sample to solubilise the resultant formazan crystals, and 100 µl of the dissolved material (DMSO-formazan solution) was transferred from each sample well to a 96-well plate (Thermo Scientific Nunc™

96 Microwell™, Fisher Scientific, UK) in triplicate, and their absorbance was measured at 540 nm via a microplate reader (Thermo Multiskan Ascent 354. MTT absorbance values were converted into cell viability percent that was calculated using the following equation:

**Equation 2.4.** Cell viability percent from MTT absorption

$$\text{Cell viability } \% = \frac{A_s - A_b}{A_c - A_b} \text{ x } 100$$

Where: $A_s$ = the absorbance of cells incubated with DTX

$A_b$ = the absorbance cell free or the culture medium only (blank)

$A_c$ = the absorbance untreated healthy cell or cells incubated with culture medium only (control)

For cancer cell lines, MCF-7, SKOV-3, and PC3 were seeded in 1 ml growth medium (according to their medium described in Table 2.3) in 24-well plates at a density of 1 $x10^5$ cells/well, then they were incubated at 37°C, in 5% $CO_2$ for 24 hours to allow cell growth. Docetaxel-loaded MPC-DPA micelles (DTX-$MPC_{90}$-$DPA_{90}$) were prepared as described in section 2.2.2.3, then a series of halving dilutions were prepared in the growth medium to provide polymer concentrations from 1000-31.25 µg $ml^{-1}$. Following incubation, polymer samples were added to the growing cells and they were incubated for 24 hours at the same conditions. After 24 hours treatment exposure, the growth medium was removed, the cells were washed with PBS (pH 7.4), and then incubated at 37°C, 5% $CO_2$ with 1 ml freshly prepared MTT solution (0.5 mg $ml^{-1}$) for 4 hours in a dark incubator. Following incubation, the MTT medium was removed and the wells were washed with PBS (pH 7.4). 1 ml of dimethyl sulphoxide (DMSO) added to each sample to solubilise the resultant formazan crystals, 100 µl of DMSO-formazan solution transferred from each sample well to a 96-well plate in

triplicate, and their absorbance was measured at 540 nm via a microplate reader (Thermo Multiskan Ascent 354). Cell viability was calculated as previously describe, using Equation 2.4.

#### *2.2.3.5.3 LDH cell viability assay*

The Lactate dehydrogenase (LDH) assay is a colorimetric assay that was developed by Wacker et al., 1956 (Wacker et al., 1956). It is well known that LDH is a cytosolic enzyme that is found in different cell species and is responsible for the conversion of pyruvate to lactate with simultaneous reduction of $NAD^+$ to NADH. LDH is a stable intracellular enzyme that can only be measured upon its release following cell lysis, which is considered as an indication of loss of cell membrane integrity (Yang et al., 2009a). The leakage of LDH into the supernatant of cell is measured in conjunction with a coupled enzymatic assay that results in the conversion of a colourless tetrazolium salt (INT) into red formazan salt. The intensity of the resultant colour is directly proportional to number of lysed cells that can be measured spectrophotometrically (Nachlas et al., 1960).

In this study, the Promega CytoTox96® Non-Radioactive Cytotoxicity Assay kit was used for the measurement of LDH release in the culture supernatant. For cancer cell lines, MCF-7, SKOV-3, and PC3 were seeded in 1 ml growth medium (according to their medium described in Table 2.3) in 24-well plates at a density of 1 $x10^5$ cells/well, and then incubated at 37°C, in 5% $CO_2$ for 24 hours to allow cell growth. Docetaxel-loaded MPC-DPA micelles (DTX-$MPC_{90}$-$DPA_{90}$) were prepared as described in section 2.2.2.3, and then a series of halving dilutions were prepared in the growth medium to provide polymer concentrations from 1000-31.25 µg $ml^{-1}$. Following incubation, polymer samples were added to the growing cells and they were incubated for 24 hours at the same conditions. The supernatant was taken (50 µl) in triplicate

and transferred to 96-well plate, and LDH substrate mixture was prepared according to the manufacturer instructions, and then added 50 µl to each cell sample. This reaction occurs at room temperature and all samples should be kept in the dark for 30 minutes. Later 50 µl of 1M acetic acid (stop solution) was added to stop the reaction, and their absorbance was measured at 492 nm via a microplate reader (Thermo Multiskan Ascent 354). The readings were converted to a measurement of cytotoxicity depending on the percentage of the released LDH from cell in relation to complete cell lysis, using the following equation:

**Equation 2.5.** Calculation of percent cytotoxicity from LDH release

$$\%\ \text{Cytotoxicity from LDH release} = \left[\frac{(S-B)-(C-B)}{(L-B)-(C-B}\right] \text{x } 100$$

Where: S = sample absorption

B = average cell free blank absorbance

C = average negative control, or non-treated healthy population absorbance value

L = average positive control, or fully lysed cell population absorbance value

Lysis solution (1% v/v Triton™-X100) was used to initiate lysis and provide a positive control to determine 100% LDH release from the standard number of cells in each sample. A blank sample of media only (without cells) was also incubated to be used as a control against all background absorbance.

In general, values over 50% were considered to be indictive of a toxic response. This equates to the median lethal dose (LD50), a crude measure of acute toxicity based on

the dose or concentration (LC50) required to kill half the members of tested population over the given treatment time (Zbinden and Flury-Roversi, 1981).

### 2.2.3.6 The Cellular Uptake Studies

The cellular uptake experiments were carried out in both normal and cancer cell lines utilising coumarin-6 (Cm-6), a hydrophobic fluorescent dye, as a probe to substitute docetaxel in the micelles. Cm-6 was incorporated into MPC-DPA micelles via nanoprecipitation. Solutions of $MPC_{20}$-$DPA_{20}$, $MPC_{50}$-$DPA_{50}$, and $MPC_{90}$-$DPA_{90}$ copolymers (40 mg $ml^{-1}$) were prepared in HPLC grade methanol (MeOH) with 0.3 mg $ml^{-1}$ Cm-6, then aliquots (500 µl) of this solution were added drop-wise to 9.5 ml of phosphate buffer saline (PBS) (pH 7.4), and the resultant samples were filtered using 0.22 µm pore size syringe filters before being used in uptake studies. In this project, the cellular uptake of Cm6-loaded micelles was assessed both qualitatively and quantitively compared with free Cm-6.

#### *2.2.3.6.1 Flow Cytometry Analysis*

Flow cytometry (FCM) is a quantitative technique that is used to analyse the physical and chemical characterisation of particles, such as cells. A flow cytometer composed of five main components, which are a flow cell, a light source (laser), an optical system, light detectors, and data processing and operating unit (computer) (Rahman, 2006). The liquid cell suspension is first injected into the flow cell and passed through a laser beam, then scattered light and fluorescence are detected and converted into digital signals that are graphically displayed by the data processing and operating unit (Hawley and Hawley, 2004; Rahman, 2006; Raveche et al., 2010).

For the quantitative assessment, cells were seeded in a 12-well cell culture plate (at 1 x $10^5$ cells/ well) and allowed to attach for 24 hours in a humified incubator (5% $CO_2$) at 37°C. Cells were then incubated with Cm-6 loaded micelles and free Cm-6 as a

control, for set lengths of time (1 min, 5 min, 10 min, 30 min, and 1 hour). Then the cells were washed with 1 ml PBS (pH 7.4) twice before trypsinisation (200 µl trypsin for 3 minutes) and centrifugation at 1000 rpm for 5 minutes. Finally, the supernatant layer was removed and cell pellets were resuspended with 500 µl PBS (7.4), then samples were examined by fluorescence intensity in cells using flow cytometry (Becton Dickinson, UK) (Shi et al., 2015a; Wang et al., 2013).

#### *2.2.3.6.2 Confocal Laser Scanning Microscope (CLSM)*

For the qualitative study, V79, Vero, MRC-5, CHO, MCF-7, SKOV-3, and PC3 cells were seeded at 5 x $10^3$ cells/ well in 12-well cell culture plates, in triplicate, and incubated overnight in a humified 5% $CO_2$ at 37°C. Cells were then incubated with Cm-6 loaded micelles for a set range of times (1 min, 5 min, 10 min, 30 min, and 1 hour), cells were washed with 1 ml PBS (pH 7.4) twice before applying drug-free fresh medium to each well, then the fluorescence in cells was observed with a Leica SP5 confocal laser scanning microscope (CLSM) (Leica, UK) using an excitation wavelength of 488 nm, and an emission collection wavelength band of 500-610 nm. Control samples of free Cm-6, blank nanocarrier, and solvent only were also tested.

#### *2.2.3.6.3 Inhibition of endocytosis*

To determine whether the uptake of Cm-6 loaded MPC-DPA nanoparticles was due to endocytosis or direct diffusion, V79, Vero, MRC-5, CHO, MCF-7, SKOV-3, and PC3 cells were seeded in 24-well plates for 24 hours in 5% $CO_2$ at 37°C. The cells were then pre-incubated for 1 hour at 4°C before being incubated with Cm-6 loaded MPC-DPA at 4°C for a further 1 hour. After co-incubation, the cells were washed with 1 ml PBS (pH 7.4) twice before trypsinisation (200 µl trypsin for 3 min) and centrifugation at 1000 rpm for 5 min. Finally, the supernatant layer was removed and cell pellets were resuspended with 500 µl PBS, then samples were examined by

fluorescence intensity in cells using flow cytometry (Snipstad et al., 2014; Wang et al., 2015a).

### 2.2.4 Statistics Analysis

All results are presented as the mean ± standard deviation of triplicate repeats from three independent experiments. Statistical analysis of the *in-vitro* data was undertaken using one-way ANOVA tests followed by post-hoc Tukey's pairwise comparisons using Minitab 18, where $p < 0.05$ was considered significant.

# CHAPTER THREE

# POLYMER SYNTHESIS

## 3.1 Introduction

The main objective of this project was to develop a series of novel amphiphilic diblock copolymers via ethanolic ATRP and evaluate their ability as drug delivery carriers, and the following results provide an overview of MPC-DPA diblock copolymer synthesis and the techniques involved to evaluate ATRP procedure.

## 3.2 Results

### 3.2.1 MPC-DPA diblock copolymer synthesis and characterisation

In this study, 2-methacryloyloxyethyl phosphorylcholine–*b*-2-(diisopropylamino)ethyl methacrylate (MPC-DPA) diblock copolymers were synthesised by atom transfer radical polymerisation (ATRP) at ambient room temperature using 2-(4-morpholino)ethyl 2-bromosiobutyrate (MEBr) as an initiator and copper bromide Cu(I)Br / 2, 2´- Bipyridyl (bpy) as the catalyst system as described in Section 2.2.1. Two sets of MPC-DPA diblock copolymers were synthesised via ATRP; 1:1 and 1:2 ratios and the resultant yields of the ATRP synthesis are shown in Table 3.1, by which a series of MPC-DPA diblock copolymers with various degree of polymerisation were successfully synthesised with a target weight yield of 5 g copolymers per ATRP.

The chemical composition of the synthesised diblock copolymers was examined by $^{1}$H NMR (Section 2.2.2.1), and the $^{1}$H NMR spectrum are shown in Figure 3.1 and 3.2 for 1:1 and 1:2 ratio respectively. In addition to $^{1}$H NMR, GPC analysis of the copolymers was also carried out (Section 2.2.2.2), by which number-average molecular weight ($M_n$), and polydispersity ($M_w/M_n$) of MPC-DPA diblock copolymers relative to PEG and PEO standards were determined by GPC, and the

unimodal GPC traces of the resultant copolymers can be seen in Figure 3.3 and 3.4, which indicated a relatively low polymer polydispersity, which was attributed to the use of the ATRP technique.

Table 3.2 details the molecular weights of the synthesised MPC-DPA diblock copolymers, with a small variation between the theoretical $M_n$, which was calculated from the molar ratios, and $M_n$ obtained from $^1H$ NMR and GPC evident. Moreover, the degree of polymerisation (DP) recorded using NMR was in close agreement with the targeted DP.

The residual ATRP copper level in the copolymers after recovery was determined via MP-AES technique (as described in (Section 2.2.1.2). The results are listed in Table 3.2 and indicated that Cu levels were in the range of 0.67-1.96 ppm for the purified MPC-DPA diblock copolymers. The data represent the mean of 3 measurements, (n=3) averaged from 3 analyses per measurement.

**Table 3.1.** The synthesised MPC-DPA diblock copolymer prepared by ethanolic ATRP at ambient temperature using sequential monomer addition route

| | **Target diblock copolymers** | **Total Reaction time (h)** | **Target yield** | **Achieved yield** | |
|---|---|---|---|---|---|
| | | | **(g)** | **(g)** | **(%)** |
| **Set 1 1:1** | $MPC_{20}$-$DPA_{20}$ | 48 | 5 | 3.88 | 77.6 |
| | $MPC_{50}$-$DPA_{50}$ | 48 | 5 | 3.66 | 73.2 |
| | $MPC_{70}$-$DPA_{70}$ | 48 | 5 | 4 | 80 |
| | $MPC_{90}$-$DPA_{90}$ | 48 | 5 | 3.20 | 64 |
| | $MPC_{120}$-$DPA_{120}$ | 48 | 5 | 3 | 60 |
| **Set 2 1:2** | $MPC_{20}$-$DPA_{40}$ | 48 | 5 | 3.52 | 70.4 |
| | $MPC_{50}$-$DPA_{100}$ | 48 | 5 | 1.32 | 26.4 |
| | $MPC_{70}$-$DPA_{140}$ | 48 | 5 | 2.59 | 51.8 |
| | $MPC_{90}$-$DPA_{180}$ | 48 | 5 | 1.25 | 25 |
| | $MPC_{120}$-$DPA_{240}$ | 48 | 5 | 2.55 | 51 |

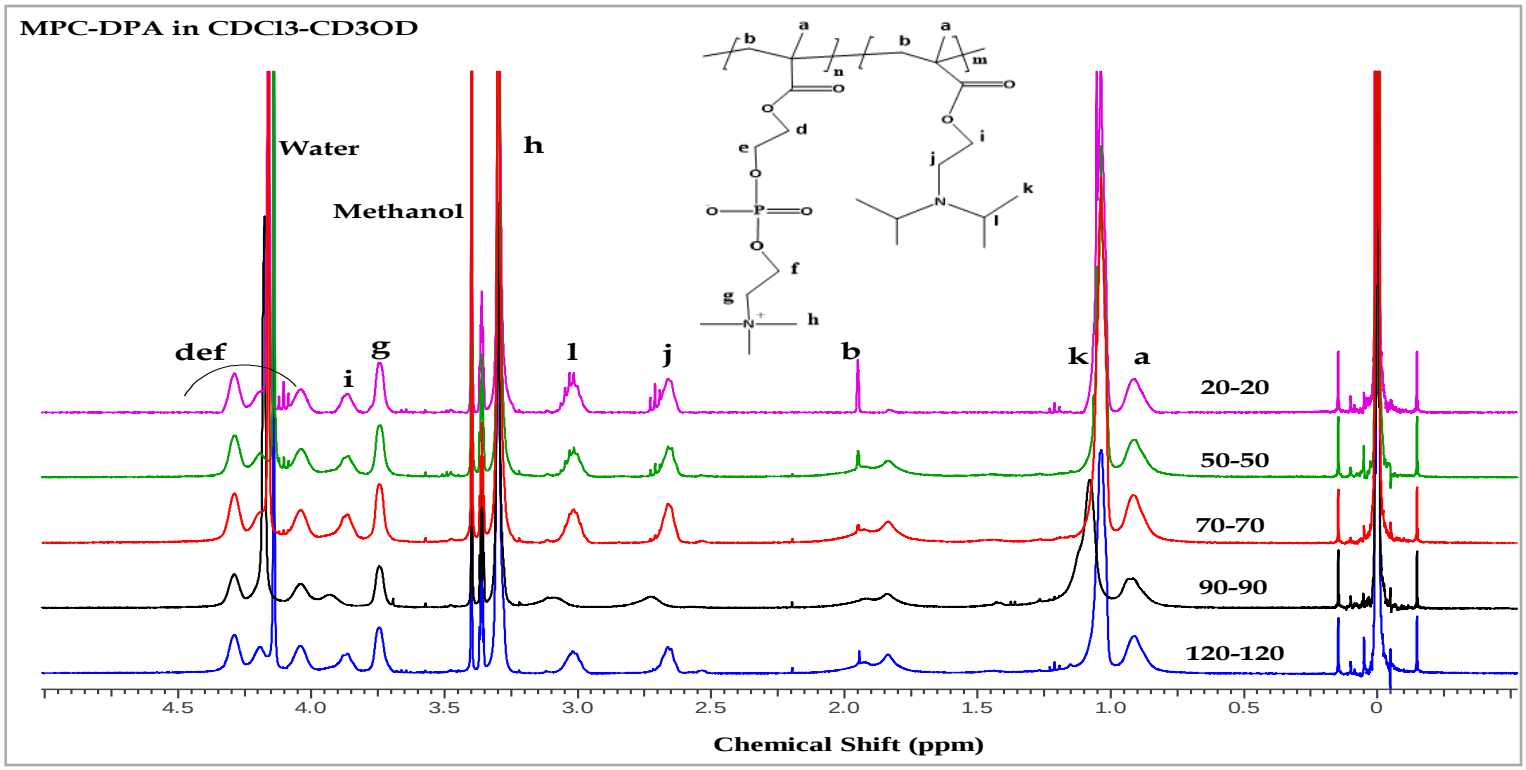


**Figure 3.1.** Assigned $^{1}H$ NMR spectrum for 1:1 ratio MPC-DPA diblock copolymers in $CDCl_3$:$CD_3OD$ solvents (3:1) (Original in colour)

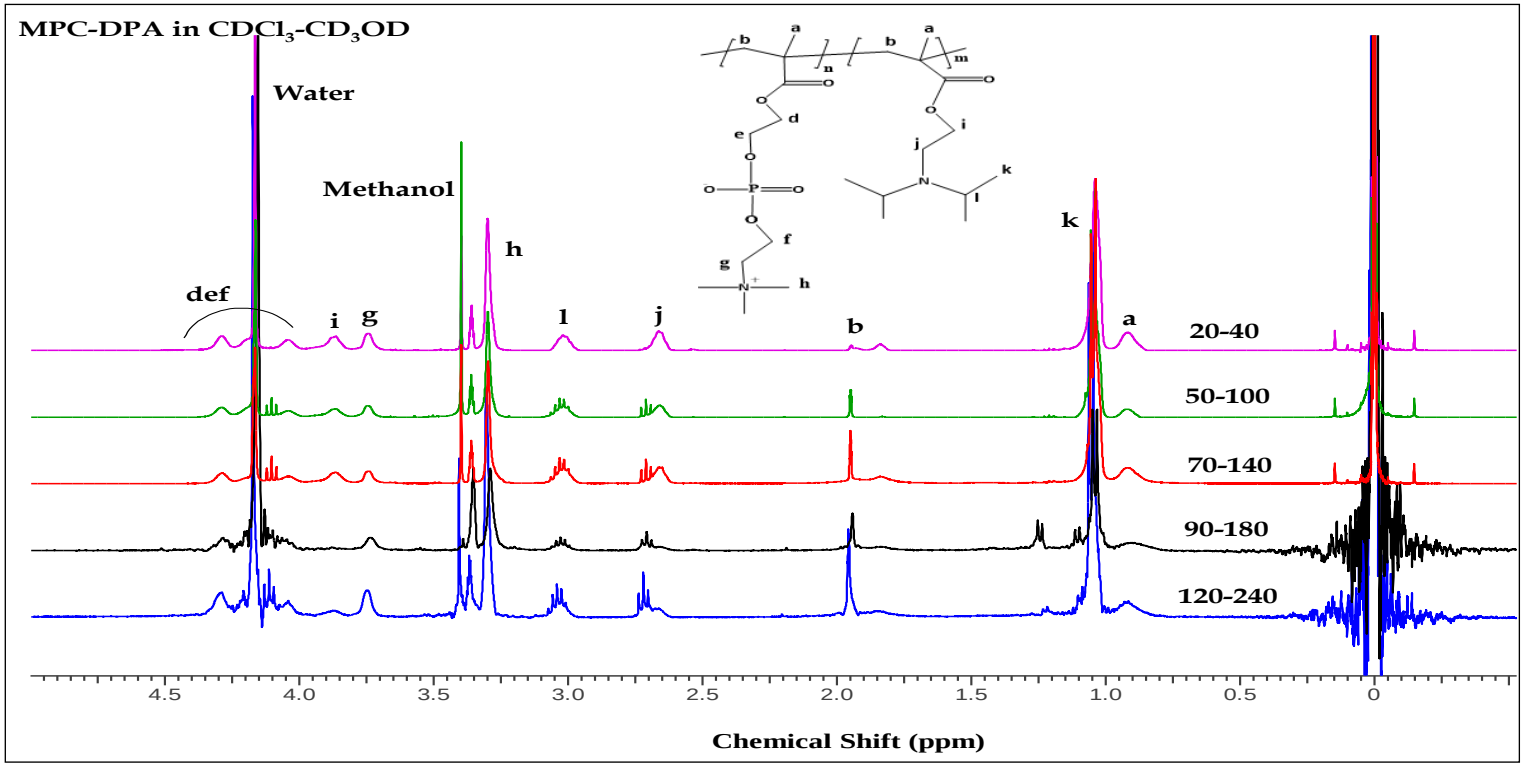


**Figure 3.2.** Assigned $^{1}H$ NMR spectrum for 1:2 ratio MPC-DPA diblock copolymers in $CDCl_3$:$CD_3OD$ solvents (3:1) (Original in colour)

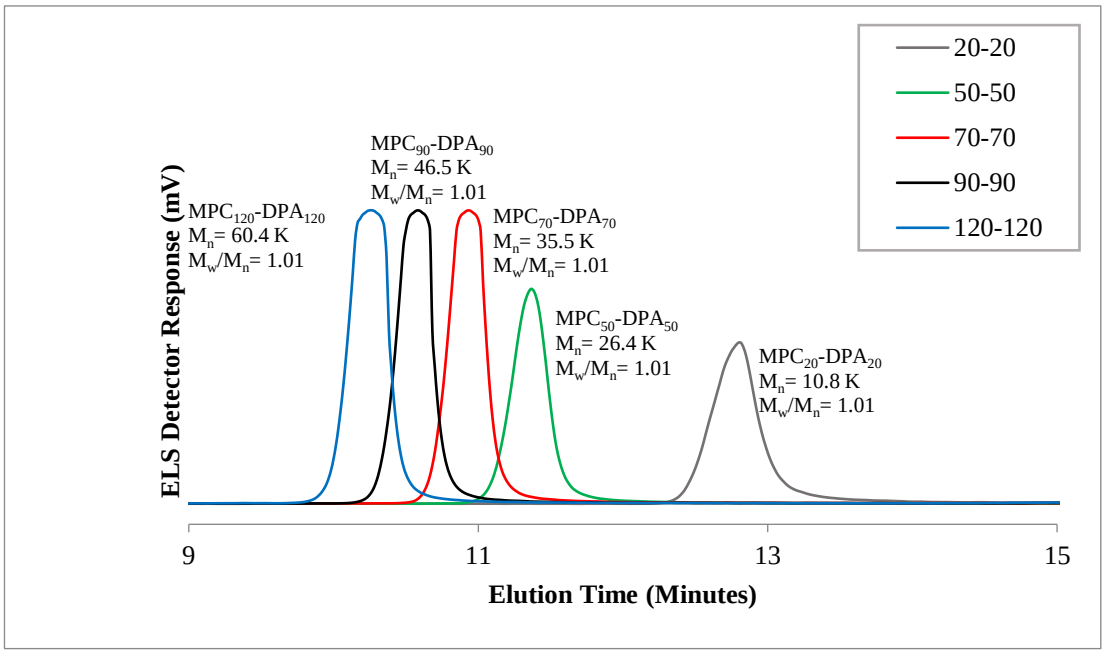


**Figure 3.3.** GPC elution profile for 1:1 MPC-DPA diblock copolymers, illustrate the synthesis of well-defined monodisperse polymers (Original in colour)

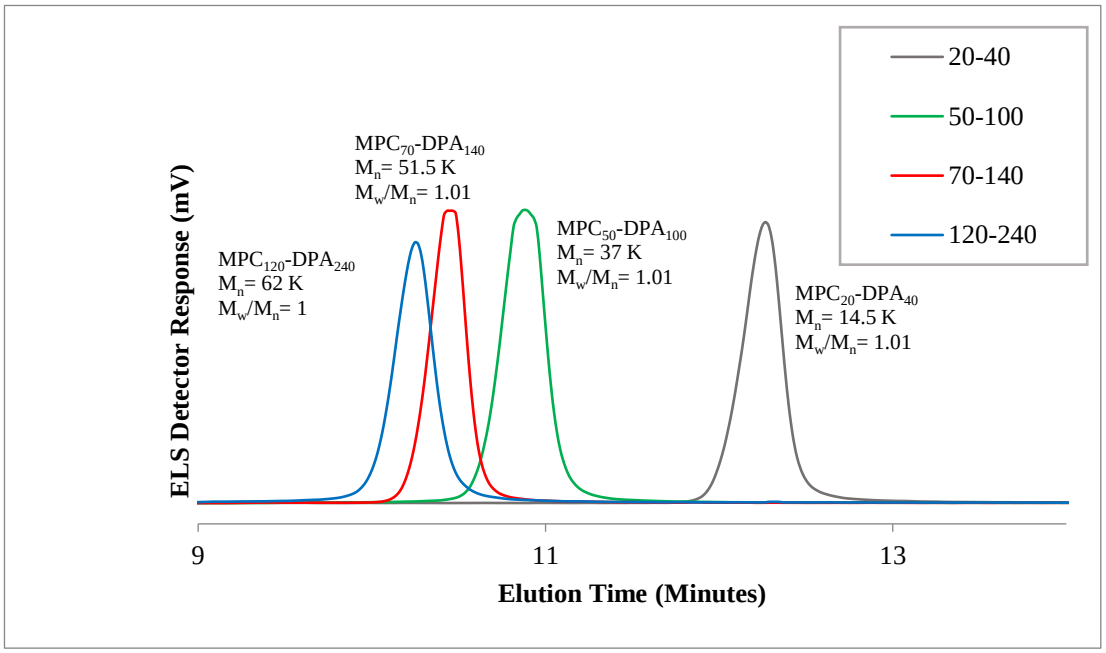


**Figure 3.4.** GPC elution profile for 1:2 MPC-DPA diblock copolymers, illustrate the synthesis of well-defined monodisperse polymers (Original in colour)

**Table 3.2.** Characteristics of MPC-DPA diblock copolymers used to prepare phosphorylcholine- based, pH-responsive self-assembled polymeric nanoparticles

| | Target MPC-DPA | Achieved MPC-DPA [a] | $M_{n,\,theo}$ [b] (g mol$^{-1}$) | $M_{n,NMR}$ [a] (g mol$^{-1}$) | $M_{n,GPC}$ [c] (g mol$^{-1}$) | $M_w/M_n$ [c] | Residual Cu content (ppm)[d] |
|---|---|---|---|---|---|---|---|
| **Set 1 1:1** | 20-20 | 20-20 | 10171 | 10100 | 10800 | 1.01 | 1.17 |
| | 50-50 | 50-40 | 25429 | 23200 | 26400 | 1.01 | 1.96 |
| | 70-70 | 70-60 | 35601 | 33400 | 35500 | 1.01 | 1.23 |
| | 90-90 | 90-76 | 45773 | 42700 | 46500 | 1.01 | 0.74 |
| | 120-120 | 120-92 | 61030 | 55000 | 60400 | 1.01 | 0.71 |
| **Set 2 1:2** | 20-40 | 20-28 | 14438 | 11800 | 14500 | 1.01 | 1.05 |
| | 50-100 | 50-93 | 36095 | 34600 | 37000 | 1.01 | 0.70 |
| | 70-140 | 70-133 | 50533 | 49000 | 51600 | 1.01 | 0.67 |
| | 90-180 | 90-81 | 64971 | 43853 | 47636 | 1.03 | 1.06 |
| | 120-240 | 120-133 | 86683 | 63800 | 62159 | 1.00 | 0.60 |

[a] determined by $^1$H NMR
[b] theoretical $M_n$
[c] determined by GPC using PEG/PEO standards for calibration
[d] Cu levels determined by MP-AES

## 3.3 Discussion

### 3.3.1 MPC-DPA diblock copolymer synthesis

In this study, and advancing from previous work, (Ma et al., 2003; Salvage et al., 2005; Salvage et al., 2016), amphiphilic MPC-DPA diblock copolymers were synthesised via ethanolic ATRP at ambient temperature, to produce a series of increasing molecular weight block copolymers. Generally, alcoholic ATRP allows a relatively fast polymerisation rate with good control over the produced polymer (Save et al., 2002), and anhydrous ethanol was used in this current polymer synthesis because of the possibility of transesterification of methacrylate monomers that may occur with methanol ATRP at ambient temperature (Bories-Azeau and Armes, 2002; Connell et al., 2012). Furthermore, and as shown in Table 3.1, MPC-DPA diblock copolymers were prepared in two set ratios; 1:1 and 1:2, hydrophilic MPC: hydrophobic DPA, based on the suggestion that the equal segment blocks lead to more stable nanoparticles, whilst longer hydrophobic block length increases the loading efficiency of nanoparticles (Giacomelli et al., 2006; Elhasi et al., 2007). The whole process of ATRP polymer synthesis was carried out at ambient temperature and the total reaction time was 48 hours (Table 3.1), during which the first 3 hours of the reaction was allocated to MPC polymerisation, then the remaining time was used for MPC-DPA polymerisation. Although 48 hours is the recommended reaction time for most MPC-DPA diblock copolymer synthesis, some of polymer compositions may require longer than 48 hours to achieve polymerisation completion, especially when longer hydrophobic DPA block chains are used, and thus resulted in the lower than expected conversions obtained. This suggestion is in close agreement with reports of $MPC_{25}$-$DPA_{90}$ synthesis, which required 96 hours at room temperature to reach completion (Yu et al., 2013). However, in the current ATRP synthesis, reaction time

was not extended beyond 48 hours, as the main aim was to determine the suitability of using ethanolic ATRP to produce a series of well-defined MPC-DPA diblock copolymers compared to methanolic ATRP, with all other factors such as temperature and time remain constant.

2-(4-morpholino)ethyl 2-bromosiobutyrate (MEBr) was chosen as the initiator for the MPC-DPA copolymer synthesis, as it has no effect on MPC-DPA properties compared to its counterpart oligo(ethylene glycol) 2-bromoisobutyrate (OEGBr), which could act as a third block in the copolymer (Robinson et al., 2002; Du et al., 2005). MEBr has been successfully used for methanolic ATRP MPC-DPA synthesis previously (Du et al., 2005; Lomas et al., 2010; Salvage et al., 2016), and ethanolic ATRP (Ruiz-Perez et al., 2015; Messager et al., 2016; Gaitzsch et al., 2016). Moreover, the copper bromide-based catalyst was considered more suitable compared to the corresponding chlorides; in terms of final polymer polydispersity due to its larger value of $k_{deact}$ (Tsarevsky and Matyjaszewski, 2007), and also lower toxicity compared to Ni and the platinum group metals (Seiler et al., 1988). The two nitrogen-based ligand namely 2, 2´-bipyridine (bpy) was chosen to complex Cu(I)Br in ATRP, as this catalyst system offers good outcomes in almost all the previously reported ATRP synthesis of MPC-DPA diblock copolymers.

The resultant yields of the ATRP synthesis are shown in Table 3.1, by which a series of MPC-DPA diblock copolymers with various degree of polymerisation were synthesised successfully with a target weight yield of 5 g copolymers per ATRP. However, the achieved weights were lower than the target, which was due to either copolymer adsorption onto silica gel during purification process or incomplete polymerisation (Ma et al., 2003). As almost all of the studies used for the synthesis of MPC-DPA diblock copolymer via ATRP depend on the same protocol employed in

this study, therefore, 10-20% loss in polymer yield is expected (Du et al., 2005; Licciardi et al., 2005).

Although ATRP represents one of the most powerful and versatile method used for polymer synthesis, it has one drawback, which is the use of relatively large amounts of catalyst, which must subsequently be removed for example by passing a solution containing the polymer and the oxidized catalyst through a column of silica gel (Tsarevsky and Matyjaszewski, 2007). In the current study, MP-AES technique was used to determine the residual copper levels in the purified MPC-DPA diblock copolymers, and as shown in Table 3.2, Cu levels were between 0.67-1.96 ppm that are comparable to results obtained from other studies involved the synthesis of MPC-DPA diblock copolymer (Ma et al., 2002; Ma et al., 2003) or other block copolymers such as PEO–NaStS (Iddon et al., 2004), MPC-DMA (Li et al., 2005). Moreover, apart from the white colour of the synthesised polymers that represented an indication for the successful purification process that was carried out utilising silica gel (Thayer, 2005), the Cu level obtained for the MPC-DPA diblock copolymers was considered very low and non-toxic according to the World Health Organization reports that recommends a daily copper dose of 0.6 mg with toxicity occurring at a dose of 10-20 g (Boyer et al., 2016). Therefore, according to these findings accompanied by the typical Cu levels obtained from MP-AES analysis, the resultant purified MPC-DPA diblock copolymers can be applied for biomedical application (Ma et al., 2002; Ma et al., 2003; Tsarevsky and Matyjaszewski, 2007).

### 3.3.2 MPC-DPA diblock copolymer characterisation

The polymer composition and the molecular weight of MPC-DPA polymer systems were determined by $^{1}$H NMR analysis, which indicated ethanolic ATRP synthesis had been successful in producing a series of well-defined MPC-DPA diblock composition

copolymers (Table 3.2). Monomer conversion to polymer in each polymer synthesis was determined using $D_2O$ during the ATRP process (Ma et al., 2003), whereas $CDCl_3$:$CD_3OD$ (3:1 v/v) mixture was used to determine the molecular weight of the final product (Pearson et al., 2013), and Tetramethyl silane (TMS) was the internal reference. As shown in Figure 3.1 and 3.2, the NMR peak assignments were consistent with previous reports of MPC-DPA synthesis (Pearson et al., 2013; Ruiz-Pérez et al., 2015; Salvage et al., 2016). According to the NMR data, MPC polymerisation was 98-99% complete after 3 hours, and the residual was consumed and polymerised after the addition of DPA monomer due to the high reactivity of MPC monomer, therefore, the target degree of polymerisation of MPC was eventually achieved. Furthermore, the DPA degree of polymerisation was confirmed by comparing the integrals of the methylene group protons in MPC block at chemical shift 4.0 ppm to that of methane group protons in DPA block at chemical shift 3.0 ppm, and methylene group protons in DPA block at chemical shift 2.6 ppm (Salvage et al., 2016), as shown in Figure 3.1 and 3.2 for 1:1 and 1:2 ratios respectively. The achieved 1:1 ratio MPC-DPA polymers were close to target as it was carried out with sufficient time for polymerisation completion. In comparison the 1:2 ratio required more time to complete DPA consumption as with this ratio DPA content was more than 2 folds greater, however, the molecular weights were as expected, and close values were obtained with NMR and GPC data.

As shown in Table 3.2, the achieved DP of DPA after 48 hours was 133 in the 1:2 ratio $MPC_{70}$-$DPA_{140}$ and $MPC_{120}$-$DPA_{240}$, which may be considered as the upper limit for DPA in this project. To the best of our knowledge that there has been no report of MPC-DPA diblock copolymers synthesised via ethanolic ATRP where the DP of DPA exceeded 72, taking into consideration that a similar reaction time, ATRP

components, and conditions were used in these studies (Ruiz-Perez et al., 2015; Messager et al., 2016; Gaitzsch et al., 2016).

GPC is another widely used technique for the determination of molecular weight and molecular weight distribution of polymers. GPC measurements, together with NMR, confirmed that successful synthesis of MPC-DPA polymers had been achieved. The molecular weight and polydispersities of the copolymers were determined by organic GPC, and the results are summarised in Table 3.2, in which the $M_n$ values of MPC-DPA diblock copolymers systematically increased according to target degree of polymerisation. Moreover, as seen in Figures 3.3 and 3.4, the GPC peaks for most of the MPC-DPA copolymers were narrow and sharp with a polydispersity ($M_w/M_n$) of less than 1.1 for all polymers (Table 3.2), which indicated synthesis of well-defined polymers was achieved. In this work, PEG/PEO standards were used for GPC calibration (Licciardi et al., 2005), with molecular weights ranging from 4000-100000 g $mol^{-1}$, which encompassed the molecular weight of the studied MPC-DPA diblock copolymers. The GPC mobile phase consisted of chloroform:methanol, 3:1 v/v% (Ruiz-Perez et al., 2015), with 0.1% acetic acid and 0.05% trifluroacetic acid as pH modifiers (Salvage et al., 2016).

As shown in Figure 3.3 and Figure 3.4, copolymers with a small molecular weight took longer time to pass through column and therefore, possess higher retention times compared to large molecular weight polymers. Furthermore, the molecular weights of MPC-DPA diblock copolymers displayed in Table 3.2, indicated that the $M_n$ values obtained from $^1$HNMR and GPC were in a good agreement with the target $M_n$ determined from the theoretical calculation of the feed ratios. However, there was some small variance between GPC and NMR data, which was most likely to be due to a deviation between the hydrodynamic volume of the polymer and monodisperse

standards used for GPC calibration (Izunobi and Higginbotham, 2011). Eventually and as expected, the $M_n$ values increased as degree of polymerisation increased, with narrow molecular weight distributions ($M_w/M_n$ = 1-1.01) being maintained, which was attributed to well-controlled and successful use of ATRP.

### 3.4. Summary

A series of well-defined MPC-DPA diblock copolymers were synthesised via ethanolic atom transfer radical polymerisation (ATRP) across a range of novel MPC-DPA block ratio compositions. $^1$H nuclear magnetic resonance spectroscopy ($^1$H NMR) and gel permeation chromatography (GPC) data confirmed the ATRP synthesis was successful, a uniform series of MPC-DPA diblock copolymers with molecular weights ranging from 10 – 64 g mol$^{-1}$, with low polydispersity, had been achieved, and thus ethanolic ATRP was well suited to MPC-DPA synthesis.

# CHAPTER FOUR

# POLYMER CHARACTERISATION

## 4.1 Introduction

After the successful synthesis of MPC-DPA diblock copolymers, the physicochemical characterisations were conducted to select the most appropriate copolymers to be further studied in terms of their application as drug delivery systems. Several methods are available for the preparation of nanoparticles from block copolymers, in this instance, nanoprecipitation using methanol as a solvent was chosen in order to produce stable nanosize self-assembled nanoparticles with low polydispersity. The nanoparticles were characterised in terms of size, dilution stability, pH-micelle formation profile, time, and temperature stability, CMC, and morphology to determine the potential for their application in pharmaceutical field.

## 4.2 Results

### 4.2.1 MPC-DPA nanoparticle characterisation

MPC-DPA polymeric nano-systems were prepared via nanoprecipitation as described in Section (2.2.2.3), where samples displayed different solubility patterns in methanol between the two MPC-DPA diblock sets, as shown in Figure 4.1.

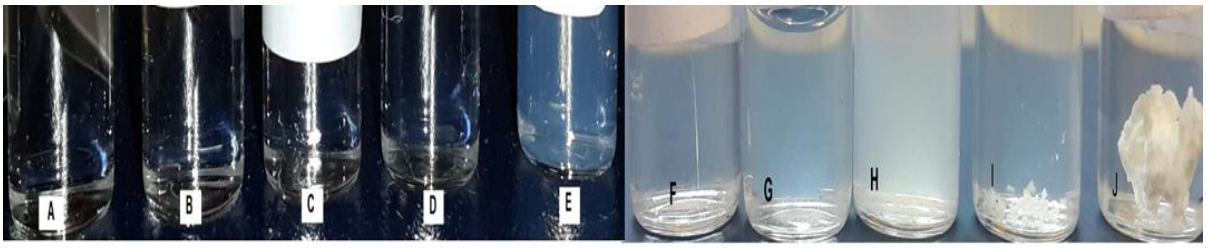


**Figure 4.1.** Images of MPC-DPA diblock copolymer samples solubility in methanol (40 mg $ml^{-1}$) as used for micelle preparation, 1:1 ratio (A-E) * and 1:2 ratio (F-J) **
* A= $MPC_{20}$-$DPA_{20}$, B= $MPC_{50}$-$DPA_{50}$, C= $MPC_{70}$-$DPA_{70}$, D= $MPC_{90}$-$DPA_{90}$, E= $MPC_{120}$-$DPA_{120}$
** F= $MPC_{20}$-$DPA_{40}$, G= $MPC_{50}$-$DPA_{100}$, H= $MPC_{70}$-$DPA_{140}$, I= $MPC_{120}$-$DPA_{240}$, J= $MPC_{90}$-$DPA_{180}$

As seen in Figure 4.1, the 1:1 ratio diblock copolymers (A-D) were completely soluble in methanol compared to the 1:2 ratio block copolymers (E-J) that showed different patterns of solubility. Usually, the cloudy appearance of MPC-DPA diblock copolymer solutions indicates the presence of clusters in the sample due to poor solubility in methanol. Moreover, the cloudy appearance was more obvious in samples H, I and J in Figure 4.1, with undissolved particles of MPC-DPA diblock copolymers still visually seen (I and J), therefore sample J, $MPC_{90}$-$DPA_{180}$ was excluded from this study.

Table 4.1 displays the particle size and polydispersity of MPC-DPA nanoparticles recorded from DLS analysis that was carried out at 25°C (Section 2.2.2.4). However, for the majority of samples produced, the particle size increased with increasing molecular weight of the diblock copolymer, with polydispersity (PDI) remaining below 0.1; except for samples; ($MPC_{120}$-$DPA_{120}$, $MPC_{50}$-$DPA_{100}$, $MPC_{70}$-$DPA_{140}$, and $MPC_{120}$-$DPA_{240}$). These results were as expected, and they were comparable to the size and PDI reported for other MPC-DPA nanoparticles (Du et al., 2005; Licciardi et al., 2006; Salvage et al., 2015), where the formation of nanoparticles with particle size below 200 nm and low polydispersity indicated the successful production of monodisperse nanoparticles via nanoprecipitation. Moreover, the larger size nanoparticles obtained from the 1:2 ratio MPC-DPA diblock copolymers, with boarder polydisperse size distributions compared to the 1:1 ratio, may have indicated the presence of larger size nanoparticles, in the form of mixed, multiple particle populations.

In summary, the results have shown that sufficiently small nanoparticles of sizes (< 200 nm) can be synthesized with fine size distribution that can reduce the RES uptake and prolong circulation time in the blood and extravasate from leaky capillaries,

thereby render these nanoparticles suitable for tumour-specific accumulation via EPR effect.

**Table 4.1.** Hydrodynamic diameter (ZAve) particle size and polydispersity of MPC-DPA nanoparticles prepared via nanoprecipitation from methanol in PBS (pH 7.4) at 25°C using DLS, (Mean ± SD, n=3)

| Target MPC-DPA | Nanoparticle diameter (nm) | Polydispersity (PDI) |
|---|---|---|
| 20-20 | 25 ± 0.7 | 0.08 ± 0.03 |
| 50-50 | 38 ± 0.8 | 0.08 ± 0.01 |
| 70-70 | 37 ± 0.9 | 0.07 ± 0.01 |
| 90-90 | 44 ± 0.7 | 0.07 ± 0.02 |
| 120-120 | 77 ± 2.1 | 0.20 ± 0 |
| 20-40 | 28 ± 0.1 | 0.04 ± 0.02 |
| 50-100 | 140 ± 36.1 | 0.32 ± 0.04 |
| 70-140 | 87 ± 14.6 | 0.37 ± 0.08 |
| 120-240 | 119 ± 10.8 | 0.27 ± 0.08 |

### 4.2.2 Effect of polymer concentration on MPC-DPA nanoparticle stability

Increasing the stability of nanoparticles upon dilution is a major challenge that must to be resolved for products intended to function as systematically administered drug delivery systems. Therefore, the effect of copolymer concentration on the self-assembled polymeric nanoparticle diameter, and particle stability upon dilution was investigated by DLS in PBS (pH 7.4) (Section 2.2.2.4.1), and the results for 1:1 and 1:2 ratios are shown in Appendix 2.0. The data demonstrated the good stability of the nanoparticles diameter upon serial halving dilutions in PBS (pH 7.4) at 25°C, down to a concentration of 100 µg $ml^{-1}$. An increase in particle size is often seen at low concentrations, when using DLS, as the ZAve variance will wider due to the very low number of particles in solutions. This was consistent with the results observed with 50 nm monodisperse polystyrene standard, which always displayed increased size at

low concentrations. Despite the apparent broadening of particle size at low concentrations, particle sizes remained detectable and measurable down to the lower limits of DLS sensitivity.

Moreover, the effect of decreasing polymer concentration on the polydispersity (PDI) for both sets of MPC-DPA nanoparticles, further supported the resistance of the nanoparticles to dilution, where PDI values were mostly below 0.1, except for the nano-systems that were above 0.1 (1:2 ratio) before dilution as seen in Appendix 3.0. As seen with size values, an increase in polydispersity at low polymer concentration was observed. This was in close agreement with PDI changes observed with 50 nm monodisperse polystyrene standard beads.

The dilution associated with decrease in nanoparticle number seen as the count rate (KCps), decrease by half with each halved concentration, but without a sudden drop in concentration that would be associated with nanoparticle dissociation (Appendix 4.0). The low number of particles present at lower concentrations resulted in some drift in particle diameter, seen as larger average particle diameters, as the particles concentration was below these required for optimum DLS measurements. However, nanoparticles diameters were still detectable and measured down to 0.0019 mg $ml^{-1}$ in both polymer sets.

For DLS method validation, 50 nm monodisperse polystyrene standard beads in 10 mM NaCl were used, and a similar trend of resistance to dilution observed with MPC-DPA polymeric nano-systems towards change in concentration was reported with standard beads, with larger size particles, increase in polydispersity, and a gradual decrease; by half, in particles count rate resulted at low concentrations.

In conclusion, the measured nanoparticle size and polydispersity data were resistant to changes in concentration down to 100 μg $ml^{-1}$, which indicated that the MPC-DPA nanoparticles displayed good particle stability upon dilution.

### 4.2.3 Effect of pH change on MPC-DPA nanoparticles

The pH response profile of MPC-DPA nanoparticles was examined using DLS analysis, at pH range (3-10) (Section 2.2.2.4.2). Figure 4.2 and Figure 4.3, showed that micellisation started at circa pH 6 and was completed by pH 7, with an associated increase in particle diameter observed at the same values. Furthermore, sample polydispersity was initially seen at pH 3, which was followed by a reduction in PDI as pH increased as seen in Figure 4.4 and Figure 4.5. The data indicate that a similar pH response behaviour was observed for both polymer sets 1:1 and 1:2 ratios, where at low pH (3), the copolymer exists in unimer form, and then with an increase in pH, an increase in size was observed, which was also associated with an increase in the polydispersity of the system. This was due to the formation of polydisperse nano-systems. With a further increase in pH; i.e. pH 7, a stable particle size was produced, which indicated the completion of the uimer to micelle transition, and was associated with a decrease in the polydispersity and the formation of monodisperse systems particularly in 1:1 ratio polymers.

A constant MPC-DPA diblock ratio (1:1), with increased molecular weight, leads to the production of monodisperse systems at physiological pH, whilst the 1:2 ratio with the longer hydrophobic DPA block, and increased molecular weight, leads to variable results related to PDI at physiological pH, in which $MPC_{20}$-$DPA_{40}$ form monodisperse systems, whilst $MPC_{50}$-$DPA_{100}$, $MPC_{70}$-$DPA_{140}$, and $MPC_{120}$-$DPA_{240}$ form polydisperse or mixed unimer-micelle systems.

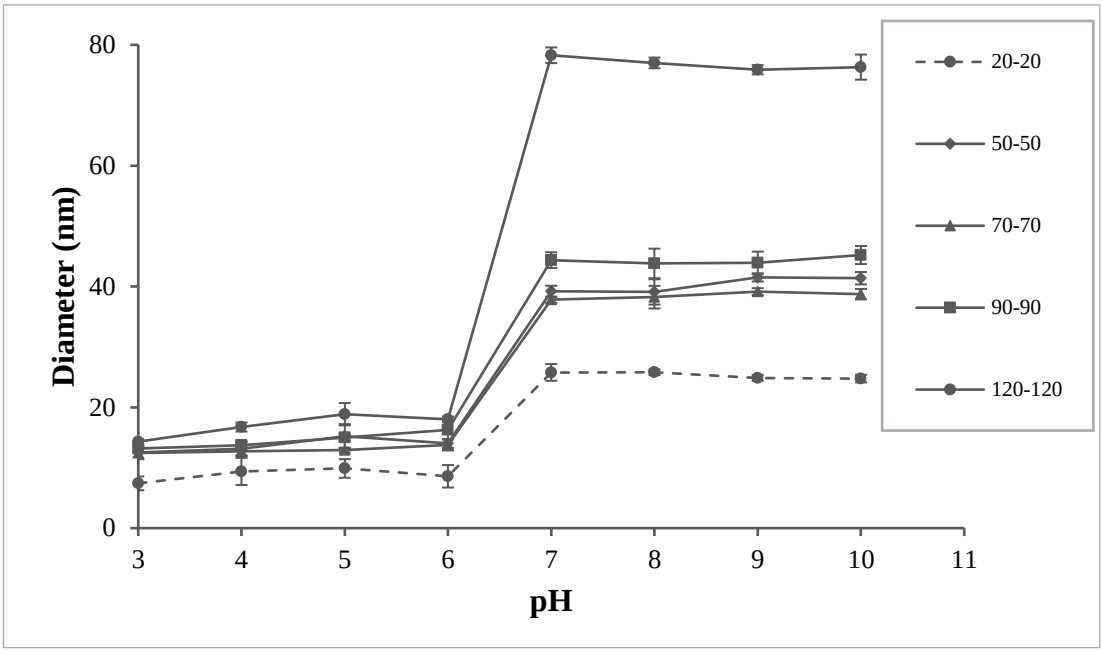


**Figure 4.2.** Effect of increasing solution pH (3-10) on particle diameter at 25°C for 1:1 ratio MPC-DPA nanoparticles (Mean ± SD, n=3)

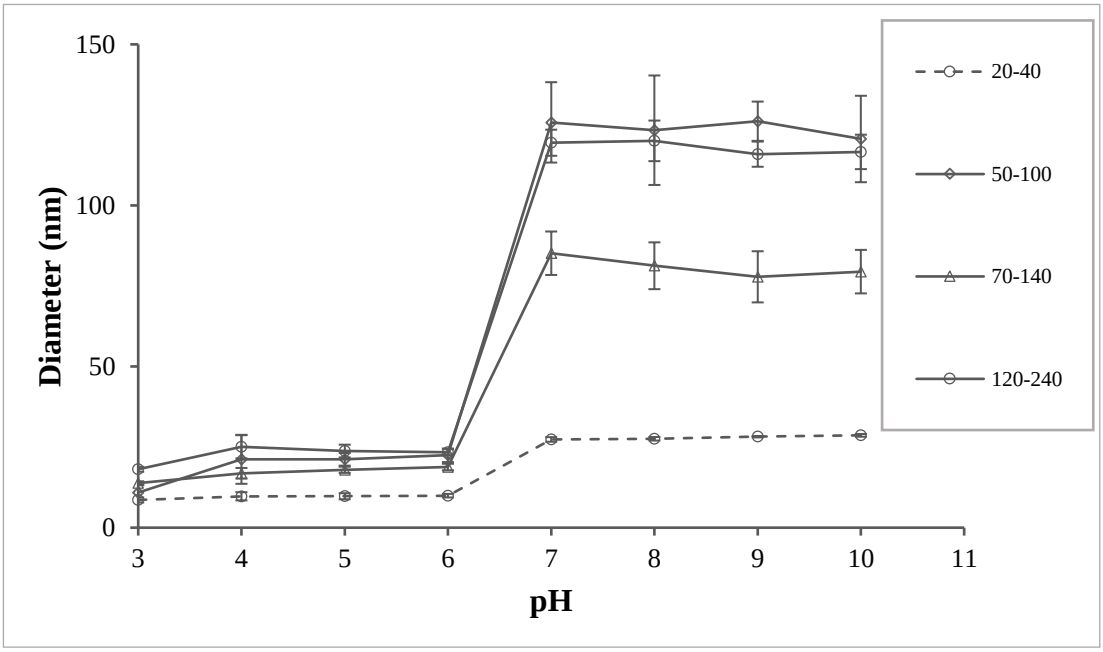


**Figure 4.3.** Effect of increasing solution pH (3-10) on particle diameter at 25°C for 1:2 ratio MPC-DPA nanoparticles (Mean ± SD, n=3)

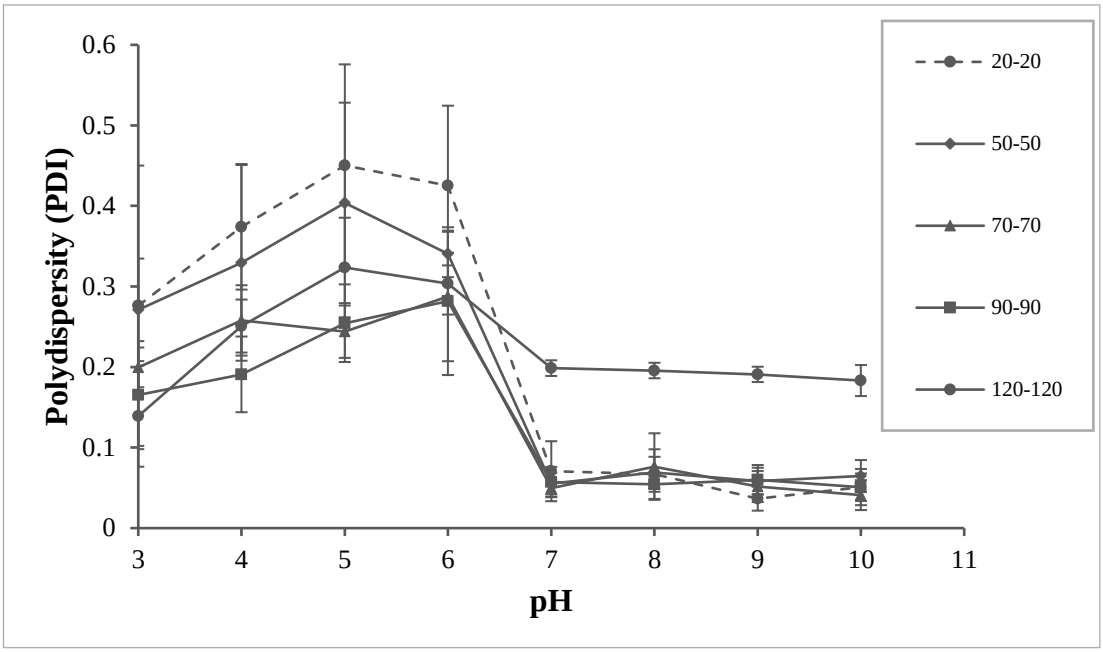


**Figure 4.4.** Effect of increasing solution pH (3-10) on particle polydispersity at 25°C for 1:1 ratio MPC-DPA nanoparticles (Mean ± SD, n=3)

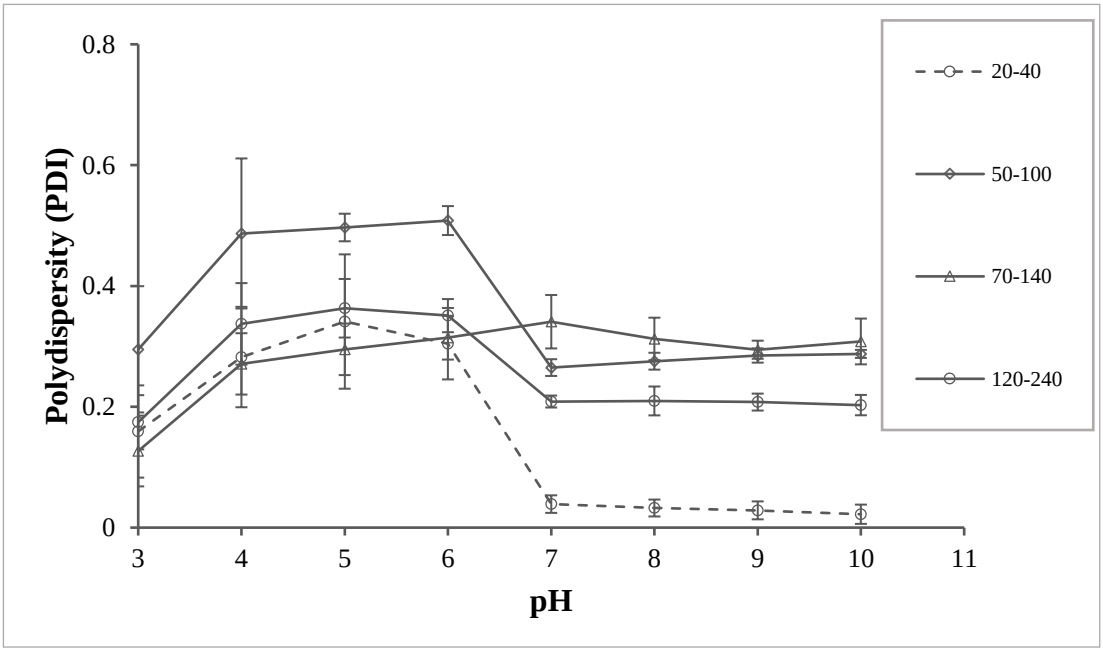


**Figure 4.5.** Effect of increasing solution pH (3-10) on particle polydispersity at 25°C for 1:2 ratio MPC-DPA nanoparticles (Mean ± SD, n=3)

The narrower pH range (6-7) was examined to determine the pH of micellisation, and the results are displayed in Table 4.2 and Table 4.3. The data indicate that self-assembly occurred primarily from pH 6.6-6.7 for 1:1 and 1:2. At lower pH values, the copolymer exists as unimers, with an increase in pH unimer/intermediate/micelle particles form, then as pH reaches 6.6-7, complete micellisation is achieved.

**Table 4.2.** Particle diameter (nm) at 25ºC for 1:1 MPC-DPA nanoparticles in buffer of differing pH values (6-7) (Mean ± SD, n=3)

| pH | MPC-DPA block ratio | | | | |
|---|---|---|---|---|---|
| | **20-20** | **50-50** | **70-70** | **90-90** | **120-120** |
| 6 | 9 ± 1.3 | 14 ± 3 | 12 ± 1.2 | 16 ± 2 | 18 ± 2 |
| 6.1 | 10 ± 3.3 | 15 ± 3 | 13 ± 1.1 | 19 ± 2 | 18 ± 0.6 |
| 6.2 | 7 ± 2 | 14 ± 1.4 | 14 ± 1 | 17 ± 2 | 20 ± 1 |
| 6.3 | 10 ± 1.3 | 13 ± 1.2 | 14 ± 3 | 18 ± 3.1 | 20 ± 2.5 |
| 6.4 | 11 ± 5 | 15 ± 1 | 13 ± 1.4 | 20 ± 4 | 89 ± 4 |
| 6.5 | 12 ± 2 | 21 ± 2.2 | 19 ± 1 | 28 ± 4 | 97 ± 1.1 |
| 6.6 | 22 ± 7 | 34 ± 7 | 27 ± 7 | 42 ± 3.7 | 94 ± 1.3 |
| 6.7 | 31 ± 2 | 40 ± 2 | 37 ± 0.2 | 45 ± 1 | 83 ± 2 |
| 6.8 | 31± 1 | 39 ± 1.1 | 37 ± 1 | 46 ± 1 | 81 ± 1 |
| 6.9 | 29 ± 1 | 38 ± 3 | 36 ± 0.4 | 44 ± 1 | 79 ± 2 |
| 7 | 24 ± 0.3 | 39 ± 3 | 37 ± 1.4 | 43 ± 0.2 | 77 ± 1 |
| | Mean ± SD | | | | |

**Table 4.3.** Particle diameter (nm) at 25ºC for 1:2 MPC-DPA nanoparticles in buffer of differing pH values (6-7) (Mean ± SD, n=3)

| pH | MPC-DPA block ratio | | | |
|---|---|---|---|---|
| | **20-40** | **50-100** | **70-140** | **120-240** |
| 6 | 10 ± 0.7 | 21 ± 2.4 | 19 ± 1.2 | 23 ± 1.7 |
| 6.1 | 10 ± 0.9 | 24 ± 5.2 | 21 ± 0.7 | 23 ± 1.8 |
| 6.2 | 10 ± 0.5 | 23 ± 0.7 | 25 ± 0.4 | 24 ± 14 |
| 6.3 | 10 ± 1.8 | 94 ± 1 | 22 ± 1 | 25 ± 3.1 |
| 6.4 | 11 ± 1.4 | 155 ± 5.6 | 133 ± 6.3 | 88 ± 1 |
| 6.5 | 29 ± 1.1 | 158 ± 5 | 135 ± 6.1 | 137 ± 3.1 |
| 6.6 | 32 ± 2 | 148 ± 3.3 | 132 ± 5 | 130 ± 3.7 |
| 6.7 | 30 ± 3 | 142 ± 4.9 | 99 ± 10 | 124 ± 2.4 |
| 6.8 | 29 ± 1.4 | 139 ± 2.8 | 94 ± 9 | 121 ± 3.6 |
| 6.9 | 28 ± 0.2 | 133 ± 4 | 95 ± 7 | 121 ± 8 |
| 7 | 28 ± 0.1 | 142 ± 2.3 | 89 ± 9.2 | 120 ± 6.3 |
| | Mean ± SD | | | |

In conclusion, the data indicated that the MPC-DPA nanoparticles possess pH responsive properties that are required for the development of *in-vivo* applications.

### 4.2.4 Temperature and time stability of MPC-DPA nanoparticles

The thermal stability and its effect on characteristics of the two ratio sets of MPC-DPA nanoparticles was examined using DLS analysis in PBS (pH 7.4), across a temperature range of 5-70°C (Section 2.2.2.4.3). The results are shown in Figure 4.6 and Figure 4.7 for effect on particle diameter, whilst the effect on polydispersity and KCps can be found in Appendix 5.0 and 6.0, respectively. All the measurements were the mean of three runs (n=3) averaged from 3 analyses per measurement, with error bars representing the standard deviation values.

As seen in Figure 4.6, all the nanoprecipitation prepared 1:1 MPC-DPA nanoparticles were thermally stable and their diameter remained unchanged across the 5-70°C temperature range, with no evidence of particle aggregation or dissociation. Due to the long block chain of $MPC_{120}$-$DPA_{120}$, a big size difference was seen when compared to other copolymers that are closer in size. The majority of 1:1 polymeric nano-systems remained monodisperse with low data variability, apart from 25 nm and 77 nm MPC-DPA nanoparticles that showed polydispersity. The count rate also remained stable across the 5-70°C temperature range for 1:1 MPC-DPA polymeric nano-systems.

Similarly, the 1:2 ratio MPC-DPA nanoparticles displayed thermal stability across the same temperature range (5-70°C), with a large difference in diameter evident between the $MPC_{20}$-$DPA_{40}$, copolymer with a shorter DPA block, relative to the other 1:2 copolymers that have diameters that are more closely spaced as shown in Figure 4.7.

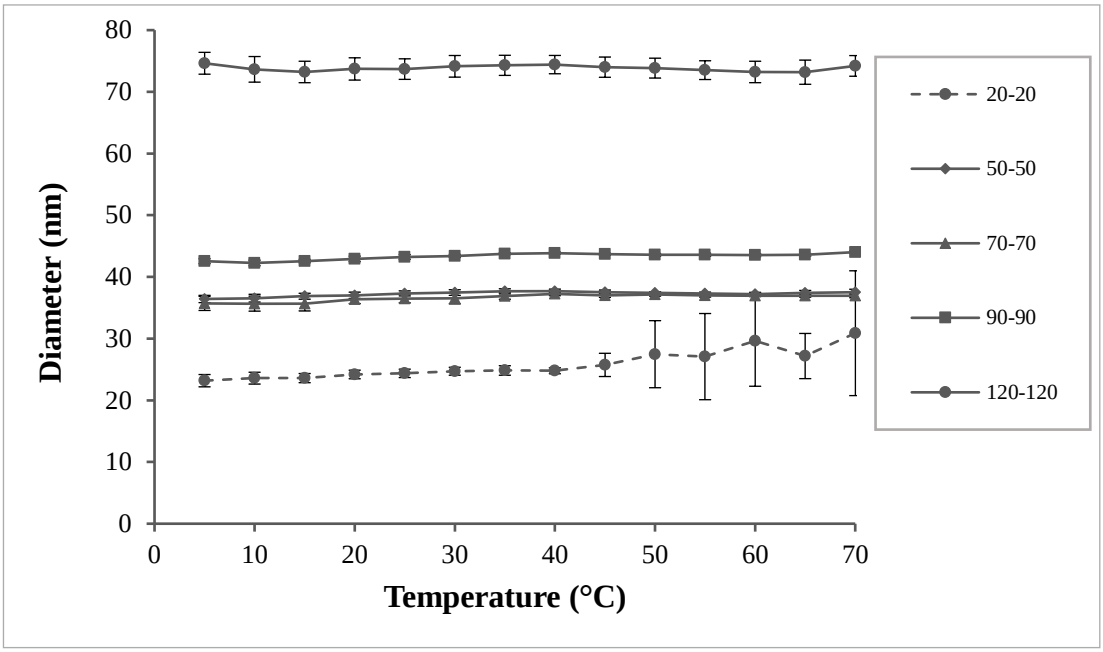


**Figure 4.6.** Effect of varying temperature (5-70°C) on particle diameter of 1:1 MPC-DPA nanoparticles formed via nanoprecipitation from methanol in PBS, pH 7.4 measured with DLS (Mean ± SD, n=3)

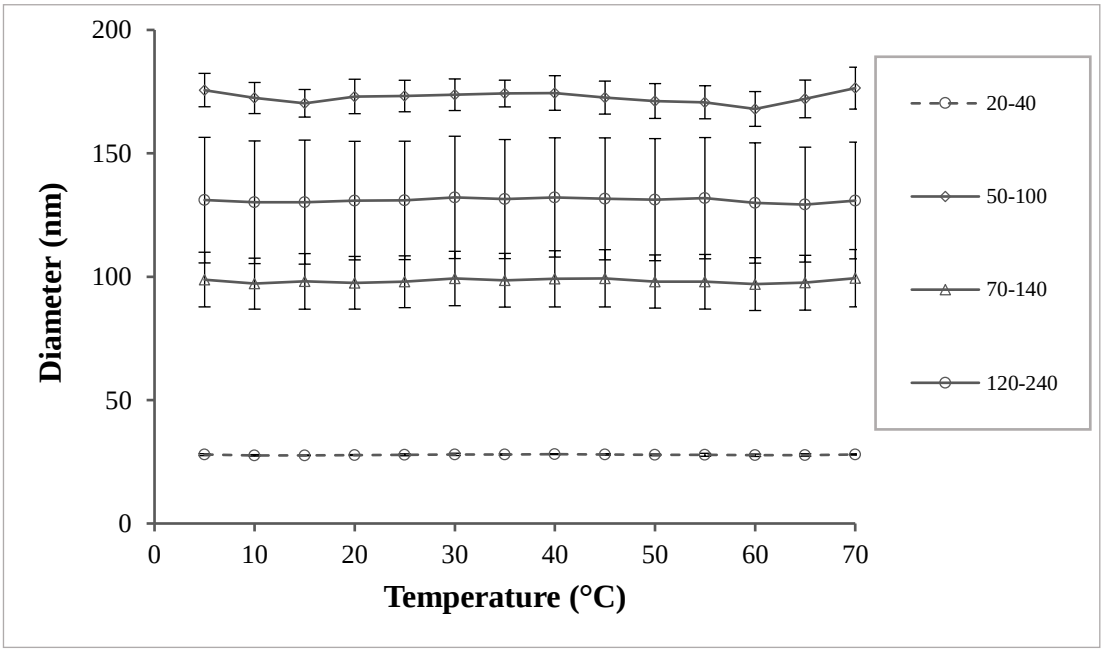


**Figure 4.7.** Effect of varying temperature (5-70°C) on particle diameter of 1:2 MPC-DPA nanoparticles formed via nanoprecipitation from methanol in PBS, pH 7.4 measured with DLS (Mean ± SD, n=3)

Moreover, stable polydispersities were observed with the 1:2 ratio MPC-DPA nanoparticles across the 5-70°C temperature range, which all remained polydisperse, with the exception of the monodisperse $MPC_{20}$-$DPA_{40}$. The count rate of 1:1 MPC-DPA nanoparticles remained stable across the 5-70°C temperature range, whilst the 1:2 MPC-DPA nanoparticles produced a higher count rate than that recorded for 1:1 MPC-DPA nanoparticles.

Additional narrow range temperature studies (30-40°C) were conducted to assess the effect of physiological temperature upon MPC-DPA nanoparticle characteristics. The data from both temperature ranges (Appendix 7.0), indicated that MPC-DPA polymeric nano-systems were thermally stable at the tested temperatures with no pronounced changes observed. All the measurements are the mean of three runs (n=3) averaged from 3 analyses per measurement. The DLS method was validated using 50 nm monodisperse polystyrene standard particles (Section 2.2.2.4.3), and the effect of temperature, for both ranges (5-70°C) and (30-40°C) on particle diameter, PDI and KCps indicated that DLS measurement was accurate and constant.

A time stability study was carried out (Section 2.2.2.4.3) and the effect of time on nanoparticle diameter, over 18 months at room temperature for 1:1 and 1:2 ratios MPC-DPA nanoparticles are displayed in Figure 4.8 and Figure 4.9. All the measurements were the mean of three runs (n=3) averaged from 3 analyses per measurement, with error bars represented the standard deviation values.

As seen in Figure 4.8, the diameter of all the nanoprecipitation prepared 1:1 MPC-DPA nanoparticles were stable at room temperature and diameter remained unchanged for the 18 months study period, with no evidence of particle aggregation or dissociation. Additionally, all 1:1 MPC-DPA nanoparticles remained monodisperse with low data variability, and the particle count rate remained unchanged over time

(Appendix 8.0 and 9.0). Similarly, the 1:2 ratio MPC-DPA nanoparticles were stable at room temperature over time in terms of particle diameter (Figure 4.9) and PDI (Appendix 8.0), with differences in diameter evident between the $MPC_{20}$-$DPA_{40}$ copolymer and the other copolymers as discussed earlier.

The count rate of 1:1 MPC-DPA nanoparticles remained stable over time, with the exception of $MPC_{120}$-$DPA_{120}$, where some variability was observed. It was again noted that the 1:2 MPC-DPA nanoparticles possessed a higher count rate than that recorded for 1:1 MPC-DPA nanoparticles, with some data variability observed with all of 1:2 MPC-DPA nanoparticles, except $MPC_{20}$-$DPA_{40}$.

The same study was conducted on MPC-DPA nanoparticle samples that had been stored at 4°C (Section 2.2.2.4.3) and the results for particle diameter are shown in Figure 4.10 and Figure 4.11. It was noted that similar size, PDI, and KCps trends were observed with MPC-DPA nanoparticle samples stored at 4°C relative to these stored at room temperature (Appendix 10.0 and 11.0).

In conclusion, the data indicated that the MPC-DPA nanoparticles displayed good thermal stability together with stability over time, which enable these nano-systems to be adaptable to a range of storage and transport conditions.

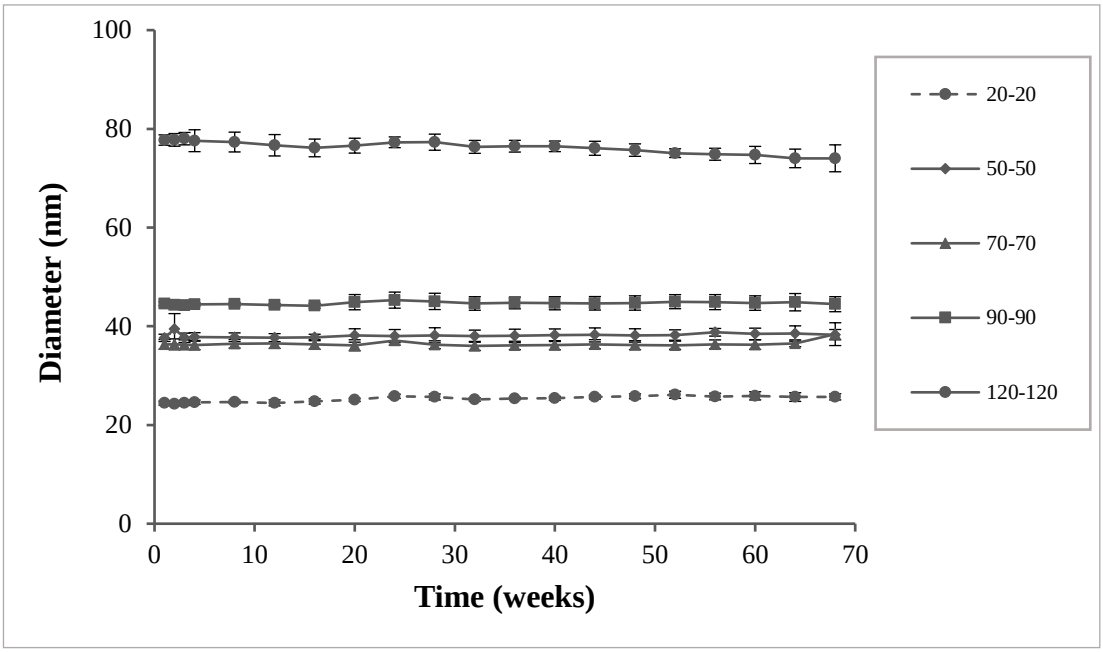


**Figure 4.8.** Time effect on particle diameter of 1:1 MPC-DPA self-assembled nanoparticles formed via nanoprecipitation from methanol in PBS, pH 7.4, stored at room temperature (Mean ± SD, n=3)

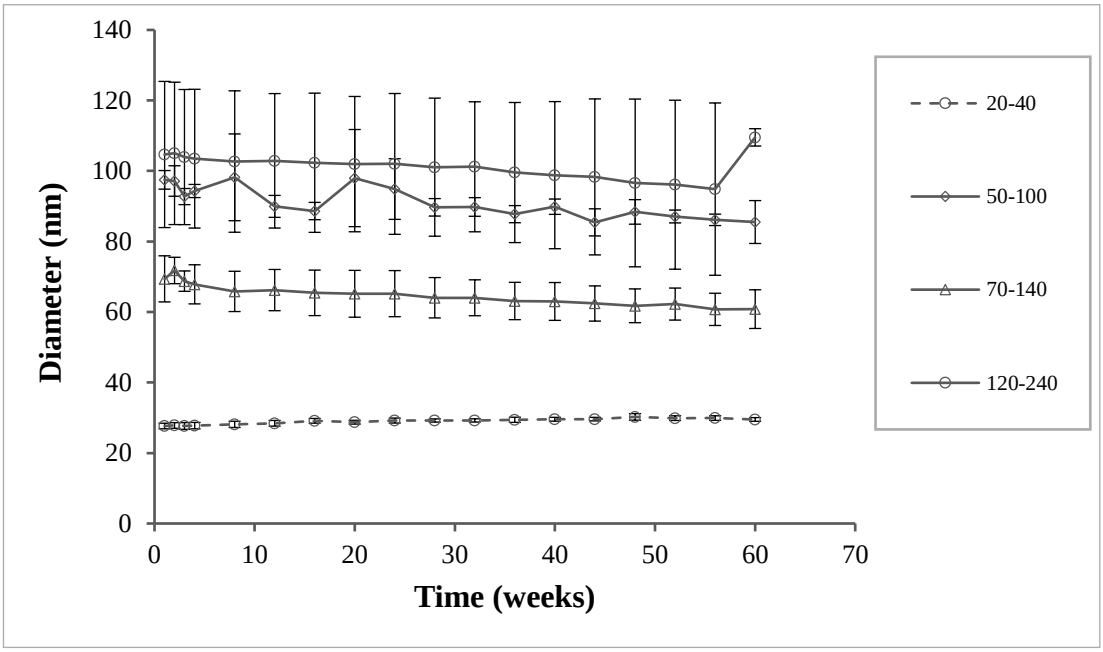


**Figure 4.9.** Time effect on particle diameter of 1:2 MPC-DPA self-assembled nanoparticles formed via nanoprecipitation from methanol in PBS, pH 7.4, stored at room temperature (Mean ± SD, n=3)

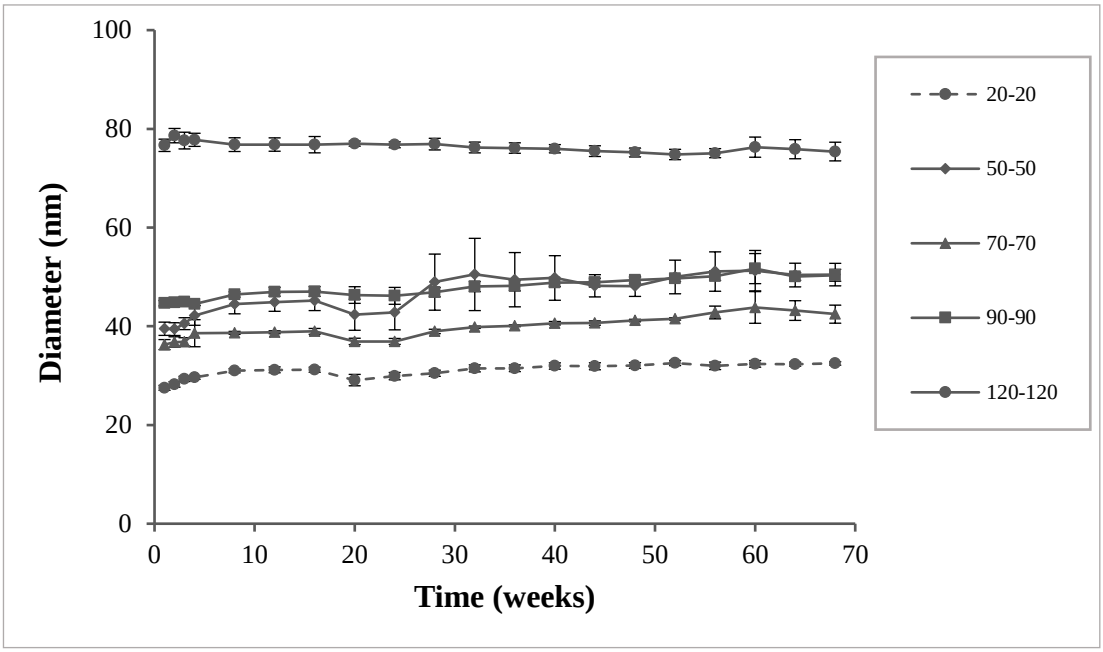


**Figure 4.10.** Time effect on particle diameter of 1:1 MPC-DPA self-assembled nanoparticles formed via nanoprecipitation from methanol in PBS, pH 7.4, stored at 4°C (Mean ± SD, n=3)

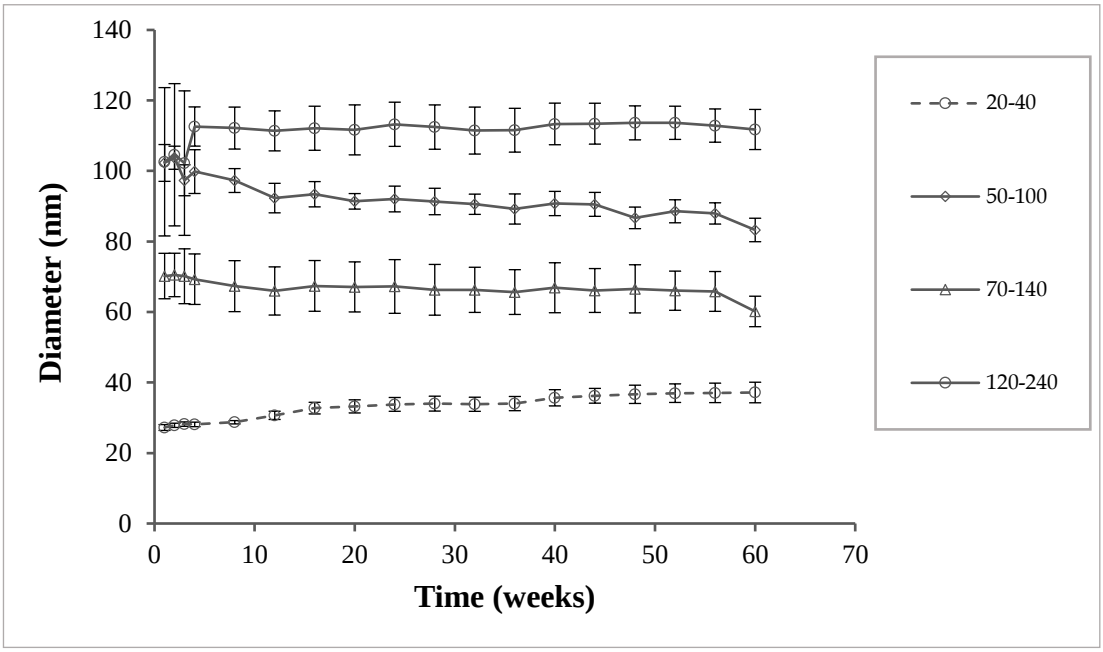


**Figure 4.11.** Time effect on particle diameter of 1:2 MPC-DPA self-assembled nanoparticles formed via nanoprecipitation from methanol in PBS, pH 7.4, stored at 4°C (Mean ± SD, n=3)

### 4.2.5 Critical micelle concentration (CMC) determination by fluorescence spectroscopy

The critical micelle concentration (CMC) values of MPC-DPA nanoparticles were determined via fluorescence spectroscopy using a pyrene as probe (Section 2.2.2.5). A representative example of the pyrene excitation spectra for decreasing PBS (pH 7.4) concentrations of MPC-DPA diblock copolymer at 25°C is displayed in Figure 4.12. The data was obtained by plotting the fluorescence intensity of peaks $I_I/I_{III}$ ($I_{373}/I_{384}$) from emission spectra versus copolymer concentration in PBS (pH 7.4), as shown in Figure 4.13. The graphical method used for the determination of CMC is displayed in Figure 4.13, from which CMC was considered as a concentration range rather than a single value, therefore, $CMC_1$ represent the start of micelle formation, with $CMC_2$ as the midpoint where uimer and micelles exist together, until endpoint $CMC_3$ is reached where micellisation is complete. Table 4.4 shows the relationship between increasing the hydrophobic block chain length and low CMC values, with the three CMC values listed. The CMC data in Table 4.4 demonstrated that CMC values of MPC-DPA diblock copolymers decrease with increasing hydrophobic DPA block length, which indicated a strong tendency for micelle formation in aqueous solution.

For method validation, sodium dodecyl sulfate (SDS) was utilised (Section 2.2.2.5), and CMC measurements carried out in the same manner as for MPC-DPA copolymers.

In conclusion, the CMC values calculated from the pyrene fluorescence method for the novel MPC-DPA diblock copolymers were low, which improves self-assembled stability and release control.

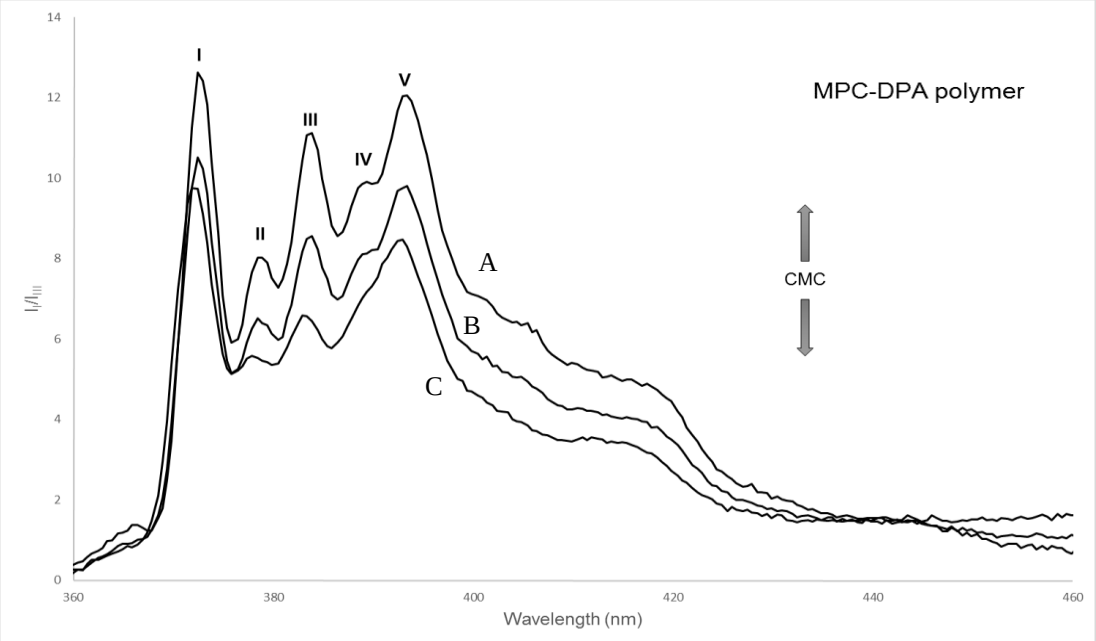


**Figure 4.12.** Fluorescence emission spectrum for pyrene probe in in PBS (7.4) of MPC-DPA diblock copolymer, (A) above CMC, (B) at CMC and (C) below CMC at 25ºC

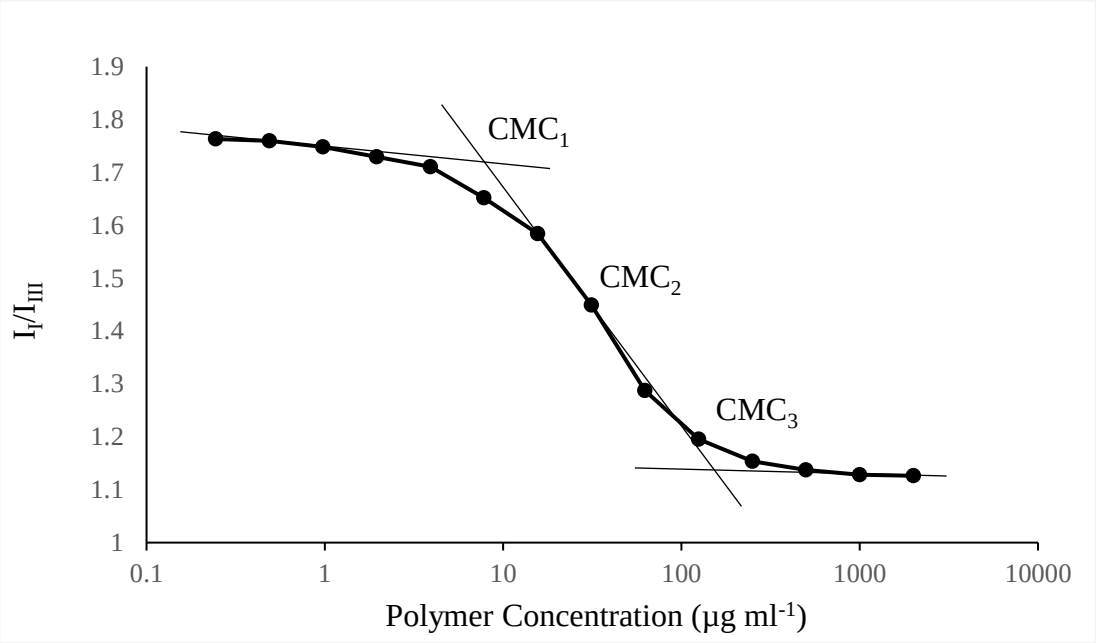


**Figure 4.13.** Example plot of pyrene vibrational band intensities ($I_I/I_{III}$) as a function of MPC-DPA diblock copolymer concentration in PBS (7.4) at 25ºC

**Table 4.4** CMC values of MPC-DPA diblock copolymers measured by florescence spectroscopy at 25ºC, (Mean ± SD)

| MPC-DPA ratio | $CMC_1$ (mg $ml^{-1}$) [a] | $CMC_2$ (mg $ml^{-1}$) [b] | $CMC_3$ (mg $ml^{-1}$) [c] |
|---|---|---|---|
| 20-20 | 0.004 ± 0.000 | 0.062 ± 0.000 | 0.450 ± 0.005 |
| 50-50 | 0.004 ± 0.000 | 0.062 ± 0.000 | 0.300 ± 0.010 |
| 70-70 | 0.004 ± 0.000 | 0.062 ± 0.000 | 0.300 ± 0.005 |
| 90-90 | 0.004 ± 0.000 | 0.062 ± 0.000 | 0.250 ± 0.005 |
| 120-120 | 0.004 ± 0.000 | 0.062 ± 0.000 | 0.100 ± 0.005 |
| 20-40 | 0.004 ± 0.000 | 0.062 ± 0.000 | 0.400 ± 0.010 |
| 50-100 | 0.004 ± 0.000 | 0.062 ± 0.000 | 0.250 ± 0.005 |
| 70-140 | 0.004 ± 0.000 | 0.062 ± 0.000 | 0.200 ± 0.010 |
| 120-240 | 0.004 ± 0.000 | 0.062 ± 0.000 | 0.350 ± 0.010 |

[a] obtained from intersection of straight line segment drawn through points in low concentration and the tangent to the sigmoid passing through its centre
[b] obtained from the centre of sigmoid [c] obtained from highest polymer concentration line

### 4.2.6 Scanning Transmission Electron Microscopy (STEM)

Amphiphilic block copolymers may assemble into different morphologies, related to block length and block copolymer composition. Therefore, all the MPC-DPA self-assembled nanoparticles were examined using the STEM technique (Section 2.2.2.6). Figure 4.14 and Figure 4.15 were examples for the 1:1 and 1:2 ratios MPC-DPA copolymer nanoparticles morphologies respectively. Method validation was performed using 50 nm polystyrene beads (Section 2.2.2.6) (Appendix 12.1).

Micelles were the predominant colloidal aggregation morphology that was seen in the 1:1 ratio example STEM images in Figure 4.14 for $MPC_{50}$-$DPA_{50}$ self-assembled nanoparticle, which was again in agreement with the DLS data (Table 4.1). It was noted that micelle size DLS data was 38 nm ± 0.8 and characterised by low polydispersity (0.08 ± 0.01), which was consistent with that observed through these images.

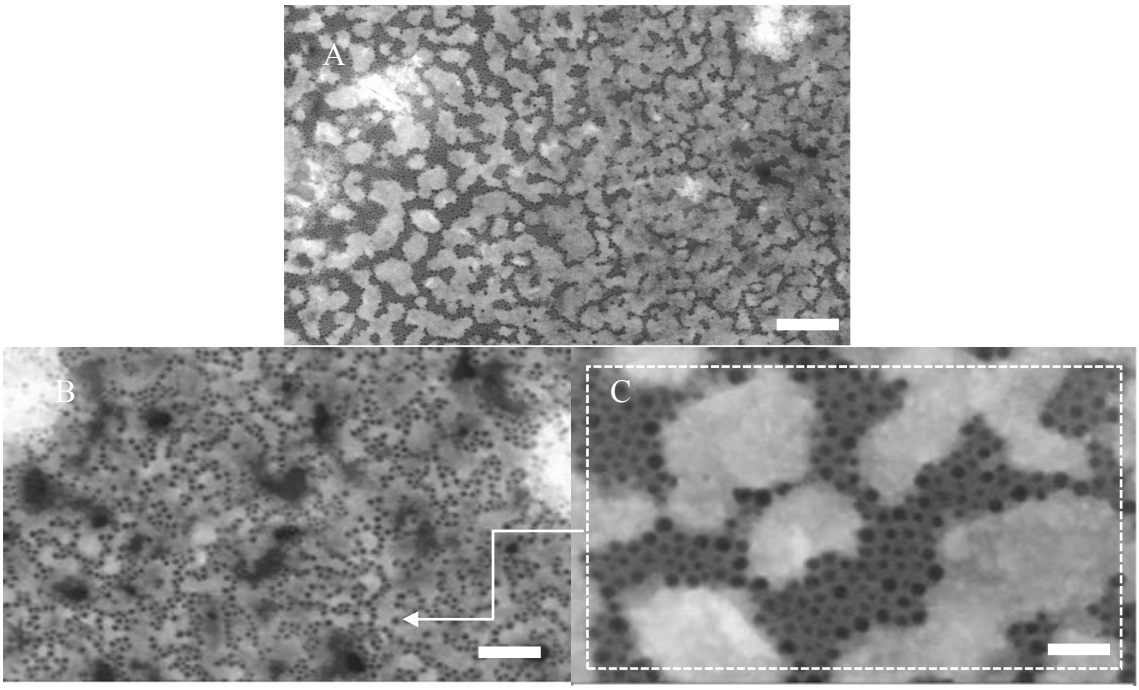


**Figure 4.14** STEM images of $MPC_{50}$-$DPA_{50}$ nanoparticles displaying wide and zoomed areas of copolymer nanoparticles. Scale bars = 100 nm, 200 nm and 20 nm for wide and zoomed areas, respectively

The STEM images for $MPC_{20}$-$DPA_{20}$ self-assembled nanoparticles (Appendix 12.2) confirmed the formation of narrow size distributed nanoscale spherical micelles that were consistent with the DLS data (Table 4.1), and indicated a particle size consistent to that of micelles (25 nm ± 0.7) with low polydispersity (0.08 ± 0.03). A similar trend was observed in the STEM images of $MPC_{70}$-$DPA_{70}$ (Appendix 12.3), in which small monodispersed spherical micelles were observed, which was consistent with DLS data (Table 4.1); size (37 ± 0.9) and polydispersity (0.07 ± 0.01 ). These micelles were similar in size and polydispersity to that observed in Figure 4.14, as they have similar size and PDI values.

Despite the increase in molecular weight, monodispersed small size micelles were also observed in the STEM images of $MPC_{90}$-$DPA_{90}$ (Appendix 12.4), which was consistent with DLS data (Table 4.1); size (44 ± 0.7 ) and polydispersity (0.07 ± 0.02). Thus, a homogenous spherical nano-system was observed with these systems.

The last 1:1 ratio MPC-DPA diblock copolymer was $MPC_{120}$-$DPA_{120}$, which according to the DLS data (Table 4.1), had a mean particle diameter of 77 ± 2.1, and PDI of 0.2, which indicated the formation of larger sized polydisperse nano-systems. These data were consistent with data obtained from the STEM images, which displaysed the presence of a mixed system of micelles and larger polymersomes (Appendix 12.5).

The STEM images for $MPC_{20}$-$DPA_{40}$ self-assembled micelles (Appendix 12.6) indicated the formation of monodisperse nanosized spherical micelles that were consistent with the DLS data (Table 4.1). The particle size observed was consistent with micelles (28 nm ± 0.1) possessing a low polydispersity (0.04 ± 0.02). This 1:2 ratio copolymer micelles were as homogenous like the 1:1 ratio copolymer micelles.

The largest (140 ± 36.1) and most polydisperse (0.32 ± 0.04) nanoparticles in this study as indicated by DLS (Table 4.1), were $MPC_{50}$-$DPA_{150}$. As shown in 1:2 ratio example STEM image in Figure 4.15, the copolymer formed a mixed system of micelles and polymersomes.

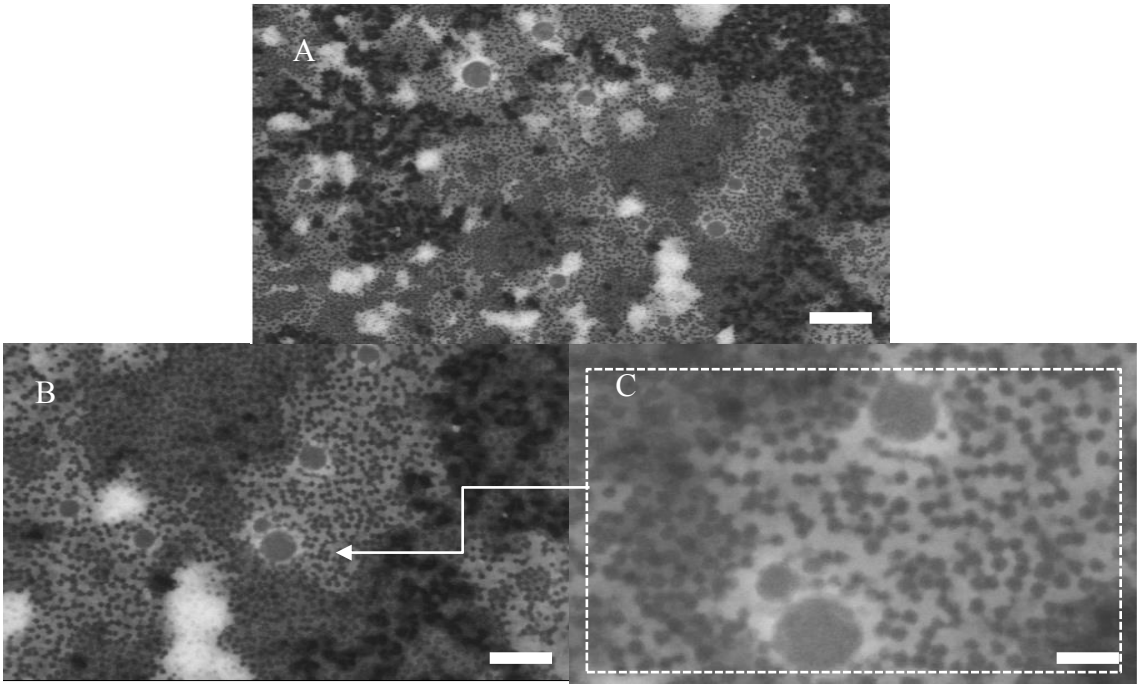


**Figure 4.15** STEM images of $MPC_{50}$-$DPA_{100}$ nanoparticles displaying wide and zoomed areas of copolymer nanoparticles. Scale bars = 200 nm and 20 nm for wide and zoomed areas, respectively

The STEM images of $MPC_{70}$-$DPA_{140}$ (Appendix 12.7), displayed the presence of a mixed system of micelles and polymersomes, which was again consistent with the DLS data (Table 4.1), in which this polymer formed polydisperse large particle size nano-system (size 87± 14.6, PDI 0.37 ± 0.08). $MPC_{120}$-$DPA_{240}$ was the final 1:2 ratio block copolymer examined, and lies between $MPC_{70}$-$DPA_{140}$ and $MPC_{50}$-$DPA_{100}$, in terms of DLS measured particle size (119 ± 10.8) and PDI (0.27 ± 0.08). $MPC_{120}$-$DPA_{240}$ STEM images (Appendix 12.8) displayed a similar trend as $MPC_{70}$-$DPA_{140}$, with the formation of multiple nano-systems (micelles and polymersomes). Although, $MPC_{120}$-$DPA_{240}$ formed mixed nano-systems, they appeared to form nanoparticles that were larger than $MPC_{70}$-$DPA_{140}$, but smaller compared to $MPC_{50}$-$DPA_{100}$. It was noted from the STEM data that the main factor which affected the morphology of the self-assembled nanoparticles appeared to be the hydrophilic-hydrophobic balance of

the MPC-DPA copolymers. The other factors, such as preparation method, nature of solvents used, and polymer concentration were the same in all formulations.

In conclusion, the STEM images observed for MPC-DPA nanoparticles were in close agreement with the DLS data, and displayed the successful self-assembly of MPC-DPA diblock copolymers to form uniform monodisperse micelles copolymers where MPC-DPA copolymer diameters were below 65 nm, whilst larger size mixed nano-systems formed when MPC-DPA copolymer diameters were above 65 nm.

## 4.3 Discussion

### 4.3.1 Nanoprecipitation

Nanoprecipitation, also called solvent displacement, is a simple, fast and reproducible method that has been widely used for nanoparticle preparation (Govender et al., 1999; Vauthier and Bouchemal, 2009; Rao and Geckeler, 2011), and its application for MPC-DPA nanoparticle preparation was recently reported using methanol as the solvent and PBS as the non-solvent (Salvage et al., 2015; Salvage et al., 2016). The mechanism of nanoparticle formation is based on the diffusion of polymer-containing solvent into the non-solvent medium resulting in polymer precipitation or aggregation, and the size of the resultant nanoparticle would depend on polymer concentration, type of solvent used and solvent to non-solvent (S/NS) ratio (Bilati et al., 2005). The affinity of polymer to solvent influences the diffusion motion in which greater affinity would hinder this motion and result in production of small nanoparticles due to the high concentration of solvent remaining in the supersaturated polymer region (Schubert et al., 2011). Furthermore, the type of solvent and non-solvent influences diffusion rate, hence nanoparticle size, with S/NS ratio adjustment facilitating the production of large amounts of the nanoparticles, whilst reducing the volume of solvent used (Bilati et al., 2005). In general, the method of synthesis, the molar ratio

of MPC:DPA in copolymer composition, or alcohol affinity are the main factors that determine the solubility of copolymers (Lewis et al., 2000). It is well known that the PC headgroup has an affinity to alcohols in blends that contain alcohol and water, therefore, MPC- based copolymers demonstrated complete solubility in these mixes, particularly a MeOH: water mix (Lewis et al., 2000; Edmondson et al., 2010).The size and shape of MPC-DPA nanoparticles can be affected by the type of solvent and it has been reported previously that methanol produced smaller monodisperse nanoparticles compared to ethanol, via nanoprecipitation (Bilati et al., 2005; Salvage et al., 2015). As seen in Figure 4.1, the 1:1 MPC-DPA diblock copolymers were totally soluble in methanol before being used in nanoparticle preparation, whilst the 1:2 diblock copolymers showed a different pattern of solubility, from being slightly soluble to completely insoluble, which can be attributed to the higher molecular weight of 1:2 MPC-DPA diblock copolymers that render them less soluble in organic solvents (Wolf, 1985; Su, 2013).

It was noted that although a relatively small volume of MeOH was used in the preparation of the nanoparticles via nanoprecipitation, MeOH toxicity remains an issue (Tephly, 1991). However, in the Salvage et al, 2015 study, the results of *in-vitro* cytotoxicity assays confirmed that there was no residual toxicity accompanied with the use of MeOH in micelle preparation. The following chapters will investigate further the issue of MeOH toxicity. Moreover, the temperature stability studies carried out via DLS demonstrated that there were no shifts or alterations at 70°C taking into consideration that the boiling point of MeOH is 65°C (Salvage et al., 2015).

### 4.3.2 MPC-DPA nanoparticles size and polydispersity measurement

The size of self-assembled nanoparticles can be predicted from the chemical structure and chain lengths of the diblock copolymers (Hamad and Qutubuddin, 1990; Xu et

al., 1992). Therefore, different MPC-DPA compositions were investigated via DLS and the results of average size and size distribution are shown in Table 4.1, which indicated that with the 1:1 MC-DPA copolymer system, the size of nanoparticles increased with increasing molecular weight of diblock copolymer, which was expected and in close agreement with comparable studies (Riley et al., 1999; Stolnik et al., 2001; Hu et al., 2003), with the exception of the $MPC_{70}$-$DPA_{70}$, which possessed a lower size (37 nm) compared to its counterpart lower molecular weight $MPC_{50}$-$DPA_{50}$ (38 nm) (Table 4.1). Although this may seem unexpected, it could be explained as other reported studies involving 1:1 ratio blocks, such as $MPC_{30}$-$DPA_{30}$ (Giacomelli et al., 2006), where despite $MPC_{30}$-$DPA_{30}$ having a longer chain length than $MPC_{20}$-$DPA_{20}$ (i.e. higher molecular weight), their particle size was 15 nm compared to 25 nm for the $MPC_{20}$-$DPA_{20}$ in the current study. Additionally, other micelle systems that were characterised by a constant particle size independent of chain length, or increased molecular weight, include the diblock copolymers poly(ethylene glycol)-poly(aspartic acid) PEG-P(Asp)/PLL, which are reported to have relatively constant particle size (ca 50 nm), regardless block copolymer chain length (Harada and Kataoka, 1997). Another explanation for the lower particle size of $MPC_{70}$-$DPA_{70}$ is related to DLS measurement, is accurate when measuring the diameter of spherical nanoparticles, therefore, DLS data for non-spherical nanoparticle diameters can vary due to multiple structures or morphologies such as rods (Malvern Instrument, 2012), which tend to form when the molecular weight of the hydrophilic block of diblock copolymers exceeds that of the hydrophobic block (Letchford and Burt, 2007). It was noted that the actual MPC-DPA diblock compositions achieved (Table 3.2) differed from the target block compositions used for polymer naming. This effect was principally confined to the DPA blocks, as the

MPC blocks had reached completion after 3 hours. The data suggested that the overall 48 hour time duration applied to the ATRP synthesis, limited the maximum achievable DPA block lengths. However, it was also noted that the molecular weights of the synthesised polymers, determined by NMR and GPC, where is close agreement with the theoretical molecular weights of the target compositions.

In addition to particle size measurement, the polydispersity of all samples was determined and as shown in Table 4.1, almost all 1:1 MPC-DPA polymer systems were monodisperse as they were < 0.1 (Lu et al., 2011), and a relatively narrow PDI was observed for $MPC_{120}$-$DPA_{120}$. In contrast, the 1:2 MPC-DPA copolymer composition data showed a different pattern, with size directly proportional to increased molecular weight for $MPC_{20}$-$DPA_{40}$ and $MPC_{50}$-$DPA_{100}$, followed by an unexpected particle size shift for the next block ratios $MPC_{70}$-$DPA_{140}$ and $MPC_{120}$-$DPA_{240}$, which were 87 nm and 119 nm respectively. This may have been attributed to the imbalance between the hydrophilic-hydrophobic ratio, and the incomplete dissolution of the samples in methanol, as shown in Figure 4.1 (I) and (J), possibly due to forming other structures or morphologies. Therefore, in general the size of the self-assembled polymeric nanoparticles was dependent on the length and ratio of hydrophilic-hydrophobic block segment as well as the nanoparticle molecular weight. Moreover, polydispersity values varied with $MPC_{20}$-$DPA_{40}$ being monodisperse with the remaining 1:2 MPC-DPA copolymers becoming relatively less homogenous with increased DPA (hydrophobic) block length, possibly due to multiple particle size populations.

Furthermore, the polymer concentration used for nanoprecipitation was 2 mg $ml^{-1}$ for all MPC-DPA systems, which could be considered relatively intermediate compared to concentrations used in other studies such as 1 and 4 mg $ml^{-1}$ for MPC-DPA 30-60

and 30-30 respectively (Giacomelli et al., 2006), 0.25 mg $ml^{-1}$ for block ratios of 25-47, 25-77, 25-94 and 25-147 (Pearson et al., 2013), 0.8 mg $ml^{-1}$ 25-120 (Du et al., 2005), and 0.4 mg $ml^{-1}$ for 100-100 block ratio (Salvage et al., 2015), however, large nanoparticles were formed at this concentration (2 mg $ml^{-1}$), which was consistent with other studies examining the effect of increasing polymer concentration on nanoparticle diameter (Bilati et al., 2005; Legrand et al., 2007; Salvage et al., 2016), and polydispersity, that increased at low concentrations. Based on the proportional relationship between molecular weight and nanoparticle size, the increment in size was more pronounced between $MPC_{20}$-$DPA_{20}$ and $MPC_{120}$-$DPA_{120}$, whereas other 1:1 MPC-DPA polymers have relatively close particle size values. This was not seen in case of 1:2 ratio, as there was a large difference between nanoparticle sizes as block length increased. The formation of stable self-assembled polymeric nanoparticles with MPC block that were too short or DPA block that were too long would be unachievable, therefore, the balance between hydrophilic and hydrophobic is essential and the assembly is mainly dependent on the hydrophobic block chain, as it has been reported that with a constant MPC block length, a short DPA block leads to nanoparticle to self-assemble into micelles (Ma et al., 2003), whilst with longer DPA blocks, vesicles were produced (Du et al., 2005).

In summary, the ethanolic ATRP had been successful in the production of a series of well-defined increasing molecule weight block compositions copolymer, which self-assembled in PBS (pH 7.4) to form nanoparticles with particle sizes highly controlled by the hydrophilic-hydrophobic ratio and type of polymer utilised.

### 4.3.3 Effect of polymer concentration on MPC-DPA nanoparticle stability

The stability of self-assembled nanoparticles in a physiological environment is one of the most important issues when designing nanoparticles as drug delivery systems, as high levels of dilution can cause dose dumping after administration, therefore, polymeric self-assembled nanoparticles should ideally be resistant to dissociation when they are diluted to a concentration below their CMC (Lu and Park, 2013). The effect of copolymer concentration on the self-assembled nanoparticles diameter and particle stability was investigated by DLS in PBS (pH 7.4), and the results demonstrated that the MPC-DPA nanoparticles were highly resistant to dilution induced dissociation of self-assembled nanoparticles, and were detected down to concentrations ranging from 0.062-0.125 mg $ml^{-1}$ (Appendix 2.0). These values are slightly higher than CMC values reported in other studies, which utilised fluorescence spectroscopy on MPC-DPA nanoparticles such as 0.025 mg $ml^{1}$ (for $MPC_{30}$-$DPA_{30}$) and 0.014 mg $ml^{-1}$ ($MPC_{30}$-$DPA_{60}$), (Giacomelli et al., 2006), and 0.004 mg $ml^{-1}$ ($MPC_{30}$-$DPA_{50}$) (Licciardi et al., 2005). Moreover, 1:1 and 1:2 MPC-DPA polymers diameters remain relatively the same upon serial dilution, but 1:2 ratio polymers were detected at lower concentrations than 1:1 ratio, which is mainly attributed to the longer hydrophobic DPA chain, which decreases the CMC and increases nanoparticle size (Wilhelm et al., 1991; Qiu and Bae, 2006). As seen in Table 4.4 MPC-DPA nanoparticle CMC, generated by pyrene fluorescence spectroscopy, were reported to decrease with longer DPA blocks for almost all polymers, with lower values observed for $MPC_{120}$-$DPA_{120}$, where nanoparticle CMC was reported down to 0.10 mg $ml^{-1}$. The polydispersity (PDI) for MPC-DPA nanoparticles were also measured by DLS, and according to reported studies, particles are considered monodisperse if their PDI values were less than 0.1(Lu et al., 2011), therefore, polydispersity increases upon

dilution were more pronounced with the large size nanoparticles, which were initially polydisperse, an indication of mixed particles population, including MPC-DPA systems: 50-100, 70-140, and 120-240, compared to the smaller size MPC-DPA systems: 20-20, 50-50, 70-70, 90-90, 120-120 and 20-40, as they were principally monodisperse and remained relatively stable upon dilution, with all MPC-DPA particle diameters were measurable down to concentration of 0.0019 mg $ml^{-1}$, an indication of DLS sensitivity (Appendix 3.0). Moreover, upon each dilution, the count rate (KCps), which is a measure of the level of light scattering, in both ratios dropped by half value in a steady state manner without unexpected or sudden drops, which indicates nanoparticles dissociation (Appendix 4.0).

For DLS method validation, a series of halving dilutions of 50 nm monodisperse polystyrene standard particles were carried out, and the particle diameter remained stable as the sample was diluted, whilst PDI displayed some drift, which suggests that even with standard size calibration particles, relative polydispersity values increase at low concentration due to the low number of particles present. The count rate (KCps) drops to half after each dilution, which indicated the DLS was capable of measuring particles parameters even at low particle numbers. In conclusion, some drift occurs at low concentration; due to being below the optimum concentration for instrument accuracy, particle size and size distribution still detected and measured.

### 4.3.4 Effect of pH change on MPC-DPA nanoparticles

The particle self-assembly pH profile of MPC-DPA copolymers were investigated by DLS, by determining the particle diameter (ZAve) and polydispersity (PDI) of self-assembled polymeric nanoparticles at different pH values, ranging from pH 3 up to pH 10, prepared to simulate the physiological condition of blood (pH 7.4), intracellular lysosome (pH 5), and the extracellular environment of solid tumour (pH

6.5-6.8) (Sun et al., 2014b) . As shown in Figure 4.2 and 4.3, at low pH (3), all MPC-DPA diblock copolymer samples were molecularly dissolved and present as unimers, as indicated by the low particle diameters, however, particle size began to increase after pH 3 until pH 6 where the self-assembly process began and was completed by pH 7, which was indicated by the increase in particle diameter that were consistent with values measured in PBS (pH 7.4). After pH 7, the particle size remained the same for the subsequently higher pH values, which indicated a complete micellisation process had been reached. In contrast, sample polydispersity was seen at pH 3, and continued to increase as pH increased, which indicated a mixed particle system (uimer, intermediate and micelle) was present. At pH 7, polydispersity reduced remarkably and continued afterwards (Figure 4.4 & Figure 4.5), which indicated the formation of monodisperse systems. These findings were consistent with previously reported data (Bütün et al., 2001; Lomas et al., 2007; Pearson et al., 2013), which indicated that the zwitterionic MPC blocks remain highly hydrophilic under various conditions, in contrast to DPA blocks that became cationic and hydrophilic due to protonation of its tertiary amine residue at low pH, and with pH adjusted to around 6-7, DPA becomes deprotonated and hydrophobic leading to the formation of self-assembled nanostructures.

In summary, at pH 7, uniform MPC-DPA nanoparticles; in terms of size and polydispersity, were produced with no evidence of aggregation or instability which indicated a complete unimer to micelle transition. For 1:1 ratio MPC-DPA nanoparticles, all polymers were close together at low pH, in terms of size, then after reaching the micellisation pH (7), a range of particle sizes were observed, related to polymer length (Figure 4.2), by which the smallest size 25 nm (20-20) was at the bottom, then the next three ratios with a relatively close size of 38, 37, and 42 nm,

whilst the larger size 77 nm polymer at the top had a larger increase than the previous ratios. In terms of PDI, all 1:1 ratio at low pH were relatively polydisperse, then at pH 7, the small size nanoparticles became monodisperse, whereas 120-120 polymers again displayed a larger increase than others, possibly due to possess the largest size and hence, was relatively polydisperse.

Furthermore, another pH range (6-7) was examined to determine the pH of nanoparticle self-assembly, and the results displayed in Table 4.2 and Table 4.3, which indicated that self-assembly occurred mainly above pH 6.4 for 1:1 and 1:2 ratio MPC-DPA copolymers, which was in close agreements with previous studies on polymeric nanoparticles (Du et al., 2005; Shen et al., 2008). As seen in Table 4.2, 1:1 ratio MPC-DPA copolymers, at low pH 6, with the block lengths 20-20, 50-50, 70-70, 90-90 and 120-120 were unimers, then particle size increases were observed at pH 6.4, 6.5, 6.6, 6.6 and 6.4 respectively, suggesting the beginning of micellisation. The next pH range increase for each copolymer displayed particle size instability suggesting the existence of mixed unimer-micelle systems until pH 7 were particle size stabilised, suggesting completion of micelle formation (Table 4.2). The 1:2 ratio MPC-DPA copolymers (Table 4.3), at low pH 6, with the block lengths 20-40, 50-100, 70-140, and 120-240 were unimers, and then particle size increased again at pH 6.5, 6.2, 6.2, and 6.4 respectively, suggesting the start of micellisation. The next pH ranges increase for each 1:2 copolymer also displayed particle size instability, again suggesting the existence of mixed uimer-micelle system until pH 7 was reached, were particle size stabilised, suggesting again micelle formation was complete.

#### 4.3.2.3 Temperature and time stability of MPC-DPA nanoparticles

Thermal stability and long-term particle stability are of great importance in manufacturing products for clinical use as storage and the way of handling products may compromise particle stability, therefore, MPC-DPA self-assembled nanoparticles were subjected to a wide range of a temperatures (5-70ºC) and (30-40ºC). The particle size and polydispersity were initially assessed across a temperature range of 5ºC to 70ºC in 5ºC incremental steps. As shown in Figures 4.6 and 4.7 for particle size of all MPC-DPA copolymer systems demonstrated good thermal stability with no cloud points and no evidence of aggregation or dissociation. Moreover, MPC-DPA (1:1 ratio) nanoparticles were stable with a small particle size difference between the 20-20 ratio and the next three ratios 50-50, 70-70, and 90-90, compared to a large size increase corresponding to the large molecular weight of 120-120 polymer. In contrast, the 1:2 ratio MPC-DPA nanoparticles, displayed a larger size increase between the smallest polymer 20-40 and the larger polymers, whilst a small and relatively similar difference in size was present between polymers with 87, 119, and 140 nm particle sizes. All those differences were attributed to differences in polymer composition, molecular weight and hydrophilic to hydrophobic ratio (Owen et al., 2012; Biswas et al., 2013). The polydispersity (PDI) and count rate for MPC-DPA nanoparticles were also measured by DLS (Appendix 5.0 and 6.0) and the results showed that the majority of 1:1 ratio MPC-DPA nanoparticles remained monodispersed and stable across the 5-70°C range.

In order to provide a closer examination on the physiological related temperature range, MPC-DPA copolymers were tested at temperatures ranging from 30-40ºC and the particle size data confirmed the thermal stability of both polymers ratios without any changes. Therefore, these data indicated that MPC-DPA nanoparticles possessed

good thermal stability in comparison to other studies that reported changes in particle diameters with temperature changes (Pearson et al., 2013), which was attributed to temperature induced micelle phase transitions. In conclusion, both ratios, would be stable at different storage and transport condition without critical micelle temperature issues, these findings were consistent with other MPC-DPA nanoparticles studies (Salvage et al., 2015).

For method and technique validation, 50 nm polystyrene standard particles were subjected to the same temperature ranges, and were stable at all temperatures with negligible fluctuation, which indicated good equipment accuracy.

Furthermore, a time stability study was conducted on the MPC-DPA systems, in the form of 18 months study on two sets of samples, the first stored at room temperature whilst the second set was kept at 4ºC. The results indicated that MPC-DPA nanoparticles were stable at different storage conditions, and possibly more so at room temperature as seen in Figure 4.8 for 1:1 ratio MPC-DPA systems and Figure 4.9 for 1:2 ratio MPC-DPA systems compared to Figure 4.10 for 1:1 set and Figure 4.11 for 1:2 at 4°C.

As described earlier, for 1:1 ratio MPC-DPA nanoparticles, stored at room temperature most of the 25 nm- 44 nm particle size were grouped together with only small size differences between them, as they had relatively narrow particle size ranges, with the exception of the larger molecular weight $MPC_{120}$-$DPA_{120}$ (77 nm), where a large size increase separated it from other nanoparticles (Figure 4.8). However, at 4ºC, there were minimal changes in particle size with an overlap present between 50-50 and 70-70 block ratio (Figure 4.10) due to a possible transition phase or the presence of different structures or morphologies. Conversely, the 1:2 ratio MPC-DPA nanoparticles, had a relatively similar size difference between the different

copolymers at 4ºC (Figure 4.11), compared to room temperature, with small difference evident between larger size copolymers (Figure 4.9).

### 4.3.6 Critical micelle concentration (CMC) determination

The critical micelle concentration (CMC) represents the concentration at which unimers start to self-assemble into micelles (Torchilin, 2007a), therefore, below CMC, amphiphilic molecules exist individually, but above CMC, unimers would exist in equilibrium with micelles, hence, the determination of CMC values of nanoparticle is essential to display nanoparticle resistance to dissociation upon dilution, and thereby, determine micellar stability (Lu and Park, 2013). There are several techniques employed for the determination of CMC such as surface tension, conductivity, chromatography and light scattering (Cho et al., 2013). Although, these methods are widely utilised for CMC determination, they have some drawbacks when measuring very low CMC values in the case of polymeric micelles (Ahmad et al., 2014). Pyrene fluorescence represents one of the most effective options, as pyrene (hydrophobic aromatic hydrocarbon) is sensitive to the minor changes in solutions and polarity of probe micro environments (Jones and Leroux, 1999), and is thus used to investigate micellar system properties thoroughly with regard to onset of micellisation and micelle structure (Aguiar et al., 2003). Generally, below CMC, there are no micelles in solution and pyrene fluorescence spectrum corresponds to that of pyrene in water, but as copolymer concentration is increased above CMC, micelles form, and the pyrene partitions towards the micellar core (the hydrophobic domain) (Astafieva et al., 1993).

Usually, in the fluorescence spectrum, pyrene displays five vibrational peaks, which are 373, 379, 384, 388 and 393 nm corresponding to $I_I$, $I_{II}$, $I_{III}$, $I_{IV}$ and $I_V$ respectively, and the intensity of peaks at $I_I$, and $I_{III}$ are considered to be the most sensitive to their

surrounding environment, thus the $I_I/I_{III}$ from the emission spectra was used in CMC determination (Figure 4.12) (Kalyanasundaram and Thomas, 1977).

In this study, CMC values were obtained by plotting the fluorescence intensity $I_I/I_{III}$ ($I_{373}/I_{384}$) from the emission spectra (the shift from 373 to 384 as pyrene partitions into micelle core) against copolymer concentration in aqueous solution, and the change in slope indicates the onset of micellisation (Domínguez et al., 1997), as shown in Figure 4.13. CMC values are frequently determined using values extracted from the intersection of a straight line segment drawn through points in the low concentration range to determine CMC (CMC1) (Licciardi et al., 2005; Giacomelli et al., 2006; Dayananda et al., 2007; Zhang et al., 2010a; Li et al., 2014b), as shown in Figure 4.13, and Table 4.4. Although many publications cite single values when reporting CMC, the CMC can be viewed as a concentration range with a start $CMC_1$, mid $CMC_2$ and endpoint $CMC_3$ (Ysambertt et al., 1998).

As shown in Table 4.4, MPC-DPA nanoparticles displayed a decrease in CMC values corresponding to the increase in hydrophobic block chain length, which is consistent with the studies that confirm the relationship between low CMC and the high hydrophobic segment in self-assembled nanoparticles, with the chain length of the hydrophilic segment kept constant (Biswas et al., 2013; Lu and Park, 2013; Ahmad et al., 2014). For example, an increase in DPA block length in MPC-DPA diblock copolymers whilst MPC block length remains constant (DP= 30) (Giacomelli et al., 2006). Various studies have demonstrated that the increase in hydrophobic chain length of polystyrene (PS) of PS-b-PEG-b-PS, poly(ethyl methacrylate) (PMMA) of PMMA-b-PEG-b-PMMA (Zhiping et al., 2009), poly(2-(dimethylamino)ethyl methacrylate)-*b*-poly(acrylic acid) (PDMAEMA) of PDMAEMA-b-PAA(Han et al., 2013), and N-isopropylacrylamide (PNIPAM) of PAM-b-PNIPAM (Wever et al.,

2014) block copolymers was associated with a reduction in CMC values. Conversely, although the effect of hydrophilic block chain length is less pronounced on CMC values, an increased PEG chain length in PEGylated phospholipid was accompanied with increased in CMC values (Ashok et al., 2004). Therefore, polymers with large hydrophobic blocks form micelles at lower concentrations and temperatures, compared to the difficulty in micelle formation seen with copolymers possessing large hydrophilic blocks (Alexandridis and Hatton, 1995).

Moreover, the low CMC values were associated with the increased micelle size due to an increased hydrophobic chain length (Torchilin et al., 2001; Qiu and Bae, 2006), thus, large size MPC-DPA copolymer nanoparticles, exhibit lower CMC values, (Table 4.4), and as expected a similar CMC value was obtained for 50-50 and 70-70 ratio MPC-DPA as they have a closer molecular weight. Therefore, all CMC data (Table 4.4) were in close agreement with the results of the copolymers dilution measured by DLS (Appendix 2.0), which confirmed the low CMC values of the synthesised MPC-DPA copolymers. Generally, for CMC measured with the DLS technique, the particle diameter of 1:1 and 1:2 ratio remained stable upon serial dilution, with particles detected down to 0.25 mg $ml^{-1}$ for almost all polymers, except for $MPC_{120}$-$DPA_{120}$ and $MPC_{120}$-$DPA_{240}$, where nanoparticles were detected down to 0.062 mg $ml^{-1}$. Moreover, as discussed earlier, the DLS technique is able to detect CMC when it occurs at a concentration within the DLS sensitivity region, in addition to the existence of secondary association; the presence of two different sized colloidal particle systems in solution, which may complicate the measurement with some copolymers such as PS-b-PEO (Khan et al., 1987; Xu et al., 1991), unlike pyrene, which is considered a highly sensitive technique for the determination of CMC.

Method validation was undertaken using sodium dodecyl sulfate (SDS), which indicated that the CMC were in close agreement with published values ($7.4 \times 10^{-3}$ mol $L^{-1)}$ (Domínguez et al., 1997; Aguiar et al., 2003). Compared to low molecular weight surfactants, polymeric micelles exhibit lower CMC values that in turn indicate a greater thermodynamic stability (Gaucher et al., 2005).

### 4.3.7 STEM analysis of MPC-DPA nanoparticle morphology

The nature of the solvent used in polymeric nanoparticle preparation, along with copolymer concentration, can affect morphology and polydispersity of particles, as demonstrated by Eisenberg and co-workers (Zhang and Eisenberg, 1996), where changes occurred with spherical micelles shifting to cylindrical, and then to vesicles when copolymer concentration was increased. Moreover, block copolymer composition and block length ratio, influence both the micellisation process and the nanoparticle morphology (Zhang and Eisenberg, 1996). Additionally, several studies have been conducted to clarify the MPC-DPA block length relationship to particle morphology, as the degree of polymerisation of MPC and DPA blocks were responsible for the type of nanoparticle obtained, whether they were micelles or vesicles (Colley et al., 2014). It was reported that copolymers with MPC block lengths of 25-30 and short DPA block lengths (< 60) produced micelles, whilst vesicles were obtained at higher DPA block ratios (70-160) (Pearson et al, 2013). Moreover, the packing parameter (p), described in Chapter 1, determines the type of configurations adopted by the self-assembled polymeric amphiphilies, hence, spherical aggregates formed spherical micelles at $p \leq 1/3$, while cylindrical micelles, which are similar to spherical micelles but their hydrophobic part packed to form rod-shaped core, are formed at $1/3 < p \leq 1/2$ resulting in worm-like structures (Smart et al., 2008). At low

curvature ($1/2 < p \leq 1$), block copolymers tend to generate membranes that wraps up to form a sac-like structure known as vesicle or polymersome.

The previous reports were in close agreement with data obtained in this study as seen in the STEM images (Appendix 12.0), which demonstrated that MPC-DPA diblock copolymer micelles were formed successfully. In general, MPC-DPA supramolecular aggregates with diameters greater than 100 nm have been reported to form vesicle like polymersomes rather than micelles, which indicated that all of the 1:1 ratio diblock copolymers should form micelles, Figure 4.14 represented an example of 1:1 ratio MPC-DPA diblock copolymers, which were all in agreement with this except for $MPC_{120}$-$DPA_{120}$, which formed a mixture of particle morphologies comprising micelles and polymersomes, which was attributed to the increase in the hydrophobic block DPA in their composition.

Additionally, the 1:1 ratio MPC-DPA diblock copolymers formed monodispersed micellar system, which was demonstrated by the DLS data (Table 4.1) and STEM images (Appendix 12.0), except for the large size 1:1 MPC-DPA diblock copolymer (77 nm), which was characterised by a broad PDI due to the presence multiple morphological particles.

Similarly, the 1:2 ratio MPC-DPA samples; apart from $MPC_{20}$-$DPA_{40}$, which formed monodisperse small micelles and DLS data (Table 4.1), displayed a combination of micelles and small vesicles as shown in example image Figure 4.15, as their average particle sizes were large, and they possessed an increased in polydispersity due to the presence of a mixture of larger sized micelles and polymersomes. Those data were consistent with results obtained from previous research that has studied the relationship between hydrophilic-hydrophobic ratio and aggregates morphology,

including other MPC-DPA combinations (Blanazs et al., 2012; Colley et al., 2014), or other types diblock copolymers (He et al., 2011; Ohno et al., 2015).

Method validation was carried out using 50 nm polystyrene standard, which confirmed the accuracy of STEM observations, in term of size and morphology. Therefore, according to the DLS and STEM data, it would appear that MPC-DPA diblock copolymers, especially the equal block length (1:1) polymers, were self-assembled predominately to form micelle nano-systems.

## 4.4 Summary

In conclusion, the DLS analysis indicated that the synthesised copolymers self-assembled and underwent the unimer-micelle transition between pH 6-7, and that these nano-systems were thermally stable across a wide temperature range (5-70°C). Additionally, all the systems demonstrated particle stability in response to dilution and exhibited low CMC values. Further investigations revealed that the MPC-DPA diblock copolymers formed a range of aggregates as seen in the STEM images, which was achieved by changing the degree of polymerisation of MPC and DPA blocks, and the STEM observations were relatively consistent with the DLS results. Therefore, self-assembled micelles preparation had been achieved, and were then considered suitable for investigation as drug delivery systems.

# CHAPTER FIVE

# BIOEVALUATION

## 5.1 Introduction

The physicochemical characteristics of nanoparticles are considered a main factor, which contributes to the development of nanoparticle cytotoxicity. Therefore, the first aim of this chapter was to evaluate the toxicological effect of MPC-DPA on different cell lines by the use of the MTT assay to determine the direct acute cytotoxicity and the cell colony formation test for long-term toxicity.

It was noted that only a few studies have focused on studying the uptake and intracellular delivery of hydrophobic agents by PC-based pH sensitive; MPC-DPA polymeric micelles compared to their counterpart polymersomes, therefore, this chapter will focus on investigating the effect of MPC-DPA characteristics on controlling the rate, extent and mechanism of micellar internalisation by cells.

As a result of the data obtained in Chapter 4, the 1:1 ratio MPC-DPA polymeric nano-systems were chosen to evaluate the potential toxicity of MPC-DPA polymeric nano-systems towards V79 Chinese hamster lung fibroblasts and 3T3 Swiss mouse NIH embryo fibrolasts. Particle size of nanoparticles plays a crucial role in the determination of uptake efficiency and kinetics, the internalisation pathway and distribution of loaded cargo, therefore, the decision was made to narrow down the choice of MPC-DPA micelles that would proceed to the bioevaluation studies to include $MPC_{20}$-$DPA_{20}$, $MPC_{50}$-$DPA_{50}$, and $MPC_{90}$-$DPA_{90}$ because they offered size ranges of 25-45 nm, which several studies considered to be optimum to evaluate nanoparticle cellular uptake (Iversen et al., 2011; Chang et al., 2016).

Therefore, the second aim of this chapter was to determine the rapid uptake of MPC-DPA micelles of different sizes using *in-vitro* studies and to identify the optimal size

for the cellular uptake of these formulations, which would then be further investigated for the delivery of the antitumour drug docetaxel. The cells lines used in this Chapter were selected based upon them being well established and widely studied *in-vitro* testing models. The V79, 3T3, Vero, MRC-5, and CHO were normal cell types used for initial bioevaluation purposes. Subsequent selective testing with cancer cell lines, MCF-7, SKOV-3, and PC-3 was undertaken in Chapter 6.

## 5.2 Results

### 5.2.1. Cytotoxicity results

The *in-vitro* cytotoxicity of MPC-DPA nanoparticles was evaluated by cell colony formation (as described in Section 2.2.3.5.1) and MTT assays (as described in Section 2.2.3.5.2), in which cells were treated with sequential concentrations of MPC-DPA nanoparticle solutions (1000-31.25 μg $ml^{-1}$). In the cell colony formation assay, the effect of MPC-DPA nanoparticles on the viability of V79 cells was examined and the results are shown in Figure 5.1, 5.2, 5.3, 5.4, and 5.5. All graphs represent the mean and SD of triplicate separate experiments and data (expressed as % of cell viability) obtained by comparing the cell colony formation of cells incubated with MPC-DPA copolymers to polymer-free cells control.

Figure 5.1 to Figure 5.5 results showed similar trends for the clonogenic assay results of the 1:1 ratio MPC-DPA polymeric nano-systems that were exposed to V79 cells at 37°C in 5% $CO_2$ humidified atmosphere for 5 days. These data indicated that minimal levels of cellular toxicity were induced over the exposure period, with the exception of the highest copolymer concentration (1000 μg $ml^{-1}$), which induced toxicity to V79 cells compared to control (MeOH).

Moreover, the subsequent copolymer concentrations displayed a lower degree of toxicity to V79 cells, which indicated that MPC-DPA copolymers had no significant

toxic effect ($p > 0.05$) on the ability of the V79 cells to proliferate. Furthermore, and as seen in all graphs (Figure 5.1 to Figure 5.5), the MeOH toxicity results indicated that there was no significant ($p > 0.05$) V79 cell toxicity observed; even with the prolonged exposure (5 days), associated with using MeOH as the solvent in the formation of MPC-DPA polymeric nano-systems via nanoprecipitation.

Overall all graphs (Figure 5.1 to Figure 5.5) illustrated that MPC-DPA nanoparticles were well tolerated in the V79 cell line tested, cell survival increased with a reduction in test sample concentration compared to the controls, and the MPC-DPA polymeric nano-systems had minimal effect on the ability of V79 to form colonies.

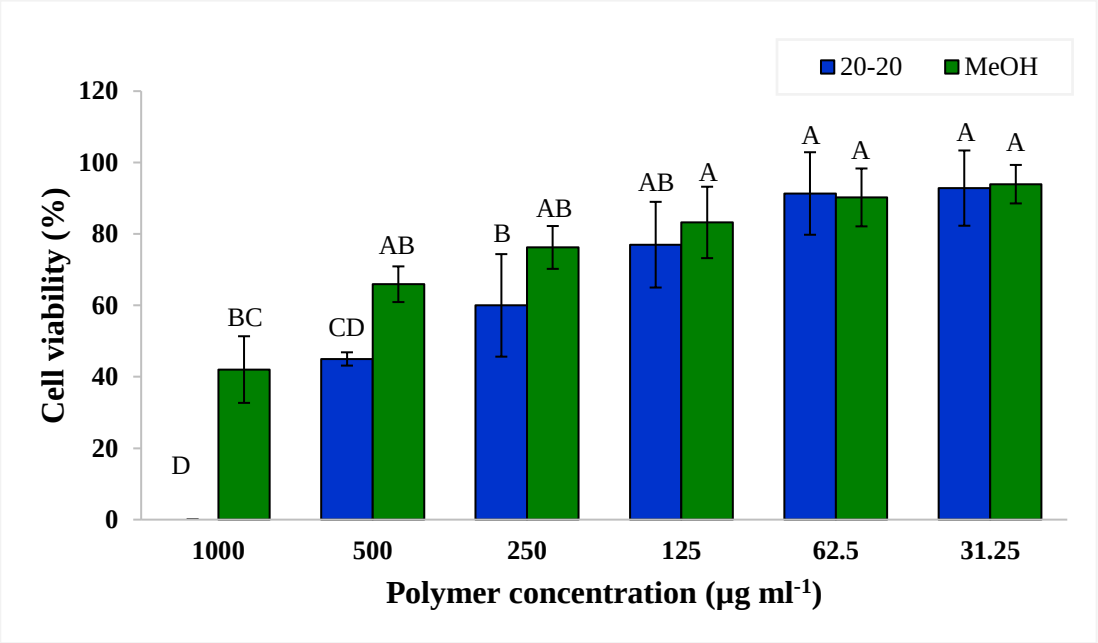


**Figure 5.1.** Cytotoxicity of 25 nm $MPC_{20}$-$DPA_{20}$ nanoparticles to V79 cells after 5 days exposure at concentrations ranging from 31.25 to 1000 µg $ml^{-1}$ at 37°C in 5% $CO_2$ determined by clonogenic assay (Mean ± SD, n=3) (Original in colour). *Bar values with different letters indicate a significant difference ($p < 0.05$) and those sharing the same letters are not significantly different ($p > 0.05$).*

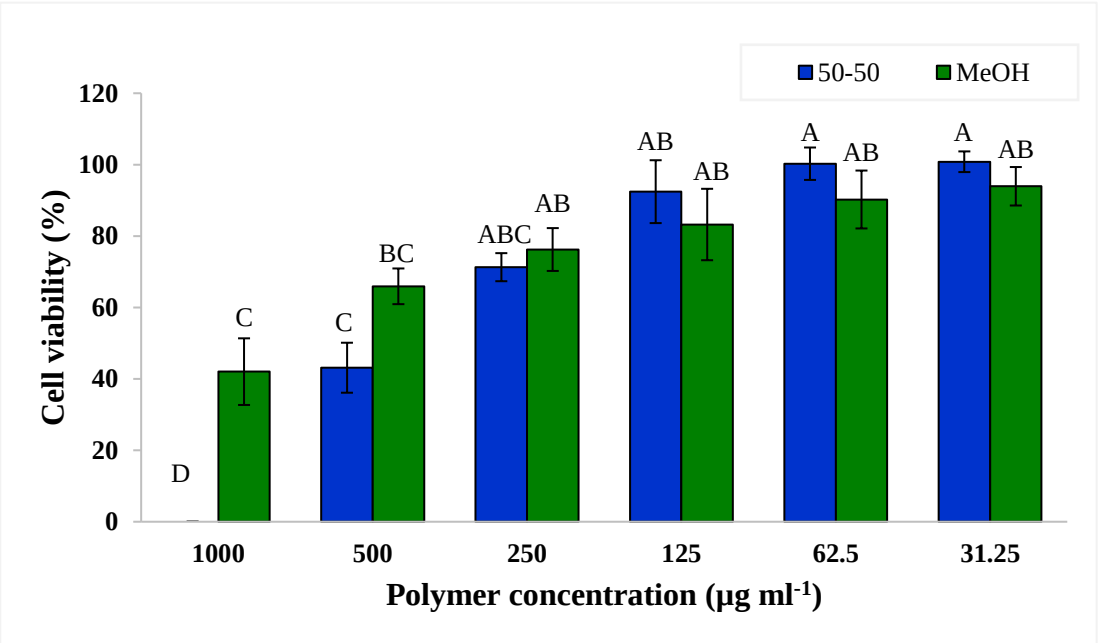


**Figure 5.2.** Cytotoxicity of 38 nm $MPC_{50}$-$DPA_{50}$ nanoparticles to V79 cells after 5 days exposure at concentrations ranging from 31.25 to 1000 µg $ml^{-1}$ at 37°C in 5% $CO_2$ determined by clonogenic assay (Mean ± SD, n=3) (Original in colour). *Bar values with different letters indicate a significant difference ($p < 0.05$) and those sharing the same letters are not significantly different ($p > 0.05$).*

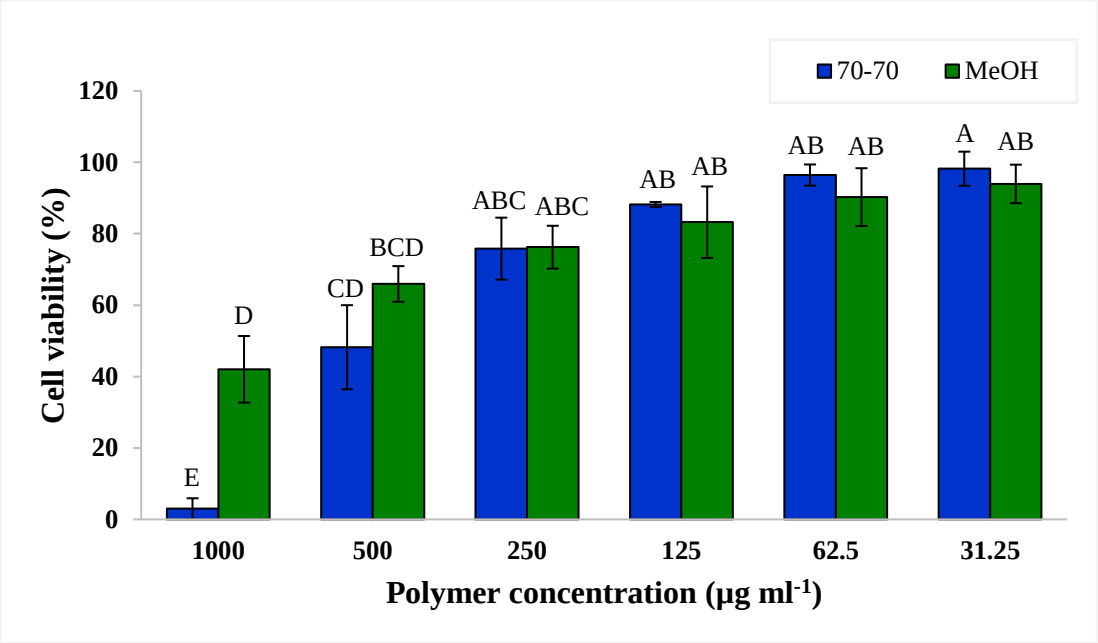


**Figure 5.3.** Cytotoxicity of 37 nm $MPC_{70}$-$DPA_{70}$ nanoparticles to V79 cells after 5 days exposure at concentrations ranging from 31.25 to 1000 µg $ml^{-1}$ at 37°C in 5% $CO_2$ determined by clonogenic assay (Mean ± SD, n=3) (Original in colour). *Bar values with different letters indicate a significant difference ($p < 0.05$) and those sharing the same letters are not significantly different ($p > 0.05$).*

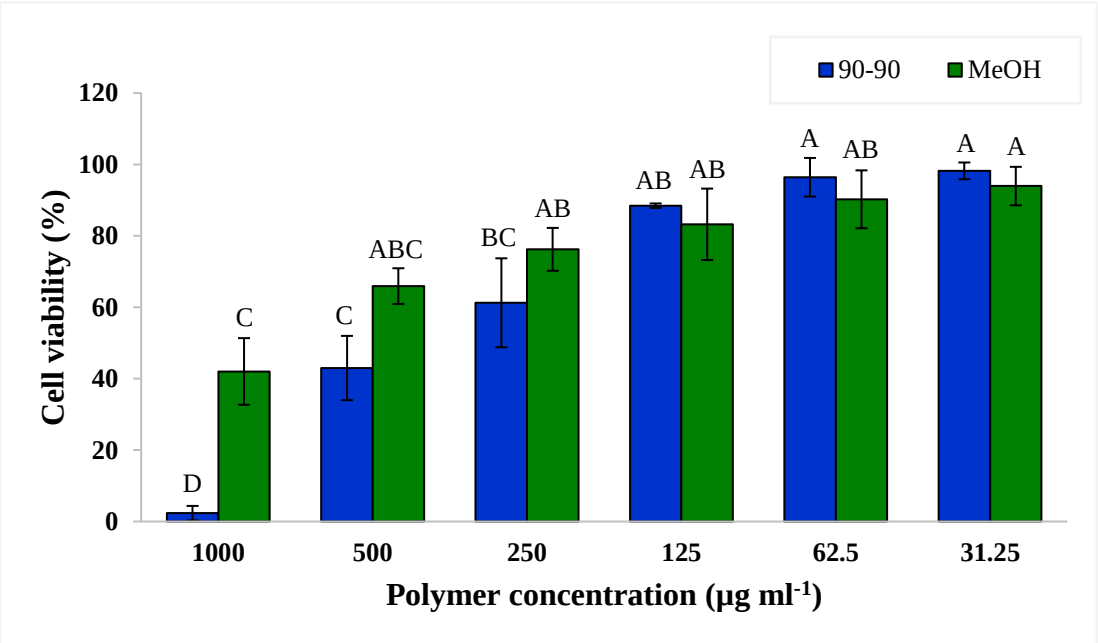


**Figure 5.4.** Cytotoxicity of 44 nm $MPC_{90}$-$DPA_{90}$ nanoparticles to V79 cells after 5 days exposure at concentrations ranging from 31.25 to 1000 µg $ml^{-1}$ at 37°C in 5% $CO_2$ determined by clonogenic assay (Mean ± SD, n=3) (Original in colour). *Bar values with different letters indicate a significant difference ($p < 0.05$) and those sharing the same letters are not significantly different ($p > 0.05$).*

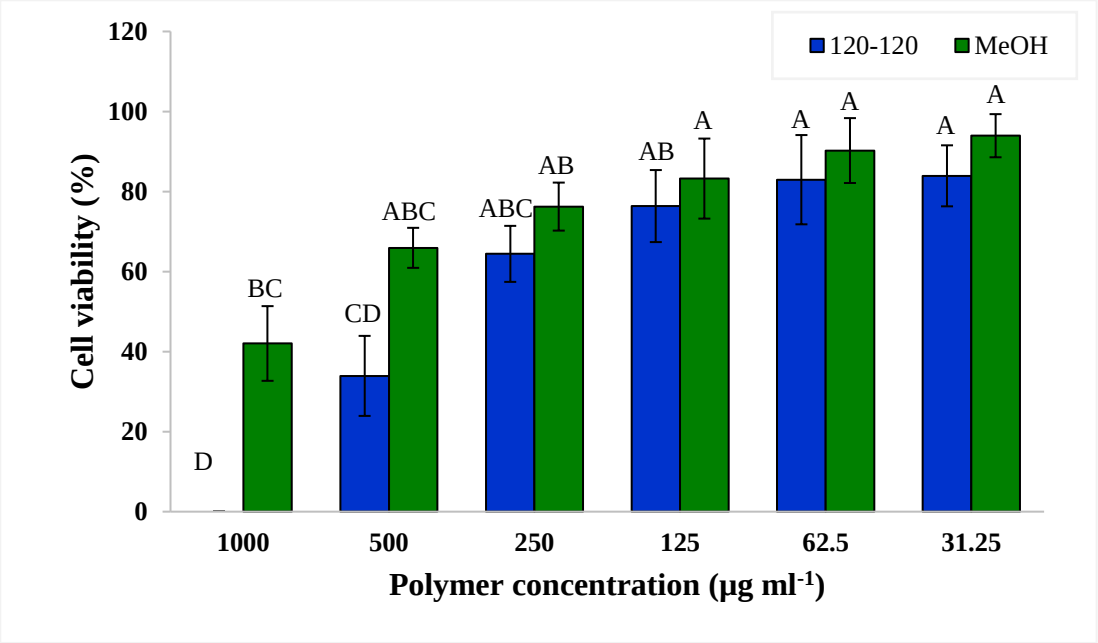


**Figure 5.5.** Cytotoxicity of 77 nm $MPC_{120}$-$DPA_{120}$ nanoparticles to V79 cells after 5 days exposure at concentrations ranging from 31.25 to 1000 µg $ml^{-1}$ at 37°C in 5% $CO_2$ determined by clonogenic assay (Mean ± SD, n=3) (Original in colour). *Bar values with different letters indicate a significant difference ($p < 0.05$) and those sharing the same letters are not significantly different ($p > 0.05$).*

The mitochondrial activity of cells exposed to six different concentrations of MPC-DPA nanoparticles was also tested via the MTT assay (as described in Section 2.2.3.5.2) to determine the cells viability after 24 h of exposure and the results are reported in the Figures 5.6 to 5.10 on two different cell types, V79 and 3T3. In the MTT assay, the number of metabolically active (viable) cells is directly correlated to the amount of MTT reduced to insoluble formazan crystals, which is quantified by measuring the absorbance at 540 nm. As observed in all graphs (Figures 5.6 A-5.10 A), the highest concentrations of MPC-DPA nanoparticles induced a statistically significant ($p < 0.05$) toxic effect on V79 cell lines. This effect was significantly reduced at the subsequent, and lower polymer nanoparticle concentrations. However, compared to the clonogenic assay results (Figure 5.1 to Figure 5.5), the cell viability at the highest concentration (1000 µg $ml^{-1}$) in the MTT assay was greater due to the shorter exposure time, 5 days versus 24 h.

A similar trend to the V79 cells was reported with the 3T3 cell line as shown in Figure 5.6 B- 5.10 B, in which the resultant cytotoxicity data revealed a statistically significant ($p < 0.05$) increase in cell viability between high and low copolymer concentrations. Moreover, the MTT toxicity results of MeOH control also demonstrated no significant toxicity to both cell lines at lower concentrations.

Overall, the cytotoxicity trends observed using the MTT assay were closely correlated with the data obtained using the clonogenic test and the MPC-DPA nanoparticles did not induce significant cytotoxicity on V79 or 3T3 cell lines in short or long exposure time at polymer concentrations 250-31.25 μg $ml^{-1}$.

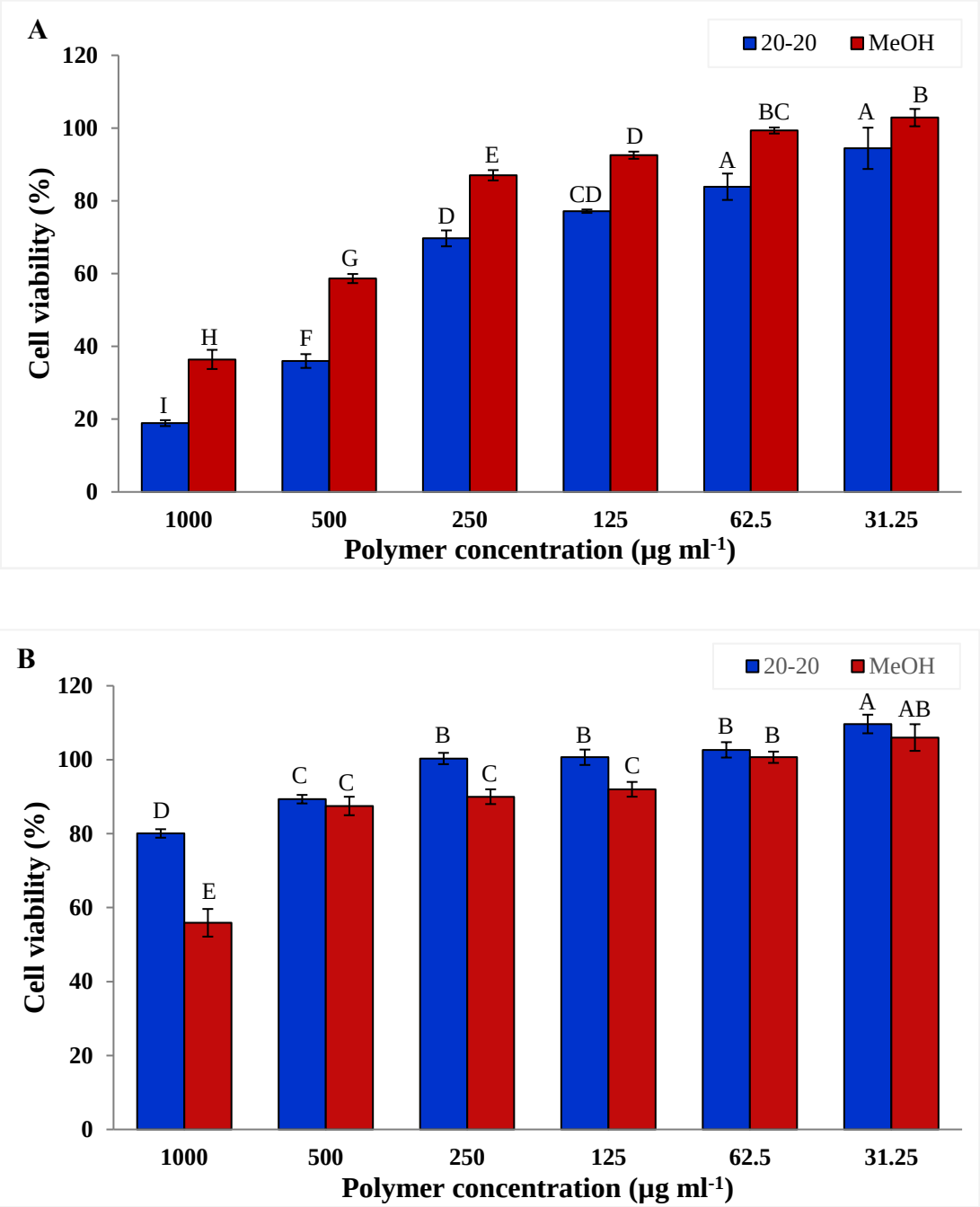


**Figure 5.6.** Cytotoxicity of 25 nm $MPC_{20}$-$DPA_{20}$ nanoparticles to (A) V79 cells and (B) 3T3 cells after 24 h exposure at concentrations ranging from 31.25 to 1000 µg $ml^{-1}$ at 37°C in 5% $CO_2$ determined by MTT assay (Mean ± SD, n=3) (Original in colour). *Bar values with different letters indicate a significant difference ($p < 0.05$) and those sharing the same letters are not significantly different ($p > 0.05$).*

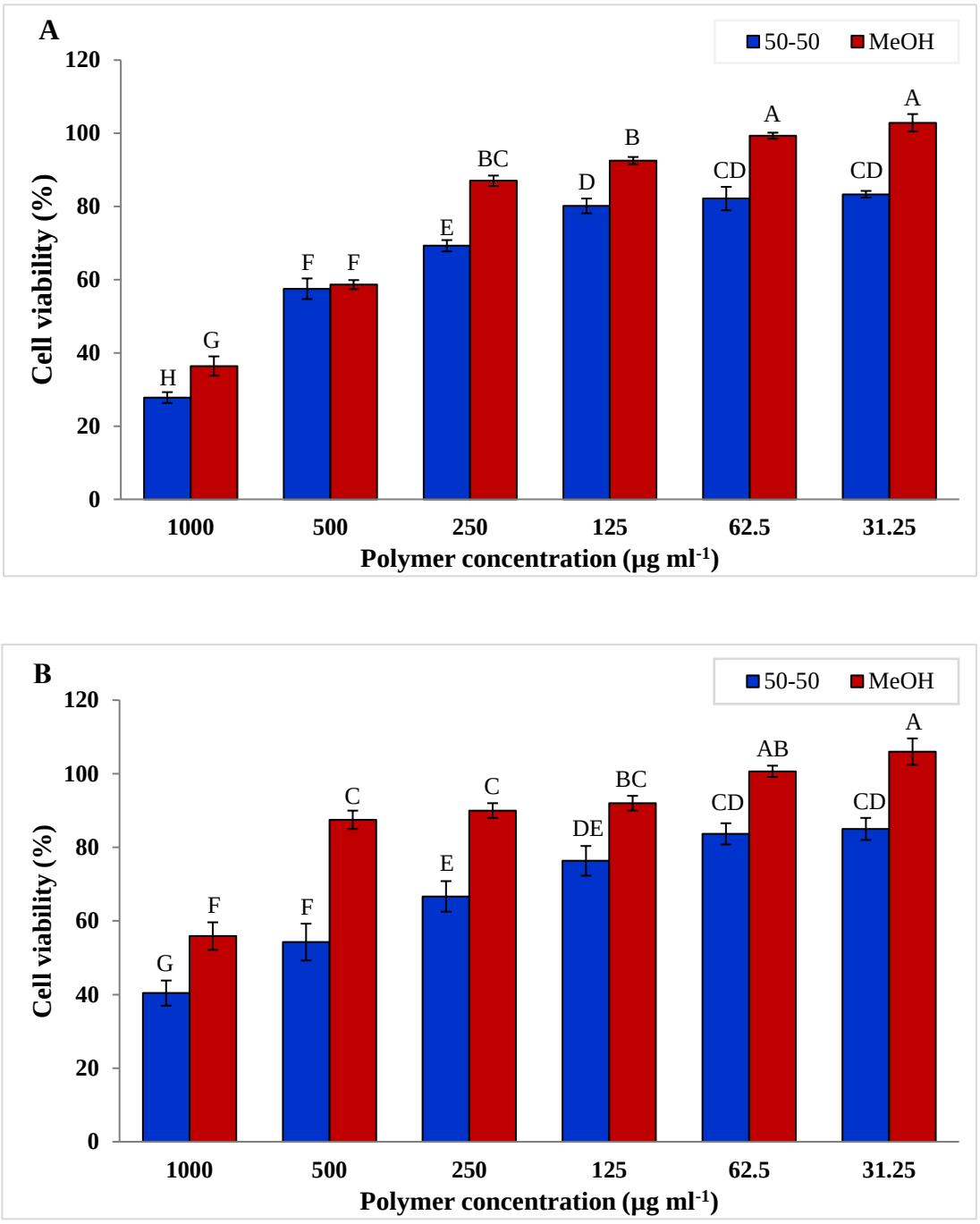


**Figure 5.7.** Cytotoxicity of 38 nm $MPC_{50}$-$DPA_{50}$ nanoparticles to (A) V79 cells and (B) 3T3 cells after 24 h exposure at concentrations ranging from 31.25 to 1000 µg $ml^{-1}$ at 37°C in 5% $CO_2$ determined by MTT assay (Mean ± SD, n=3) (Original in colour). *Bar values with different letters indicate a significant difference ($p < 0.05$) and those sharing the same letters are not significantly different ($p > 0.05$).*

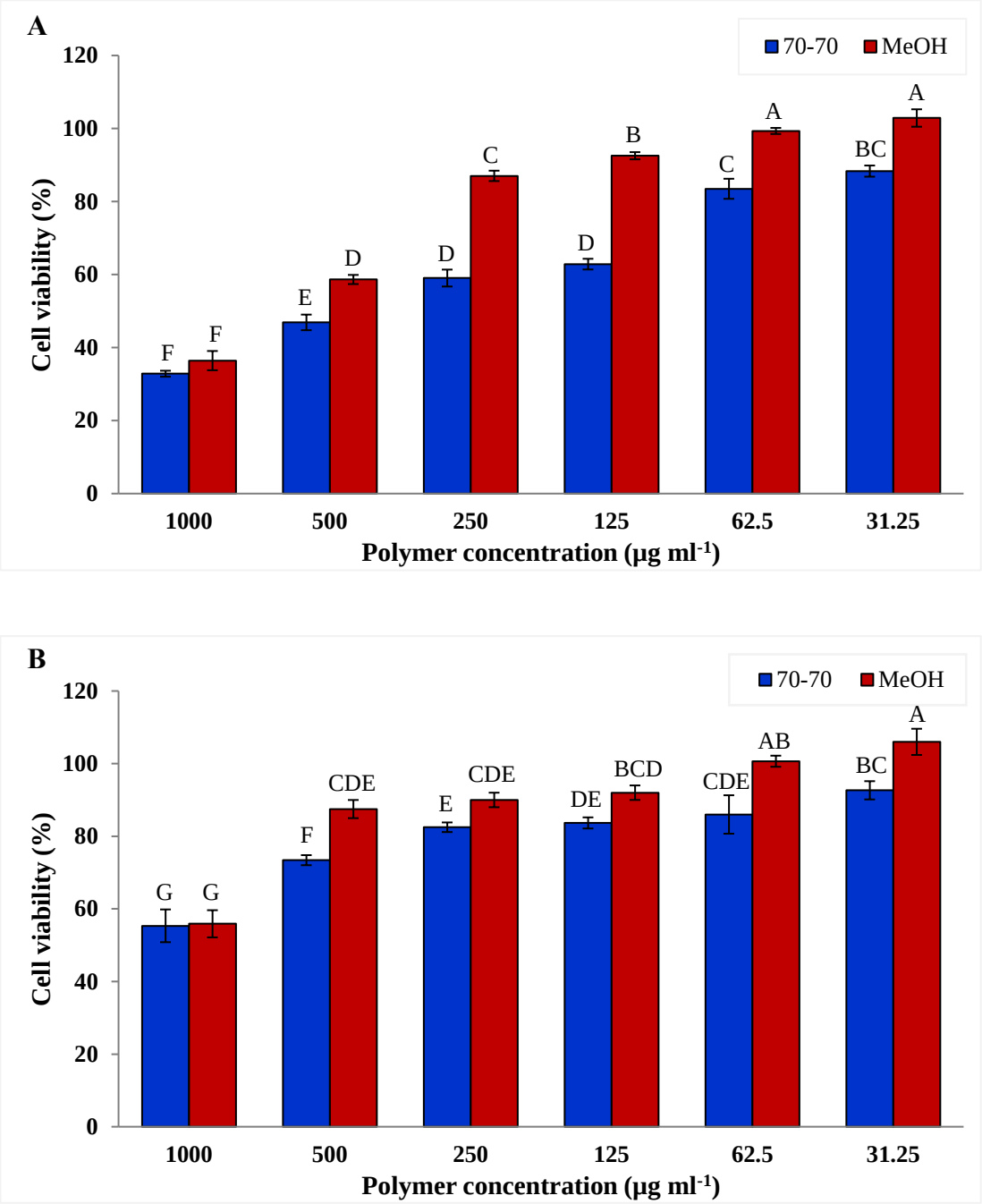


**Figure 5.8.** Cytotoxicity of 37 nm $MPC_{70}$-$DPA_{70}$ nanoparticles to (A) V79 cells and (B) 3T3 cells after 24 h exposure at concentrations ranging from 31.25 to 1000 µg $ml^{-1}$ at 37°C in 5% $CO_2$ determined by MTT assay (Mean ± SD, n=3) (Original in colour). *Bar values with different letters indicate a significant difference ($p < 0.05$) and those sharing the same letters are not significantly different ($p > 0.05$).*

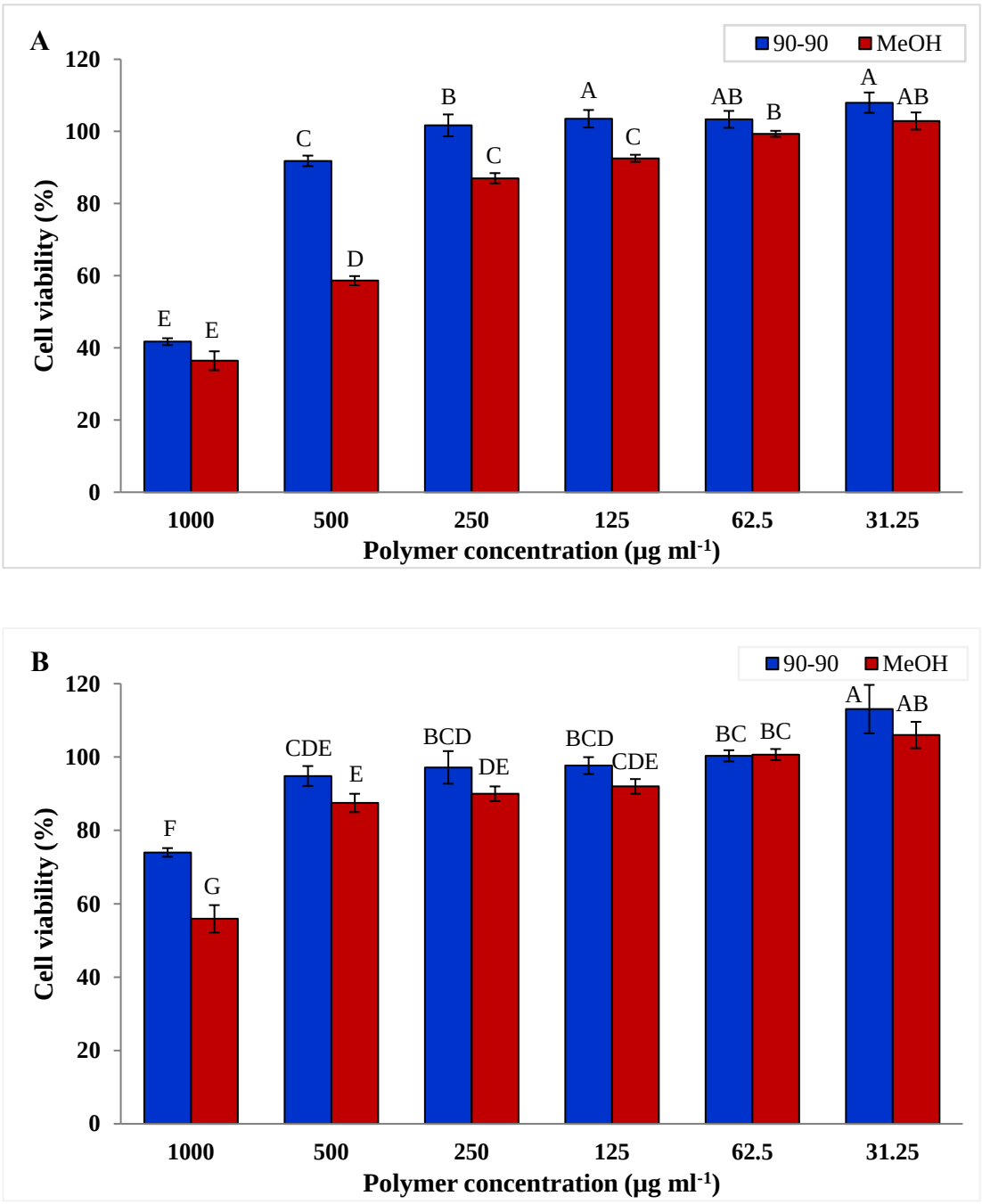


**Figure 5.9.** Cytotoxicity of 44 nm $MPC_{90}$-$DPA_{90}$ nanoparticles to (A) V79 cells and (B) 3T3 cells after 24 h exposure at concentrations ranging from 31.25 to 1000 µg $ml^{-1}$ at 37°C in 5% $CO_2$ determined by MTT assay (Mean ± SD, n=3) (Original in colour). *Bar values with different letters indicate a significant difference ($p < 0.05$) and those sharing the same letters are not significantly different ($p > 0.05$).*

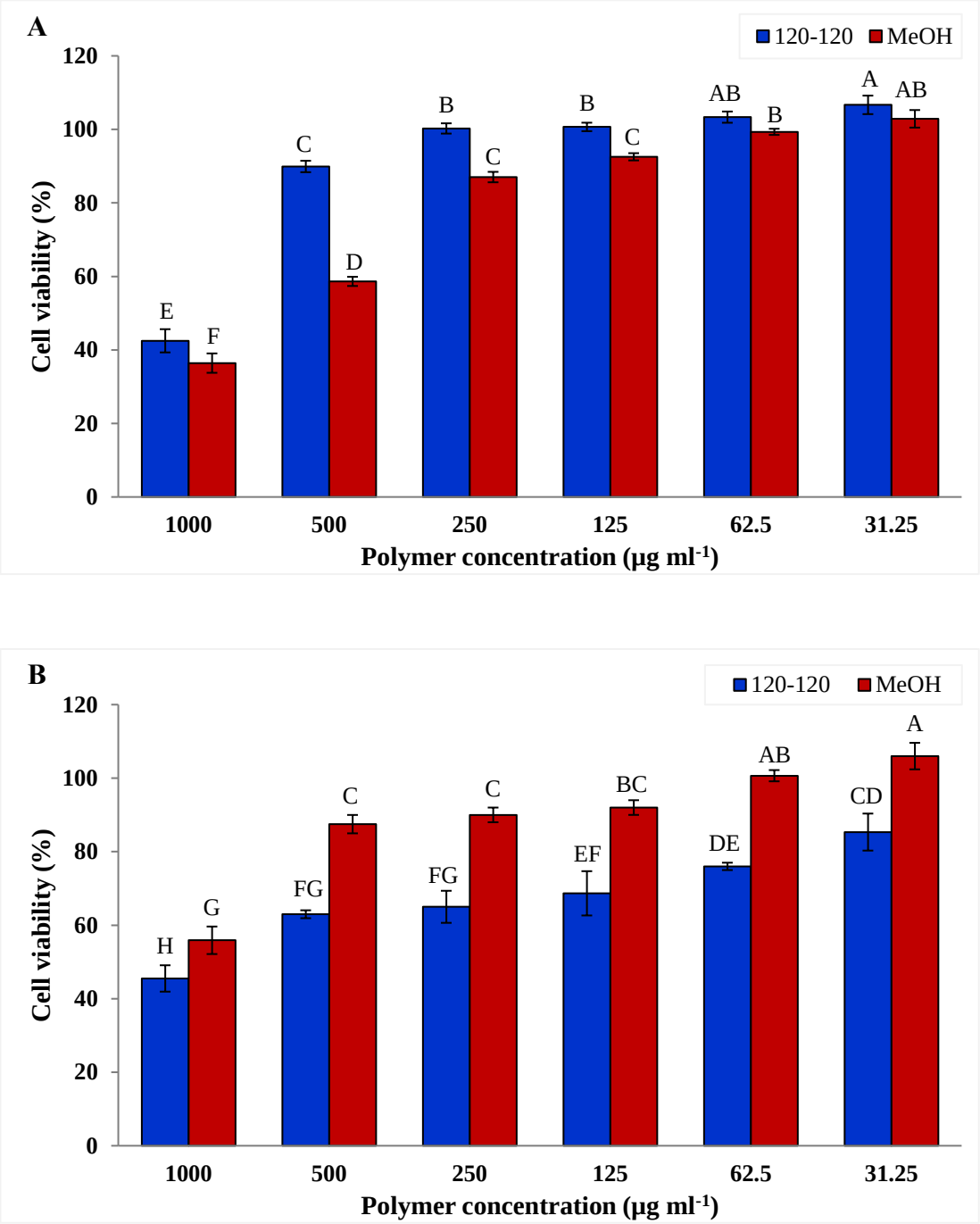


**Figure 5.10.** Cytotoxicity of 77 nm $MPC_{120}$-$DPA_{120}$ nanoparticles to (A) V79 cells and (B) 3T3 cells after 24 h exposure at concentrations ranging from 31.25 to 1000 µg $ml^{-1}$ at 37°C in 5% $CO_2$ determined by MTT assay (Mean ± SD, n=3) (Original in colour). *Bar values with different letters indicate a significant difference ($p < 0.05$) and those sharing the same letters are not significantly different ($p > 0.05$).*

### 5.2.2. Cellular uptake studies and flow cytometric analysis

In this project, the confocal laser scanning microscopy (CLSM) (as described in Section 2.2.3.6.2) and flow cytometry (FCM) (as described in Section 2.2.3.6.1); alongside the use of Coumarin-6 (Cm-6) as a fluorescent probe, were employed to monitor the uptake and internalisation of fluorescent MPC-DPA micelles into four different normal cell lines that were chosen as *in-vitro* models, namely Chinease hamester lung (V79), African green monkey kidney (Vero), human foetal lung (MRC-5), and Chinese hamester ovary (CHO). These cells were used to provide a platform to examine the uptake process and to evaluate the time-dependent intracellular incorporation after incubation with Cm-6-loaded MPC-DPA micelles for 1 min, 5 min, 10 min, 30 min, and 1 hour.

The CLSM images of V79 cells incubated with Cm-6-loaded MPC-DPA micelles showed that Cm-6-loaded MPC-DPA micelles were densely accumulated around the nuclei; in the cytoplasm, which indicated that the fluorescent micelles had been internalised into the cells successfully and a very rapid uptake was observed in the V79 cell line within 1 minute of incubation, as demonstrated by the high fluorescence intensity in Figure 5.11. Moreover, and despite that the intracellular uptake is time-dependent process, there was no statistically significant difference ($p > 0.05$) in the fluorescence intensity of Cm-6-loaded MPC-DPA micelles observed with longer incubation times (5 min, 10 min, 30 min, and 1 hour) as shown in CLSM images and the flow cytometric profiles of Cm-6-loaded MPC-DPA micelles in Appendix 13.0.

These results were consistent with the results obtained from flow cytometric analysis displayed with each incubation time as shown in Figure 5.12, which showed that the Cm-6-loaded MPC-DPA micelles exhibited a statistically significant ($p < 0.05$) higher uptake compared to free Cm-6, with the exception of the data recorded after 1 min

incubation time. Furthermore, it was well reported that the uptake process of nanoparticles is size-dependent, therefore, the smallest micelle (25 nm) had the highest cellular uptake; represented as the fluorescent intensity value which shifted depending on nanoparticle size, compared to the 38 nm and 44 nm micelles, as shown in flow cytometric histograms in all graphs of uptake in V79 cells (Figure 5.11 and Appendix 13.0).

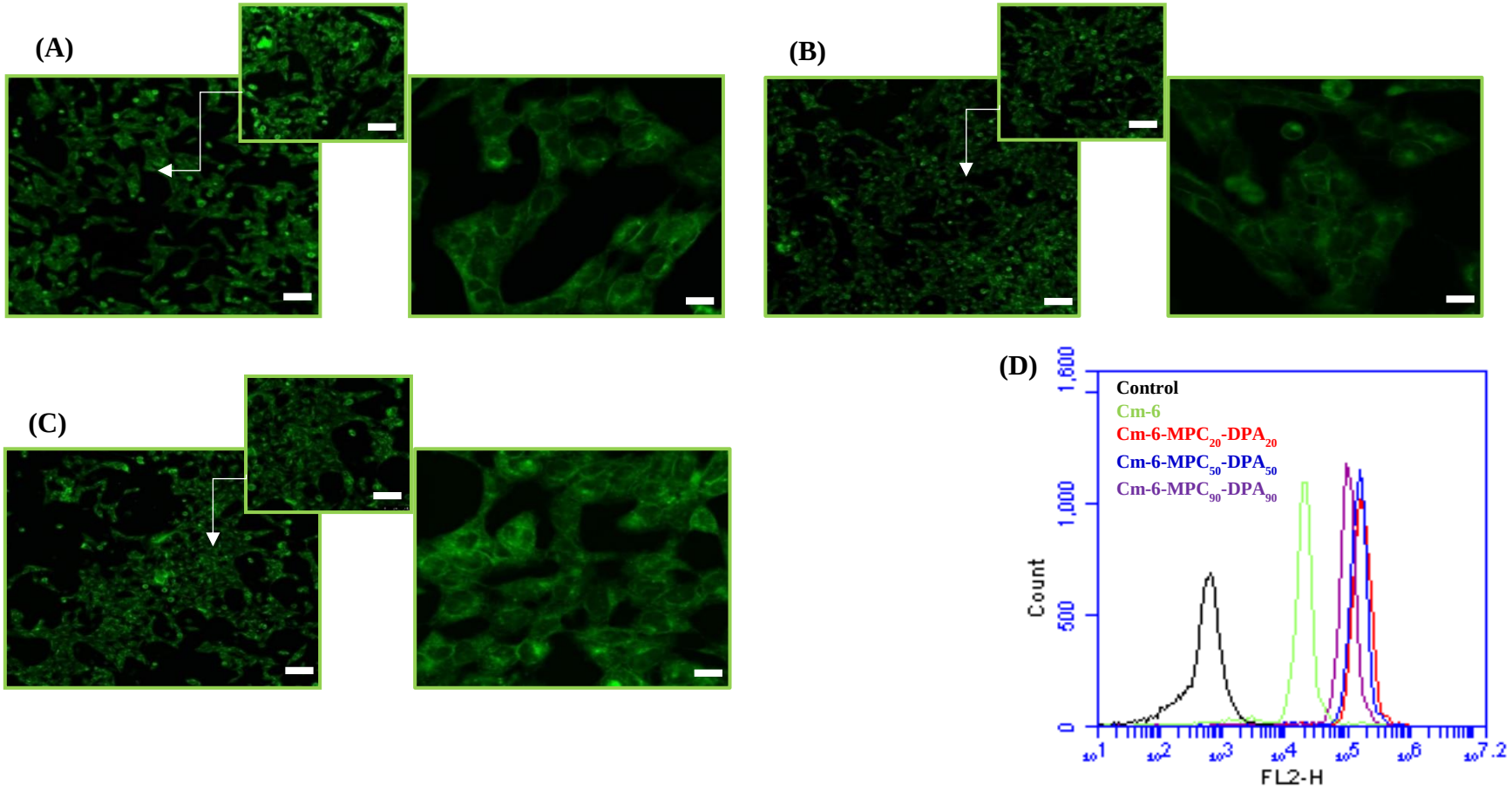


**Figure 5.11.** Confocal laser scanning microscopy (CLSM) images and flow cytometry histogram of V79 cells after 1 min incubation with Cm-6-loaded MPC-DPA micelles (A) Cm-6-$MPC_{20}$-$DPA_{20}$, (B) Cm-6-$MPC_{50}$-$DPA_{50}$, (C) Cm-6-$MPC_{90}$-$DPA_{90}$, (D) Flow cytometric profiles. Scale bars = 100, 50, and 25 µm. (Original in colour)

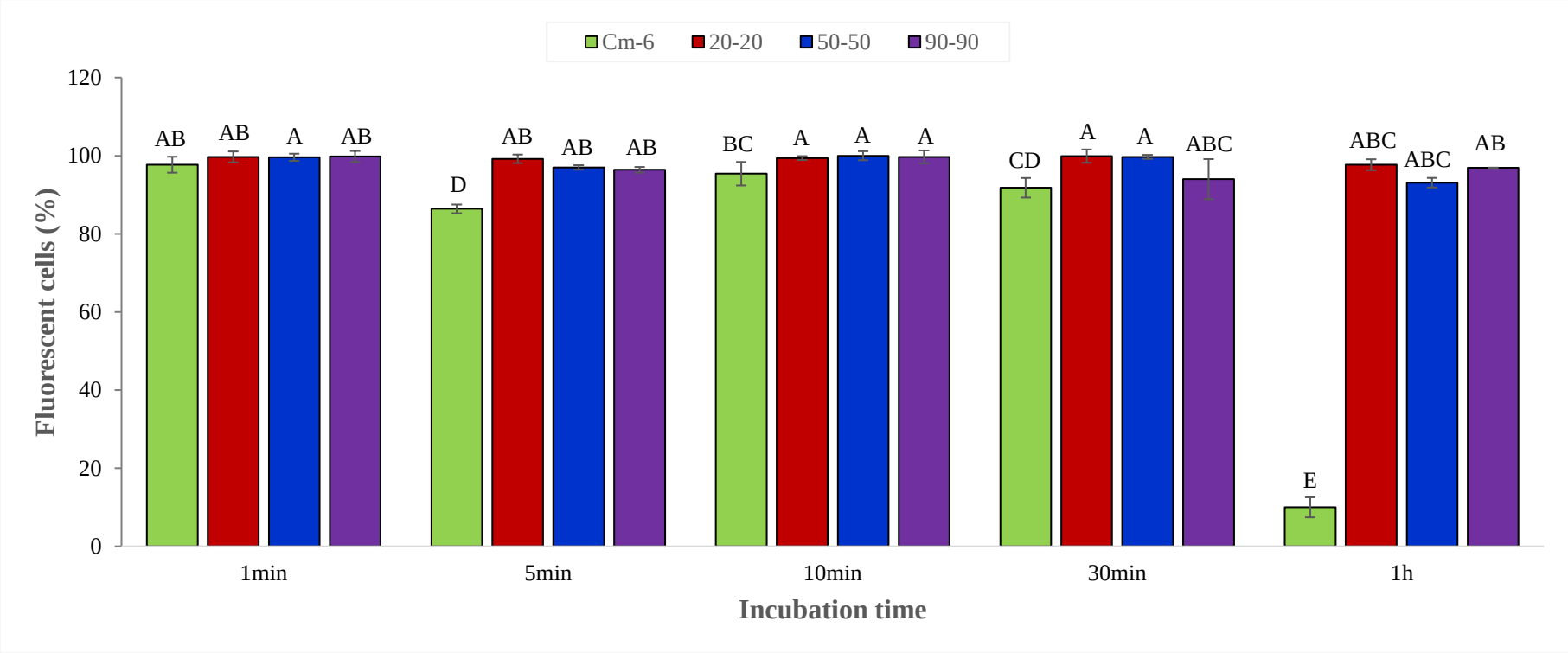


**Figure 5.12.** Quantification of the cellular uptake of Cm-6-loaded MPC-DPA micelles in V79 cells after incubation at 37°C at set time points. Flow cytometry determined the percentage of NP-positive cells (Mean ± SD, n=3) (Original in colour). *Bar values with different letters indicate a significant difference ($p < 0.05$) and those sharing the same letters are not significantly different ($p > 0.05$).*

Figure 5.13, displayed the CLSM images and flow cytometric profile of Vero cells incubated with Cm-6-loaded MPC-DPA micelles and a similar trend to that observed with the cellular uptake of Cm-6-loaded MPC-DPA micelles in V79 cell was observed (Figure 5.11), in that the fluorescent micelles were localised in the cytoplasm around the nuclei, which again indicated that the micelles had been internalised by the Vero cells successfully. Moreover, a very rapid uptake was again observed in the Vero cell line within 1 minute of incubation, as demonstrated by the high fluorescence intensity seen in Figure 5.13. There was no visual difference compared to the fluorescence intensity observed with longer incubation times (5 min, 10 min, 30 min, and 1 hour) as shown in Appendix 13.0. However, a time-dependent cellular uptake was observed with Vero cells incubated with Cm-6-loaded MPC-DPA micelles for extended times, and also compared to the cellular uptake of free Cm-6 as a function of incubation time as shown in Figure 5.14.

These results were consistent with the data obtained from the flow cytometric analysis displayed with each incubation time (Figure 5.14), which showed that the Cm-6-loaded MPC-DPA micelles exhibited statistically significant ($p < 0.05$) higher uptake compared to free Cm-6.

Generally, the fluorescent intensity values in the flow cytometry histograms tended to shift to the right in a size-dependent manner, therefore, higher uptake values were reported with 25 nm MPC-DPA micelles compared to the 38 nm and 44 nm MPC-DPA micelles, as shown in flow cytometric histograms in all graphs for uptake in Vero cell (Figure 5.13 and Appendix 13.0)

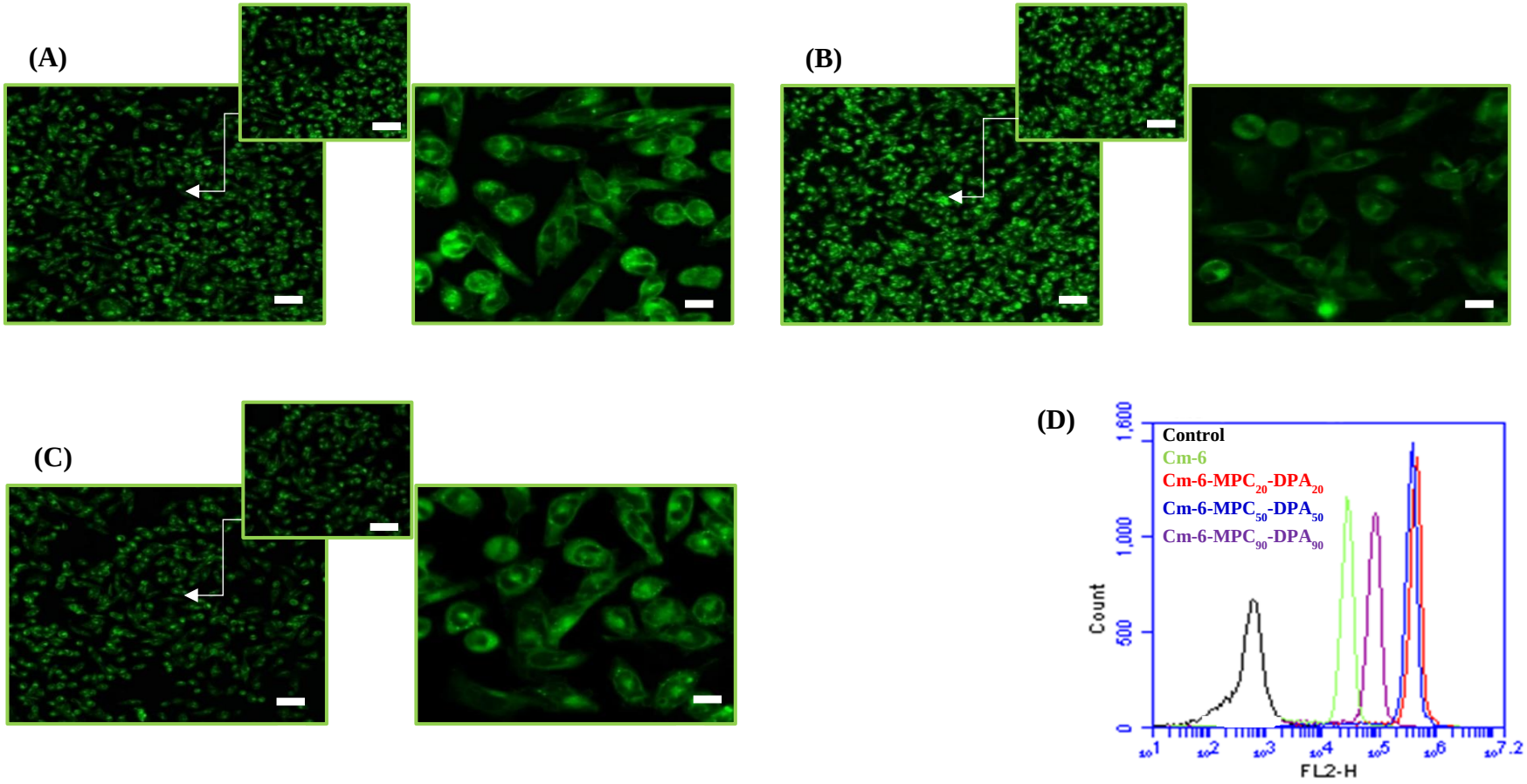


**Figure 5.13.** Confocal laser scanning microscopy (CLSM) images and flow cytometry histogram of Vero cells after 1 min incubation with Cm-6-loaded MPC-DPA micelles. (A) Cm-6-MPC$_{20}$-DPA$_{20}$, (B) Cm-6-MPC$_{50}$-DPA$_{50}$, (C) Cm-6-MPC$_{90}$-DPA$_{90}$, (D) Flow cytometric profiles. Scale bars = 100, 50, and 25 µm. (Original in colour)

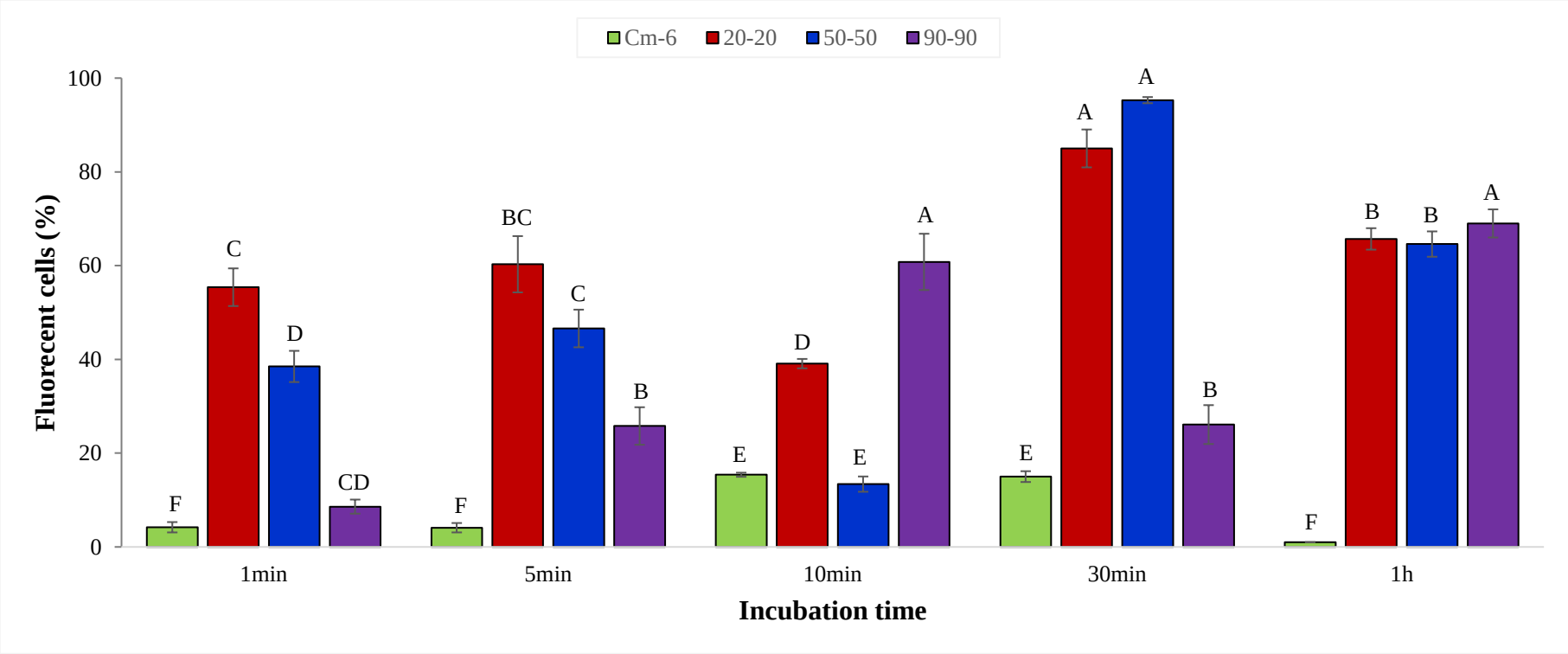


**Figure 5.14.** Quantification of the cellular uptake of Cm-6-loaded MPC-DPA micelles in Vero cells after incubation at 37°C at set time points. Flow cytometry determined the percentage of NP-positive cells, (Mean ± SD, n=3) (Original in colour). *Bar values with different letters indicate a significant difference ($p < 0.05$) and those sharing the same letters are not significantly different ($p > 0.05$).*

As drug uptake is a cell-dependent process (Sahay et al., 2010), other types of cells were therefore selected to examine the uptake in different cell lines. Figure 5.15, displayed the CLSM images and flow cytometric profile of MRC-5 cells incubated with Cm-6-loaded MPC-DPA micelles, which displayed that the fluorescent micelles were internalised into the cell cytoplasm as demonstrated by the high fluorescence intensity. Moreover, very rapid uptake was observed in the MRC-5 cell line within 1 minute of incubation, as demonstrated in Figure 5.15, with no visible difference compared to the fluorescence intensity observed with the longer incubation time (1 hour) as shown in Appendix 13.0. These results were again consistent with the data obtained from the flow cytometric analysis displayed in Figure 5.16 at a set range of time (1 min, 5 min, 10 min, 30 min, and 1 hour), which confirmed there was no statistically significant ($p > 0.05$) difference in the cellular uptake of Cm-6-loaded MPC-DPA micelles observed with longer incubation times. A similar result was obtained with free Cm-6, in which the cellular uptake did not vary under longer incubation times as shown in Figure 5.16.

Moreover, and as shown in Figure 5.16, a higher percentage of fluorescent cells was again detected with Cm-6-loaded MPC-DPA micelles compared to free Cm-6.

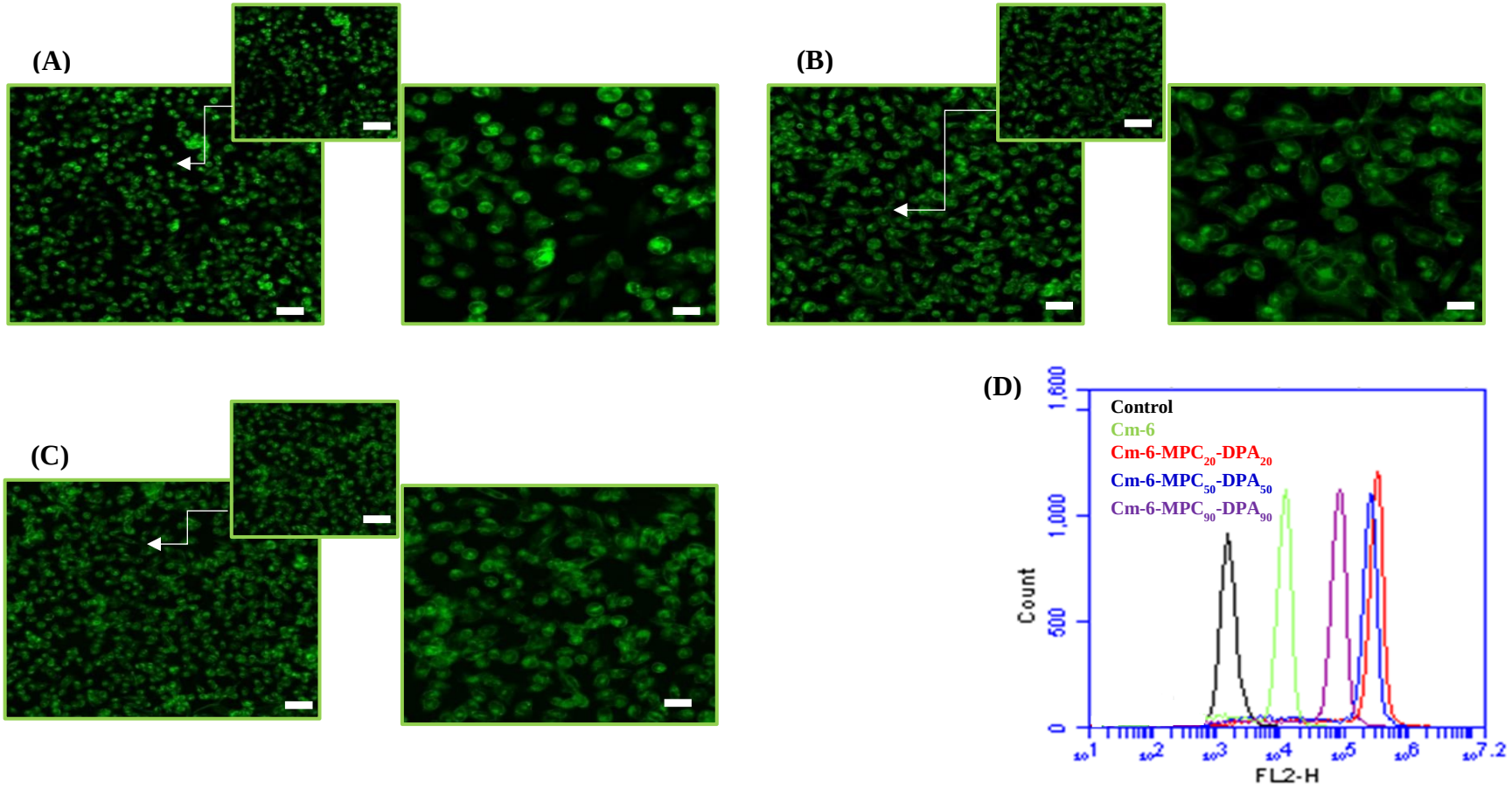


**Figure 5.15.** Confocal laser scanning microscopy (CLSM) images and flow cytometry histogram MRC-5 cells after 1 min incubation with Cm-6-loaded MPC-DPA micelles. (A) Cm-6-$MPC_{20}$-$DPA_{20}$, (B) Cm-6-$MPC_{50}$-$DPA_{50}$, (C) Cm-6-$MPC_{90}$-$DPA_{90}$, (D) Flow cytometric profiles. Scale bars = 100, 50, and 25 µm. (Original in colour)

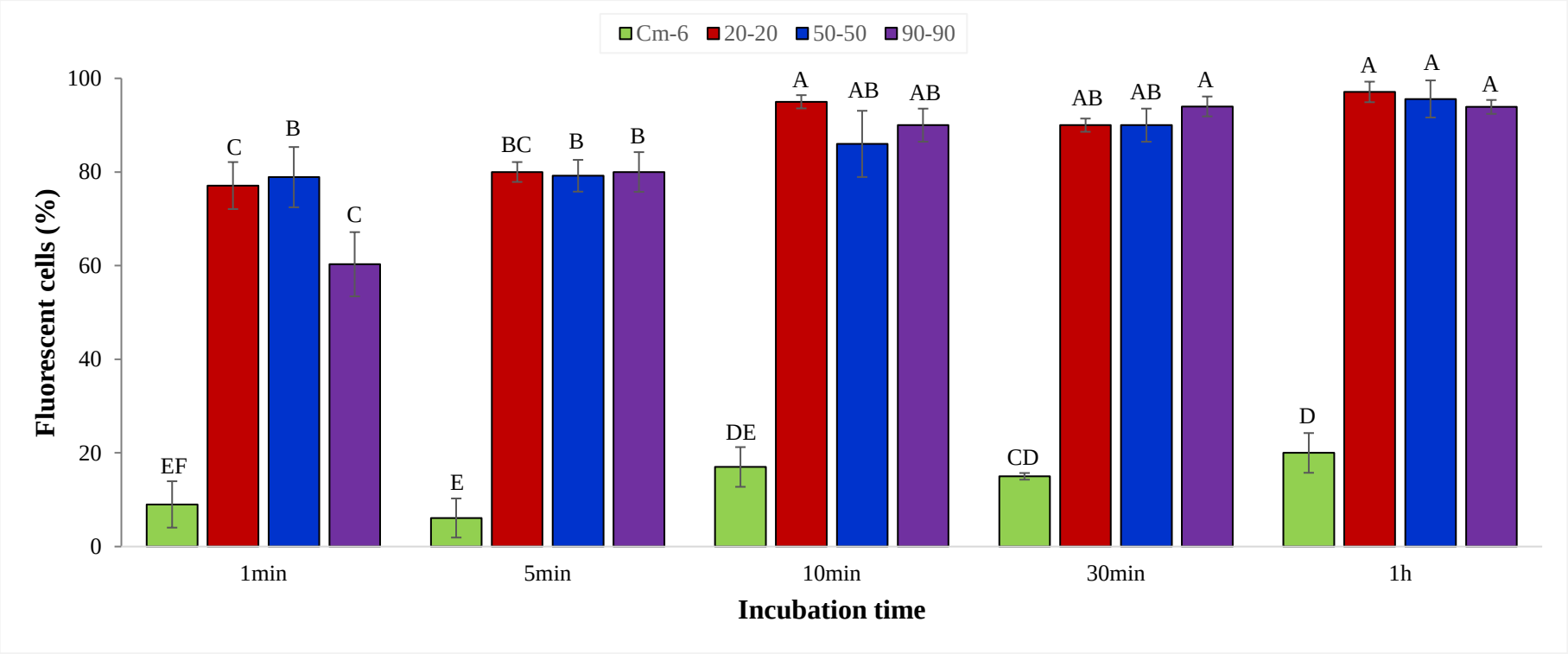


**Figure 5.16.** Quantification of the cellular uptake of Cm-6-loaded MPC-DPA micelles in MRC-5 cells after incubation at 37°C at set time points. Flow cytometry determined the percentage of NP-positive cells, (Mean ± SD, n=3) (Original in colour). *Bar values with different letters indicate a significant difference ($p < 0.05$) and those sharing the same letters are not significantly different ($p > 0.05$).*

Figure 5.17, displayed the CLSM images of Cm-6-loaded MPC-DPA micelles as a function of incubation time (1 min) in the CHO cell line, which indicated that the fluorescently labelled MPC-DPA micelles were internalised rapidly into the cells cytoplasm as demonstrated by the high fluorescence intensity. Moreover, very rapid uptake was once again observed in the CHO cell line within 1 minute of incubation, as demonstrated in Figure 5.17, with no visible difference compared to the fluorescence intensity observed with a longer incubation time (1 hour) as shown in Appendix 13.0. A quantitative analysis via flow cytometry was again carried out (as described in Section 2.2.3.6.1) to outline the effect of a set range of incubation times on the percentage of fluorescent cell uptake and the results are shown in Figure 5.18, which confirmed the successful uptake of Cm-6-loaded MPC-DPA micelles.

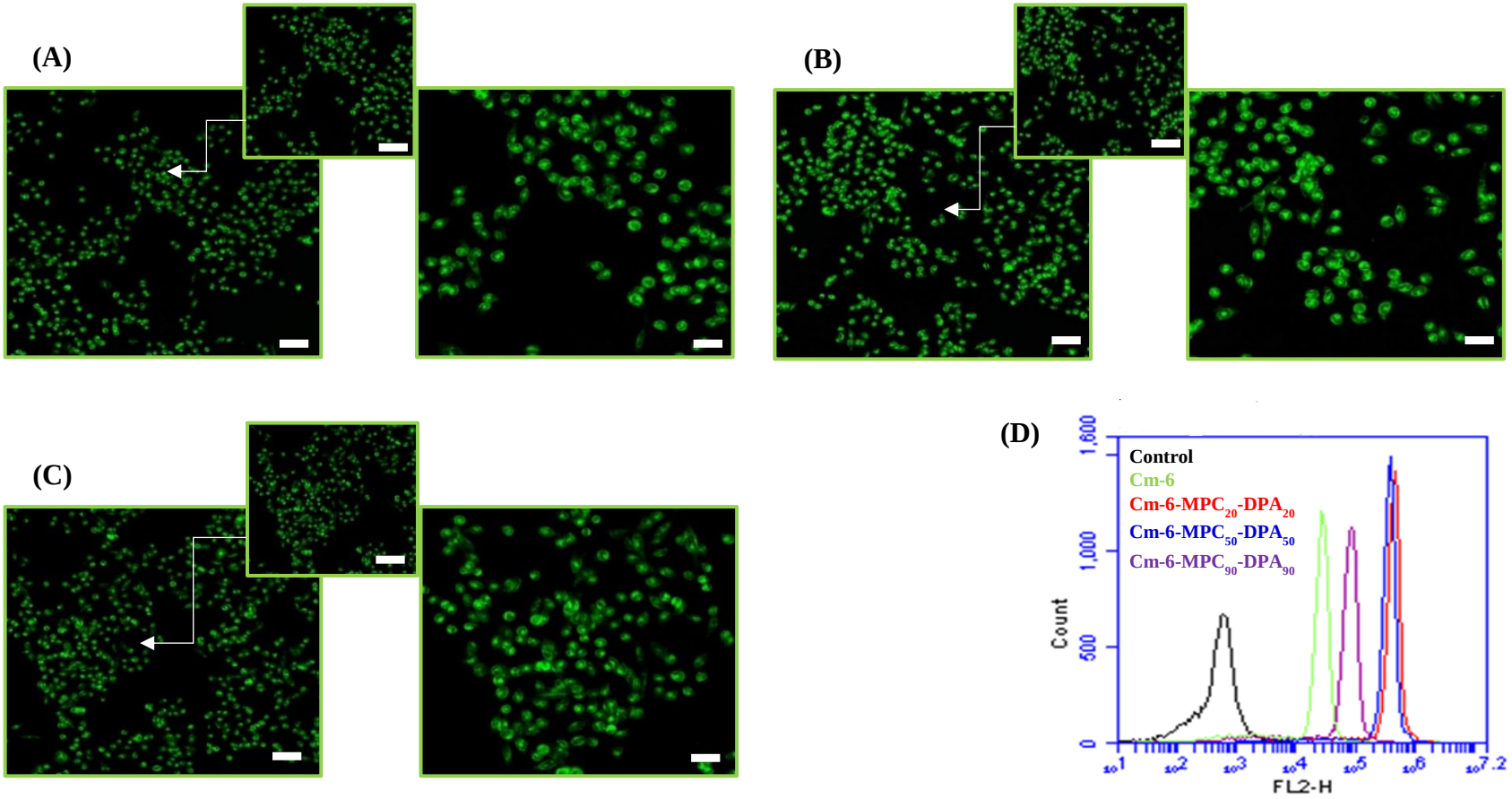


**Figure 5.17.** Confocal laser scanning microscopy (CLSM) images and flow cytometry histogram CHO cells after 1 min incubation with Cm-6-loaded MPC-DPA micelles. (A) Cm-6-$MPC_{20}$-$DPA_{20}$, (B) Cm-6-$MPC_{50}$-$DPA_{50}$, (C) Cm-6-$MPC_{90}$-$DPA_{90}$, (D) Flow cytometric profiles. Scale bars = 100, 50, and 25 µm. (Original in colour)

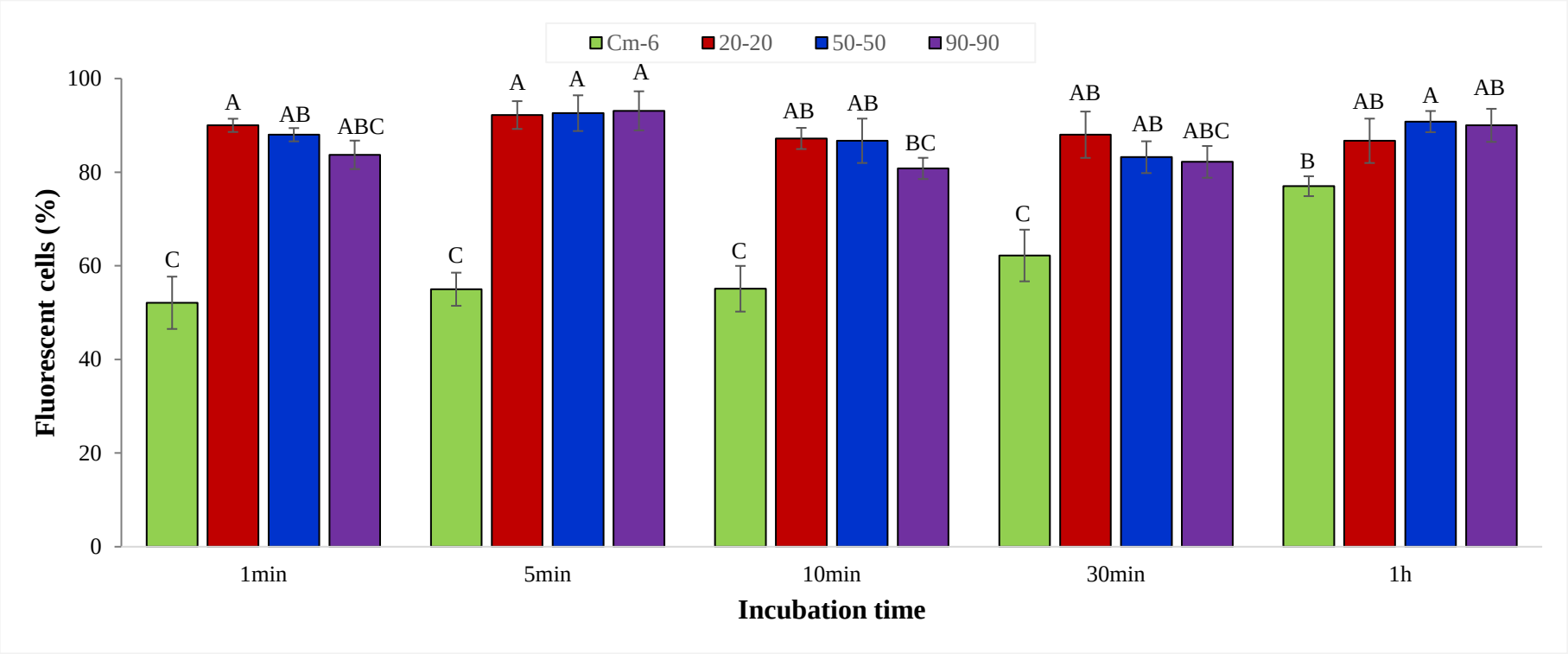


**Figure 5.18.** Quantification of the cellular uptake of Cm-6-loaded MPC-DPA micelles in CHO cells after incubation at 37°C at set time points. Flow cytometry determined the percentage of NP-positive cells, (Mean ± SD, n=3) (Original in colour). *Bar values with different letters indicate a significant difference ($p < 0.05$) and those sharing the same letters are not significantly different ($p > 0.05$).*

### 5.2.3. Uptake mechanism studies

It was reported that micelles are primarily internalised into cells via endocytic mechanisms (Xiao et al., 2011; Li et al., 2014c), whilst free drug molecule uptake is via passive diffusion mechanisms. However, some studies have demonstrated that endocytosis is not always responsible for the uptake of nanoparticles, especially when a rapid uptake has taken place (within minutes). Therefore, inhibition studies of endocytosis were carried out on all of the cell lines involved in this project, with the data obtained via the flow cytometry technique (as described in Section 2.2.3.6.3). A decrease in the incubation temperature from 37°C to 4°C is considered an effective means to inhibit endocytosis (Dausend et al., 2008; Cartiera et al., 2009), therefore, this method was used here, and the data are shown in Figure 5.19, 5.20, 5.21, and 5.22 for V79, Vero, MRC-5, and CHO cell lines, respectively.

The result for V79 cells incubated with Cm-6-loaded MPC-DPA micelles for 1 hour at 37°C and 4°C are displayed in Figure 5.19, and show that a statistically significant ($p < 0.05$) inhibition of endocytosis took place with all of the Cm-6-loaded MPC-DPA micelles at 4°C compared to 37°C, which indicated that the endocytosis was the uptake mechanism in V79 cells. Moreover, a statistically significant ($p < 0.05$) increase in cellular uptake was seen with the V79 cells treated with free Cm-6 at 4°C, which indicated that free Cm-6 uptake was via a passive diffusion mechanism.

As shown in Figure 5.20 for Vero cells incubated with Cm-6-loaded MPC-DPA micelles for 1 hour at 37°C and 4°C, a statistically significant ($p < 0.05$) inhibition of endocytosis had occurred, except for the 25 nm Cm-6-loaded MPC-DPA micelles. The 25 nm micelles exhibited an increased uptake, even after endocytosis inhibition, compared to that reported with 38 nm and 44 nm Cm-6-loaded MPC-DPA micelles.

Moreover, there was no statistically significant ($p > 0.05$) effect between the Vero cells treated with free Cm-6 at 37°C and 4°C.

The results for MRC-5 cells incubated with Cm-6-loaded MPC-DPA micelles for 1 hour at 37°C and 4°C are displayed in Figure 5.21, and again a statistically significant ($p < 0.05$) inhibition of endocytosis had occurred with all of the Cm-6-loaded MPC-DPA micelles at 4°C, which indicated that the endocytosis was the uptake mechanism in MRC-5 cells. Furthermore, there was no statistically significant ($p > 0.05$) difference between the MRC-5 cells treated with free Cm-6 at 4°C compared to 37°C.

The fourth selected cells to examine the mechanism of cellular uptake were CHO cells, and Figure 5.22 displayed the results for CHO cells incubated with Cm-6-loaded MPC-DPA micelles for 1 hour at 37°C and 4°C. No statistically significant ($p > 0.05$) inhibition of uptake was observed with all of the Cm-6-loaded MPC-DPA micelles at 4°C compared to that at 37°C. Moreover, a statistically significant ($p < 0.05$) increase in the uptake of free Cm-6 took place after incubation at 4°C, which indicated that the diffusion process was the uptake mechanism in CHO cells.

In conclusion, the MPC-DPA micelles with their entrapped drug (Cm-6) have been internalised into the cytoplasm of four different cell lines, as visually confirmed by CLSM images and quantitively via FCM, with a high cellular uptake achieved in different cell lines via different mechanisms.

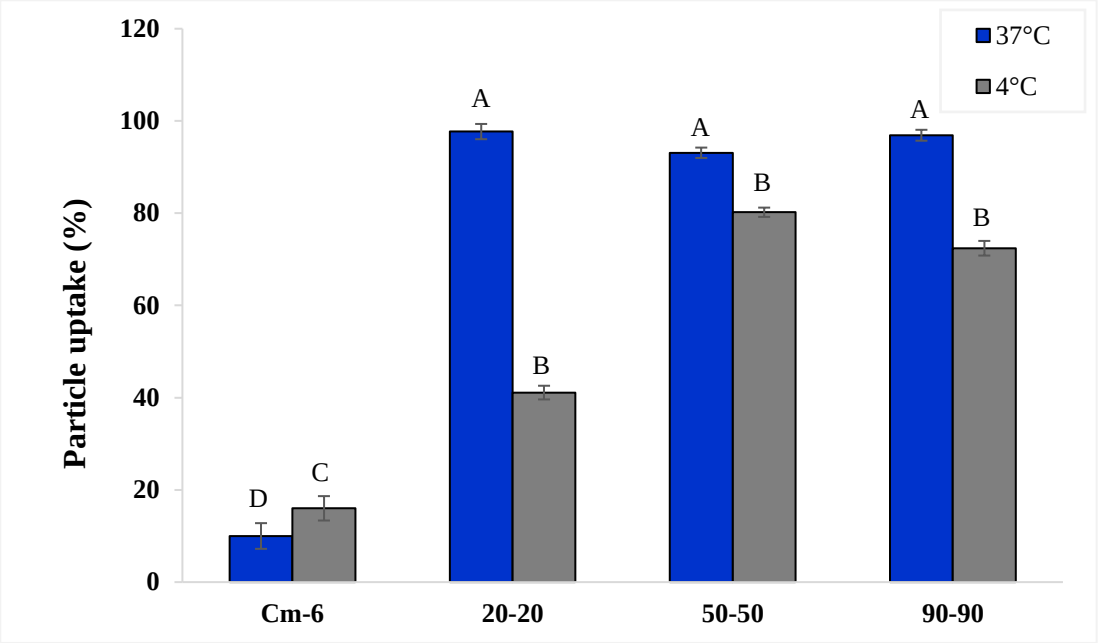


**Figure 5.19.** Uptake of Cm-6-loaded MPC-DPA micelles by V79 cells incubated at 37°C and 4°C for 1 hour determined by flow cytometry (Mean ± SD, n=3) (Original in colour). *Bar values with different letters indicate a significant difference ($p < 0.05$) and those sharing the same letters are not significantly different ($p > 0.05$).*

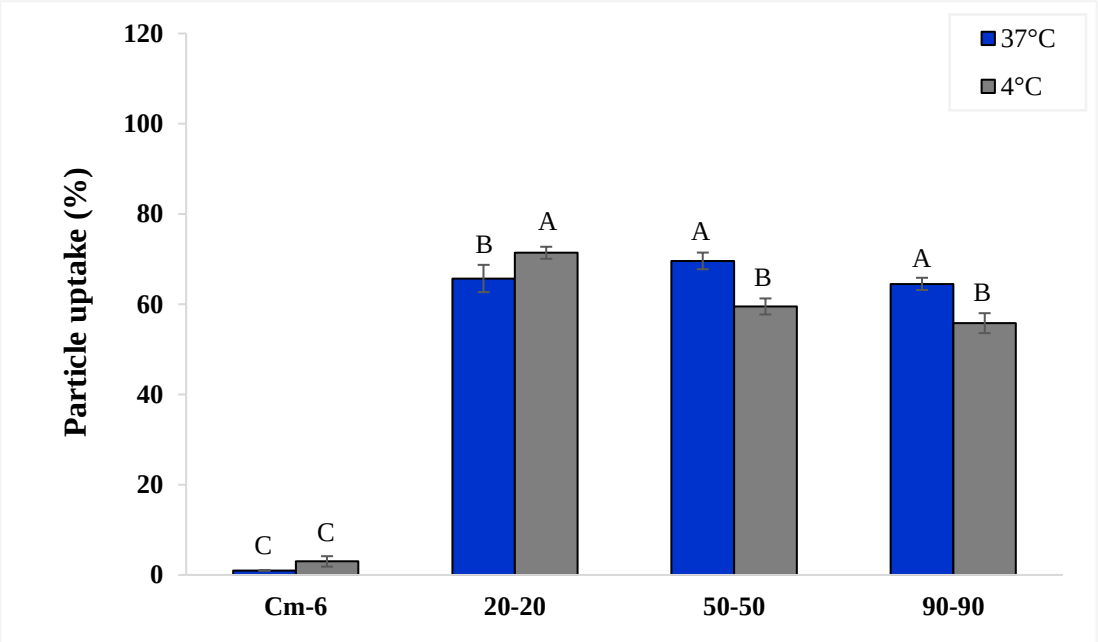


**Figure 5.20.** Uptake of Cm-6-loaded MPC-DPA micelles by Vero cells incubated at 37°C and 4°C for 1 hour determined by flow cytometry (Mean ± SD, n=3) (Original in colour). *Bar values with different letters indicate a significant difference ($p < 0.05$) and those sharing the same letters are not significantly different ($p > 0.05$).*

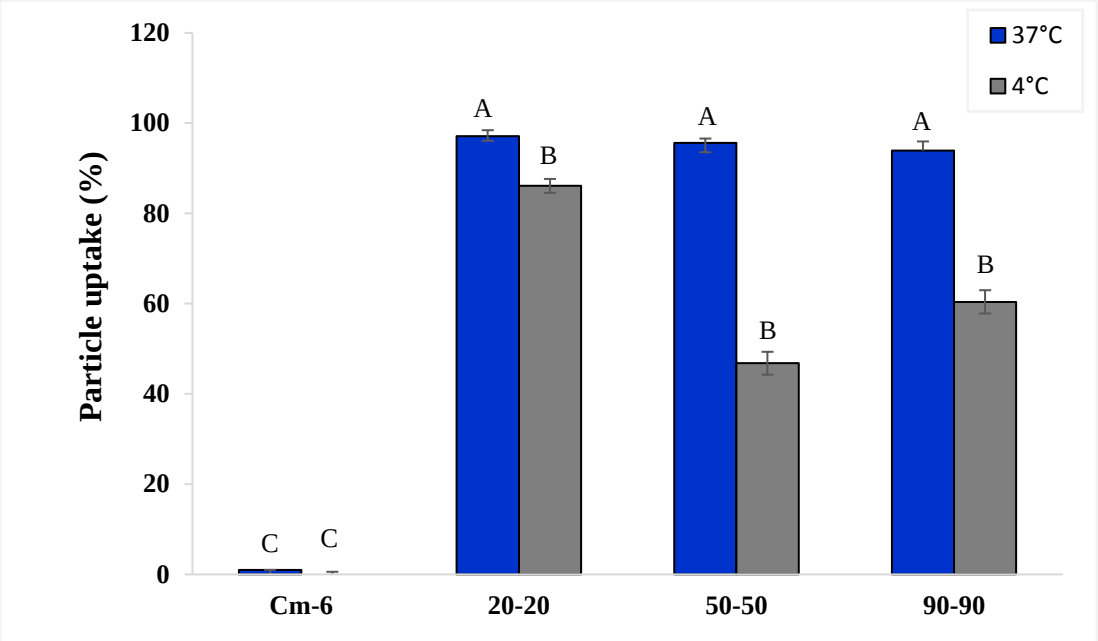


**Figure 5.21.** Uptake of Cm-6-loaded MPC-DPA micelles by MRC-5 cells incubated at 37°C and 4°C for 1 hour determined by flow cytometry (Mean ± SD, n=3) (Original in colour). *Bar values with different letters indicate a significant difference ($p < 0.05$) and those sharing the same letters are not significantly different ($p > 0.05$).*

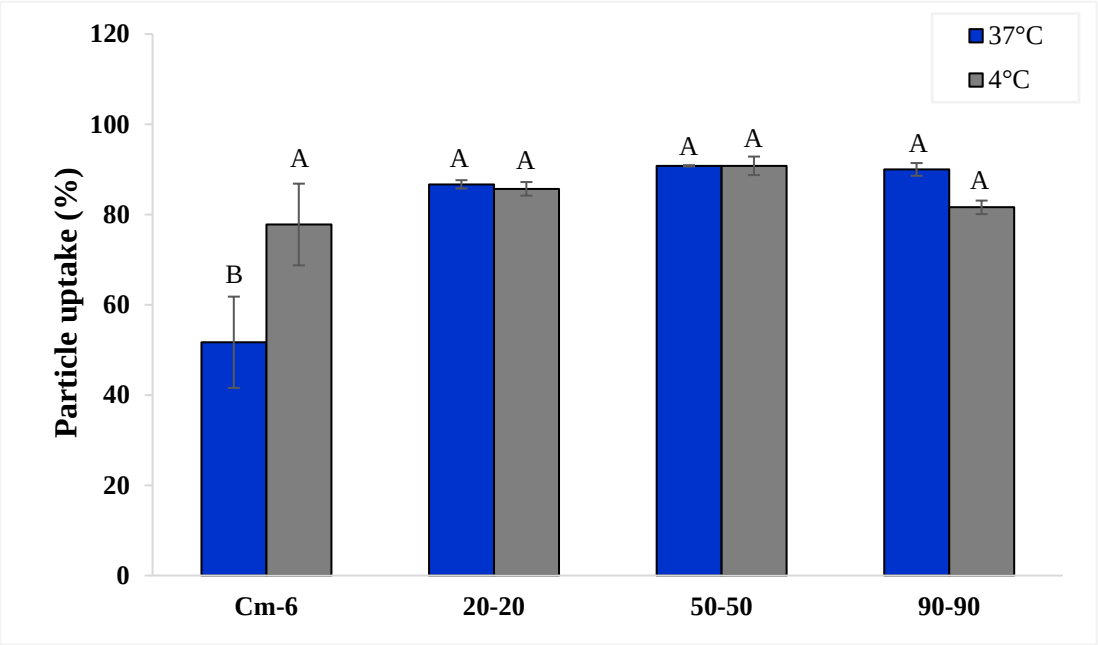


**Figure 5.22.** Uptake of Cm-6-loaded MPC-DPA micelles by CHO cells incubated at 37°C and 4°C for 1 hour determined by flow cytometry (Mean ± SD, n=3) (Original in colour). *Bar values with different letters indicate a significant difference ($p < 0.05$) and those sharing the same letters are not significantly different ($p > 0.05$).*

## 5.3. Discussion

The aim of this chapter was to examine how different cells respond to MPC-DPA micelles of variable sizes through monitoring their cell viability, cellular uptake and potential mechanisms of uptake, in order to improve the safety and efficacy of the developed nanoparticles. Therefore, the uptake of MPC-DPA polymeric micelles by different cell types and the cytotoxicity associated with micelles exposure was investigated.

### 5.3.1. Effect of MPC-DPA self-assembled nanoparticles on cell viability

Due to the rise in the number and the type of nanoparticles used in various fields of nanotechnology, a growing concern about their toxicity and their effect on the body has become an increasingly important issue (Kong et al., 2011). Currently, several approaches have been used to assess nanoparticle cytotoxicity via *in-vitro* and *in-vivo* examinations. However, although *in-vivo* and *in-vitro* experiments may provide different outcomes, *in-vitro* investigations are widely used to provide preliminary results regarding the potential toxicity of nanoparticles, as the application, control and interpretation of the results are relatively straightforward compared to *in-vivo* tests (Mei et al., 2009; Kong et al., 2011; Bahadar et al., 2016).

In this project, the *in-vitro* cytotoxicity tests were carried out to verify that the products used in the synthesis (e.g. copper catalyst) and preparation (e.g. methanol) of MPC-DPA nanoparticles did not lead to the formation of toxic compounds that could compromise patient health when they utilise as drug delivery system. However, despite the low levels of copper reported in all synthesised MPC-DPA diblock copolymer as mentioned earlier in Chapter 3 (Table 3.2), and no reported cytotoxicity associated with the use of methanol in MPC-DPA formulations in previous studies

(Salvage et al., 2015; Salvage et al., 2016), *in-vitro* cell cytotoxicity studies were conducted on the selected 1:1 MPC-DPA nanoparticles.

There are a wide range of *in-vitro* cytotoxicity assays that have been developed to test the cytotoxicity of nanoparticles with the conventional colorimetric-based assays providing an indication of the effect of nanoparticles on cell proliferation and viability. Therefore, the colony forming or clonogenic assay was used to determine the effect of a range of MPC-DPA nanoparticles concentrations (31.25-1000 μg $ml^{-1}$) on the ability of cells to multiply to form colonies, and the results (Figure 5.1- Figure 5.5) indicated the low cellular toxicity of MPC-DPA copolymers, which was in a good agreement with previous reports using MPC-DPA as a nanocarrier (Salvage et al., 2005; Massignani et al., 2009; Salvage et al., 2016).

However, there was a statistically significant ($p < 0.05$) reduction in cell survival at high concentrations that can be attributed to cell growth disruption caused by a reduction in cell medium due to the dilution process that cause cell stress or reduced cell growth (as described in Section 2.2.3.5.1) (Salvage et al., 2015). Furthermore, no statistically significant ($p > 0.05$) toxicity was observed with the use of methanol as a control, and cell survival was comparable to that of MPC-DPA nanoparticles. An exception was seen at the highest polymer concentration (1000 μg $ml^{-1}$) in which MPC-DPA polymeric nano-systems caused a reduction in cell viability compared to methanol that can be attributed to the 50% media dilution used as mentioned previously.

Although the cell colony formation assay is a well-established test (Franken et al., 2006), it does not provide a direct indication of cell death or survival, therefore, other assays can be used to provide more detail about cell viability. One of the most widely used cell assays for the quantitative determination of drug sensitivity and cytotoxicity

is the MTT assay, which is considered rapid, versatile, and a highly reproducible test. Generally, the nanoparticles cytotoxicity is highly dependent on the type of cell tested as the variation in cell physiology, proliferation rate and membrane characteristics that exist between different cell lines can affect MTT result. Therefore, in this study, the MTT assay was used to determine the viability of V79 and 3T3 cells after 24 hours exposure to MPC-DPA nanoparticles, and as seen from Figure 5.6 to Figure 5.10, MPC-DPA nanoparticles had only a limited or not significant effect in both cell lines, which can be attributed to the biomimetic zwitterionic properties of the MPC monomer. These results were in close agreement with other reported studies (Massignani et al., 2009; Salvage et al., 2016). Moreover, it was noted that in all cytotoxicity graphs (Figure 5.1- Figure 5.10), there was no residual MeOH toxicity, which indicated that using MeOH in the formation of nanoparticles via nanoprecipitation was acceptable for *in-vitro* testing. These findings were consistent with cytotoxicity results reported from other MeOH-based nanoprecipitation prepared MPC-DPA micelles (Salvage et al., 2015; Salvage et al., 2016). It was noted that the MPC-DPA polymeric nano-systems caused a higher reduction in the cell viability in some MTT assay graphs compared to methanol and this is attributed to the higher cellular uptake of nanoparticles, which mediated a higher cytotoxicity than that observed with the solvent used (Misra et al., 2015).

In both *in-vitro* cytotoxicity assays (Figure 5.1- Figure 5.10), a size-dependent toxicity was recorded, in which small MPC-DPA polymeric nano-systems displayed a relatively higher reduction in cellular viability compared to the larger nanoparticles, as the former possess a high surface area relative to their total mass that increases the chance of interaction with the surrounding biomolecules and thereby induces adverse responses (Pan et al., 2007; Kyung et al., 2009; Shang et al., 2014b).

### 5.3.2. The intracellular uptake kinetics of Cm-6-loaded MPC-DPA micelles in normal cells

In order to examine the characteristics of cellular uptake of MPC-DPA micelles, Cm-6 was used as a fluorescent probe to investigate the uptake kinetics of different size MPC-DPA micelles, at different time points, at 37°C, as described in Section 2.2.3.6.1 and 2.2.3.6.2), which was observed via confocal laser scanning microscopy and flow cytometry. Although, a number of techniques are available to monitor nanoparticle internalisation into cells, confocal laser scanning microscopy (CLSM) and flow cytometry (FCM) are considered the most commonly used techniques to study the cellular uptake of nanoparticles, qualitatively and quantitatively (Shi et al., 2015b; Jiang et al., 2016; Li et al., 2017).

Moreover, the hydrophobic fluorescent dye coumarin-6 (Cm-6) is one of the most widely used probes to substitute for hydrophobic drugs in micelles (Shi et al., 2015b; Salvage et al., 2016; Kumar et al., 2017; Hu et al., 2017), due to its biocompatibility and high fluorescence activity (Zhang et al., 2010b). In general, the efficiency of nanoparticle uptake and internalisation depends on nanoparticle physicochemical characteristics, incubation time, and type of cells used (Shang et al., 2014a). Therefore, MPC-DPA micelles uptake was studied in normal and malignant cells to examine if MPC-DPA micelles demonstrated different uptake mechanisms depending on the cell type.

#### 5.3.2.1. Effect of incubation time

The incubation time in several reported studies had an impact on nanoparticle uptake, in which a gradual increase in uptake was observed with an increase in the exposure time (Davda and Labhasetwar, 2002; Li et al., 2014c; Li et al., 2016; Hu et al., 2017). Here in, a strong Cm-6 fluorescence was observed in the cell cytoplasm after

incubation with Cm-6-loaded MPC-DPA micelles compared to cells treated with free Cm-6 (control), indicating that micelles facilitated Cm-6 intracellular uptake, this was consistent with previous reports for both MPC-DPA micelles (Salvage et al., 2016), and other nanoparticles (Zhang et al., 2014; Zeng et al., 2015). Moreover, the cellular uptake of Cm-6 loaded MPC-DPA micelles assayed at different incubation time points, 1 min, 5 min, 10 min, 30 min, and 1 hour, demonstrated that fluorescence aggregates were present in all of the analysed cells (Figure 5.11-Figure 5.18), and increased with extended exposure time in some cell lines (Vero and MRC-5), where micelles accumulated around the nucleus and between cell organelles. However, in V79 and CHO cell lines, a high fluorescent intensity after 1 min was observed that did not vary with extended exposure time, as uptake is a cell-dependent process and cells vary with their responses to nanoparticles (Sohaebuddin et al., 2010; Adjei et al., 2014; Sulheim et al., 2016).

Additionally, and as shown in CLSM images and the quantitative analysis of cellular uptake via FCM (Figure 5.11-Figure 5.18) the cellular internalisation process was very rapid; within 1 min after incubation with fluorescent MPC-DPA micelles in all cell lines tested, which may have indicated that the uptake occurred via a less-energy dependent mechanism such as cell contact diffusion rather than endocytosis (Snipstad et al., 2014).

#### 5.3.2.2. Effect of nanoparticle size and shape

It is well reported that nanoparticle size is among the most important parameters that affect the fate of cancer nanomedicines (Sahay et al., 2010), as size has an impact on nanoparticle circulation in blood compartments, tumour accumulation via EPR effect, tissue penetration and tumour cell internalisation, and finally intracellular drug release (Wang et al., 2015b). For example, micelles of 100 nm had long circulation times and

better accumulation at tumour sites compared small size micelles (i.e. 30 nm) but they had a lower penetration efficacy (Sun et al., 2014a). Moreover, Cabral et al, found that micelles with diameters of 30-100 nm penetrated a highly permeable tumour (Cabral et al., 2011), therefore, despite the contradictory results obtained from studies involved in investigating the effect of nanoparticle size on cellular uptake, there are several other studies that have reported that the particle size range of 20-50 nm were more rapidly uptaken than other larger or smaller particles (Iversen et al., 2011; Chang et al., 2016). In addition to size, nanoparticle shape also affects cellular uptake, as cells tend to internalise spherical nanoparticles more efficiently than rod-shaped or cylindrical nanoparticles (Chithrani et al., 2006; Zhang et al., 2009; Yuan and Zhang, 2010), due to the different curvature of the adsorbed nanoparticles experienced by the cell (Florez et al., 2012). In this project, Cm-6 was loaded into spherical MPC-DPA micelles as confirmed by STEM data in Chapter 4.

As shown in the CLSM images and flow cytometer results (Figure 5.11-Figure 5.18 and Appendix 13.0), there was a trend observed in the cell types used in the experiments by which the smaller particle sized micelles (25 nm), had relatively higher cellular uptake compared to the other MPC-DPA micelles (38 nm and 44 nm). This effect can be attributed to the high degree of binding of small nanoparticles to cell membrane receptors, which affects their cellular uptake (Bhattacharjee et al., 2012). These findings were in close agreement with previously reported studies that a higher intracellular uptake observed with smaller nanoparticles (Zhang et al., 2010b).

#### 5.3.2.3. Uptake mechanism

Polymeric micelles are predominately internalised into cells via endocytosis (Xiao et al., 2011), and endocytosis was the main uptake pathway reported in most MPC-DPA nanoparticles studies. Moreover, this process is energy-dependent, and is blocked at

low temperatures, therefore, cooling the cells to 4°C should inhibit the uptake process of nanoparticles (Dausend et al., 2008; Cartiera et al., 2009). The endocytosis inhibition experiments were performed by the incubation of four different cell lines at 4°C for 1 hour only (as described in Section 2.2.3.6.3) as endocytosis processes are very fast and blocking one route of uptake may lead to the activation of other pathways of endocytosis (Harush-Frenkel et al., 2007).

The endocytosis inhibition results seen in Figure 5.19, Figure 5.20 and Figure 5.21, demonstrated that there was a statistically significant ($p < 0.05$) reduction in the cellular uptake of Cm-6-loaded-MPC-DPA micelles at 4°C compared to that at 37°C in V79, Vero, and MRC-5 cell lines, which indicated that the internalisation of Cm-6-loaded-MPC-DPA micelles was mediated by endocytosis in these cells. These results were in close agreement with other reported studies, which demonstrated that endocytosis is the mechanism of nanoparticles uptake with V79 (Canton and Battaglia, 2012), Vero (Díaz-Moscoso et al., 2010; Sun et al., 2017), and MRC-5 cells (Ng et al., 2015).

However, there was no significant decrease ($p > 0.05$) in the cellular uptake of Cm-6-loaded-MPC-DPA micelles at 4°C observed with CHO cells, as seen in Figure 5.22, which suggested that an energy independent pathway; most likely due to a passive process such as diffusion, may contribute to the internalisation of Cm-6-loaded-MPC-DPA micelles. These findings were consistent with some studies that involved nanoparticles uptake in CHO cells (Jiang et al., 2015).

In summary, the uptake and inhibition studies were used to investigate the mechanism of cellular entry by the MPC-DPA nanoparticles. The controls used were free Cm-6, which is a very hydrophobic compound (Zhang et al., 2010b), and thus the uptake mechanism for free Cm-6 is thought to be via passive diffusion across the hydrophobic

lipid containing cell membrane (Shi et al., 2015b), rather than by endocytosis. Endocytosis is an active process that involves the formation of vesicles with an aqueous core (Yameen et al., 2014), which the hydrophobic Cm-6 would be repelled from. In contrast the MPC-DPA nanoparticles are characterised by a hydrophilic outer corona, and would therefore be more compatible with endocytosis than free Cm-6. The data presented appears to support this, with lower uptake of free Cm-6 controls compared to MPC-DPA nanoparticle loaded Cm-6 seen over a 1 hour period in Figures 5.14, 5.16, and 5.18. However, these Figures did not differentiate or identify the uptake mechanisms responsible. Subsequent further studies using low temperature (4 °C) incubation to inhibit endocytosis indicated that an active uptake process was involved in MPC-DPA nanoparticle cellular internalisation, as seen in Figures 5.19, 5.20, and 5.21, whilst a passive process was responsible for free Cm-6 control uptake, and remained unchanged by lowering the temperature. It was noted that there were some limitations to the study, principally that the inhibition study was run for a single 1 hour time period in (Figures 5.19, 5.20, and 5.21), which did not fully explore the possible uptake mechanisms responsible for the data reported at 1 min, 5 min, 10 min, and 30 min presented in the uptake study (Figures 5.14, 5.16, and 5.18). It was also noted that the uptake data for V79 cells (Figure 5.12) and inhibition data for CH0 cells (Fig 5.22) differed from the behaviour seen with the other cells. Additional experimental work would help elucidate these matters further, as cell entry can be affected by many factors, such as the cell phenotype, growing conditions, cell density, and presence of growth factors (Sahay et al., 2010).

## 5.4. Summary

In summary, this chapter provided an insight of the cytotoxicity profile and the size and cell-specific cellular uptake of MPC-DPA micelles. Therefore, based on the high cellular uptake and biocompatibility of the MPC-DPA micelles, it was concluded that the self-assembled pH-sensitive MPC-DPA micelles might be a suitable candidate for anticancer drug delivery applications.

# CHAPTER SIX

# DRUG LOADING POTENTIAL OF MPC-DPA MICELLES

## 6.1. Introduction

At this stage of the project, the aim was to evaluate the efficiency of the synthesised novel MPC-DPA diblock copolymers to encapsulate the selected hydrophobic anticancer drug, docetaxel and to establish the capacity of MPC-DPA nano-systems for *in-vitro* delivery of docetaxel to relevant cancer cell models. Docetaxel was selected as a model drug due to its high therapeutic activity against a wide range of tumours that have been hampered by its low aqueous solubility and systemic toxicity accompanied by using Tween 80 and ethanol. Therefore, several approaches have previously been proposed based on nanoparticles, micelles, liposomes, macromolecular conjugations, and prodrugs to enhance the solubility and bioavailability of DTX.

One of these approaches has been to use polymeric micelles, therefore, this chapter focused on the determination of loading and release efficiency of docetaxel from MPC-DPA nanoparticles, the effect of nanoparticle size on the docetaxel delivery system, and the efficacy of docetaxel delivered to suitable cell lines. Based on the characterisation data presented in Chapter 4, 1:1 MPC-DPA diblock copolymers ($MPC_{20}$-$DPA_{20}$, $MPC_{50}$-$DPA_{50}$, and $MPC_{90}$-$DPA_{90}$) were chosen because of the nanoparticle size range they provided (25 nm, 38 nm, and 44 nm, respectively). Moreover, and in order to quantify and study the kinetics of loaded MPC-DPA micelles uptake in Caucasian human cell lines, breast adenocarcinoma (MCF-7), ovary adenocarcinoma (SKOV-3), and prostate adenocarcinoma (PC3) were incubated with the different sized Cm-6-loaded MPC-DPA micelles for increasing lengths of time, and the cell-associated fluorescence measured by flow cytometry. Subsequently,

$MPC_{90}$-$DPA_{90}$ micelles were selected to study the antitumor efficacy of DTX via MTT and LDH assays.

## 6.2 Results

### 6.2.1 Preparation and characterisation of Docetaxel (DTX)-loaded MPC-DPA micelles:

The nanoparticle size and size distribution of DTX-loaded MPC-DPA micelles prepared by nanoprecipitation were measured by DLS (as described in Section 2.2.3.1), and as shown in Table 6.1. The nanoparticle sizes of the DTX-loaded micelles were comparable to that of blank micelles and they tended to form monodispersed nano-systems in MeOH-PBS (pH 7.4). As PC polymers are reported to display different solubility profiles in different solvent blends with an affinity mainly to alcohols (Lewis et al., 2000), EtOH was also used in the preparation of MPC-DPA micelles via nanoprecipitation to evaluate the impact of solvent selection on the particle size of the MPC-DPA micelles. As shown in Table 6.1, the sizes of DTX-loaded micelles in EtOH-PBS (pH 7.4) were larger than that produced with MeOH-PBS (pH 7.4) systems, with the nano-systems tending to be polydisperse. Moreover, the sizes of DTX-loaded micelles in EtOH-PBS (pH 7.4) were in close agreement with the corresponding blank MPC-DPA micelles, but with a tendency to form a polydisperse systems.

**Table 6.1.** Characterisation of micelles formed via nanoprecipitation from MeOH and EtOH in PBS (pH 7.4) at 25°C (Mean ± SD, n=3)

| Copolymers | DTX-loaded micelle (MeOH) | | DTX-loaded micelle (EtOH) | |
|---|---|---|---|---|
| | Micelle size (nm) | Polydispersity (PDI) | Micelle size (nm) | Polydispersity (PDI) |
| $MPC_{20}$-$DPA_{20}$ | 22 ± 0.3 | 0.05 ± 0.02 | 41 ± 2.4 | 0.14 ± 0.01 |
| $MPC_{50}$-$DPA_{50}$ | 33 ± 0.3 | 0.06 ± 0.01 | 128 ± 3.6 | 0.26 ± 0.01 |
| $MPC_{90}$-$DPA_{90}$ | 39 ± 0.2 | 0.05 ± 0.01 | 141 ± 9.0 | 0.25 ± 0.01 |

In order to assess the effect of micelle preparation methods, an additional MPC-DPA nanoparticle system was prepared (as described in Section 2.2.3.1), firstly via nanoprecipitation, then a dialysis process was carried out to remove any residual solvents (MeOH or EtOH), prior to drug entrapment via direct dissolution (as described in Section 2.2.3.1). The effect on the nanoparticle size and PDI is summarised in Table 6.2 and Table 6.3 for MeOH-PBS and EtOH-PBS systems respectively. Although the dialysis process had a relatively minor effect on MPC-DPA micelle size, as displayed in Table 6.2, a small increase in the size of DTX-loaded MPC-DPA micelles was observed with an associated development of polydispersed nano-systems compared to the pre-dialysed monodispersed systems. Conversely, the EtOH-PBS MPC-DPA nanoparticle systems displayed a large decrease in the size of MPC-DPA micelles after dialysis and consequently the size of DTX-loaded MPC-DPA micelle also decreased, compared to the pre-dialysis MPC-DPA micelles, with the nano-systems tending to be polydisperse at all stages, as shown in Table 6.3.

**Table 6.2.** Particle diameter and polydispersity of MPC-DPA micelles measured with DLS (25°C), formed via nanoprecipitation from MeOH in PBS (pH 7.4), pre-and post-dialysis (Mean ± SD, n=3)

| **Copolymers** | **Micelle size (nm)** | | |
|---|---|---|---|
| | Blank micelle (Pre-dialysis) | Blank micelle (Post dialysis) | DTX-loaded micelle |
| $MPC_{20}$-$DPA_{20}$ | 22 ± 0.2 | 23 ± 1.1 | 27 ± 3.0 |
| $MPC_{50}$-$DPA_{50}$ | 32 ± 0.3 | 35 ± 0.4 | 43 ± 3.3 |
| $MPC_{90}$-$DPA_{90}$ | 39 ± 0.1 | 39 ± 0.3 | 42 ± 0.8 |
| **Polydispersity (PDI)** | | | |
| $MPC_{20}$-$DPA_{20}$ | 0.04 ± 0.01 | 0.07 ± 0.01 | 0.23 ± 0.10 |
| $MPC_{50}$-$DPA_{50}$ | 0.08 ± 0.01 | 0.16 ± 0.03 | 0.29 ± 0.06 |
| $MPC_{90}$-$DPA_{90}$ | 0.07 ± 0.01 | 0.11 ± 0.01 | 0.18 ± 0.02 |

**Table 6.3.** Particle diameter and polydispersity of MPC-DPA micelles measured with DLS (25°C), formed via nanoprecipitation from EtOH in PBS (pH 7.4), pre-and post-dialysis (Mean ± SD, n=3)

| Copolymers | Micelle size (nm) | | |
|---|---|---|---|
| | Blank micelle (Pre-dialysis) | Blank micelle (Post dialysis) | DTX-loaded micelle |
| $MPC_{20}$-$DPA_{20}$ | 42 ± 2.0 | 33 ± 1.0 | 38 ± 6.0 |
| $MPC_{50}$-$DPA_{50}$ | 128 ± 6.3 | 99 ± 7.5 | 97 ± 8.4 |
| $MPC_{90}$-$DPA_{90}$ | 136 ± 12.1 | 111 ± 11.1 | 109 ± 10.5 |
| **Polydispersity (PDI)** | | | |
| $MPC_{20}$-$DPA_{20}$ | 0.13 ± 0.01 | 0.13 ± 0.07 | 0.23 ± 0.10 |
| $MPC_{50}$-$DPA_{50}$ | 0.27 ± 0.01 | 0.25 ± 0.01 | 0.22 ± 0.01 |
| $MPC_{90}$-$DPA_{90}$ | 0.25 ± 0.01 | 0.25 ± 0.01 | 0.24 ± 0.01 |

### 6.2.2 Determination of Docetaxel content:

The encapsulation efficiency (EE) and drug loading (DL) of docetaxel in each MPC-DPA diblock copolymer micelle formulation was calculated using UV-visible spectroscopy (as described in Section 2.2.3.2) and the results are summarised in Table 6.4 and 6.5 for nanoprecipitation and direct dissolution preparation methods, respectively. For DTX- MPC-DPA loaded micelles prepared by nanoprecipitation, EE and DL % in MeOH-PBS (pH 7.4) increased with an associated increase in block length (DPA) compared to those prepared using EtOH-PBS (pH 7.4), which showed higher percentages with $MPC_{50}$-$DPA_{50}$ (EE= 80.8 ± 0.27, DL=2.1± 0.1), as shown in Table 6.4. These results differed from the data recorded for DTX-loaded MPC-DPA micelles prepared via direct dissolution, in which low EE and DL % were obtained in MeOH-PBS (pH 7.4) prepared nano-systems, whilst high values of EE and DL % were observed with the EtOH-PBS (pH 7.4) MPC-DPA nano-systems as shown in Table 6.5.

**Table 6.4.** Encapsulation efficiency (EE), drug loading (DL) and the concentration of docetaxel in MPC-DPA micelles prepared via nanoprecipitation (feed weight ratio of DTX to block copolymer was 1:40) (Mean ± SD, n=3)

| Copolymers | DTX-loaded micelle (MeOH+PBS) | | | DTX-loaded micelle (EtOH+PBS) | | |
|---|---|---|---|---|---|---|
| | Encapsulation Efficiency (EE%) | Drug Loading (DL%) | DTX Conc. (μg $ml^{-1}$) | Encapsulation Efficiency (EE%) | Drug Loading (DL%) | DTX Conc. (μg $ml^{-1}$) |
| $MPC_{20}$-$DPA_{20}$ | 56.73 ± 0.38 | 1.42 ± 0.01 | 28.37 ± 0.01 | 54.90 ± 0.11 | 1.37 ± 0.04 | 27.45 ± 0.04 |
| $MPC_{50}$-$DPA_{50}$ | 59.40 ± 0.17 | 1.49 ± 0.05 | 29.70 ± 0.05 | 80.81 ± 0.27 | 2.02 ± 0.01 | 40.40 ± 0.01 |
| $MPC_{90}$-$DPA_{90}$ | 70.73 ± 0.42 | 1.77 ± 0.01 | 35.37 ± 0.01 | 43.56 ± 0.07 | 1.09 ± 0.02 | 21.78 ± 0.02 |

**Table 6.5.** Encapsulation efficiency (EE), drug loading (DL) and the concentration of docetaxel MPC-DPA micelles prepared via direct dissolution (feed weight ratio of DTX to block copolymer was 1:40) (Mean ± SD, n=3)

| Copolymers | DTX-loaded micelle (MeOH) | | | DTX-loaded micelle (EtOH) | | |
|---|---|---|---|---|---|---|
| | Encapsulation Efficiency (EE%) | Drug Loading (DL%) | DTX Conc. (μg $ml^{-1}$) | Encapsulation Efficiency (EE%) | Drug Loading (DL%) | DTX Conc. (μg $ml^{-1}$) |
| $MPC_{20}$-$DPA_{20}$ | 36.44 ± 0.17 | 0.91 ± 0.01 | 18.22 ± 0.01 | 70.48 ± 0.25 | 1.76 ± 0.02 | 35.24 ± 0.02 |
| $MPC_{50}$-$DPA_{50}$ | 28.52 ± 0.43 | 0.71 ± 0.01 | 14.26 ± 0.01 | 69.40 ± 0.59 | 1.73 ± 0.07 | 34.70 ± 0.07 |
| $MPC_{90}$-$DPA_{90}$ | 33.40 ± 0.71 | 0.84 ± 0.06 | 16.79 ±0.06 | 70.32 ± 0.11 | 1.75 ± 000 | 35.16 ± 000 |

### 6.2.3 *In-vitro* Docetaxel release profiles:

The cumulative *in-vitro* release profiles of DTX from MPC-DPA micelles at 37°C in PBS (pH 7.4) were carried out to assess the ability of nanoparticles to release the encapsulated content quickly to its target site (as described in Section 2.2.3.3). The release pattern of DTX from the different MPC-DPA micelles are presented in Figure 6.1 and 6.2 for DTX loaded MPC-DPA micelles via nanoprecipitation and direct dissolution, respectively. Both loaded MPC-DPA micelle nano-systems displayed an initial burst release of DTX with the first hours followed primarily by sustained release from the MPC-DPA micelles for up to 96 hours. As shown in Figure 6.1, an initial release of DTX was observed in all MPC-DPA micelle samples with more than 60% release from DTX- loaded $MPC_{50}$-$DPA_{50}$ and $MPC_{90}$-$DPA_{90}$ micelles and 90 % from $MPC_{20}$-$DPA_{20}$ micelles based on nanoprecipitation in MeOH, and less than 30% release from DTX-loaded MPC-DPA micelles based on EtOH within the first 6 hours. Moreover, in MPC-DPA micelles loaded by direct dissolution (Figure 6.2), more than 80% of DTX was released from $MPC_{50}$-$DPA_{50}$ and $MPC_{90}$-$DPA_{90}$ micelles, compared to 50% release from $MPC_{20}$-$DPA_{20}$ micelles after 6 hours.

Furthermore, in DTX-loaded MPC-DPA micelles prepared via nanoprecipitation (MeOH and EtOH), the DTX release was higher for smaller particles MPC-DPA micelles, compared to the other two larger particle size MPC-DPA micelles as shown in Figure 6.1, whilst a reverse trend was observed for DTX-loaded micelles via direct dissolution as shown in Figure 6.2.

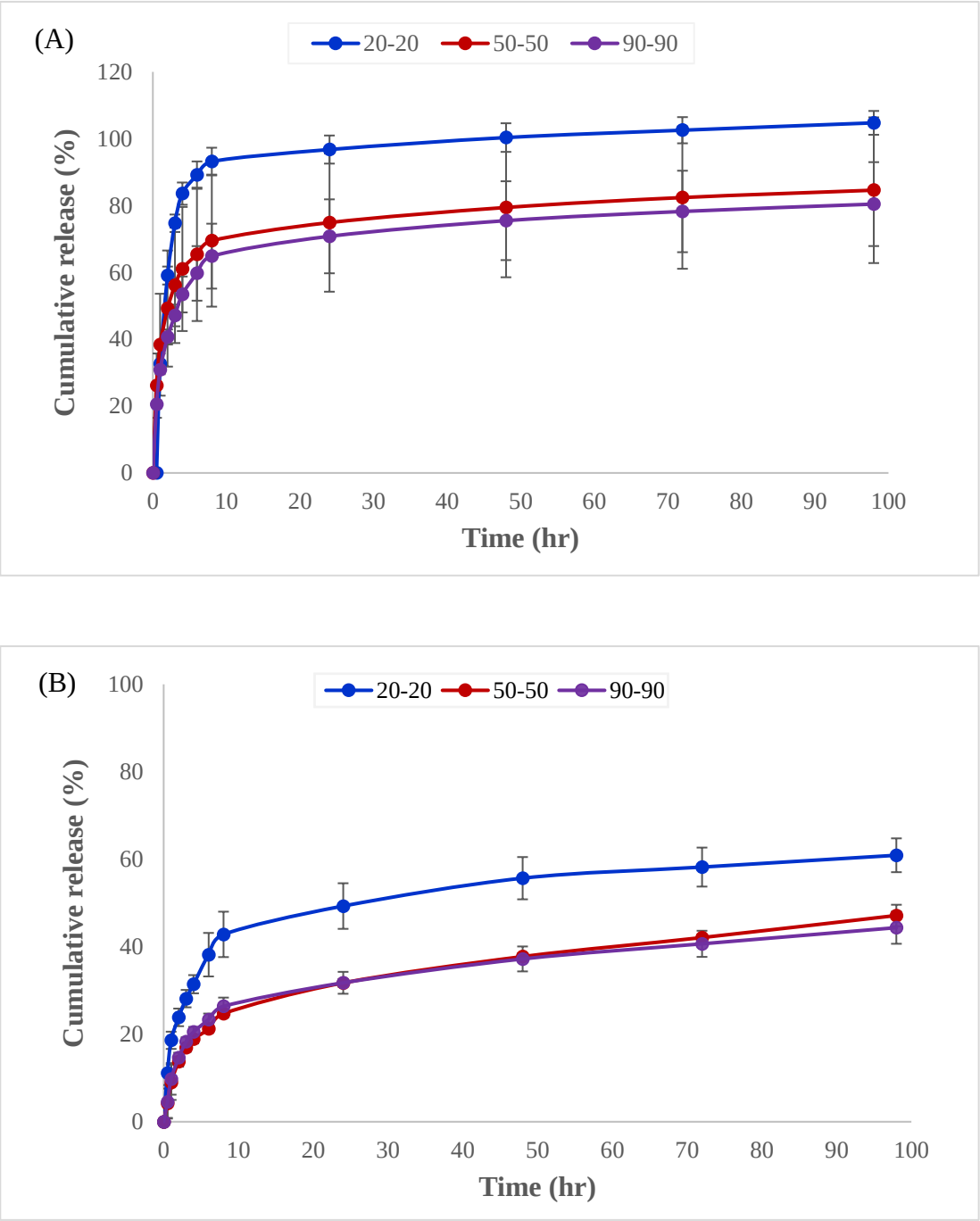


**Figure 6.1.** The cumulative *in-vitro* release profiles of DTX-loaded MPC-DPA micelles in PBS (pH 7.4) prepared via nanoprecipitation in (A) MeOH and (B) EtOH (mean ± SD, n=3) (Original in colour)

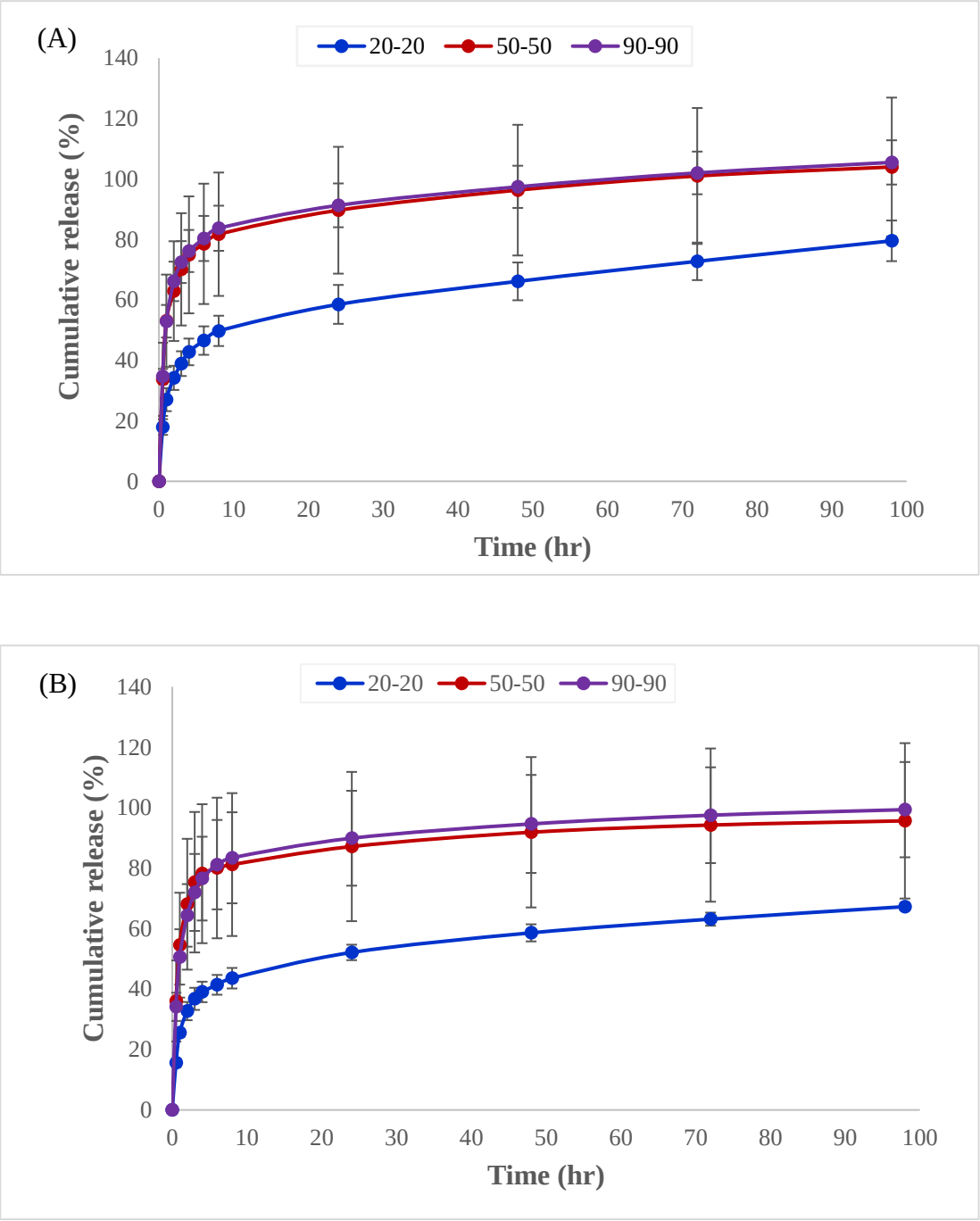


**Figure 6.2.** The cumulative *in-vitro* release profiles of DTX-loaded MPC-DPA micelles in PBS (pH 7.4) prepared via direct dissolution after dialysis to remove (A) MeOH and (B) EtOH (mean ± SD, n=3) (Original in colour)

### 6.2.4 The cellular uptake studies:

The cellular uptake of MPC-DPA micelles with different nanoparticle sizes was measured qualitatively via CLSM and quantitively via flow cytometry using coumarin-6 (Cm-6) as a model fluorescent molecule to replace DTX (a described in Section 2.2.3.6.1 and Section 2.2.3.6.2). Figure 6.3, 6.5, and 6.7 displayed human cancer cells MCF-7, SKOV-3, and PC3 cancer cells after 1 h incubation with different Cm-6-loaded MPC-DPA micelles, which demonstrated the presence of fluorescent MPC-DPA micelles in all cancer cells analysed, which were located in the cytoplasm of the cells and adjacent to the peripheral region of nuclei, indicating the successful internalisation of MPC-DPA nanoparticles into relevant cancer cell lines. Moreover, the treated cells showed an increase in fluorescence intensity compared to untreated control cells, as shown in the flow cytometry histograms, which were shown to be highly dependent on the size of loaded MPC-DPA micelles, therefore, a higher uptake percentage of Cm-6-loaded-$MPC_{90}$-$DPA_{90}$ was reported compared to that reported for Cm-6-loaded $MPC_{20}$-$DPA_{20}$ and $MPC_{50}$-$DPA_{50}$. Moreover, and as per Chapter five, the time-dependence intracellular uptake was evaluated at different time intervals and data displayed in Figure 6.4, 6.6, and 6.8 for MCF-7, SKOV-3, and PC3 cells respectively. The data showed a rapid uptake (1 min) of Cm-6-loaded MPC-DPA micelles in all cell types tested.

After 1 min of incubation in MCF-7 cells, Figure 6.4, a high percentage of fluorescence cells detected via flow cytometry were observed, and despite the uptake process being a time-dependent one, there were no statistically significant ($p > 0.05$) changes in the percentage of Cm-6-loaded MPC-DPA micelles with longer incubation times in the $MPC_{50}$-$DPA_{50}$ and $MPC_{90}$-$DPA_{90}$ loaded micelles. However, $MPC_{20}$-$DPA_{20}$ loaded micelles did display significant ($p < 0.05$) variability. Additionally, and as shown in

Figure 6.4, there was no significant difference ($p > 0.05$) in the cellular uptake of free Cm-6 as a function of incubation time with MCF-7 cells. Moreover, a significant difference ($p < 0.05$) between the cellular uptake of Cm-6-loaded MPC-DPA micelles compared to free Cm-6 was recorded in MCF-7 cells, which indicated that MPC-DPA micelles facilitated Cm-6 intracellular uptake. It was reported that a higher percentage uptake of Cm-6 were observed with the larger size MPC-DPA micelles ($MPC_{50}$-$DPA_{50}$ and $MPC_{90}$-$DPA_{90}$ loaded micelles) compared to smaller size $MPC_{20}$-$DPA_{20}$ loaded micelles, in contrast with the data observed in the cellular uptake studies on normal cell lines (Chapter 5).

In Figure 6.6, a similar trend was reported for SKOV-3 cell quantitative uptake in which there were no significant ($p > 0.05$) changes in the percentage of Cm-6-loaded MPC-DPA micelles with longer incubation, in addition to the no significant ($p > 0.05$) difference in the cellular uptake of free Cm-6 as a function of incubation time. However, a significant difference ($p < 0.05$) between the cellular uptake of Cm-6-loaded MPC-DPA micelles compared to free Cm-6 which seen for prolonged incubation times (30 min-1 hour), which indicated that MPC-DPA micelles facilitated Cm-6 intracellular uptake. Furthermore, $MPC_{20}$-$DPA_{20}$ loaded micelles once again showed a significantly ($p < 0.05$) lower cellular percentage uptake compared to the results seen with $MPC_{50}$-$DPA_{50}$ and $MPC_{90}$-$DPA_{90}$ loaded micelles with extended incubation times.

In Figure 6.8 for PC3 cells uptake, there were no significant ($p > 0.05$) changes in the percentage of Cm-6-loaded MPC-DPA micelles with longer incubation times in $MPC_{50}$-$DPA_{50}$ and $MPC_{90}$-$DPA_{90}$ loaded micelles, however, $MPC_{20}$-$DPA_{20}$ loaded micelles displayed significant ($p < 0.05$) reduction in their uptake with prolonged incubation times. Additionally, and as shown in Figure 6.8, there was no significant

difference ($p > 0.05$) in the cellular uptake of free Cm-6 as a function of incubation time at 1 min, 5 min, and 10 min. However, a significant ($p < 0.05$) increase in the Cm-6 uptake after 30 min and 1 h incubation was seen. Moreover, a significant difference ($p < 0.05$) between the PC3 cellular uptake of Cm-6-loaded MPC-DPA micelles compared to free Cm-6 was observed, which indicated that MPC-DPA micelles facilitated Cm-6 intracellular uptake.

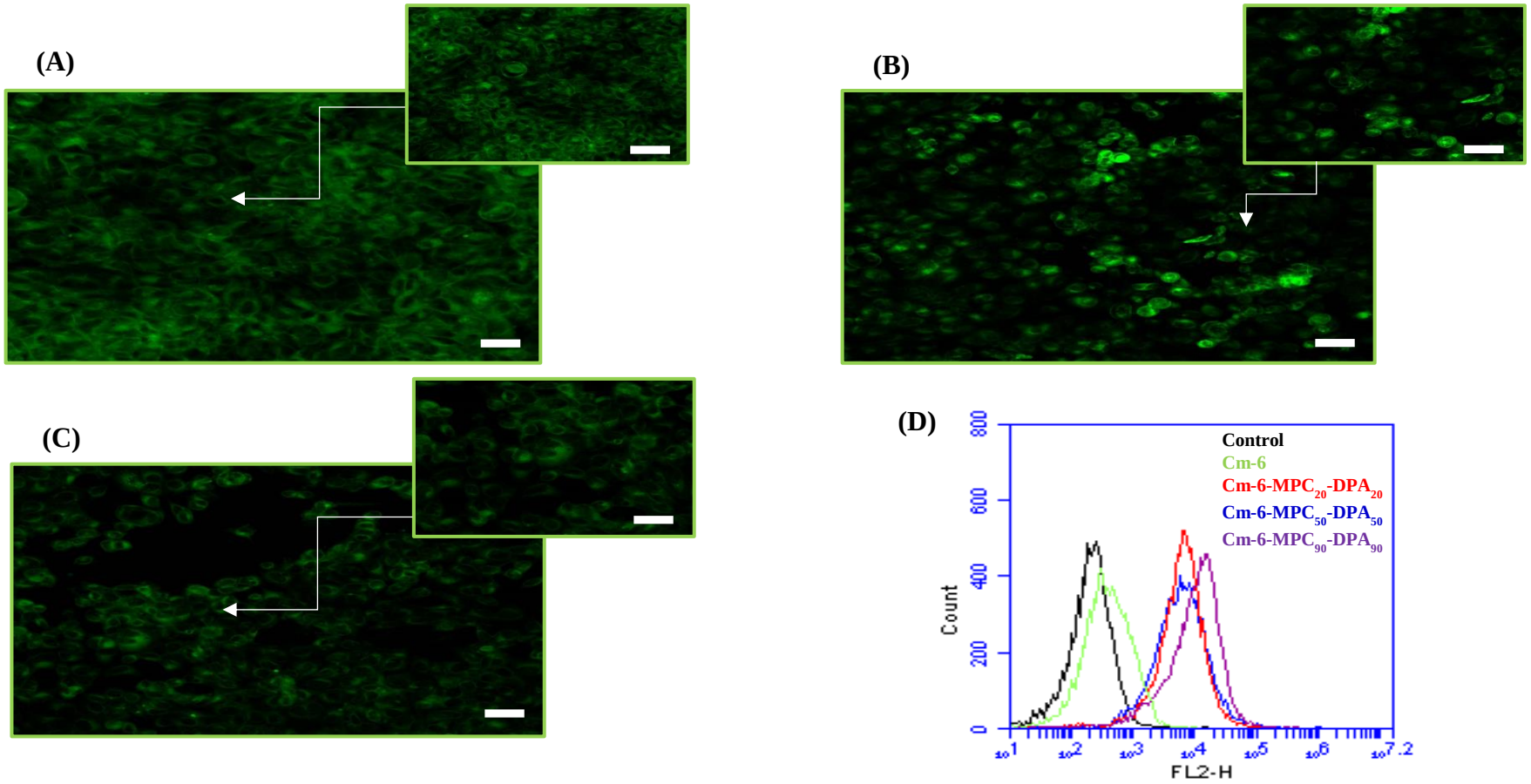


**Figure 6.3.** Confocal laser scanning microscopy (CLSM) images and flow cytometry histogram of MCF-7 cells after 1 h incubation with Cm-6-loaded MPC-DPA micelles. (A) Cm-6-$MPC_{20}$-$DPA_{20}$, (B) Cm-6-$MPC_{50}$-$DPA_{50}$, (C) Cm-6-$MPC_{90}$-$DPA_{90}$, (D) Flow cytometric profiles. Scale bars = 50, and 25 µm. (Original in colour)

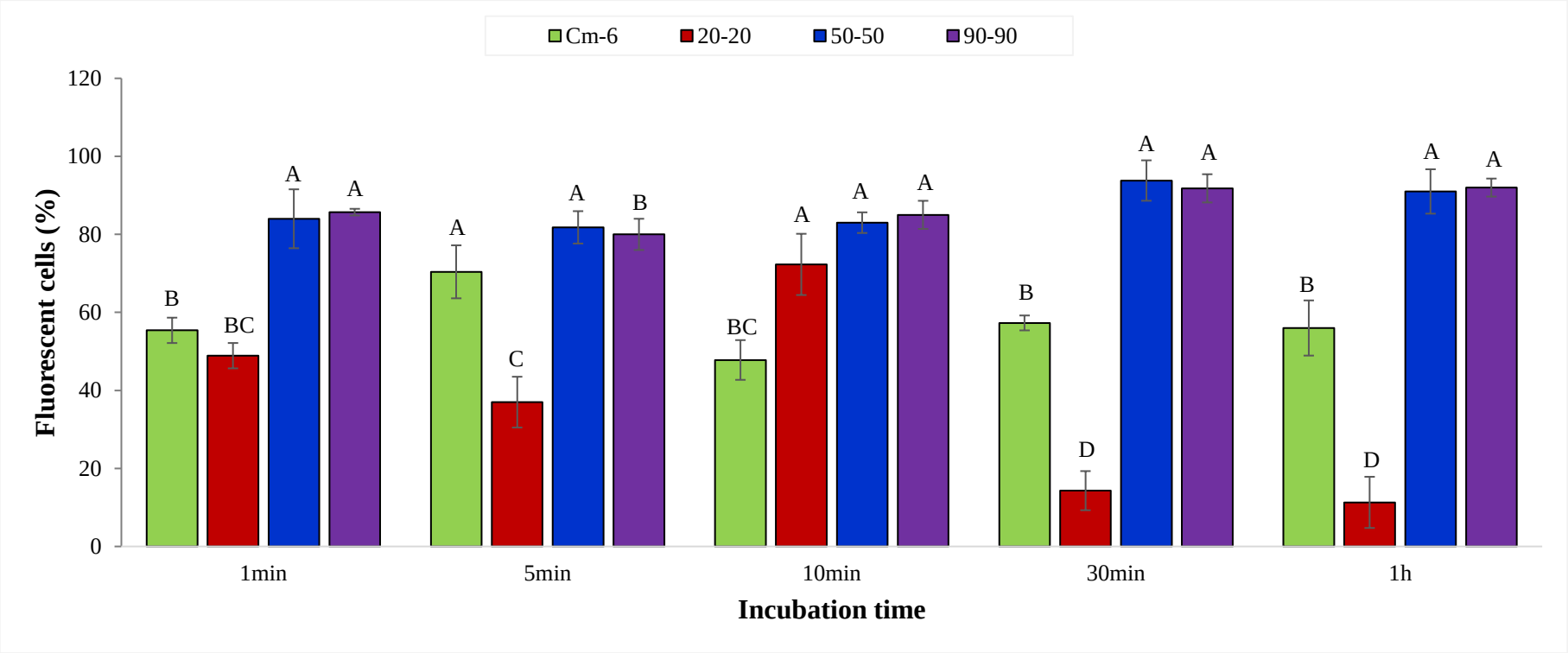


**Figure 6.4.** Quantification of the cellular uptake of Cm-6-loaded MPC-DPA micelles in MCF-7 cancer cells after incubation at 37°C at set time points. Flow cytometry determined the percentage of NP-positive cells (Mean ± SD, n=3) (Original in colour). *Bar values with different letters indicate a significant difference ($p < 0.05$) and those sharing the same letters are not significantly different ($p > 0.05$).*

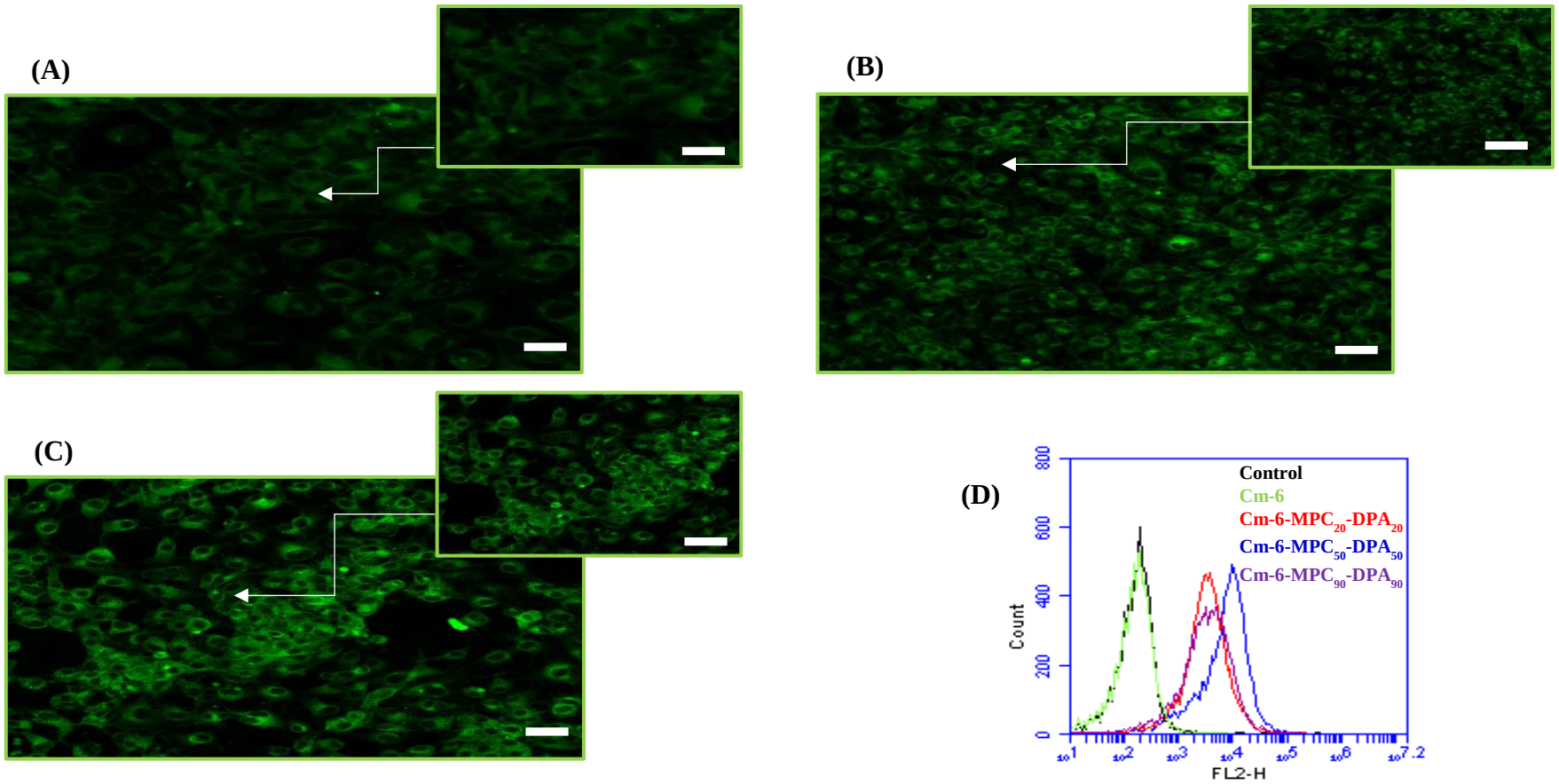


**Figure 6.5.** Confocal laser scanning microscopy (CLSM) images and flow cytometry histogram of SKOV-3 cells after 1 h incubation with Cm-6-loaded MPC-DPA micelles. (A) Cm-6-MPC$_{20}$-DPA$_{20}$, (B) Cm-6-MPC$_{50}$-DPA$_{50}$, (C) Cm-6-MPC$_{90}$-DPA$_{90}$, (D) Flow cytometric profiles. Scale bars = 50, and 25 µm. (Original in colour)

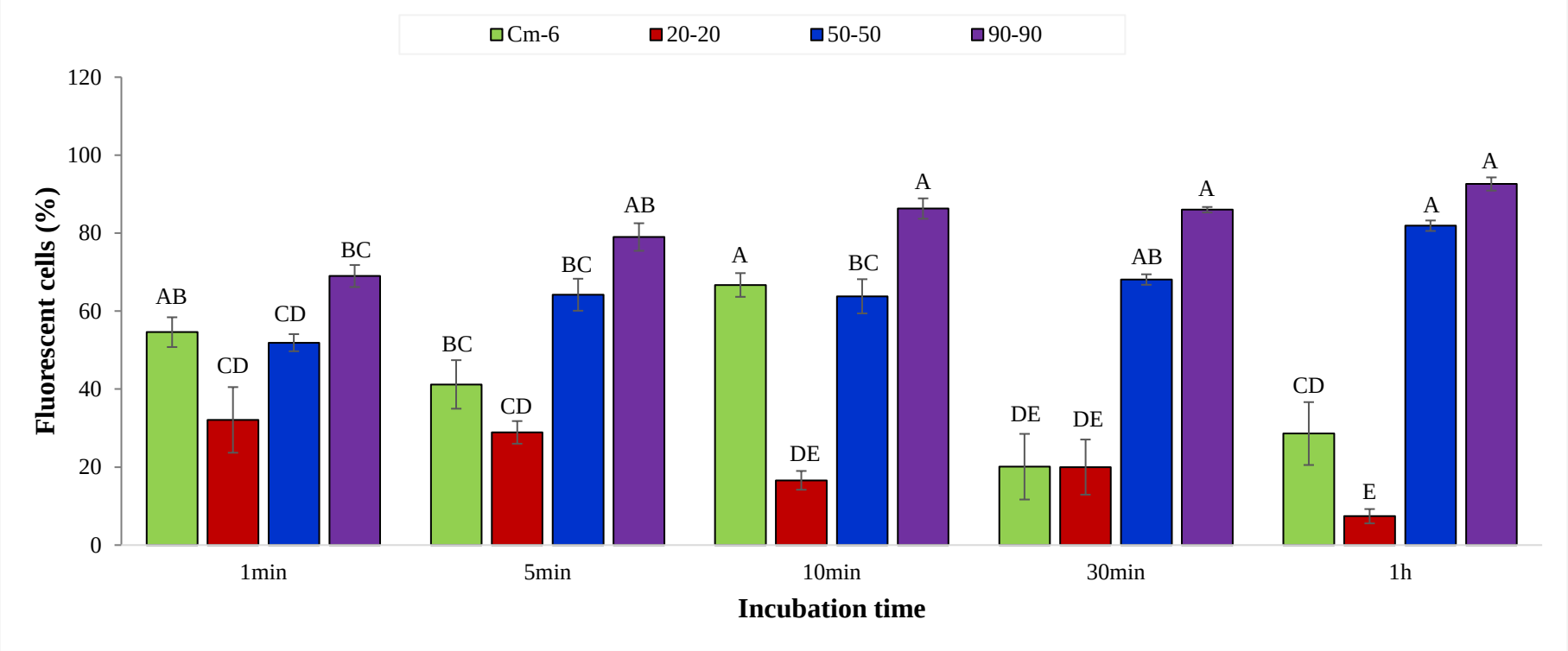


**Figure 6.6.** Quantification of the cellular uptake of Cm-6-loaded MPC-DPA micelles in SKOV-3 cancer cells after incubation at 37°C at set time points. Flow cytometry determined the percentage of NP-positive cells (Mean ± SD, n=3) (Original in colour). *Bar values with different letters indicate a significant difference ($p < 0.05$) and those sharing the same letters are not significantly different ($p > 0.05$).*

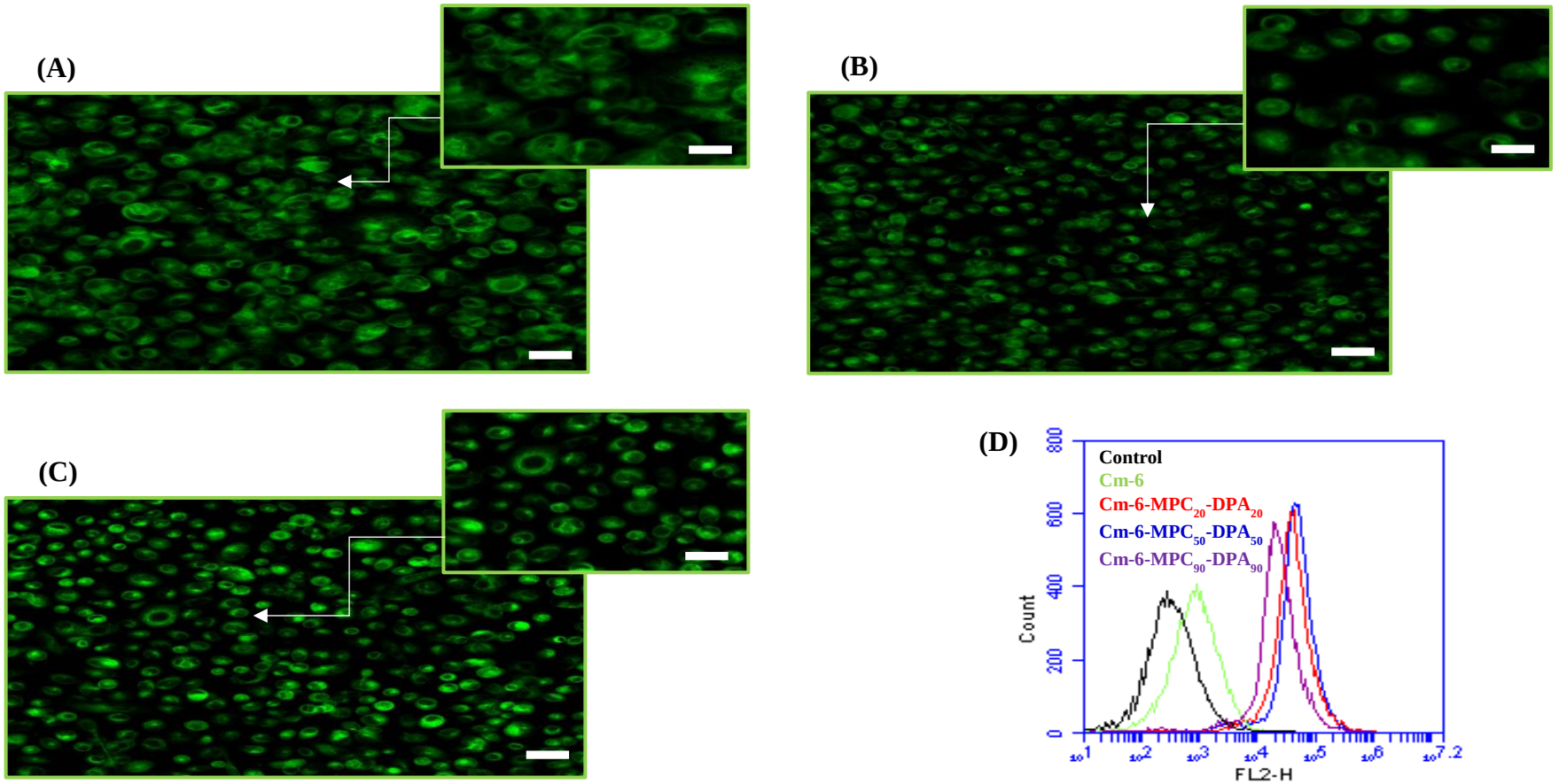


**Figure 6.7.** Confocal laser scanning microscopy (CLSM) images and flow cytometry histogram of PC3 cells after 1 h incubation with Cm-6-loaded MPC-DPA micelles. (A) Cm-6-$MPC_{20}$-$DPA_{20}$, (B) Cm-6-$MPC_{50}$-$DPA_{50}$, (C) Cm-6-$MPC_{90}$-$DPA_{90}$, (D) Flow cytometric profiles. Scale bars = 50, and 25 µm. (Original in colour)

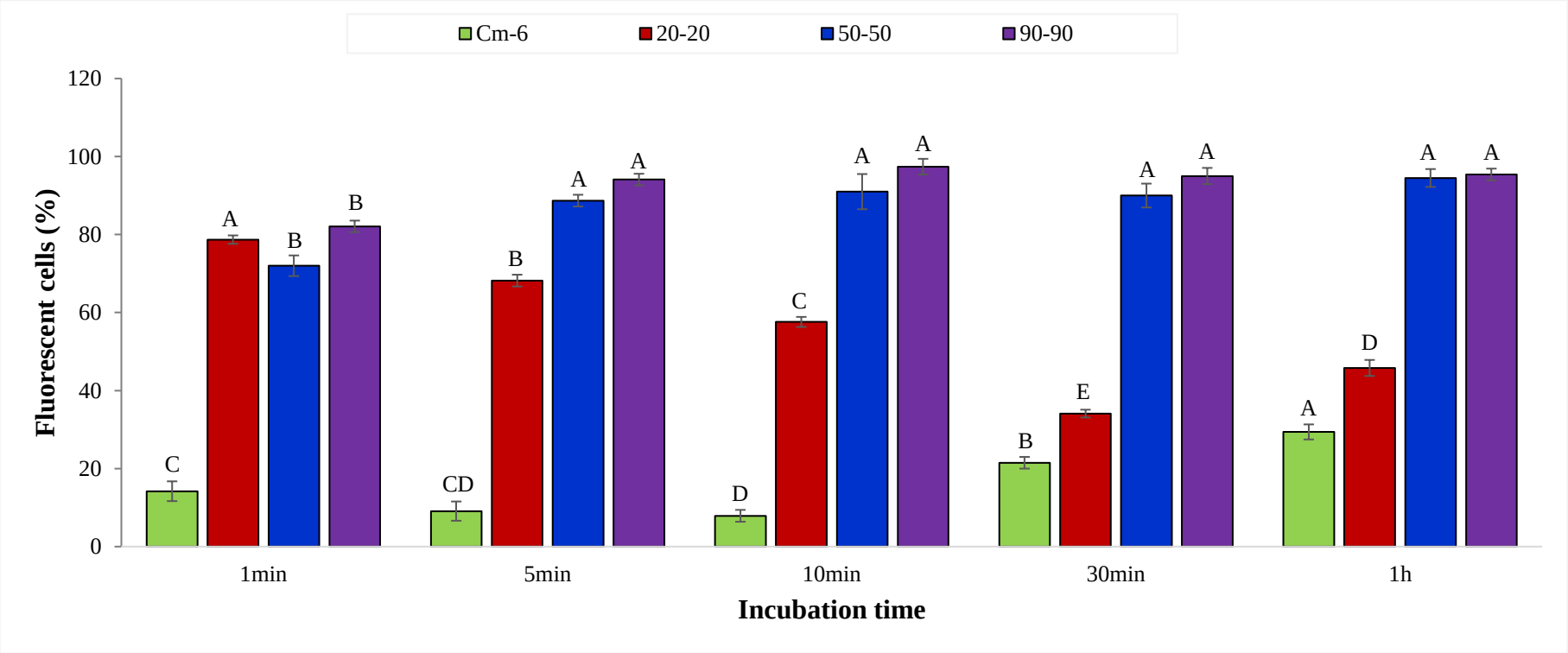


**Figure 6.8.** Quantification of the cellular uptake of Cm-6-loaded MPC-DPA micelles in PC3 cancer cells after incubation at 37°C at set time points. Flow cytometry determined the percentage of NP-positive cells (Mean ± SD, n=3) (Original in colour). *Bar values with different letters indicate a significant difference ($p < 0.05$) and those sharing the same letters are not significantly different ($p > 0.05$).*

In order to determine the mechanism of the *in-vitro* cellular uptake of the synthesised MPC-DPA micelles, MCF-7, SKOV-3, and PC3 cells were incubated with free Cm-6 and Cm-6-loaded MPC-DPA micelles at 37 °C and 4 °C; as endocytosis is an energy dependent process and is blocked at low temperatures, and the results obtained via flow cytometry assay.

As shown in Figure 6.9, the decrease in temperature (4 °C) significantly ($p < 0.05$) reduced the cellular uptake of Cm-6-loaded $MPC_{50}$-$DPA_{50}$ and Cm-6-loaded $MPC_{90}$-$DPA_{90}$ micelles by MCF-7 cancer cells compared to 37 °C. In contrast the cellular uptake of free Cm-6 was not affected by temperature (no significant difference $p > 0.05$), which indicated the involvement of energy-independent mechanisms. An unexpected increase in the uptake of 25 nm Cm-6-loaded MPC-DPA micelles by MCF-7 cells was seen, which may have originated from a difference in the mechanism of cellular uptake of these micelles. A similar trend was obtained with SKOV-3 cells incubated with Cm-6-loaded MPC-DPA micelles at 4 °C (Figure 6.10), in which a significant ($p < 0.05$) decrease in the cellular uptake at 4 °C was observed with $MPC_{50}$-$DPA_{50}$ and $MPC_{90}$-$DPA_{90}$ compared to 37 °C, while the cellular uptake of free Cm-6 was again not affected by temperature (no significant difference $p > 0.05$), indicating that endocytosis was the uptake mechanism in SKOV-3. No significant changes ($p > 0.05$) were observed with the smaller Cm-6-loaded MPC-DPA micelles (25 nm), however, these loaded micelles were still significantly different ($p < 0.05$) when compared to free Cm-6. Figure 6.11 displayed the uptake of free Cm-6 and Cm-6-loaded MPC-DPA micelles by PC3 cancer cells after incubation at 37 °C and 4 °C for 1 h. A significant reduction ($p < 0.05$) in the cellular uptake of all Cm-6-loaded MPC-DPA micelles samples occurred at 4 °C compared to that at 37 °C. However, the cellular uptake of free Cm-6 was not affected by temperature (no significant difference

$p > 0.05$), which indicated the involvement of energy-independent mechanisms for free Cm-6 uptake.

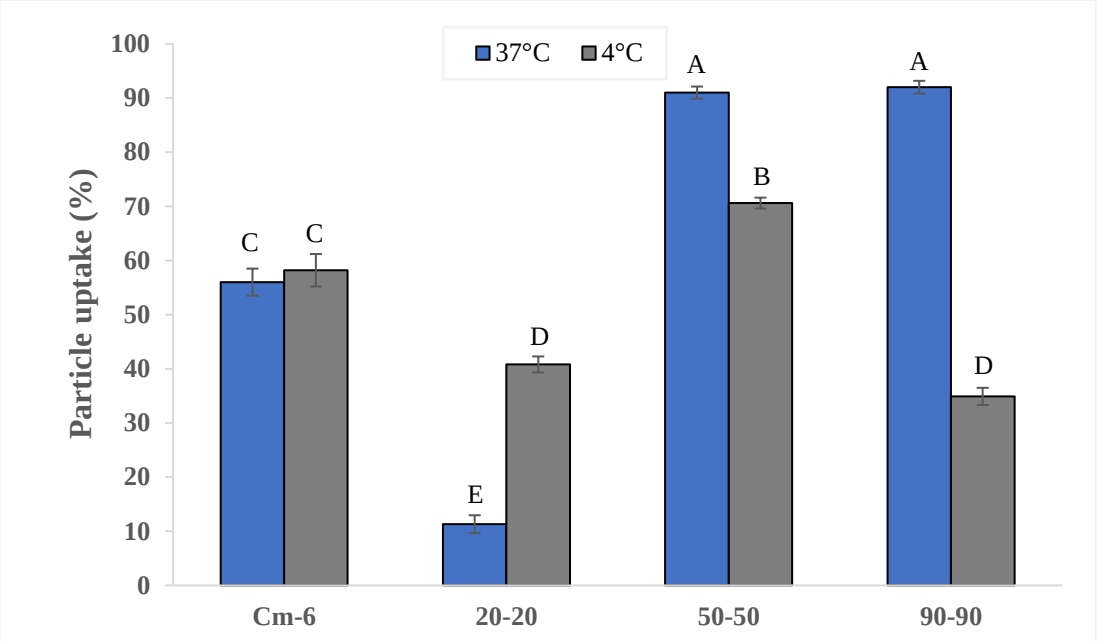


**Figure 6.9.** Uptake of Cm-6-loaded MPC-DPA nanoparticles by MCF-7 cancer cells with incubation at 37°C and 4°C for 1 hour determined by flow cytometry (Mean ± SD, n=3) (Original in colour). *Bar values with different letters indicate a significant difference ($p < 0.05$) and those sharing the same letters are not significantly different ($p > 0.05$).*

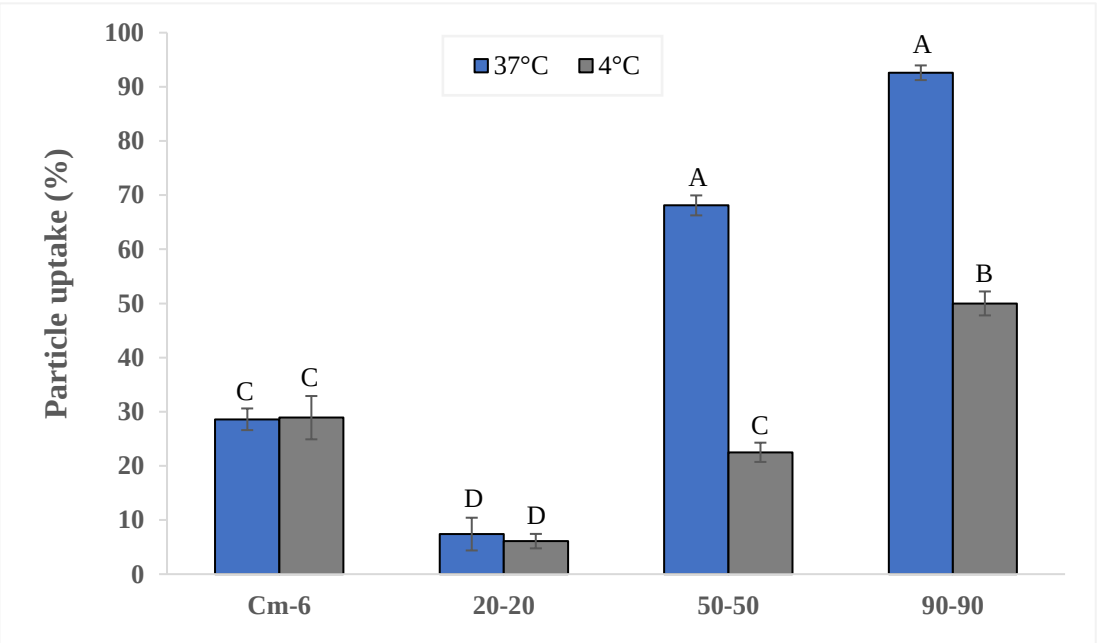


**Figure 6.10.** Uptake of Cm-6-loaded MPC-DPA nanoparticles by SKOV-3 cancer cells with incubation at 37°C and 4°C for 1 hour determined by flow cytometry (Mean ± SD, n=3) (Original in colour). *Bar values with different letters indicate a significant difference ($p < 0.05$) and those sharing the same letters are not significantly different ($p > 0.05$).*

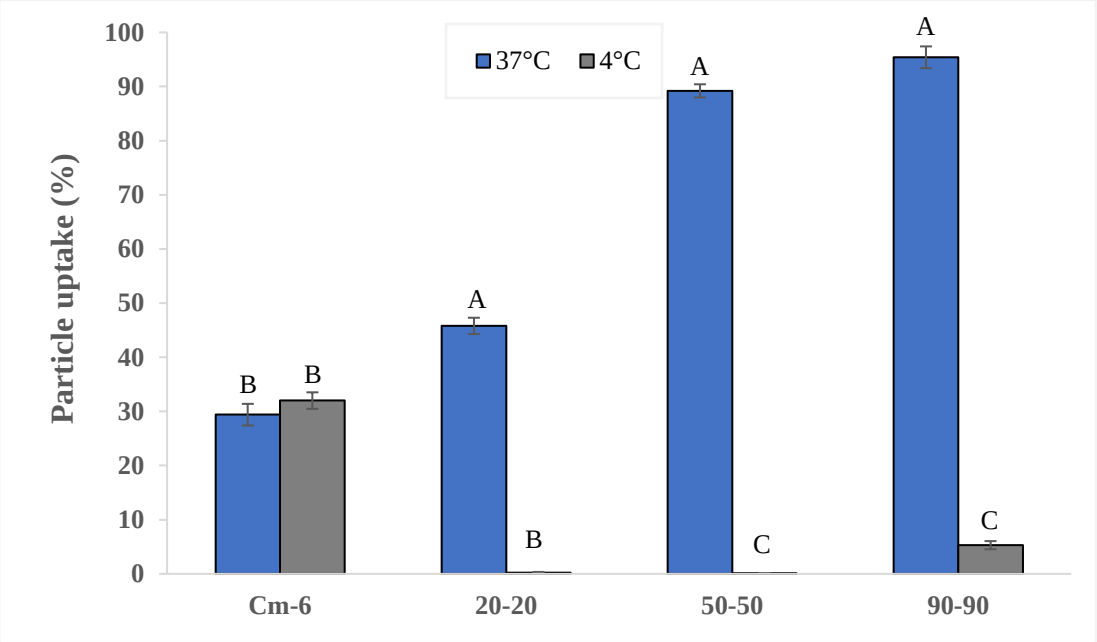


**Figure 6.11.** Uptake of Cm-6-loaded MPC-DPA nanoparticles by PC3 cancer cells with incubation at 37°C and 4°C for 1 hour determined by flow cytometry (Mean ± SD, n=3) (Original in colour). *Bar values with different letters indicate a significant difference ($p < 0.05$) and those sharing the same letters are not significantly different ($p > 0.05$).*

### 6.2.5 *In-vitro* cytotoxicity assay of DTX-loaded $MPC_{90}$-$DPA_{90}$ micelles:

The *in-vitro* cytotoxic activity of blank $MPC_{90}$-$DPA_{90}$ and DTX-loaded $MPC_{90}$-$DPA_{90}$ micelles were evaluated by incubating three human tumour cell lines; namely MCF-7, SKOV-3, and PC3 for 24 h at six designated drug concentrations (31.25-1000 µg $ml^{-1}$) using MTT (cell viability) and LDH (cell mortality) cytotoxicity assays.

Figure 6.12 (A) and Figure 6.13 (A), showed the MTT cytotoxicity results of nanoprecipitation prepared DTX-loaded $MPC_{90}$-$DPA_{90}$ micelles to MCF-7 cells after 24 h exposure. As seen from these figures, blank $MPC_{90}$-$DPA_{90}$ micelles did not induce cytotoxic effects to MCF-7 cells, and free DTX exerted a significantly ($p < 0.05$) higher anticancer effect on MCF-7 cells compared to DTX-loaded $MPC_{90}$-$DPA_{90}$ micelles (MeOH) (Figure 6.12 A). Moreover, there was no significant difference ($p > 0.05$) in the reduction of cell viability between free DTX and DTX-

loaded $MPC_{90}$-$DPA_{90}$ micelles (EtOH) as shown in Figure 6.12 A. These results were in close agreement with the LDH assay results after 24 h exposure as shown in Figure 6.12 (B) and Figure 6.13 (B).

Conversely, the MTT cytotoxicity results of DTX-loaded $MPC_{90}$-$DPA_{90}$ micelles prepared by direct dissolution against MCF-7 cells after 24 h exposure, as shown in Figure 6.14 (A) and Figure 6.15 (A), also confirmed the safety and non-toxicity of blank $MPC_{90}$-$DPA_{90}$ micelles, whilst DTX-loaded $MPC_{90}$-$DPA_{90}$ micelles (MeOH) caused a significant reduction in the metabolically active of viable cells and induced cellular toxicity at the highest polymer concentration than that observed for free DTX (Figure 6.14 A). Statistically significant ($p < 0.05$) cytotoxicity was observed with DTX-loaded $MPC_{90}$-$DPA_{90}$ micelles (EtOH) (except at 1000 µg $ml^{-1}$) compared to free DTX as shown in Figure 6.15 A. These results were consistent with the LDH results after 24 h exposure as shown in Figure 6.14 (B) and Figure 6.15 (B).

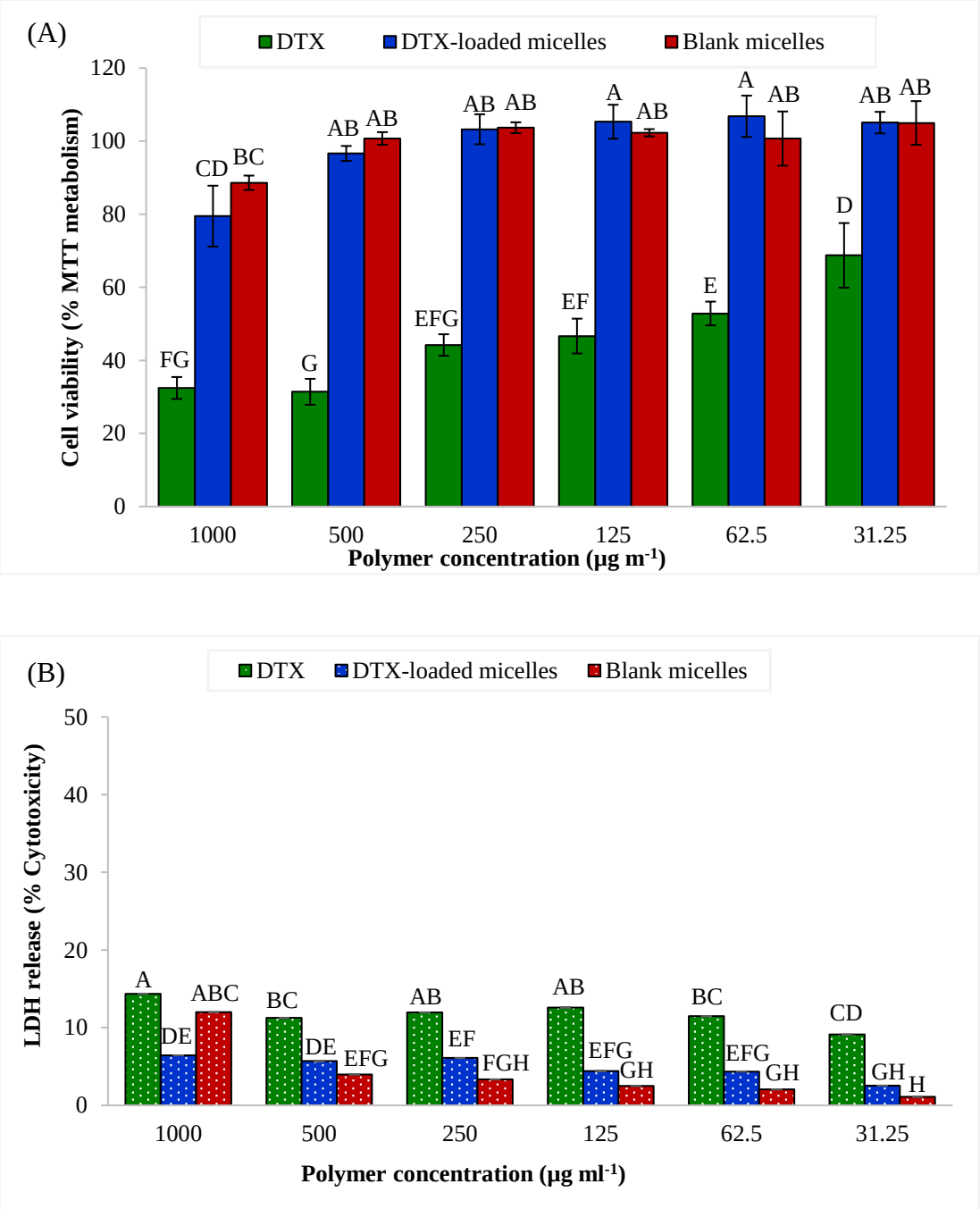


**Figure 6.12.** (A) Cell viability (%) tested by MTT assay and (B) Cytoxicity (%) by LDH assay performed on MCF-7 cancer cells exposed to set concentrations of free DTX, DTX-loaded $MPC_{90}$-$DPA_{90}$ micelles, and blank micelles prepared via nanoprecipitation (MeOH) (Mean ± SD, n=3) (Original in colour). *Bar values with different letters indicate a significant difference ($p < 0.05$) and those sharing the same letters are not significantly different ($p > 0.05$).*

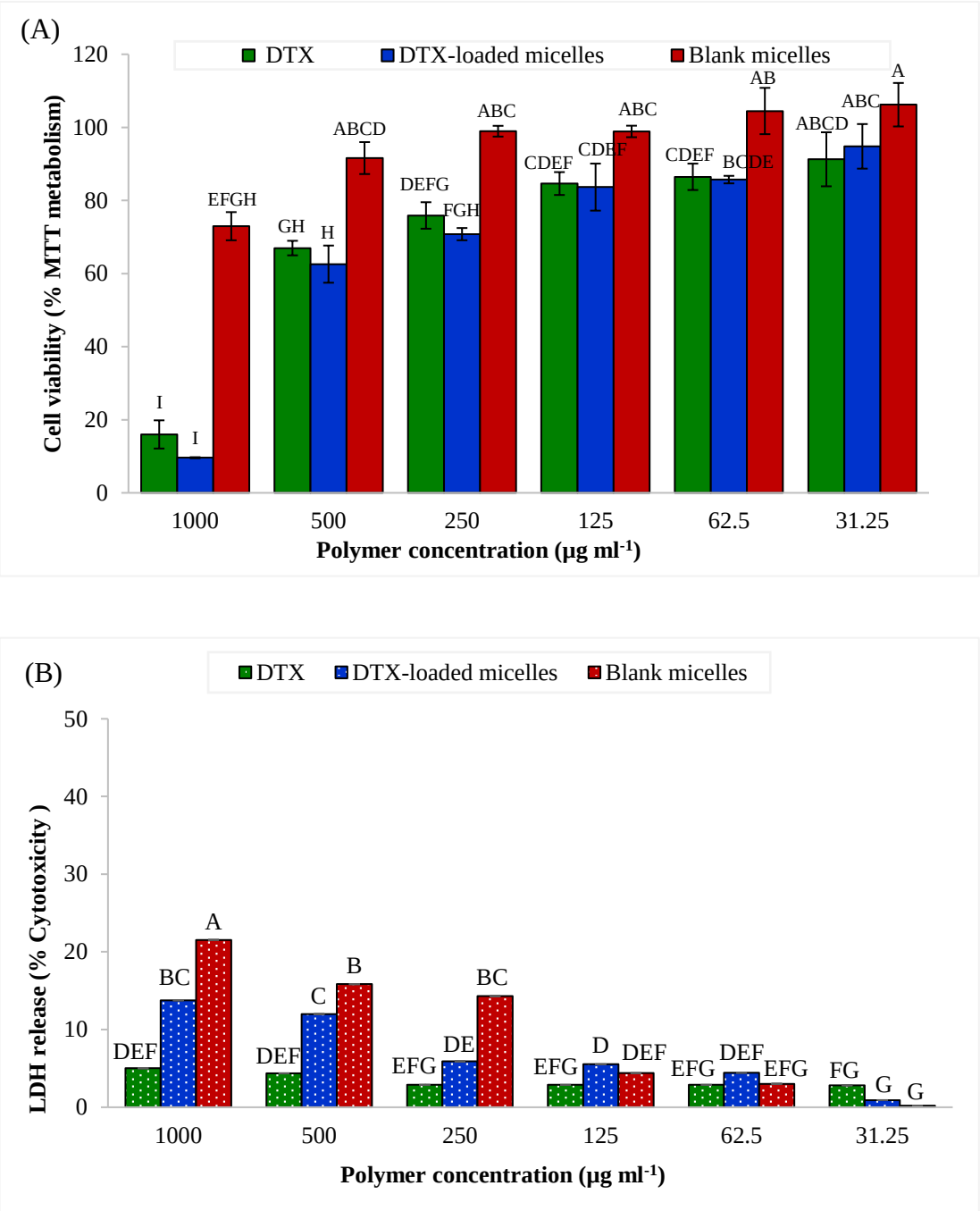


**Figure 6.13.** (A) Cell viability (%) tested by MTT assay and (B) Cytoxicity (%) by LDH assay performed on MCF-7 cancer cells exposed to set concentrations of free DTX, DTX-loaded $MPC_{90}$-$DPA_{90}$ micelles, and blank micelles prepared via nanoprecipitation (EtOH) (Mean ± SD, n=3) (Original in colour). *Bar values with different letters indicate a significant difference ($p < 0.05$) and those sharing the same letters are not significantly different ($p > 0.05$).*

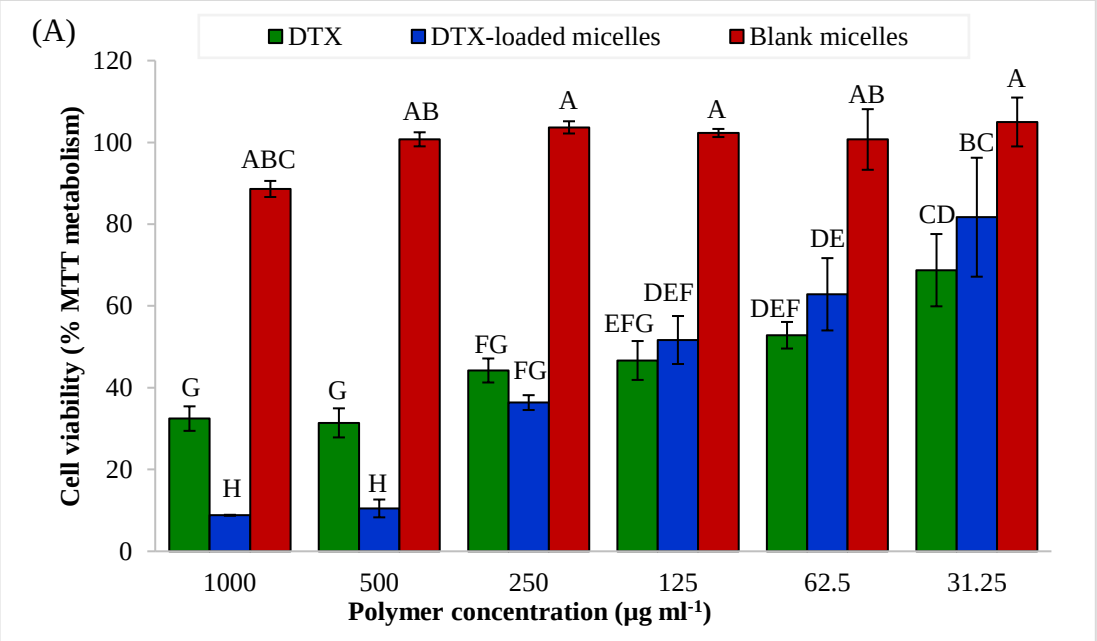


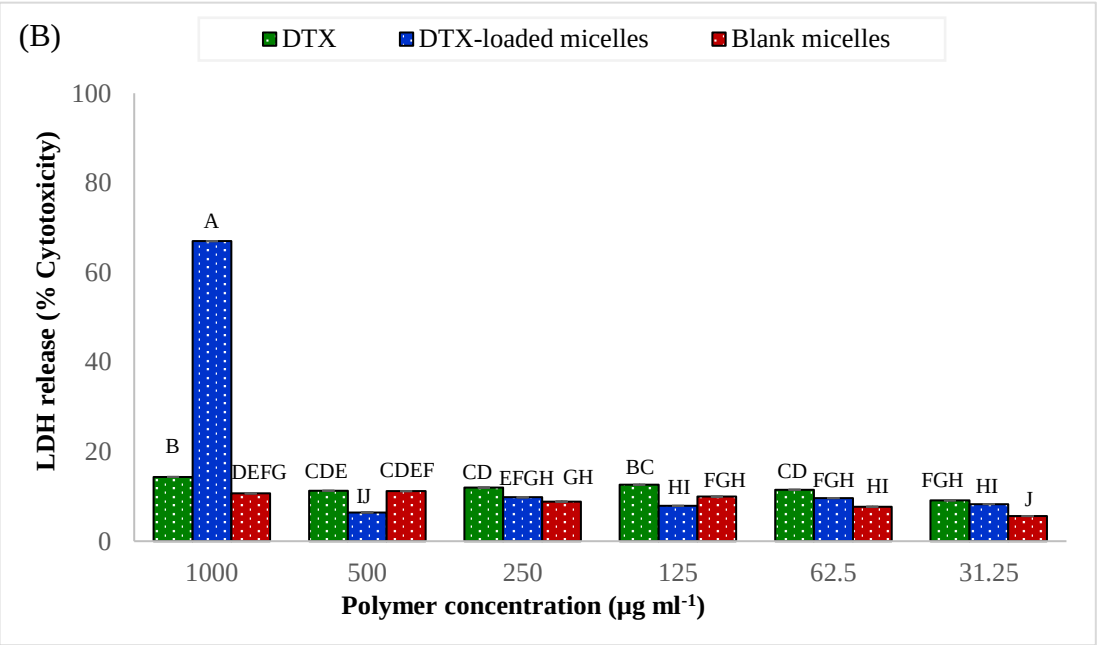


**Figure 6.14.** (A) Cell viability (%) tested by MTT assay and (B) Cytoxicity (%) by LDH assay performed on MCF-7 cancer cells exposed to set concentrations of free DTX, DTX-loaded $MPC_{90}$-$DPA_{90}$ micelles, and blank micelles prepared via direct dissolution (MeOH). (Mean ± SD, n=3) (Original in colour). *Bar values with different letters indicate a significant difference ($p < 0.05$) and those sharing the same letters are not significantly different ($p > 0.05$).*

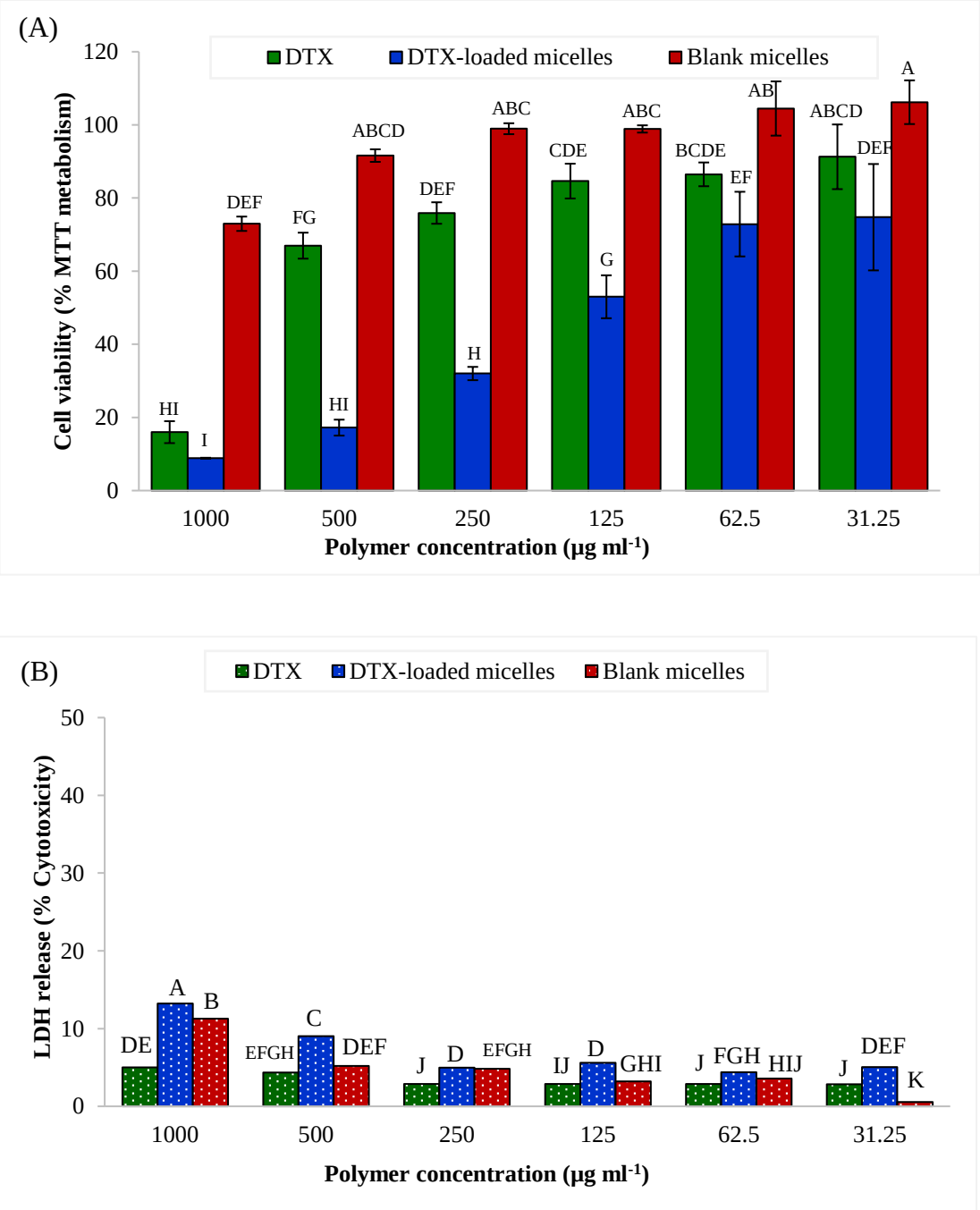


**Figure 6.15.** (A) Cell viability (%) tested by MTT assay and (B) Cytoxicity (%) by LDH assay performed on MCF-7 cancer cells exposed to set concentrations of free DTX, DTX-loaded $MPC_{90}$-$DPA_{90}$ micelles, and blank micelles prepared via direct dissolution (EtOH) (Mean ± SD, n=3) (Original in colour). *Bar values with different letters indicate a significant difference ($p < 0.05$) and those sharing the same letters are not significantly different ($p > 0.05$).*

The MTT cytotoxicity results for nanoprecipitation prepared DTX-loaded $MPC_{90}$-$DPA_{90}$ micelles to SKOV-3 cells after 24 h exposure were presented in Figure 6.16 (A) and Figure 6.17 (A), and the results indicated that blank $MPC_{90}$-$DPA_{90}$ micelles did not induce cytotoxic effects to SKOV-3 cells, whilst free DTX produced a significant ($p < 0.05$) cytotoxic activity against SKOV-3 cells compared to DTX-loaded $MPC_{90}$-$DPA_{90}$ micelles (MeOH) at the highest polymer concentration only (1000 µg $ml^{-1}$) with no significant difference ($p > 0.05$) in toxicity observed afterwards. Furthermore, there was no significant difference ($p > 0.05$) in cytotoxicity between free DTX and DTX-loaded $MPC_{90}$-$DPA_{90}$ micelles (EtOH) as displayed in Figure 6.17 A. These results were in close agreement with LDH assay results after 24 h exposure as shown in Figure 6.16 (B) and Figure 6.17 (B).

In contrast, the MTT cytotoxicity results of DTX-loaded $MPC_{90}$-$DPA_{90}$ micelles prepared by direct dissolution to SKOV-3 cells after 24 h exposure showed a similar trend to that observed with MCF-7 cells, by which DTX-loaded $MPC_{90}$-$DPA_{90}$ micelles produced a significantly ($p < 0.05$) higher cytotoxicity compared to free DTX as shown in Figure 6.18 (A) and Figure 6.19 (A). These results were consistent with the LDH results after 24 h exposure as shown in Figure 6.18 (B) and Figure 6.19 (B). Moreover, for the blank $MPC_{90}$-$DPA_{90}$ micelles in both formulations there was no significant ($p > 0.05$) cytotoxicity after 24 h incubation.

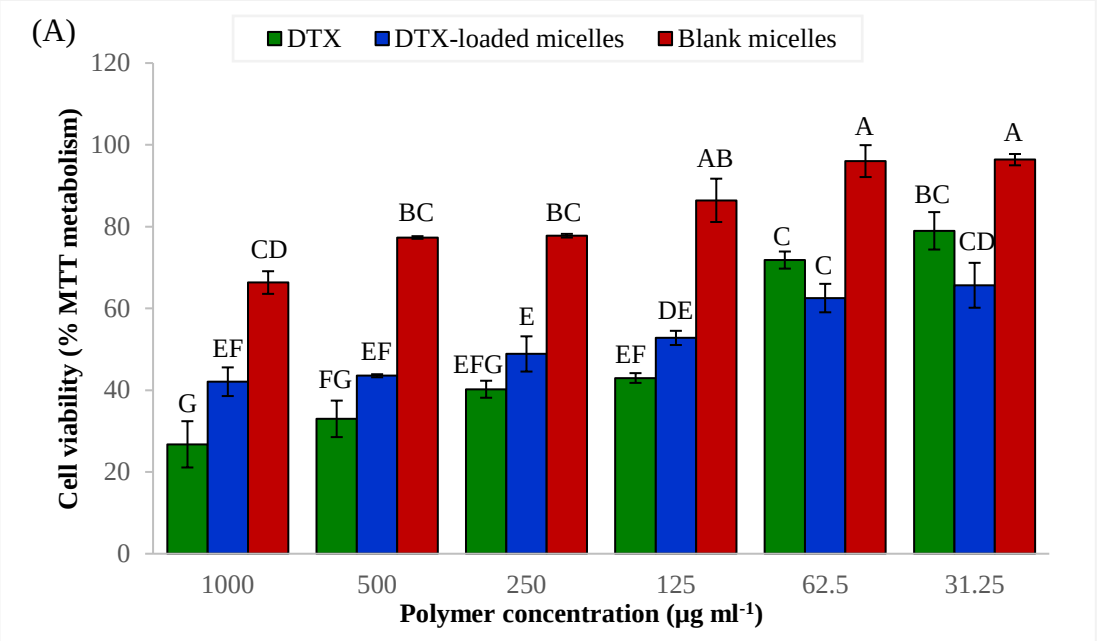


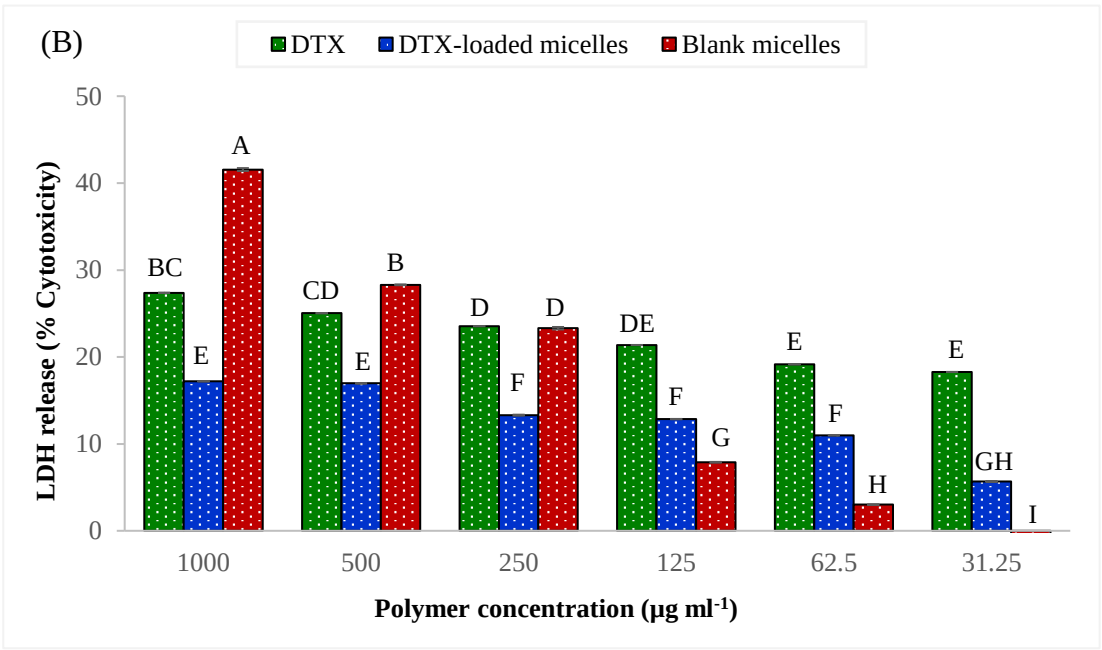


**Figure 6.16.** (A) Cell viability (%) tested by MTT assay and (B) Cytoxicity (%) by LDH assay performed on SKOV-3 cancer cells exposed to set concentrations of free DTX, DTX-loaded $MPC_{90}$-$DPA_{90}$ micelles, and blank micelles prepared via nanoprecipitation (MeOH). (Mean ± SD, n=3) (Original in colour). *Bar values with different letters indicate a significant difference ($p < 0.05$) and those sharing the same letters are not significantly different ($p > 0.05$).*

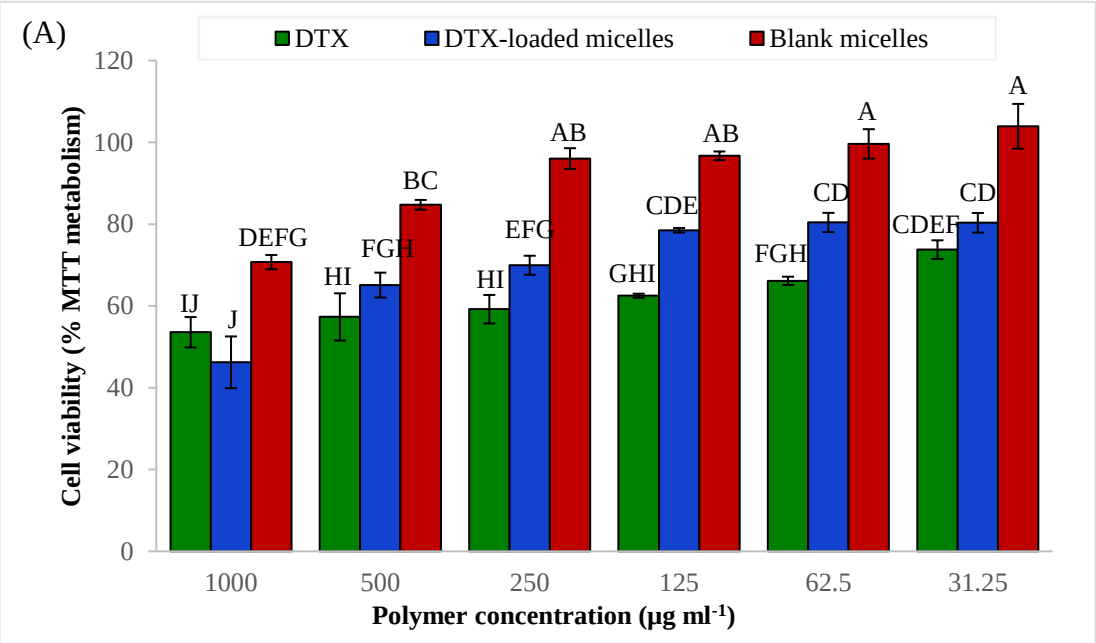


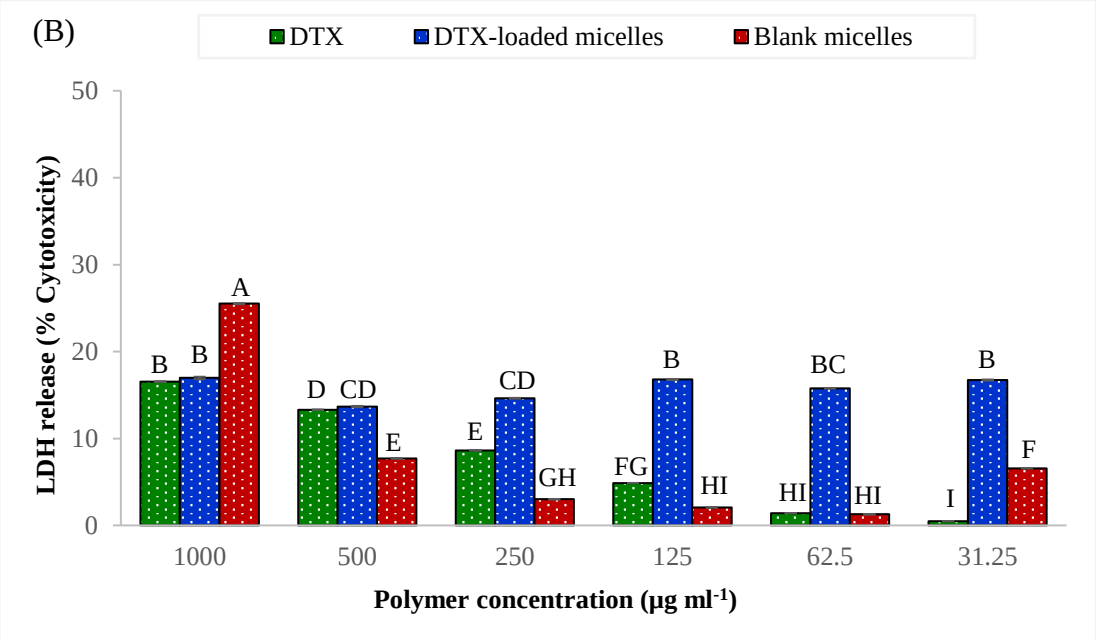


**Figure 6.17.** (A) Cell viability (%) tested by MTT assay and (B) Cytoxicity (%) by LDH assay performed on SKOV-3 cancer cells exposed to set concentrations of free DTX, DTX-loaded $MPC_{90}$-$DPA_{90}$ micelles, and blank micelles prepared via nanoprecipitation (EtOH). (Mean ± SD, n=3) (Original in colour). *Bar values with different letters indicate a significant difference ($p < 0.05$) and those sharing the same letters are not significantly different ($p > 0.05$).*

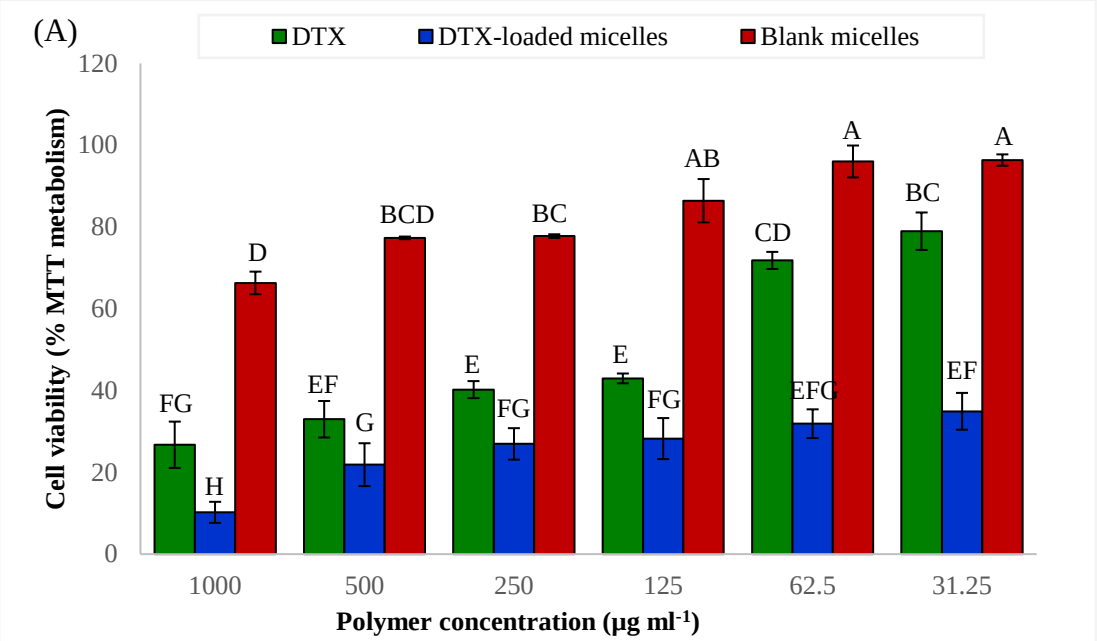


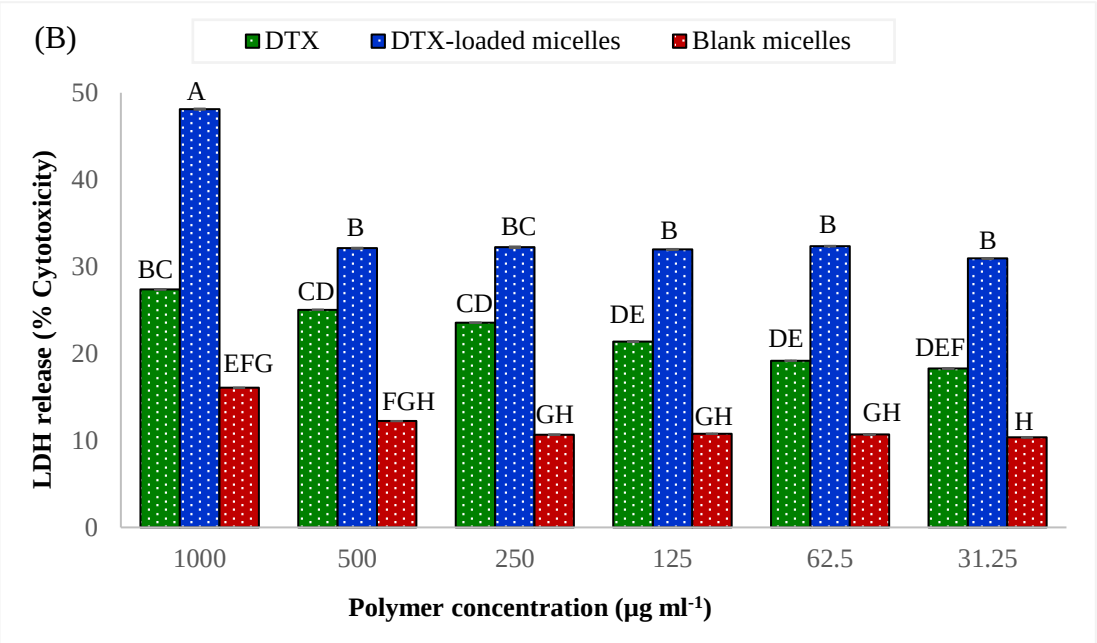


**Figure 6.18.** (A) Cell viability (%) tested by MTT assay and (B) Cytoxicity (%) by LDH assay performed on SKOV-3 cancer cells exposed to set concentrations of free DTX, DTX-loaded $MPC_{90}$-$DPA_{90}$ micelles, and blank micelles prepared via direct dissolution (MeOH). (Mean ± SD, n=3) (Original in colour). *Bar values with different letters indicate a significant difference ($p < 0.05$) and those sharing the same letters are not significantly different ($p > 0.05$).*

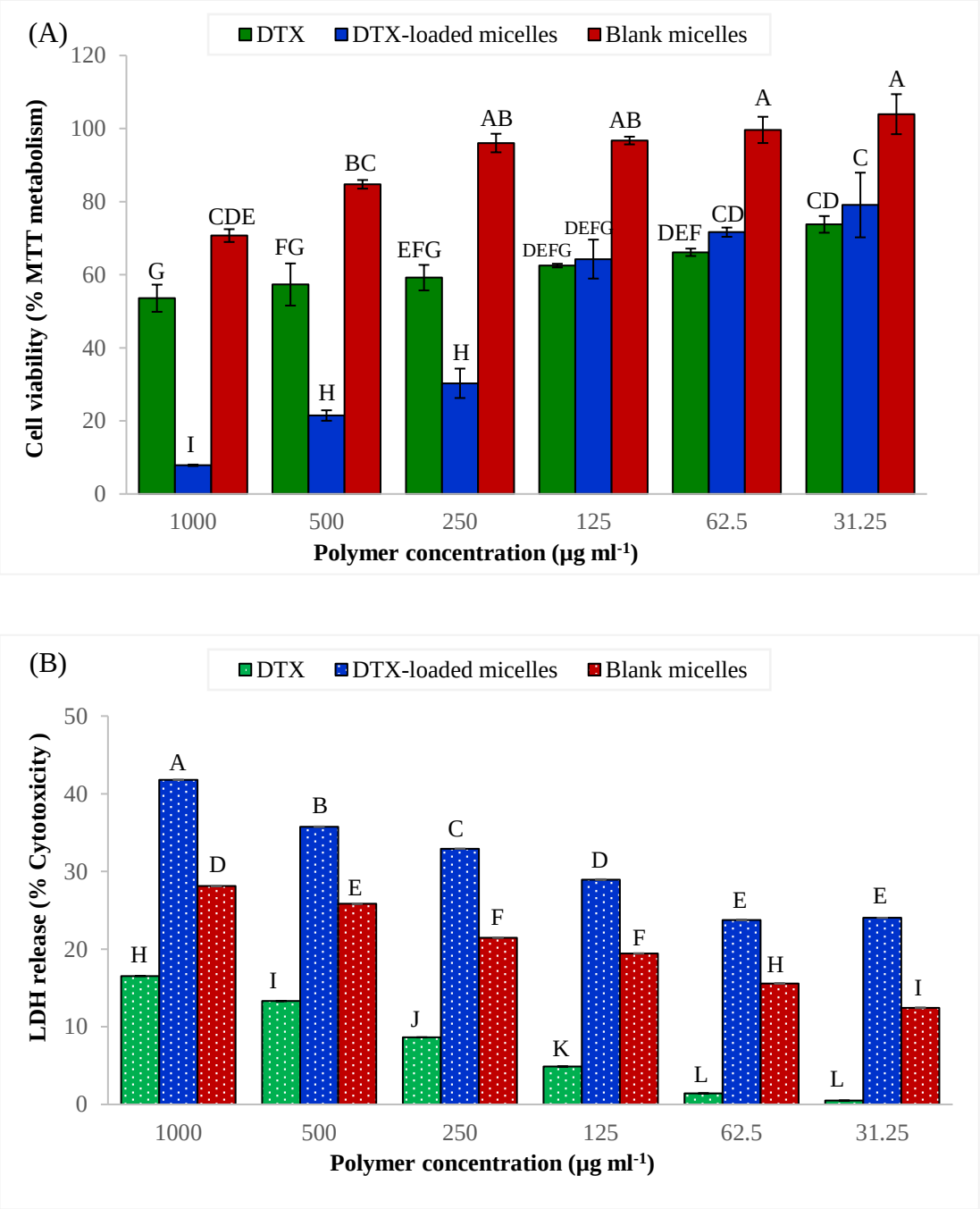


**Figure 6.19.** (A) Cell viability (%) tested by MTT assay and (B) Cytoxicity (%) by LDH assay performed on SKOV-3 cancer cells exposed to set concentrations of free DTX, DTX-loaded $MPC_{90}$-$DPA_{90}$ micelles, and blank micelles prepared via direct dissolution (EtOH). (Mean ± SD, n=3) (Original in colour). *Bar values with different letters indicate a significant difference ($p < 0.05$) and those sharing the same letters are not significantly different ($p > 0.05$).*

As shown in Figure 6.20 (A) and Figure 6.21 (A), blank $MPC_{90}$-$DPA_{90}$ micelles did not produce cytotoxicity after exposure for 24 h in PC-3 cells in the MTT assays. The free DTX and DTX-loaded $MPC_{90}$-$DPA_{90}$ micelles prepared by nanoprecipitation (MeOH) also displayed a no significant difference ($p > 0.05$) in the cytotoxic activity against PC-3 cells. However, free DTX and DTX-loaded $MPC_{90}$-$DPA_{90}$ micelles prepared by nanoprecipitation (EtOH) showed comparably high cytotoxic effects, but no significant differences ($p > 0.05$). These results were in close agreement with LDH assay results after 24 h exposure as shown in Figure 6.20 (B) and Figure 6.21 (B).

The MTT cytotoxicity results of DTX-loaded $MPC_{90}$-$DPA_{90}$ micelles prepared by direct dissolution for PC-3 cells after 24 h exposure showed a similar trend to that observed in MCF-7 and SKOV-3 cells, by which DTX-loaded $MPC_{90}$-$DPA_{90}$ micelles (MeOH) showed a significantly ($p < 0.05$) decrease in cell viability compared to free DTX as shown in Figure 6.22 (A). Both free DTX and DTX-loaded $MPC_{90}$-$DPA_{90}$ micelles (EtOH) showed a comparable reduction in the cell viability effect, but no significant differences ($p < 0.05$) as displayed in Figure 6.23 (A). These results were consistent with the LDH results after 24 h exposure as shown in Figure 6.22 (B) and Figure 6.23 (B). Moreover, the blank $MPC_{90}$-$DPA_{90}$ micelles in both formulations did not show cytotoxicity after 24 h incubation.

Overall, the ability of DTX-loaded $MPC_{90}$-$DPA_{90}$ micelles to inhibit cell growth varies depending on cells type and micelle loading method, in which nanoprecipitation based loaded micelles showed similar trends in the three cell lines, of limited cytotoxicity compared to micelles loaded with DTX via direct dissolution. Moreover, free DTX showed limited toxicity compared to DTX-loaded micelles (via direct dissolution).

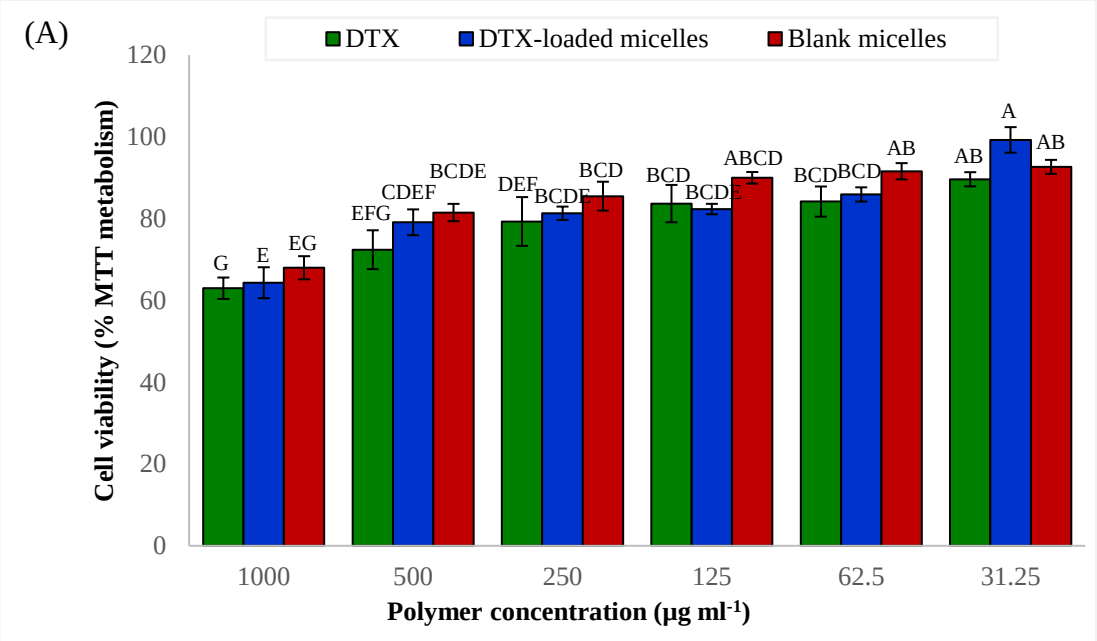


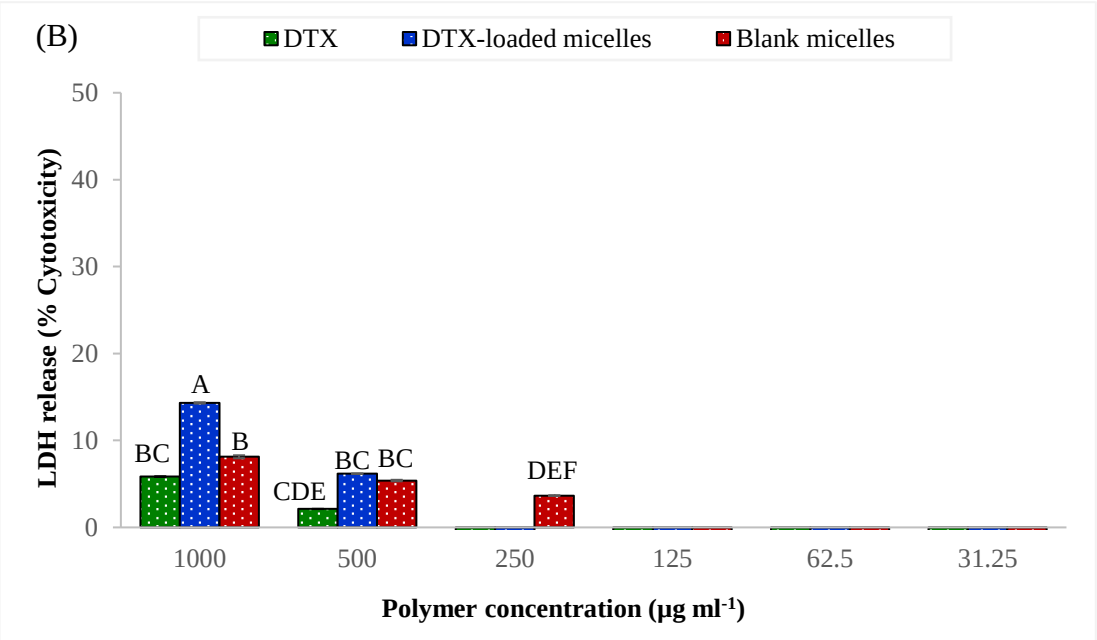


**Figure 6.20.** (A) Cell viability (%) tested by MTT assay and (B) Cytoxicity (%) by LDH assay performed on PC3 cancer cells exposed to set concentrations of free DTX, DTX-loaded $MPC_{90}$-$DPA_{90}$ micelles, and blank micelles prepared via nanoprecipitation (MeOH). (Mean ± SD, n=3) (Original in colour). *Bar values with different letters indicate a significant difference ($p < 0.05$) and those sharing the same letters are not significantly different ($p > 0.05$).*

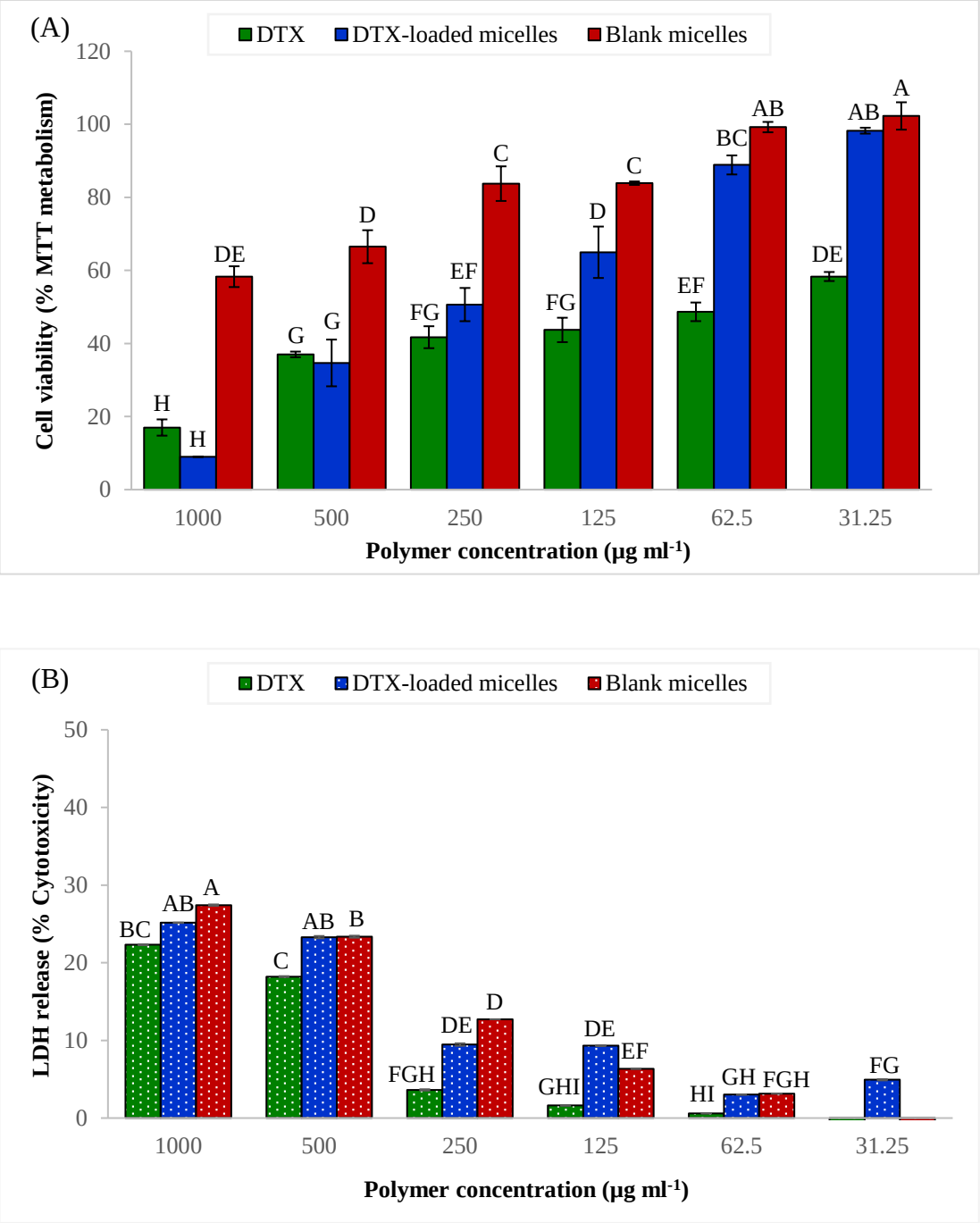


**Figure 6.21.** (A) Cell viability (%) tested by MTT assay and (B) Cytoxicity (%) by LDH assay performed on PC3 cancer cells exposed to set concentrations of free DTX, DTX-loaded $MPC_{90}$-$DPA_{90}$ micelles, and blank micelles prepared via nanoprecipitation (EtOH). (Mean ± SD, n=3) (Original in colour). *Bar values with different letters indicate a significant difference ($p < 0.05$) and those sharing the same letters are not significantly different ($p > 0.05$).*

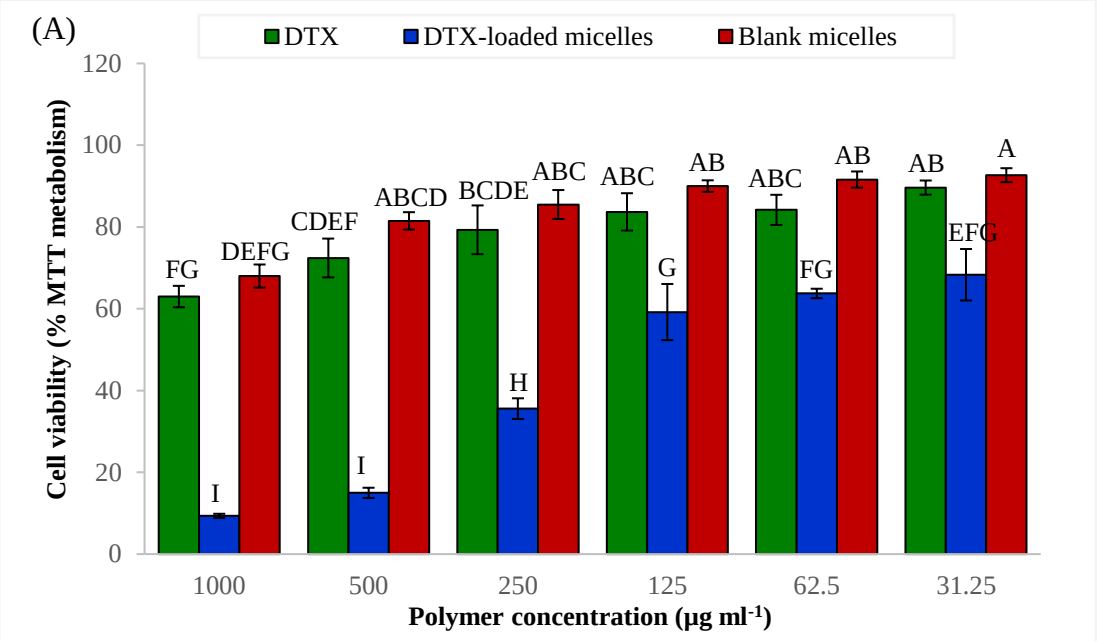


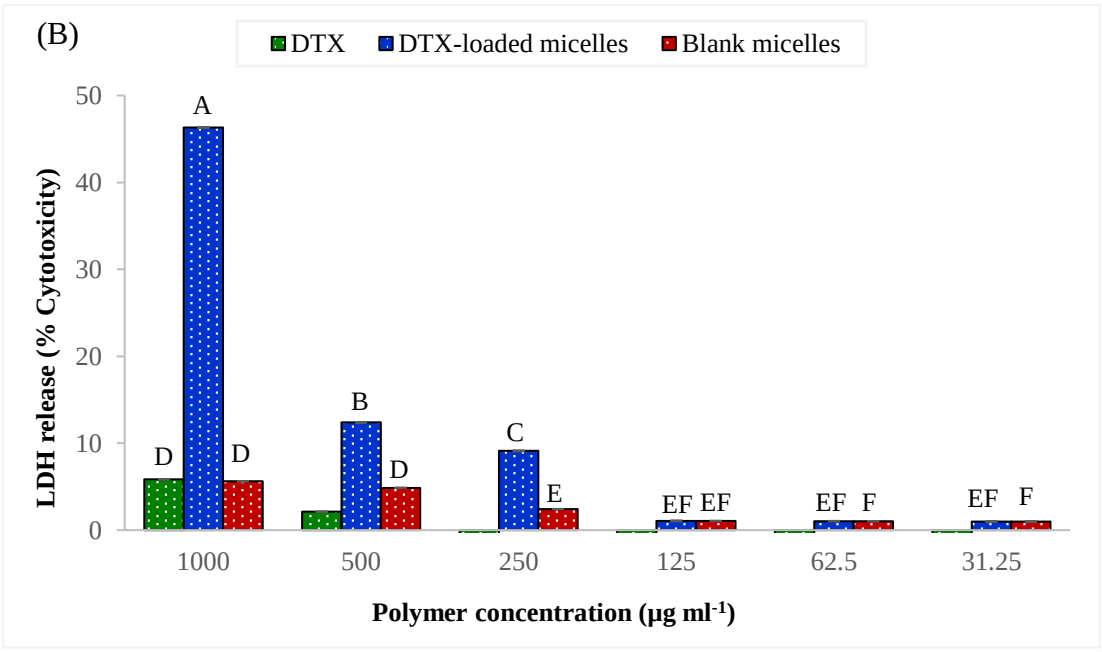


**Figure 6.22.** (A) Cell viability (%) tested by MTT assay and (B) Cytoxicity (%) by LDH assay performed on PC3 cancer cells exposed to set concentrations of free DTX, DTX-loaded $MPC_{90}$-$DPA_{90}$ micelles, and blank micelles prepared via direct dissolution (MeOH). (Mean ± SD, n=3) (Original in colour). *Bar values with different letters indicate a significant difference ($p < 0.05$) and those sharing the same letters are not significantly different ($p > 0.05$).*

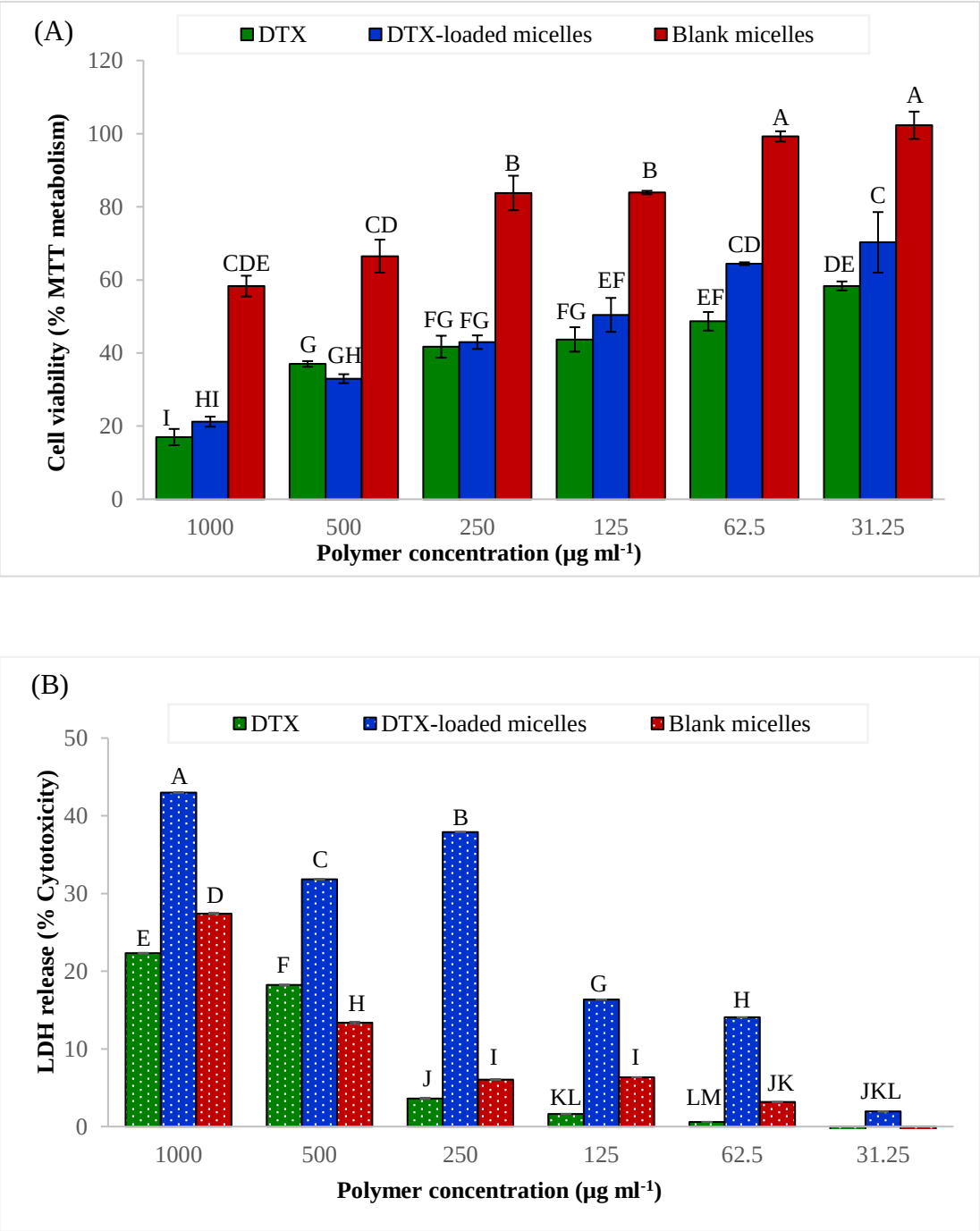


**Figure 6.23.** (A) Cell viability (%) tested by MTT assay and (B) Cytoxicity (%) by LDH assay performed on PC3 cancer cells exposed to set concentrations of free DTX, DTX-loaded $MPC_{90}$-$DPA_{90}$ micelles, and blank micelles prepared via direct dissolution (EtOH). (Mean ± SD, n=3) (Original in colour). *Bar values with different letters indicate a significant difference ($p < 0.05$) and those sharing the same letters are not significantly different ($p > 0.05$).*

## 6.3 Discussion

An effective drug delivery system is usually characterised by efficient drug encapsulation and release at the site of action. Therefore, this chapter was designed to investigate the behaviour of MPC-DPA micelles as future nano-systems for delivering the anticancer agent docetaxel to a site of action, through studying the *in-vitro* anticancer efficacy, uptake, and internalisation of DTX-loaded MPC-DPA micelles in human cancer cell lines.

### 6.3.1 Characterisation of Docetaxel (DTX)-loaded micelles

Docetaxel (DTX) is a hydrophobic semisynthetic analogue of paclitaxel (PTX) that is derived from 10-deacetyl baccatin III and is widely used in the treatment of a range of cancers (Rowinsky, 1997; Naik et al., 2012). DTX is an antimitotic agent that disrupts microtubule dynamics through binding to the tubulin, leading to mitotic arrest and apoptosis, i.e. interfering with cell division (Morikawa et al., 2012). Compared to PTX, DTX has been reported to produce more antitumor activity both *in-vitro* and *in-vivo* studies (Esmaeili et al., 2008; Hu et al., 2015a). Although DTX is an important chemotherapeutic agent against cancer, it has very poor water solubility (3 μg $ml^{-1}$), low selective distribution, and rapid phagocytic activity, and renal clearance, which limit its clinical applications (Chen et al., 2013). Therefore, in order to overcome the aforementioned limitations, DTX is formulated using high concentrations of the nonionic surfactant Tween 80 (polysorbate 80) and ethanol (50:50, v/v) in order to dissolve the DTX in the current commercial available formulation (Immordino et al., 2003; Liu et al., 2008). Unfortunately, intravenous DTX administration of the commercial formulation has been associated with acute hypersensitivity reactions, peripheral neuropathy and cumulative fluid retention (Engels and Verweij, 2005; Baker et al., 2009), which have been attributed to the use of Tween 80 (Engels and

Verweij, 2005; Hennenfent and Govindan, 2005; Li et al., 2016). Therefore, efforts have focused on reformulating DTX to use less toxic and better tolerated Tween-80 free formulations in order to overcome the drawbacks associated with the presence of Tween 80. One of these alternative drug delivery systems has been based on polymeric micelles (Liu et al., 2008; Gaucher et al., 2010; Ostacolo et al., 2010; Gu et al., 2012; Chen et al., 2013).

Different preparation methods for loading DTX into micelles were assessed to select the best method to produce formulations with the most favourable characteristics. Therefore, in this Chapter, two preparation methods were utilised to encapsulate DTX within MPC-DPA micelles, in order to highlight the effect of preparation method and solvent selection on MPC-DPA micelle size, PDI and drug loading. The first method was nanoprecipitation, an easy and reproducible method, which offers a promising process for the preparation of a range of nanoparticle systems (Barichello et al., 1999; Betancourt et al., 2007; Zhao et al., 2012; Salvage et al., 2015), and the second was direct dissolution that has been commonly employed for loading drugs into polymeric micelles (Chiappetta et al., 2008; Yang et al., 2009b; Ding et al., 2012b).

In this project, both MeOH and EtOH were the solvents used in the preparation method, due to the changes they have previously provided on the physicochemical properties of MPC based polymers (Edmondson et al., 2010; Salvage et al., 2015).

For DTX-loaded MPC-DPA micelles prepared via nanoprecipitation, and as shown in Table 6.1, DTX-loaded MPC-DPA micelles prepared in MeOH-PBS (pH 7.4) systems produced small monodisperse micelles compared to micelles prepared in EtOH-PBS (pH 7.4) systems, and this can be attributed to the highest dielectric constant of methanol that result in the production of small nanoparticles (Singh et al., 1999). These results were consistent with the data reported from other studies that explored

the effect of solvent selection in polymeric micelle preparation (Bilati et al., 2005; Schubert and Müller-Goymann, 2003; Salvage et al., 2015).

For loaded MPC-DPA nano-systems prepared via direct dissolution; after being dialysed against PBS (pH 7.4); a small increase in the size of DTX loaded MPC-DPA micelles was recorded with the development of polydisperse nano-systems compared to the pre-dialysed monodisperse nano-systems as shown in Table 6.2 for MeOH-PBS systems. These data agreed with data reported from other studies, where loaded micelles were slightly larger than the corresponding blank micelles (Licciardi et al., 2006; Sezgin et al., 2006; Shi et al., 2015b; Salvage et al., 2016). Conversely, a decrease in the size of DTX-loaded MPC-DPA micelle was observed compared to the pre-dialysis MPC-DPA micelle, where the systems tended to be polydisperse, as shown in Table 6.2 for EtOH-PBS systems, which can be attributed to the strong hydrophobic interactions between the encapsulated drug and DPA core (Licciardi et al., 2006; Shi et al., 2015b).

### 6.3.2 DTX loading and encapsulation efficiency

In general, the length of the core-forming block, the compatibility between the drug and the core, and the preparation of drug-loaded micelles are the main factors that influence the drug loading efficiency (Allen et al., 1999; Liu et al., 2006; Rapoport, 2007).

The drug loading (DL%) and encapsulation efficiency (EE%) of DTX were investigated and the results presented in Table 6.4 and 6.5 for DTX loaded via nanoprecipitation and direct dissolution respectively. These data showed that both the DL and EE for most samples increased with an increase in the hydrophobic block of MPC-DPA micelle (DPA block) as greater drug entrapment is usually obtained with longer hydrophobic blocks (Allen et al., 1999).

The EE and DL increased with increased nanoparticle size in MeOH based nanoprecipitation prepared MPC-DPA micelle and micelles loaded via direct dissolution after EtOH removal. These results were comparable with other MPC-DPA reports (Colley et al., 2014; Salvage et al., 2016) and studies which involved DTX loaded into other micelles (Liu et al., 2010; Mi et al., 2011; Shi et al., 2015a). However, the DL% was relatively lower than that obtained in previous MPC-DPA reports as the starting drug: polymer ratio here was 1:40 compared to 1:10 (Giacomelli et al., 2006; Licciardi et al., 2006) or 1:5 (Chu et al., 2009) ratios in other studies, as the DL was restricted by DTX solubility in MeOH and EtOH.

It was noted that the direct dissolution method yielded a comparable loading efficiency to that observed with nanoprecipitation prepared micelles, which can be further increased by the increasing the stirring time required for drug encapsulation (Yang et al., 2009b).

### 6.3.3 *In-vitro* Docetaxel release studies

The ability of micelles to entrap hydrophobic drugs to prolong system circulation time is an important factor for drug accumulation in tumours via the EPR effect. Therefore, the *in-vitro* DTX release profile against time was studied in physiological conditions; PBS (pH 7.4) to simulate the environment of blood and body temperature (37°C) (as described in Section 2.2.3.3).

As shown in Figure 6.1 and 6.2, a burst DTX release from all MPC-DPA micelle samples was observed for an initial 6 hours then followed by a sustained release from the MPC-DPA micelles for the experimental duration of 4 days. In DTX loaded MPC-DPA micelles based on nanoprecipitation from MeOH, more than 60% of the total drug was released by 6 hours compared to less than 30% for DTX loaded MPC-DPA micelles based on EtOH. Moreover, the amount of DTX released after 6 hours from

most of the DTX loaded MPC-DPA micelles samples prepared by direct dissolution reached 80% with the exception of $MPC_{20}$-$DPA_{20}$ micelles, which had a burst release of less than 50%. The burst release may be attributed to the rapid diffusion of DTX on the surface of nanoparticles. Thus, DTX was deposited at the region near or within the MPC shell and has access to the aqueous medium without the need for extended diffusion times (Zhang et al., 2004; Hu et al., 2015a). The subsequent sustained release was due to the slow diffusion of DTX from the core of the hydrophobic carrier (DPA) (Hu et al., 2015a), in which circa 85% of the total loaded DTX (via nanoprecipitation in MeOH) diffused from MPC-DPA micelle within 4 days, whilst the release from MPC-DPA micelles based on EtOH was less than 50%. Moreover, more than 90% of DTX was released by most of the loaded MPC-DPA micelles nano-systems prepared by direct dissolution over the 4 days except for $MPC_{20}$-$DPA_{20}$ micelles, which released 70-80% of DTX in the same period. Generally, the small particles possess a large surface area-to-volume ratio; therefore, most of the drug associated with small particles would be at or near the particle surface with the small diffusion distances encountered in the particles allowing trapped drugs to diffuse out rapidly and also for the release medium to diffuse in, leading to faster drug release. Conversely, the large particles possess large cores, which allow more drug to be encapsulated per particle and hence lead to a slower release (Redhead et al., 2001).

It is well reported that the molecular weight of the hydrophobic block is one of the main factors that determines the size of micelle cores and thereby affects the rate of drug release from micelles (Liu et al., 2006). Therefore, a longer hydrophobic chain forms a larger micelle core, which should release drugs at a slower rate than copolymers with a smaller molecular weight (Liu et al., 2006; Shi et al., 2015a). This concept was consistent with the results obtained, in which the release rate of DTX

from MPC-DPA micelles decreased with the increase in the molecular weight or size of the DPA block. Furthermore, the drug release from the core-shell structure of micelles is largely dependent on the interaction between the drug and core, therefore, an increase in this interaction can occur with a larger hydrophobic block of the MPC-DPA, which in turn requires a longer time for DTX to diffuse across the MPC-DPA micelles to the release medium due to strong hydrophobic interaction (Rajagopal et al., 2010; Shi et al., 2015b).

It was noted that DTX release data (Figure 6.1 and Figure 6.2) of MPC-DPA micelles were relatively close particularly with the DTX- loaded $MPC_{50}$-$DPA_{50}$ and DTX-loaded $MPC_{90}$-$DPA_{90}$ micelles, which attributed to the close actual polymer compositions of the two micelles (i.e. the achieved MPC-DPA diblock copolymers) and the equivalent amount of DTX contained in MPC-DPA nanoparticles. Additionally, and as shown in Table 6.4 and Table 6.5, the reported encapsulation efficacy and drug loading results displayed no marked variability between DTX loading to the different MPC-DPA compositions, although some deviations were observed which was expected due to the different loading preparation method and the utilised solvent.

In general, an initial burst release followed by slow and sustained release of drug from polymeric micelles is considered advantageous for the drug delivery applications, as it limits the dose frequency and enables prolonged drug release after single dose.

### 6.3.4 The cellular uptake of Cm-6-loaded micelles:

The successful internalisation of anticancer drugs into cancer cells is an essential step in the achievement of therapeutic effects, as delivering drugs via nanocarriers to the surface of cells is not an indication that the drugs have reached their target. It is well reported that the cancer cells are more porous than the normal cells, therefore, they

can uptake polymeric micelles quite easily and once they enter the cellular compartment through either endocytosis or other pathways; they conjugate with the acidic lysosomal vesicles in the cellular compartment, which makes environment very acidic and consequently, the degradation of the polymeric micelles can occur with the concomitant release of the entrapped drug molecules in the lysosomal pH (Laskar et al., 2014). Therefore, the differential endocytic pathways between normal and cancer cell lines can be the gateway for the selective targeting of novel nanoparticles into tumours (Sahay et al., 2010).

In this project Cm-6 was used to represent DTX (as described in Section 2.2.3.6) due to its biocompatibility and its high fluorescence activity, which enables the evaluation of cellular uptake (Shi et al., 2015b). As shown in the CLSM images in Figure 6.3, 6.5, and 6.7, Cm-6-loaded MPC-DPA micelles were localised extensively in the cytoplasmic region near the cell membrane after 1 h in all cancer cells tested, MCF-7, SKOV-3, and PC3 cells. These results were consistent with the flow cytometric data that showed a higher accumulation percent of fluorescent MPC-DPA micelles compared to free Cm-6 in all cancer cell types tested at the same conditions. Therefore, it can be concluded that MPC-DPA micelles play an important role in mediating the intracellular uptake of drugs.

As cellular uptake is a time-dependent process, MCF-7, SKOV-3, and PC3 cells were incubated with Cm-6 loaded MPC-DPA micelles at different times (1min, 5min, 10 min, 30 min, and 1 hour) (as described in Section 2.2.3.6.1). However, and as shown in Figure 6.4, 6.6, and 6.8, there was no significant difference ($p > 0.05$) in the fluorescent intensity observed with increased exposure time, these results were in close agreement with other studies involving nanoparticles uptake (Peñaloza et al., 2017). It was noted that among the loaded MPC-DPA micelles, 38 nm and 44 nm

MPC-DPA micelles showed higher uptake than the smaller 25 nm micelles, this trend was observed in cancer cell lines, which differed from that observed in the normal cell lines, due to the difference between healthy and cancer cells, which confirmed that uptake varies from cell to cell and is affected by the size of nanoparticles. These findings were in close agreement with reports which have studied nanoparticle uptake such as gold nanoparticles (Chithrani et al., 2006), polystyrene nanoparticles (Varela et al., 2012), and micelles (Tu et al., 2011). Additionally, these results may suggest that the higher uptake of larger micelles could be due to the strong adhesion to the cell surface compared to the smaller micelles, as the small nanoparticles have a smaller van der Waals adhesion force and higher diffusion that can be contributed to the lower uptake rate when compared with the other two larger studied micelles (Israelachvili, 1992).

In order to elucidate the cellular uptake mechanism, and to validate that the loaded MPC-DPA micelles were internalised by an energy-dependent process, an endocytosis inhibition studies were carried out by incubating cancer cells with an equivalent concentration (15 µg $ml^{-1}$) of free Cm-6 and Cm-6 loaded MPC-DPA micelles at 37°C and 4°C to minimise the endocytosis process for 1 hour (Fredericksen et al., 2002) (as described in Section 2.2.3.6.3). These experiments were performed for 1 h as blocking one route of endocytosis might activate other routes, therefore, this short time is preferable (Conner and Schmid, 2003; Harush-Frenkel et al., 2007). As shown in Figure 6.9, 6.10, and 6.11 for MCF-7, SKOV-3, and PC3 cells respectively, a significant ($p < 0.05$) decrease in micelle internalisation was observed in most cells, which suggested endocytosis inhibition; with the exception of 25 nm Cm-6-loaded MPC-DPA micelles entry into MCF-7 cells. This confirmed that most micelles were taken up via endocytosis, whilst free drugs entered cells via a passive diffusion

mechanism (Massignani et al., 2009; Ostacolo et al., 2010; de Melo-Diogo et al., 2014; Wang et al., 2015a). These results were consistent with previous studies that investigated the mechanisms involved in the internalisation of nanoparticles in MCF-7 (Mahmud and Lavasanifar, 2005; Shi et al., 2015b), SKOV-3 (Koopaei et al., 2014; Peñaloza et al., 2017), and PC3 cells (Sulheim et al., 2016; Snipstad et al., 2017).

### 6.3.5 *In-vitro* anticancer efficacy:

As it was previously reported that receptor-based endocytosis was highest for 40-50 nm nanoparticles (Chithrani et al., 2006; Jiang et al., 2008), and considering the physicochemical characterisations and data obtained in the uptake and release studies, $MPC_{90}$-$DPA_{90}$ was chosen at this stage for further study of the efficacy of DTX-loaded $MPC_{90}$-$DPA_{90}$ formulations to defeat selected cancer cell lines (MCF-7, SKOV-3, and PC3) by assaying their cytotoxicity.

Although, there are a wide variety of assays that can be utilised to assess the cytotoxicity of nanoparticles, the most commonly used one was the MTT assay which measured the mitochondrial activity of cells. In conjugation with MTT, an LDH assay was also used, which measured the activity of intracellular LDH that was released to the extracellular media by damaged cells (Stone et al., 2009; Ratoi et al., 2014).

In MTT and LDH assays, the blank $MPC_{90}$-$DPA_{90}$ micelles were used in the equivalent concentrations to that used in DTX-loaded $MPC_{90}$-$DPA_{90}$ micelles and as shown in Figure 6.12-6.23, limited or no toxicity results were obtained ($p < 0.05$), which were consistent with the results reported in Chapter 5, thereby these MPC-DPA diblock copolymers can be considered safe and suitable for biomedical applications. Moreover, the cell viability of DTX-loaded $MPC_{90}$-$DPA_{90}$ micelles was lower than that of blank $MPC_{90}$-$DPA_{90}$ micelles in almost all samples, which indicated a statistically significant ($p < 0.05$) cytotoxicity was obtained by encapsulating DTX

into $MPC_{90}$-$DPA_{90}$ micelles. Furthermore, the nanoprecipitation based DTX-loaded $MPC_{90}$-$DPA_{90}$ micelles showed limited cytotoxicity compared to $MPC_{90}$-$DPA_{90}$ micelles loaded with DTX via direct dissolution, which confirmed the effect of different loading processes.

As shown in the cytotoxicity data for MCF-7, SKOV-3, and PC3 cells incubated with DTX-loaded $MPC_{90}$-$DPA_{90}$ micelles prepared by nanoprecipitation, free DTX displayed a statistically significant ($p < 0.05$) cytotoxicity than DTX-loaded $MPC_{90}$-$DPA_{90}$ micelles, which can be attributed to the ability of free DTX to enter cells via passive diffusion process which was faster than endocytosis in addition to the slow sustained release of DTX from micelles producing lower concentrations of the drug compared to free drug at the same time (Xie et al., 2013; Wang et al., 2016). Conversely, the cytotoxicity results of MCF-7 (Figure 6.15), SKOV-3 (Figure 6.18), and PC3 (Figure 6.22) cells incubated with DTX-loaded $MPC_{90}$-$DPA_{90}$ micelles prepared via direct dissolution, free DTX displayed a limited toxicity compared to DTX-loaded $MPC_{90}$-$DPA_{90}$ micelles, which can be due to a more efficient intracellular drug release.

It was noted that DTX blocks cell cycle progress at a specific phase, i.e. DTX exerts its effect on tumour cells by the inhibition of cell mitosis in the late G2 and M phase. Therefore, the capability of DTX-loaded $MPC_{90}$-$DPA_{90}$ micelles to sustain drug release acts selectively on a higher number of cells in a specific phase of cell cycle; through induced polymerisation of tubulin monomer and depolymerisation leading to mitotic arrest, compared to a bolus DTX administration (Aggarwal et al., 2009; Tu et al., 2011; Shi et al., 2015b).

It was reported previously that the incubation time and concentration have a role in *in-vitro* cytotoxicity of DTX (Liu et al., 2010; Shi et al., 2015b), therefore, a low cell

viability and/or higher cell mortality were associated with higher drug concentrations in all cell lines as shown in Figure 6-12-6.23. Moreover, the survival rate for both the MTT and LDH assays was measured after only 24 h exposure, therefore, time-dependent cytotoxicity was less applicable here. The reported results were as expected, as most cytotoxicity studies involving DTX-loaded nanoparticles (Liu et al., 2010; Ostacolo et al., 2010; Zeng et al., 2015; Guan et al., 2017; Tang et al., 2015) or other anticancer drugs (Danhier et al., 2009; Tu et al., 2011; Tabatabaei Mirakabad et al., 2016; Thomas et al., 2016) were carried out for extended time period rather than 24 hour only. This resulted in dramatic reductions in cell viability with increasing incubation time. Furthermore, it was previously reported that nanoparticle loaded DTX requires a 72 hour incubation period to kill some types of tumour cells such as MCF-7 (Zeng et al., 2015), SKOV-3 (Ganta et al., 2016; Hami et al., 2017), and PC3 (Sanna et al., 2011; Dubey et al., 2016). Therefore, a longer incubation period may be required for DTX-loaded $MPC_{90}$-$DPA_{90}$ micelles due to the sustained release of DTX from MPC-DPA micelles as demonstrated in the earlier *in-vitro* release studies (Gu et al., 2012).

### 6.4 Summary

In conclusion, MPC-DPA based micelles were able to encapsulate and release docetaxel and demonstrated their applicability for the delivery of docetaxel to relevant cancer cells. Moreover, it was shown that the incorporation of DTX in MPC-DPA micelles enhanced the anti-tumoral efficacy of DTX compared to free DTX, particularly with SKOV-3 and PC3 cell lines. Therefore, MPC-DPA micelles were considered promising nano-system for DTX delivery.

# CHAPTER SEVEN

# GENERAL DISCUSSION AND CONCLUSION

## 7.1 Study general discussion

This project aimed to develop novel diblock copolymer nano-systems that were composed of 2-methacryloyloxyethyl phosphorylcholine (MPC) with 2-(diisopropylamino)ethyl methacrylate (DPA) for pharmaceutical applications. The MPC block was considered a suitable hydrophilic shell block candidate for the formation of drug delivery micelles, because of its non-thrombogenic properties and biocompatibility (Lewis, 2000).

Moreover, the pH-responsive properties of DPA have attracted wide attention and have been used as the core block in polymeric micelles for the encapsulation of a wide variety of hydrophobic drugs. Therefore, these MPC-DPA diblock copolymers were designed to entrap hydrophobic drugs in the hydrophobic core, form micelles at neutral pH, and then release the drug in response to a decrease in pH (Licciardi et al., 2006; Giacomelli et al., 2006).

This project was an integrated body of work based on the achievement of three main tasks:

(1) MPC-DPA diblock copolymer synthesis, which involved the establishment of ethanolic ATRP for polymer synthesis that lead to the production of novel ratio composition block copolymers.

(2) MPC-DPA diblock copolymer characterisation, which focused on the ability of this copolymer to form micelles, and the effect of copolymer concentration, solution pH, and temperature, and time on nanoparticle size, polydispersity and morphology assessment.

(3) Bioevaluation, which involved the following:

a. *In-vitro* cell cytotoxicity assays of MPC-DPA nano-systems.

b. Cellular uptake of MPC-DPA nano-systems using *in-vitro* cell lines.

c. Drug loading and release profiles of MPC-DPA nanoparticles.

d. Delivery of the anticancer drug docetaxel to relevant *in-vitro* cancer cell lines.

This project built upon previous work and contributed novel data to fill gaps in the predictive matrix of characteristics for MPC-DPA copolymers, which have demonstrated biocompatible traits in the form of negligible *in-vitro* cytotoxicity. Moreover, several key questions were proposed relative to the aims and objectives when this project was designed, and this chapter will help in clarify them.

***Q1- Does ethanol offer the same controllability for ATRP to produce a well-defined MPC-DPA diblock copolymers?***

A series of MPC-DPA diblock copolymers were synthesised using ethanolic atom transfer radical polymerization (ATRP), a method widely adopted by researchers for polymer synthesis due to its robustness and versatility to produce well-defined block copolymers. Because of the possibility of transesterification of methacrylate monomers that may occur with methanol ATRP at ambient temperature (Bories-Azeau and Armes, 2002), anhydrous ethanol was used instead of methanol for polymer synthesis, which resulted in the formation of two sets of 1:1 and 1:2, hydrophilic MPC: hydrophobic DPA block ratio, MPC-DPA copolymers.

$^{1}$H NMR data indicated the successful production of well-defined MPC-DPA diblock copolymers (Table 3.2). These findings were consistent with GPC data (Figure 3.3 and Figure 3.4) of the synthesised copolymer, which displayed a unimodal size distribution with narrow polydispersity for all MPC-DPA diblock copolymers.

Therefore, ethanolic ATRP was considered suitable for a wide range of MPC-DPA diblock copolymers.

***Q2- What effects do MPC-DPA compositions have on nanoparticle size and particle stability?***

It is well reported that the size of particles is a major factor in their biodistribution and clearance by the reticuloendothelial system (RES), in which particles with a diameter of 5 nm are usually cleared from systemic circulation via renal filtration, whilst particles > 200 nm are subjected to clearance via the liver and spleen (Allen et al., 1999). Therefore, nanoparticles with diameters of 50-200 nm are considered appropriate candidates for therapeutic drug delivery applications. In this current work, the particle size of MPC-DPA nanoparticles prepared via nanoprecipitation from methanol in PBS (pH 7.4) were measured using dynamic light scattering (DLS). The mean particle diameters produced ranged from 25-140 nm, and these diameters increased as the molecular weight of the MPC-DPA diblock copolymers increased (Table 4.1). Therefore, subject to being an appropriate size, it is suggested that MPC-DPA nanoparticles may resist elimination through the renal glomeruli (Rapoport, 1999; Kabanov et al., 2002) and RES clearance (Moghimi et al., 2001; Yoo and Park, 2001; Kedar et al., 2010).

Furthermore, all 1:1 ratio MPC-DPA copolymer systems were monodispersed (Table 4.1), compared to the 1:2 ratio MPC-DPA copolymer systems, which tended to be polydisperse (Table 4.1) due to the presence of multiple particle size populations. These data were visually investigated via scanning transmission electron microscopy (STEM), which confirmed the successful formation of MPC-DPA diblock copolymer monodisperse micelles in 1:1 ratio (Figure 4.14), with the exception of 77 nm $MPC_{120}$-$DPA_{120}$ nanoparticles, which formed a mix of micelles and polymersomes (Appendix 12.5). In contrast, the STEM images for the 1:2 ratio MPC-DPA diblock copolymers, displayed polydisperse nano-systems due to the presence of a mixture of larger size

micelles and polymersomes (Figure 4.15), with the exception of the monodisperse micelles formed by 28 nm $MPC_{20}$-$DPA_{40}$ diblock copolymer (Appendix 12.6). These data were consistent with previous studies which reported the effect of the hydrophilic-hydrophobic block ratio on the morphology of polymer aggregates, in which spherical micelle morphology was reported for short DPA block lengths (< 60 nm), whilst polymersomes formed at higher DPA ratios (70-160) (Du et al., 2005; Pearson et al., 2013).

DLS was also used to assess the stability of self-assembled MPC-DPA nanoparticles toward dilution induced nanoparticle dissociation. The results reported (Appendix 2.0) indicated that MPC-DPA nanoparticles were highly resistant to dilution, and were thus consistent with previous reports (Salvage et al., 2005; Salvage et al., 2015). This indicated that dose dumping should not be expected after systemic administration of MPC-DPA nanoparticles. These data were also in close agreement with the CMC values determined for the MPC-DPA nanoparticles measured using the pyrene method (Table 4.4). It is well reported that the CMC values of amphiphilic block copolymers usually decrease as the hydrophobicity of a copolymer increases (Gaucher et al., 2005), and this was consistent with the CMC values recorded for the MPC-DPA nanoparticles (Table 4.4), which indicated that the lowest CMC values were reported with largest hydrophobic block (DPA) in the self-assembled nanoparticles (Licciardi et al., 2005; Giacomelli et al., 2006). Studies suggest that polymers with low CMC values are considered more stable *in-vivo* (Rangel-Yagui et al., 2005; Sezgin et al., 2006; Gaucher et al., 2010). Therefore, it was hypothesised that MPC-DPA nano-systems might be suitable candidates for the loading and release of therapeutic agents, with minimised release of these drugs before reaching the target site.

Alterations to the pH of the MPC-DPA copolymer solutions was also investigated using DLS, in order to determine the potential for release mechanism *in-vitro*, and it was concluded from the sharp transition (unimers to self-assembled nanoparticles) between pH 6 to pH 7 (Figure 4.2-4.5, Table 4.2 and Table 4.3), that the MPC-DPA based nanoparticles were stable at high pH values (> pH 7) and would dissemble when exposed to low pH conditions (< pH 6). This would facilitate the release of a loaded drug in low pH tissue such as cancer tumour (Salvage et al., 2005; Licciardi et al., 2005; Du et al., 2005).

The MPC-DPA nanoparticles also displayed high stability towards temperature changes (5°C-70°C) (Figure 4.6 and Figure 4.7), together with the stability over an extended period of time (18 months) observed at room temperature and at 4°C (Figure 4.8-4.11), which indicated that the MPC-DPA nanoparticles would be suitable for a range of storage and transport options.

Therefore, the synthesised MPC-DPA copolymers formed nanoparticle systems relative to copolymer composition, were pH responsive, and were resistant to shifts in concentration, temperature, and time.

***Q3- Does MPC-DPA nanoparticle size affect the rate of in-vitro cellular uptake and cytotoxicity?***

Due to the small particle size of nanoparticles, they can penetrate cells and translocate to other cells or tissues around the body, therefore, the possible toxic effect of these nanoparticles is considered a key concern of nanoparticles use. Based on the findings in Chapter 4, the 1:1 ratio MPC-DPA nano-systems were selected to undergo further testing and development, including the assessment of MPC-DPA nanoparticle cytotoxicity. The results of the *in-vitro* clonogenic cytotoxicity assay after 5 days exposure of V79 Chinese hamster lung fibroblasts cells, indicated that the MPC-DPA

copolymers were of low cellular toxicity (Figure 5.1-5.5), and the ability of the V79 cells to form colonies was not affected by MPC-DPA copolymers, which was in a good agreement with other MPC-DPA nanoparticle studies (Salvage et al., 2005; Licciardi et al., 2008; Lomas et al., 2008; Salvage et al., 2015; Salvage et al., 2016). Moreover, the acute toxicity of the MPC-DPA copolymers were assessed using an MTT assay and an incubation time of 24 hour, with two of most widely used *in-vitro* cell lines, which were V79 and 3T3. All the MTT assay data for the V79 cells (Figure 5.6 A -5.10 A) were consistent with V79 colony assay data (Figure 5.1-5.5), where the MPC-DPA copolymers were essentially non-toxic. Similarly, the MPC-DPA copolymers had no cytotoxic effects on the 3T3 cells as indicated by the MTT assay results (Figure 5.6 B -5.10 B). These findings were consistent with published literature, where MPC-DPA nanoparticles were reported as having no cellular toxicity in both colony formation and MTT assays (Salvage et al., 2016). Therefore, the MPC-DPA copolymers were considered suitable for further *in-vitro* cell uptake studies.

Although the cytotoxicity assays used give an indication of cell colony formation, cell viability, and cell metabolic and mitochondrial activities, they do not provide positive confirmation of nanoparticle cell penetration and internalisation. Therefore, confocal laser scanning microscopy (CLSM) and flow cytometry (FCM) were used to investigate the cellular internalisation and the possible uptake mechanisms of the MPC-DPA nanoparticles and thus compliment the cytotoxicity data.

In this project, CLSM together with FCM were employed to investigate the uptake of three types of fluorescent (Cm-6) loaded MPC-DPA micelles, $MPC_{20}$-$DPA_{20}$, $MPC_{50}$-$DPA_{50}$, and $MPC_{90}$-$DPA_{90}$ that were 25 nm, 38 nm and 44 nm in diameter respectively, after *in-vitro* incubation for 1 min, 5 min, 10 min, 30 min, and 1 hour with four different healthy cell lines; V79, Vero, MRC-5, and CHO cells. CLSM

images of all cell types displayed concentrated areas of fluorescent Cm-6 within the cytoplasm surrounding the nuclei after 1 min exposure (Figure 5.11, 5.13, 5.15, and 5.17), which was indicative of successful MPC-DPA micelle uptake and delivery of Cm-6. The was no apparent increase in the fluorescent intensity of Cm-6 with extended exposure time, and the very rapid uptake that occurred within minutes of exposure may have suggested that the uptake was the result of a diffusion mechanism rather than endocytosis (Snipstad et al., 2014). Therefore, endocytosis inhibition studies were conducted by cooling the cells to 4°C in order to elucidate the mechanism of cellular uptake within the tested cell lines. FCM results (Figure 5.19, 5.20, and 5.21), indicated that endocytosis was the uptake mechanism for V79, Vero, and MRC-5 cells, whilst cell contact diffusion may have been the primary uptake mechanism in CHO cells (Figure 5.22).

***Q4- Are MPC-DPA nano-systems able to deliver docetaxel in-vitro to cancer cell lines?***

Following determination that the MPC-DPA micelles were non-toxic and successfully mediated the intracellular delivery of Cm-6, the potential application of MPC-DPA micelles as anticancer drug delivery vehicles was studied using docetaxel (DTX) as the anticancer model drug. Docetaxel (DTX) is a potent hydrophobic anticancer drug that is available commercially in formulations containing large amounts of Tween 80, which can be physically unstable and has demonstrate toxicity during its use (Zhao et al., 2010; Gu et al., 2012). Therefore, the high stability, low toxicity, and technical simplicity of the MPC-DPA micelles, offered an opportunity for DTX loading in order to minimise toxicity, remove Tween 80, and enhance the bioavailability and thus the therapeutic action of the DTX.

DTX was loaded into MPC-DPA micelles, $MPC_{20}$-$DPA_{20}$, $MPC_{50}$-$DPA_{50}$, and $MPC_{90}$-$DPA_{90}$ via two methods, nanoprecipitation and direct dissolution, with resultant particle size and polydispersity measured via DLS. When using nanoprecipitation, larger and polydisperse DTX-MPC-DPA micelles were obtained with ethanol based preparation compared to methanol based DTX-MPC-DPA micelles (Table 6.1). This was attributed to the PC headgroup of the MPC-DPA, which was less soluble in an ethanol-water mix than a methanol-water mix (Lewis et al., 2000; Edmondson et al., 2010). These findings were consistent with previous studies that examined the solubility of the MPC-DPA copolymers in different solvents, and the effect on the MPC-DPA polymer characterisations (Licciardi et al., 2005; Salvage et al., 2015; Elyafi et al., 2017). Furthermore, the particle size and polydispersity of the MPC-DPA micelles prepared by direct dissolution method, displayed a small increase in nanoparticle size after DTX loading of methanol-free MPC-DPA micelles compared to a size decrease observed with ethanol-free DTX-loaded MPC-DPA micelles, with both systems being polydisperse (Table 6.2 and Table 6.3).

The DTX loading achieved with the MPC-DPA micelles in this study was lower compared with previous reports, and the variation in DTX loading may have been due to the different parameters used for loading DTX, such as drug: polymer ratio, molecular weight of polymers, encapsulation procedure, and the solvent used (Upadhyay et al., 2010; Shi et al., 2015b; Zeng et al., 2015; Salvage et al., 2016). However, the objective at this stage was to optimise the novel MPC-DPA diblock copolymer formulation parameters for use as a drug delivery system, rather than maximising DTX loading.

In the DTX release experiment (Figure 6.1 and Figure 6.2), burst release of DTX was initially observed from all of the MPC-DPA micelles, $MPC_{20}$-$DPA_{20}$, $MPC_{50}$-$DPA_{50}$, and $MPC_{90}$-$DPA_{90}$, which would require further study and work, followed by slow and sustained release of DTX from the MPC-DPA micelles. Based on these findings, it was proposed that the diffusion mechanism was primarily responsible for the release of DTX from the MPC-DPA micelles, which was consistent with previous reports of DTX release from other micelle systems (Upadhyay et al., 2010; Chen et al., 2013; Zeng et al., 2015).

From the project data it was therefore concluded that the $MPC_{90}$-$DPA_{90}$ micelles was the best performing formulation compared to the other MPC-DPA micelles, in terms of particle size, drug loading, drug release profile, and *in-vitro* cytotoxicity and cellular uptake. Therefore, the 42 nm $MPC_{90}$-$DPA_{90}$ micelles was selected for assessment of delivery of DTX into appropriate human cancer cell lines; MCF-7, SKOV-3, and PC3.

MTT and LDH assays were used to assess the anticancer effect of free DTX, and DTX-loaded MPC-DPA micelles. The results indicated that an anticancer effect of the DTX-loaded MPC-DPA micelles was observed in human ovarian cancer cells SKOV-3 and prostate adenocarcinoma PC3 cells, which was in consistent with previous studies investigating the delivery of DTX from other micelle formulations into SKOV-3 (Hami et al., 2017) and PC3 cells (Luo et al., 2010).

## 7.2 Conclusion

In conclusion, the data generated and presented in this thesis fulfilled the aims of the project, and supported the project hypothesis.

The novel MPC-DPA diblock copolymer compositions were successfully synthesised via ethanolic ATRP, these amphiphilic block copolymers self-assembled in an aqueous environment (pH 6-7) form core-shell nanostructures and possessed low CMC values compared to low molecular weight surfactants. The MPC-DPA micelles were successfully prepared by nanoprecipitation, with nanoparticle sizes and morphologies relative to MPC-DPA block composition observed. *In-vitro* studies produced a rapid and high cellular uptake of the MPC-DPA micelles. Moreover, the MPC-DPA micelles were able to encapsulate and release the anticancer drug DTX and effectively deliver DTX to SKOV-3 and PC3 cells.

## 7.3 Future study

The data findings, and conclusions of this project have generated new questions to be answered, which will require further study, these were as follow:

Q1- Would an extend ATRP duration (> 48 hours), affect the final DPA block length using ethanol?

Q2- What effect would an extended *in-vitro* exposure time (> 24 hours), using the MTT and LDH assays have on cytotoxicity?

Q3- How can DTX loading to MPC-DPA micelles being optimised or maximised?

Q4- What effect would changes in pH have on DTX release from MPC-DPA micelles *in-vitro*?

Q5- What effect would DTX concentration have on the level and rate of *in-vitro* uptake?

Q6- What morphology do DTX-loaded MPC-DPA nanoparticles form?

Q7- Is the *in-vitro* delivery of DTX loaded MPC-DPA micelles to human ovarian SKOV-3 and human prostate adenocarcinoma PC3 cells reproducible *in-vivo*?

Q8- What other drugs could the MPC-DPA nano-systems be used for?

### 7.4 Original contribution to knowledge

This project provided a novel contribution to scientific knowledge by creation of the following novel data and findings:

1- It reported for the first time ethanolic ATRP of novel MPC-DPA diblock copolymer compositions, and identified the limit of synthesis.

2- It reported for the first time the relationship between the novel MPC-DPA copolymer compositions and the particle size and the morphology formed.

3- It was the first report of the relationship between MPC-DPA nanoparticle size and *in-vitro* cellular uptake.

4- It was the first study, and first report of DTX loading, release, and delivery using MPC-DPA nano-systems.

5- It was the first study, and first report of MPC-DPA nano-systems mediated the *in-vitro* delivery of DTX to MCF-7, SKOV-3 and PC3 cells, which produced an anticancer effect in the SKOV-3 and PC3 cells.

**References:**


Abreu CM, Mendonça PV, Serra AC, et al. (2012) Accelerated Ambient-Temperature ATRP of Methyl Acrylate in Alcohol–Water Solutions with a Mixed Transition-Metal Catalyst System. *Macromolecular Chemistry and Physics* 213: 1677-1687.

Abuchowski A, McCoy JR, Palczuk NC, et al. (1977) Effect of covalent attachment of polyethylene glycol on immunogenicity and circulating life of bovine liver catalase. *Journal of Biological Chemistry* 252: 3582-3586.

Adams ML, Lavasanifar A and Kwon GS. (2003) Amphiphilic block copolymers for drug delivery. *Journal of pharmaceutical sciences* 92: 1343-1355.

Adjei IM, Sharma B and Labhasetwar V. (2014) Nanoparticles: cellular uptake and cytotoxicity. *Nanomaterial.* Springer, 73-91.

Aggarwal P, Hall JB, McLeland CB, et al. (2009) Nanoparticle interaction with plasma proteins as it relates to particle biodistribution, biocompatibility and therapeutic efficacy. *Advanced drug delivery reviews* 61: 428-437.

Agrawal AK, Urimi D and Jain S. (2015) Multifunctional Polymeric Nano-Carriers in Targeted Drug Delivery. *Targeted Drug Delivery: Concepts and Design.* Springer, 461-500.

Aguiar J, Carpena P, Molina-Bolıvar J, et al. (2003) On the determination of the critical micelle concentration by the pyrene 1: 3 ratio method. *Journal of colloid and interface science* 258: 116-122.

Ahl PL, Bhatia SK, Meers P, et al. (1997) Enhancement of the in vivo circulation lifetime of l-α-distearoylphosphatidylcholine liposomes: importance of liposomal aggregation versus complement opsonization. *Biochimica et Biophysica Acta (BBA)-Biomembranes* 1329: 370-382.

Ahmad Z, Shah A, Siddiq M, et al. (2014) Polymeric micelles as drug delivery vehicles. *RSC Advances* 4: 17028-17038.

Aillon KL, Xie Y, El-Gendy N, et al. (2009) Effects of nanomaterial physicochemical properties on in vivo toxicity. *Advanced drug delivery reviews* 61: 457-466.

Akimoto J, Nakayama M and Okano T. (2014) Temperature-responsive polymeric micelles for optimizing drug targeting to solid tumors. *Journal of controlled release* 193: 2-8.

Albanese A, Tang PS and Chan WC. (2012) The effect of nanoparticle size, shape, and surface chemistry on biological systems. *Annual review of biomedical engineering* 14: 1-16.

Alexandridis P and Hatton TA. (1995) Poly (ethylene oxide) · poly (propylene oxide) · poly (ethylene oxide) block copolymer surfactants in aqueous solutions and at interfaces: thermodynamics, structure, dynamics, and modeling. *Colloids and surfaces A: physicochemical and engineering aspects* 96: 1-46.

Alexandridis P and Lindman B. (2000) *Amphiphilic block copolymers: self-assembly and applications*: Elsevier.

Allen C, Maysinger D and Eisenberg A. (1999) Nano-engineering block copolymer aggregates for drug delivery. *Colloids and Surfaces B: biointerfaces* 16: 3-27.

Almgren M. (2000) Mixed micelles and other structures in the solubilization of bilayer lipid membranes by surfactants. *Biochimica et Biophysica Acta (BBA)-Biomembranes* 1508: 146-163.

Amin A and El-Gaffar M. (2008) Synthesis of novel polyamide-hyperbranched polymers via self condensing Atom Transfer Radical Polymerization. *Polymer-Plastics Technology and Engineering* 47: 984-990.

Ashok B, Arleth L, Hjelm RP, et al. (2004) In vitro characterization of PEGylated phospholipid micelles for improved drug solubilization: effects of PEG chain length and PC incorporation. *Journal of pharmaceutical sciences* 93: 2476-2487.

Astafieva I, Zhong XF and Eisenberg A. (1993) Critical micellization phenomena in block polyelectrolyte solutions. *Macromolecules* 26: 7339-7352.

Aw MS, Kurian M and Losic D. (2013) Polymeric micelles for multidrug delivery and combination therapy. *Chemistry-A European Journal* 19: 12586-12601.

Bader H, Dorn K, Hupfer B, et al. (1985) Polymeric monolayers and liposomes as models for biomembranes. *Polymer Membranes*: 1-62.

Bae Y, Nishiyama N, Fukushima S, et al. (2005) Preparation and biological characterization of polymeric micelle drug carriers with intracellular pH-triggered drug release property: tumor permeability, controlled subcellular drug distribution, and enhanced in vivo antitumor efficacy. *Bioconjugate chemistry* 16: 122-130.

Bahadar H, Maqbool F, Niaz K, et al. (2016) Toxicity of nanoparticles and an overview of current experimental models. *Iranian biomedical journal* 20: 1.

Baker J, Ajani J, Scotté F, et al. (2009) Docetaxel-related side effects and their management. *European Journal of Oncology Nursing* 13: 49-59.

Barahuie F, Hussein MZ, Fakurazi S, et al. (2014) Development of drug delivery systems based on layered hydroxides for nanomedicine. *International journal of molecular sciences* 15: 7750-7786.

Barichello JM, Morishita M, Takayama K, et al. (1999) Encapsulation of hydrophilic and lipophilic drugs in PLGA nanoparticles by the nanoprecipitation method. *Drug development and industrial pharmacy* 25: 471-476.

Benoit GG, Naud CF, Simard MA, et al. (1997) Noninterference of cytochrome P4501A2 in the cytotoxicity of tacrine using genetically engineered V79 Chinese hamster cells for stable expression of the human or rat isoform and two human hepatocyte cell lines. *Biochemical pharmacology* 53: 423-427.

Berridge MV and Tan AS. (1993) Characterization of the cellular reduction of 3-(4, 5-dimethylthiazol-2-yl)-2, 5-diphenyltetrazolium bromide (MTT): subcellular localization, substrate dependence, and involvement of mitochondrial electron transport in MTT reduction. *Archives of biochemistry and biophysics* 303: 474-482.

Berridge MV, Tan AS, McCoy KD, et al. (1996) The biochemical and cellular basis of cell proliferation assays that use tetrazolium salts. *Biochemica* 4: 14-19.

Betancourt T, Brown B and Brannon-Peppas L. (2007) Doxorubicin-loaded PLGA nanoparticles by nanoprecipitation: preparation, characterization and in vitro evaluation. *Nanomedicine* 2: 219-232.

Bhattacharjee S, Ershov D, Fytianos K, et al. (2012) Cytotoxicity and cellular uptake of tri-block copolymer nanoparticles with different size and surface characteristics. *Particle and fibre toxicology* 9: 11.

Bilati U, Allémann E and Doelker E. (2005) Development of a nanoprecipitation method intended for the entrapment of hydrophilic drugs into nanoparticles. *European Journal of Pharmaceutical Sciences* 24: 67-75.

Biswas S, Vaze OS, Movassaghian S, et al. (2013) Polymeric micelles for the delivery of poorly soluble drugs. John Wiley & Sons: New York, 411-476.

Blanazs A, Ryan A and Armes S. (2012) Predictive phase diagrams for RAFT aqueous dispersion polymerization: effect of block copolymer composition, molecular weight, and copolymer concentration. *Macromolecules* 45: 5099-5107.

Bonté F, Taupin C and Puisieux F. (1987) Kinetics of solid-fluid phase separation in mixed monolayers of phospholipids. *Journal of colloid and interface science* 115: 268-270.

Bories-Azeau X and Armes SP. (2002) Unexpected transesterification of tertiary amine methacrylates during methanolic ATRP at ambient temperature: a cautionary tale. *Macromolecules* 35: 10241-10243.

Bories-Azeau X, Armes SP and van den Haak HJ. (2004) Facile synthesis of zwitterionic diblock copolymers without protecting group chemistry. *Macromolecules* 37: 2348-2352.

Boyer C, Corrigan NA, Jung K, et al. (2015) Copper-Mediated Living Radical Polymerization (Atom Transfer Radical Polymerization and Copper (0) Mediated Polymerization): From Fundamentals to Bioapplications. *Chemical reviews*.

Boyer C, Corrigan NA, Jung K, et al. (2016) Copper-mediated living radical polymerization (atom transfer radical polymerization and copper (0) mediated polymerization): from fundamentals to bioapplications. *Chem. Rev* 116: 1803-1949.

Brigger I, Dubernet C and Couvreur P. (2002) Nanoparticles in cancer therapy and diagnosis. *Advanced drug delivery reviews* 54: 631-651.

Burris HA, Infante JR, Greco FA, et al. (2016) A phase I dose escalation study of NK012, an SN-38 incorporating macromolecular polymeric micelle. *Cancer chemotherapy and pharmacology* 77: 1079-1086.

Bütün V, Armes S and Billingham N. (2001) Synthesis and aqueous solution properties of near-monodisperse tertiary amine methacrylate homopolymers and diblock copolymers. *Polymer* 42: 5993-6008.

Cabral H and Kataoka K. (2014) Progress of drug-loaded polymeric micelles into clinical studies. *Journal of controlled release* 190: 465-476.

Cabral H, Matsumoto Y, Mizuno K, et al. (2011) Accumulation of sub-100 nm polymeric micelles in poorly permeable tumours depends on size. *Nature nanotechnology* 6: 815-823.

Canton I and Battaglia G. (2012) Endocytosis at the nanoscale. *Chemical Society Reviews* 41: 2718-2739.

Carmody WR. (1961) Easily prepared wide range buffer series. *J. Chem. Educ* 38: 559.

Cartiera MS, Johnson KM, Rajendran V, et al. (2009) The uptake and intracellular fate of PLGA nanoparticles in epithelial cells. *Biomaterials* 30: 2790-2798.

Chanan-Khan A, Szebeni J, Savay S, et al. (2003) Complement activation following first exposure to pegylated liposomal doxorubicin (Doxil®): possible role in hypersensitivity reactions. *Annals of Oncology* 14: 1430-1437.

Chang T, Gosain P, Stenzel MH, et al. (2016) Drug-loading of poly(ethylene glycol methyl ether methacrylate) (PEGMEMA)—based micelles and mechanisms of uptake in colon carcinoma cells. *Colloids and Surfaces B: biointerfaces* 144: 257-264.

Chatterjee U, Jewrajka SK and Mandal BM. (2005) The amphiphilic block copolymers of 2-(dimethylamino) ethyl methacrylate and methyl methacrylate: Synthesis by atom transfer radical polymerization and solution properties. *Polymer* 46: 10699-10708.

Chen L, Sha X, Jiang X, et al. (2013) Pluronic P105/F127 mixed micelles for the delivery of docetaxel against Taxol-resistant non-small cell lung cancer:

optimization and in vitro, in vivo evaluation. *International journal of nanomedicine* 8: 73.

Chen W, Inoue Y and Ishihara K. (2015) Preparation of photoreactive phospholipid polymer nanoparticles to immobilize and release protein by photoirradiation. *Colloids and Surfaces B: biointerfaces* 135: 365-370.

Chiappetta DA, Degrossi J, Teves S, et al. (2008) Triclosan-loaded poloxamine micelles for enhanced topical antibacterial activity against biofilm. *European journal of pharmaceutics and biopharmaceutics* 69: 535-545.

Chithrani BD, Ghazani AA and Chan WC. (2006) Determining the size and shape dependence of gold nanoparticle uptake into mammalian cells. *Nano lett* 6: 662-668.

Cho EJ, Holback H, Liu KC, et al. (2013) Nanoparticle characterization: state of the art, challenges, and emerging technologies. *Molecular pharmaceutics* 10: 2093.

Cho HK, Cheong IW, Lee JM, et al. (2010) Polymeric nanoparticles, micelles and polymersomes from amphiphilic block copolymer. *Korean Journal of Chemical Engineering* 27: 731-740.

Christie RJ, Matsumoto Y, Miyata K, et al. (2012) Targeted polymeric micelles for siRNA treatment of experimental cancer by intravenous injection. *ACS nano* 6: 5174-5189.

Chu H, Liu N, Wang X, et al. (2009) Morphology and in vitro release kinetics of drug-loaded micelles based on well-defined PMPC–b–PBMA copolymer. *International journal of pharmaceutics* 371: 190-196.

Clarke S, Davies MC, Roberts CJ, et al. (2000) Surface mobility of 2-methacryloyloxyethyl phosphorylcholine-co-lauryl methacrylate polymers. *Langmuir* 16: 5116-5122.

Coessens VM and Matyjaszewski K. (2010) Fundamentals of atom transfer radical polymerization. *Journal of Chemical Education* 87: 916-919.

Colley HE, Hearnden V, Avila-Olias M, et al. (2014) Polymersome-mediated delivery of combination anticancer therapy to head and neck cancer cells: 2D and 3D in vitro evaluation. *Molecular pharmaceutics* 11: 1176-1188.

Connell LS, Jones JR and Weaver JV. (2012) Transesterification of functional methacrylate monomers during alcoholic copper-catalyzed atom transfer radical polymerization: formation of compositional and architectural side products. *Polymer Chemistry* 3: 2735-2738.

Conner SD and Schmid SL. (2003) Regulated portals of entry into the cell. *Nature* 422: 37.

Craparo EF, Sardo C, Serio R, et al. (2014) Galactosylated polymeric carriers for liver targeting of sorafenib. *International journal of pharmaceutics* 466: 172-180.

Cureton DK, Massol RH, Saffarian S, et al. (2009) Vesicular stomatitis virus enters cells through vesicles incompletely coated with clathrin that depend upon actin for internalization. *PLoS Pathog* 5: e1000394-e1000394.

Dadwal M, Solan D and Pradesh H. (2014) Polymeric Nanoparticles as Promising Novel Carriers for Drug Delivery: An Overview. *Journal of Advanced Pharmacy Education & Research Jan-Mar* 4.

Dahe GJ, Teotia RS, Kadam SS, et al. (2011) The biocompatibility and separation performance of antioxidative polysulfone/vitamin E TPGS composite hollow fiber membranes. *Biomaterials* 32: 352-365.

Danhier F, Danhier P, De Saedeleer CJ, et al. (2015) Paclitaxel-loaded micelles enhance transvascular permeability and retention of nanomedicines in tumors. *International journal of pharmaceutics* 479: 399-407.

Danhier F, Lecouturier N, Vroman B, et al. (2009) Paclitaxel-loaded PEGylated PLGA-based nanoparticles: in vitro and in vivo evaluation. *Journal of controlled release* 133: 11-17.

Dausend J, Musyanovych A, Dass M, et al. (2008) Uptake mechanism of oppositely charged fluorescent nanoparticles in HeLa cells. *Macromolecular bioscience* 8: 1135-1143.

Davda J and Labhasetwar V. (2002) Characterization of nanoparticle uptake by endothelial cells. *International journal of pharmaceutics* 233: 51-59.

Davis KA and Matyjaszewski K. (2000) Atom transfer radical polymerization of tert-butyl acrylate and preparation of block copolymers. *Macromolecules* 33: 4039-4047.

Dayananda K, Kim MS, Kim BS, et al. (2007) Synthesis and characterization of MPEG-b-PDPA amphiphilic block copolymer via atom transfer radical polymerization and its pH-dependent micellar behavior. *Macromolecular Research* 15: 385-391.

de Melo-Diogo D, Gaspar VM, Costa EC, et al. (2014) Combinatorial delivery of Crizotinib–Palbociclib–Sildenafil using TPGS-PLA micelles for improved cancer treatment. *European journal of pharmaceutics and biopharmaceutics* 88: 718-729.

Deng C, Jiang Y, Cheng R, et al. (2012) Biodegradable polymeric micelles for targeted and controlled anticancer drug delivery: promises, progress and prospects. *Nano Today* 7: 467-480.

di Lena F and Matyjaszewski K. (2010) Transition metal catalysts for controlled radical polymerization. *Progress in Polymer Science* 35: 959-1021.

Díaz-Moscoso A, Vercauteren D, Rejman J, et al. (2010) Insights in cellular uptake mechanisms of pDNA–polycationic amphiphilic cyclodextrin nanoparticles (CDplexes). *Journal of controlled release* 143: 318-325.

Ding H, Wang X, Zhang S, et al. (2012a) Applications of polymeric micelles with tumor targeted in chemotherapy. *Journal of Nanoparticle Research* 14: 1254.

Ding J, Chen J, Li D, et al. (2012b) Biocompatible reduction-responsive polypeptide micelles as nanocarriers for enhanced chemotherapy efficacy in vitro. *Journal of Materials Chemistry B* 1: 69-81.

Dobrovolskaia MA and McNeil SE. (2007) Immunological properties of engineered nanomaterials. *Nature nanotechnology* 2: 469-478.

Doherty GJ and McMahon HT. (2009) Mechanisms of endocytosis. *Annual review of biochemistry* 78: 857-902.

Domínguez A, Fernández A, González N, et al. (1997) Determination of critical micelle concentration of some surfactants by three techniques. *J. Chem. Educ* 74: 1227.

Dong H and Matyjaszewski K. (2008) ARGET ATRP of 2-(dimethylamino) ethyl methacrylate as an intrinsic reducing agent. *Macromolecules* 41: 6868-6870.

Du J and Armes SP. (2008) Preparation of Primary Amine-Based Block Copolymer Vesicles by Direct Dissolution in Water and Subsequent Stabilization by Sol−Gel Chemistry. *Langmuir* 24: 13710-13716.

Du J, Tang Y, Lewis AL, et al. (2005) pH-sensitive vesicles based on a biocompatible zwitterionic diblock copolymer. *Journal of the American Chemical Society* 127: 17982-17983.

Dubey SK, Thomas A and Samanta MK. (2016) Development of docetaxel-PLGA-nanoparticles and in vitro anti-tumor activity in PC3 cells Targeted to Prostate Tumor. *Int J Sci Eng Res* 7: 671-678.

Duncan R and Richardson SC. (2012) Endocytosis and intracellular trafficking as gateways for nanomedicine delivery: opportunities and challenges. *Molecular pharmaceutics* 9: 2380-2402.

Durrani AA, Hayward JA and Chapman D. (1986) Biomembrnanes as models for polymer surfaces: II. The syntheses of reactive species for covalent coupling of phosphorylcholine to polymer surfaces. *Biomaterials* 7: 121-125.

Edmondson S, Nguyen NT, Lewis AL, et al. (2010) Co-nonsolvency effects for surface-initiated poly (2-(methacryloyloxy) ethyl phosphorylcholine) brushes in alcohol/water mixtures. *Langmuir* 26: 7216-7226.

Ehrlich P. (1907) Chemotherapeutische trypanosomen-studien. *Berliner Munch Tierarztl Wochenschr* 11: 233-238.

Elhasi S, Astaneh R and Lavasanifar A. (2007) Solubilization of an amphiphilic drug by poly (ethylene oxide)-block-poly (ester) micelles. *European journal of pharmaceutics and biopharmaceutics* 65: 406-413.

Elsaesser A and Howard CV. (2012) Toxicology of nanoparticles. *Advanced drug delivery reviews* 64: 129-137.

Elyafi AKE, Standen G, Meikle ST, et al. (2017) Development of MPC-DPA polymeric nanoparticle systems for inhalation drug delivery applications. *European Journal of Pharmaceutical Sciences* 106: 362-380.

Emami J, Rezazadeh M, Hasanzadeh F, et al. (2015) Development and in vitro/in vivo evaluation of a novel targeted polymeric micelle for delivery of paclitaxel. *International journal of biological macromolecules* 80: 29-40.

Engels FK and Verweij J. (2005) Docetaxel administration schedule: from fever to tears? A review of randomised studies. *European Journal of Cancer* 41: 1117-1126.

Esmaeili F, Ghahremani MH, Ostad SN, et al. (2008) Folate-receptor-targeted delivery of docetaxel nanoparticles prepared by PLGA–PEG–folate conjugate. *Journal of drug targeting* 16: 415-423.

Faccia PA and Amalvy JI. (2013) Synthesis, characterization, and swelling behavior of new pH-sensitive hydrogels derived from copolymers of 2-hydroxyethyl methacrylate and 2-(diisopropylamino) ethylmethacrylate. *Journal of applied polymer science* 127: 1974-1980.

Fadeel B, Fornara A, Toprak MS, et al. (2015) Keeping it real: The importance of material characterization in nanotoxicology. *Biochemical and biophysical research communications* 468: 498-503.

Fang J, Nakamura H and Maeda H. (2011) The EPR effect: unique features of tumor blood vessels for drug delivery, factors involved, and limitations and augmentation of the effect. *Advanced drug delivery reviews* 63: 136-151.

Florez L, Herrmann C, Cramer JM, et al. (2012) How shape influences uptake: interactions of anisotropic polymer nanoparticles and human mesenchymal stem cells. *Small* 8: 2222-2230.

Franken NA, Rodermond HM, Stap J, et al. (2006) Clonogenic assay of cells in vitro. *Nature protocols* 1: 2315.

Fredericksen BL, Wei BL, Yao J, et al. (2002) Inhibition of endosomal/lysosomal degradation increases the infectivity of human immunodeficiency virus. *Journal of virology* 76: 11440-11446.

Gaitzsch J, Delahaye M, Poma A, et al. (2016) Comparison of metal free polymer–dye conjugation strategies in protic solvents. *Polymer Chemistry* 7: 3046-3055.

Ganta S, Singh A, Rawal Y, et al. (2016) Formulation development of a novel targeted theranostic nanoemulsion of docetaxel to overcome multidrug resistance in ovarian cancer. *Drug delivery* 23: 958-970.

Gao H and Matyjaszewski K. (2008) Synthesis of star polymers by a new "core-first" method: sequential polymerization of cross-linker and monomer. *Macromolecules* 41: 1118-1125.

Gaucher G, Dufresne M-H, Sant VP, et al. (2005) Block copolymer micelles: preparation, characterization and application in drug delivery. *Journal of controlled release* 109: 169-188.

Gaucher G, Marchessault RH and Leroux J-C. (2010) Polyester-based micelles and nanoparticles for the parenteral delivery of taxanes. *Journal of controlled release* 143: 2-12.

Gaynor SG, Qiu J and Matyjaszewski K. (1998) Controlled/ "living" radical polymerization applied to water-borne systems. *Macromolecules* 31: 5951-5954.

Giacomelli C, Le Men L, Borsali R, et al. (2006) Phosphorylcholine-based pH-responsive diblock copolymer micelles as drug delivery vehicles: light scattering, electron microscopy, and fluorescence experiments. *Biomacromolecules* 7: 817-828.

Giacomelli FC, Stepánek P, Giacomelli C, et al. (2011) pH-triggered block copolymer micelles based on a pH-responsive PDPA (poly [2-(diisopropylamino) ethyl methacrylate]) inner core and a PEO (poly (ethylene oxide)) outer shell as a potential tool for the cancer therapy. *Soft Matter* 7: 9316-9325.

Gnach A, Lipinski T, Bednarkiewicz A, et al. (2015) Upconverting nanoparticles: assessing the toxicity. *Chemical Society Reviews* 44: 1561-1584.

Gobeil F, Juneau C and Plante S. (2002) Thrombus formation on guide wires during routine PTCA procedures: a scanning electron microscopic evaluation. *The Canadian journal of cardiology* 18: 263-269.

Goda T and Ishihara K. (2006) Soft contact lens biomaterials from bioinspired phospholipid polymers. *Expert review of medical devices* 3: 167-174.

Goda T, Matsuno R, Konno T, et al. (2009) Protein adsorption resistance and oxygen permeability of chemically crosslinked phospholipid polymer hydrogel for ophthalmologic biomaterials. *Journal of Biomedical Materials Research Part B: Applied Biomaterials* 89: 184-190.

Góis JR, Rocha N, Popov AV, et al. (2014) Synthesis of well-defined functionalized poly (2-(diisopropylamino) ethyl methacrylate) using ATRP with sodium dithionite as a SARA agent. *Polymer Chemistry* 5: 3919-3928.

Gong C, Xie Y, Wu Q, et al. (2012) Improving anti-tumor activity with polymeric micelles entrapping paclitaxel in pulmonary carcinoma. *Nanoscale* 4: 6004-6017.

Govender T, Stolnik S, Garnett MC, et al. (1999) PLGA nanoparticles prepared by nanoprecipitation: drug loading and release studies of a water soluble drug. *Journal of controlled release* 57: 171-185.

Gref R, Minamitake Y, Peracchia MT, et al. (1994) Biodegradable long-circulating polymeric nanospheres. *Science* 263: 1600-1604.

Grislain L, Couvreur P, Lenaerts V, et al. (1983) Pharmacokinetics and distribution of a biodegradable drug-carrier. *International journal of pharmaceutics* 15: 335-345.

Gu PF, Xu H, Sui BW, et al. (2012) Polymeric micelles based on poly (ethylene glycol) block poly (racemic amino acids) hybrid polypeptides: conformation-facilitated drug-loading behavior and potential application as effective anticancer drug carriers. *International journal of nanomedicine* 7: 109.

Guan Q, Zhang G, Sun D, et al. (2017) In vitro and in vivo evaluation of docetaxel-loaded stearic acid-modified Bletilla striata polysaccharide copolymer micelles. *PloS one* 12: e0173172.

Haddleton DM, Crossman MC, Dana BH, et al. (1999) *J. Macromolecules* 32: 2110.

Haddleton DM, Jasieczek CB, Hannon MJ, et al. (1997) *J. Macromolecules* 30: 2190.

Hamad E and Qutubuddin S. (1990) Theory of micelle formation by amphiphilic side-chain polymers. *Macromolecules* 23: 4185-4191.

Hamaguchi T, Doi T, Eguchi-Nakajima T, et al. (2010) Phase I study of NK012, a novel SN-38–incorporating micellar nanoparticle, in adult patients with solid tumors. *Clinical cancer research* 16: 5058-5066.

Hamaguchi T, Kato K, Yasui H, et al. (2007) A phase I and pharmacokinetic study of NK105, a paclitaxel-incorporating micellar nanoparticle formulation. *British journal of cancer* 97: 170.

Hami Z, Amini M, Ghazi-Khansari M, et al. (2014) Synthesis and in vitro evaluation of a pH-sensitive PLA–PEG–folate based polymeric micelle for controlled delivery of docetaxel. *Colloids and Surfaces B: biointerfaces* 116: 309-317.

Hami Z, Rezayat SM, Gilani K, et al. (2017) In-vitro cytotoxicity and combination effects of the docetaxel-conjugated and doxorubicin-conjugated poly (lactic acid)-poly (ethylene glycol)-folate-based polymeric micelles in human ovarian cancer cells. *Journal of pharmacy and pharmacology* 69: 151-160.

Hammer MR. (2008) A magnetically excited microwave plasma source for atomic emission spectroscopy with performance approaching that of the inductively coupled plasma. *Spectrochimica Acta Part B: Atomic Spectroscopy* 63: 456-464.

Han X, Zhang X, Zhu H, et al. (2013) Effect of Composition of PDMAEMA-b-PAA Block Copolymers on Their pH- and Temperature-Responsive Behaviors. *Langmuir* 29: 1024-1034.

Harada A and Kataoka K. (1997) Formation of stable and monodispersive polyion complex micelles in aqueous medium from poly (L-lysine) and poly (ethylene glycol)-poly (aspartic acid) block copolymer. *Journal of Macromolecular Science, Part A: Pure and Applied Chemistry* 34: 2119-2133.

Harush-Frenkel O, Debotton N, Benita S, et al. (2007) Targeting of nanoparticles to the clathrin-mediated endocytic pathway. *Biochemical and biophysical research communications* 353: 26-32.

Hasenstein JR, Shin H-C, Kasmerchak K, et al. (2012) Antitumor activity of Triolimus: a novel multidrug-loaded micelle containing Paclitaxel, Rapamycin, and 17-AAG. *Molecular cancer therapeutics* 11: 2233-2242.

Hawley TS and Hawley RG. (2004) *Flow cytometry protocols*: Springer.

Hayward JA and Chapman D. (1984) Biomembrane surfaces as models for polymer design: the potential for haemocompatibility. *Biomaterials* 5: 135-142.

Hayward JA, Durrani AA, Lu Y, et al. (1986a) Biomembranes as models for polymer surfaces: IV. ESCA analyses of a phosphorylcholine surface covalentiy bound to hydroxylated substrates. *Biomaterials* 7: 252-258.

Hayward JA, Durrani AA, Shelton CJ, et al. (1986b) Biomembpanes as models for polymer surfaces: III. Characterization of a phosphorylcholine surface covalenay bound to glass. *Biomaterials* 7: 126-131.

He C, Hu Y, Yin L, et al. (2010) Effects of particle size and surface charge on cellular uptake and biodistribution of polymeric nanoparticles. *Biomaterials* 31: 3657-3666.

He W-D, Sun X-L, Wan W-M, et al. (2011) Multiple morphologies of PAA-b-PSt assemblies throughout RAFT dispersion polymerization of styrene with PAA Macro-CTA. *Macromolecules* 44: 3358-3365.

He W, Jiang H, Zhang L, et al. (2013) Atom transfer radical polymerization of hydrophilic monomers and its applications. *Polymer Chemistry* 4: 2919-2938.

Hennenfent K and Govindan R. (2005) Novel formulations of taxanes: a review. Old wine in a new bottle? *Annals of Oncology* 17: 735-749.

Hernández-Ortiz JC, Vivaldo-Lima E, Dubé MA, et al. (2014) Modeling of Network Formation in the Atom Transfer Radical Co-Polymerization (ATRP) of Vinyl/Divinyl Monomers Using a Multifunctional Polymer Molecule Approach. *Macromolecular Theory and Simulations* 23: 429-441.

Hsiue GH, Lo CL, Cheng CH, et al. (2007) Preparation and characterization of poly (2-methacryloyloxyethyl phosphorylcholine)-block-poly (D, L-lactide) polymer nanoparticles. *Journal of Polymer Science Part A: Polymer Chemistry* 45: 688-698.

Hu L, Pang S, Hu Q, et al. (2015a) Enhanced antitumor efficacy of folate targeted nanoparticles co-loaded with docetaxel and curcumin. *Biomedicine & Pharmacotherapy* 75: 26-32.

Hu Q, Rijcken CJ, Bansal R, et al. (2015b) Complete regression of breast tumour with a single dose of docetaxel-entrapped core-cross-linked polymeric micelles. *Biomaterials* 53: 370-378.

Hu X, Yang F-F, Liu C-Y, et al. (2017) In vitro uptake and transport studies of PEG-PLGA polymeric micelles in respiratory epithelial cells. *European journal of pharmaceutics and biopharmaceutics* 114: 29-37.

Hu Y, Jiang X, Ding Y, et al. (2003) Preparation and drug release behaviors of nimodipine-loaded poly(caprolactone)–poly(ethylene oxide)–polylactide amphiphilic copolymer nanoparticles. *Biomaterials* 24: 2395-2404.

Hub HH, Hupfer B, Koch H, et al. (1980) Polymerizable phospholipid analogues—new stable biomembrane and cell models. *Angewandte Chemie International Edition in English* 19: 938-940.

Hussain SM, Warheit DB, Ng SP, et al. (2015) At the crossroads of nanotoxicology in vitro: past achievements and current challenges. *Toxicological Sciences* 147: 5-16.

Iddon PD, Robinson KL and Armes SP. (2004) Polymerization of sodium 4-styrenesulfonate via atom transfer radical polymerization in protic media. *Polymer* 45: 759-768.

Immordino ML, Brusa P, Arpicco S, et al. (2003) Preparation, characterization, cytotoxicity and pharmacokinetics of liposomes containing docetaxel. *Journal of controlled release* 91: 417-429.

Ishida T, Maeda R, Ichihara M, et al. (2003) Accelerated clearance of PEGylated liposomes in rats after repeated injections. *Journal of controlled release* 88: 35-42.

Ishihara K. (1997) Novel polymeric materials for obtaining blood-compatible surfaces. *Trends in polymer science* 5: 401-407.

Ishihara K. (2000) Bioinspired phospholipid polymer biomaterials for making high performance artificial organs. *Science and Technology of Advanced Materials* 1: 131-138.

Ishihara K and Iwasaki Y. (2000) Biocompatible elastomers composed of segmented polyurethane and 2-methacryloyloxyethyl phosphorylcholine polymer. *Polymers for Advanced Technologies* 11: 626-634.

Ishihara K, Nomura H, Mihara T, et al. (1998) Why do phospholipid polymers reduce protein adsorption? *Journal of biomedical materials research* 39: 323-330.

Ishihara K, Oda H, Aikawa T, et al. (2015) Bioinspired phospholipid polymer hydrogel system for cellular engineering. *Macromolecular Symposia.* Wiley Online Library, 69-77.

Ishihara K and Takai M. (2009) Bioinspired interface for nanobiodevices based on phospholipid polymer chemistry. *Journal of the Royal Society Interface* 6: S279-S291.

Ishihara K, Tanaka S, Furukawa N, et al. (1996) Improved blood compatibility of segmented polyurethanes by polymeric additives having phospholipid polar groups. I. Molecular design of polymeric additives and their functions. *Journal of Biomedical Materials Research Part A* 32: 391-399.

Ishihara K, Ueda T and Nakabayashi N. (1990) Preparation of phospholipid polymers and their properties as polymer hydrogel membranes. *Polym J* 22: 355-360.

Ishii T, Miyata K, Anraku Y, et al. (2016) Enhanced target recognition of nanoparticles by cocktail PEGylation with chains of varying lengths. *Chemical Communications* 52: 1517-1519.

Israelachvili JN. (1992) Adhesion forces between surfaces in liquids and condensable vapours. *Surface Science Reports* 14: 109-159.

Iversen T-G, Skotland T and Sandvig K. (2011) Endocytosis and intracellular transport of nanoparticles: present knowledge and need for future studies. *Nano Today* 6: 176-185.

Iwasaki Y and Ishihara K. (2012) Cell membrane-inspired phospholipid polymers for developing medical devices with excellent biointerfaces. *Science and Technology of Advanced Materials* 13: 064101.

Iwasaki Y, Nakabayashi N and Ishihara K. (2003) In vitro and ex vivo blood compatibility study of 2-methacryloyloxyethyl phosphorylcholine (MPC) copolymer-coated hemodialysis hollow fibers. *Journal of Artificial Organs* 6: 260-266.

Iwasaki Y, Takami U, Sawada S-i, et al. (2008) Interfacing biomembrane mimetic polymer surfaces with living cells–Surface modification for reliable bioartificial liver. *Applied Surface Science* 255: 523-528.

Izunobi JU and Higginbotham CL. (2011) Polymer molecular weight analysis by 1H NMR spectroscopy. *Journal of Chemical Education* 88: 1098-1104.

Jiang X, Miclăuş T, Wang L, et al. (2015) Fast intracellular dissolution and persistent cellular uptake of silver nanoparticles in CHO-K1 cells: implication for cytotoxicity. *Nanotoxicology* 9: 181-189.

Jiang Y, Yang N, Zhang H, et al. (2016) Enhanced in vivo antitumor efficacy of dual-functional peptide-modified docetaxel nanoparticles through tumor targeting and Hsp90 inhibition. *Journal of controlled release* 221: 26-36.

Jones M-C and Leroux J-C. (1999) Polymeric micelles–a new generation of colloidal drug carriers. *European journal of pharmaceutics and biopharmaceutics* 48: 101-111.

Kabanov AV, Batrakova EV and Alakhov VY. (2002) Pluronic® block copolymers as novel polymer therapeutics for drug and gene delivery. *Journal of controlled release* 82: 189-212.

Kabanov AV, Chekhonin V, Alakhov VY, et al. (1989) The neuroleptic activity of haloperidol increases after its solubilization in surfactant micelles: micelles as microcontainers for drug targeting. *FEBS letters* 258: 343-345.

Kadoma Y. (1978) Synthesis and hemolysis test of the polymer containing phosphorylcholine groups. *Koubunshi Ronbunshu* 35: 423-427.

Kalyanasundaram K and Thomas J. (1977) Environmental effects on vibronic band intensities in pyrene monomer fluorescence and their application in studies of micellar systems. *Journal of the American Chemical Society* 99: 2039-2044.

Kasko AM, Heintz AM and Pugh C. (1998) The effect of molecular architecture on the thermotropic behavior of poly [11-(4 ‘-cyanophenyl-4 ‘‘-phenoxy) undecyl acrylate] and its relation to polydispersity. *Macromolecules* 31: 256-271.

Kaszuba M, McKnight D, Connah MT, et al. (2008) Measuring sub nanometre sizes using dynamic light scattering. *Journal of Nanoparticle Research* 10: 823-829.

Kataoka K, Harada A and Nagasaki Y. (2001) Block copolymer micelles for drug delivery: design, characterization and biological significance. *Advanced drug delivery reviews* 47: 113-131.

Kato K, Chin K, Yoshikawa T, et al. (2012) Phase II study of NK105, a paclitaxel-incorporating micellar nanoparticle, for previously treated advanced or recurrent gastric cancer. *Investigational new drugs* 30: 1621-1627.

Kato M, Kamigaito M, Sawamoto M, et al. (1995) Polymerization of methyl methacrylate with the carbon tetrachloride/dichlorotris-(triphenylphosphine) ruthenium (II)/methylaluminum bis (2, 6-di-tert-butylphenoxide) initiating system: possibility of living radical polymerization. *Macromolecules* 28: 1721-1723.

Ke X-Y, Ng VWL, Gao S-J, et al. (2014) Co-delivery of thioridazine and doxorubicin using polymeric micelles for targeting both cancer cells and cancer stem cells. *Biomaterials* 35: 1096-1108.

Kedar U, Phutane P, Shidhaye S, et al. (2010) Advances in polymeric micelles for drug delivery and tumor targeting. *Nanomedicine: Nanotechnology, Biology and Medicine* 6: 714-729.

Kettler K, Veltman K, van de Meent D, et al. (2014) Cellular uptake of nanoparticles as determined by particle properties, experimental conditions, and cell type. *Environmental toxicology and chemistry* 33: 481-492.

Khan TN, Mobbs RH, Price C, et al. (1987) Synthesis and colloidal behaviour of a polystyrene-b-poly(ethylene oxide) block copolymer. *European Polymer Journal* 23: 191-194.

Kim H, Choi W, Lee S, et al. (2014) Synthesis of biomembrane-mimic polymers with various phospholipid head groups. *Polymer* 55: 517-524.

Kloover J, Den Bakker M, Gelderblom H, et al. (2004) Fatal outcome of a hypersensitivity reaction to paclitaxel: a critical review of premedication regimens. *British journal of cancer* 90: 304.

Kong B, Seog JH, Graham LM, et al. (2011) Experimental considerations on the cytotoxicity of nanoparticles. *Nanomedicine* 6: 929-941.

Koo OM, Rubinstein I and Onyuksel H. (2005) Role of nanotechnology in targeted drug delivery and imaging: a concise review. *Nanomedicine: Nanotechnology, Biology and Medicine* 1: 193-212.

Koopaei MN, Khoshayand MR, Mostafavi SH, et al. (2014) Docetaxel loaded PEG-PLGA nanoparticles: optimized drug loading, in-vitro cytotoxicity and in-vivo antitumor effect. *Iranian journal of pharmaceutical research: IJPR* 13: 819.

Kore G, Kolate A, Nej A, et al. (2014) Polymeric micelle as multifunctional pharmaceutical carriers. *Journal of nanoscience and nanotechnology* 14: 288-307.

Kotani Y, Kamigaito M and Sawamoto M. (2000) Living Radical Polymerization of Para-Substituted Styrenes and Synthesis of Styrene-Based Copolymers with Rhenium and Iron Complex Catalysts 1. *Macromolecules* 33: 6746-6751.

Kumar R, Kumar P, Singh B, et al. (2017) In vivo pharmacokinetic studies and intracellular delivery of methotrexate by means of glycine-tethered PLGA-based polymeric micelles. *International journal of pharmaceutics* 519: 138-144.

Kunzmann A, Andersson B, Thurnherr T, et al. (2011) Toxicology of engineered nanomaterials: focus on biocompatibility, biodistribution and biodegradation. *Biochimica et Biophysica Acta (BBA)-General Subjects* 1810: 361-373.

Kwiatkowski P, Jurczak J, Pietrasik J, et al. (2008) High molecular weight polymethacrylates by AGET ATRP under high pressure. *Macromolecules* 41: 1067-1069.

Kwon GS and Kataoka K. (2012) Block copolymer micelles as long-circulating drug vehicles. *Advanced drug delivery reviews* 64: 237-245.

Kwon GS and Okano T. (1996) Polymeric micelles as new drug carriers. *Advanced drug delivery reviews* 21: 107-116.

Kyomoto M, Moro T, Saiga K, et al. (2012) Biomimetic hydration lubrication with various polyelectrolyte layers on cross-linked polyethylene orthopedic bearing materials. *Biomaterials* 33: 4451-4459.

Kyomoto M, Moro T, Yamane S, et al. (2014) Poly (2-methacryloyloxyethyl phosphorylcholine) grafting and vitamin E blending for high wear resistance and oxidative stability of orthopedic bearings. *Biomaterials* 35: 6677-6686.

Kyung OY, Grabinski CM, Schrand AM, et al. (2009) Toxicity of amorphous silica nanoparticles in mouse keratinocytes. *Journal of Nanoparticle Research* 11: 15-24.

Lasic DD. (1998) Novel applications of liposomes. *Trends in biotechnology* 16: 307-321.

Laskar P, Samanta S, Ghosh SK, et al. (2014) In vitro evaluation of pH-sensitive cholesterol-containing stable polymeric micelles for delivery of camptothecin. *Journal of colloid and interface science* 430: 305-314.

Lawrence MJ. (1994) Surfactant systems: their use in drug delivery. *Chemical Society Reviews* 23: 417-424.

Lee ES, Na K and Bae YH. (2003a) Polymeric micelle for tumor pH and folate-mediated targeting. *Journal of controlled release* 91: 103-113.

Lee H-i, Pietrasik J, Sheiko SS, et al. (2010a) Stimuli-responsive molecular brushes. *Progress in Polymer Science* 35: 24-44.

Lee H-S, Lee HJ and Suh HJ. (2011) Silk protein hydrolysate increases glucose uptake through up-regulation of GLUT 4 and reduces the expression of leptin in 3T3-L1 fibroblast. *Nutrition research* 31: 937-943.

Lee SB, Russell AJ and Matyjaszewski K. (2003b) ATRP synthesis of amphiphilic random, gradient, and block copolymers of 2-(dimethylamino) ethyl methacrylate and n-butyl methacrylate in aqueous media. *Biomacromolecules* 4: 1386-1393.

Lee SH, Dreyer DR, An J, et al. (2010b) Polymer brushes via controlled, surface-initiated atom transfer radical polymerization (ATRP) from graphene oxide. *Macromolecular rapid communications* 31: 281-288.

Legrand P, Lesieur S, Bochot A, et al. (2007) Influence of polymer behaviour in organic solution on the production of polylactide nanoparticles by nanoprecipitation. *International journal of pharmaceutics* 344: 33-43.

Leng C, Hung H-C, Sun S, et al. (2015) Probing the surface hydration of nonfouling zwitterionic and PEG materials in contact with proteins. *ACS applied materials & interfaces* 7: 16881-16888.

Letchford K and Burt H. (2007) A review of the formation and classification of amphiphilic block copolymer nanoparticulate structures: micelles, nanospheres, nanocapsules and polymersomes. *European journal of pharmaceutics and biopharmaceutics* 65: 259-269.

Lewis A, Tolhurst L and Stratford P. (2002) Analysis of a phosphorylcholine-based polymer coating on a coronary stent pre-and post-implantation. *Biomaterials* 23: 1697-1706.

Lewis AL. (2000) Phosphorylcholine-based polymers and their use in the prevention of biofouling. *Colloids and Surfaces B: biointerfaces* 18: 261-275.

Lewis AL, Berwick J, Davies MC, et al. (2004) Synthesis and characterisation of cationically modified phospholipid polymers. *Biomaterials* 25: 3099-3108.

Lewis AL, Cumming ZL, Goreish HH, et al. (2001) Crosslinkable coatings from phosphorylcholine-based polymers. *Biomaterials* 22: 99-111.

Lewis AL, Hughes PD, Kirkwood LC, et al. (2000) Synthesis and characterisation of phosphorylcholine-based polymers useful for coating blood filtration devices. *Biomaterials* 21: 1847-1859.

Li J, Wu J, Zhang J, et al. (2016) Oral bioavailability and evaluation of docetaxel–nicotinamide complex loaded chitosan nanoparticles. *RSC Advances* 6: 35354-35364.

Li J, Zhang J, Wang Y, et al. (2017) Synergistic inhibition of migration and invasion of breast cancer cells by dual docetaxel/quercetin-loaded nanoparticles via Akt/MMP-9 pathway. *International journal of pharmaceutics* 523: 300-309.

Li L, Yang Q, Zhou Z, et al. (2014a) Doxorubicin-loaded, charge reversible, folate modified HPMA copolymer conjugates for active cancer cell targeting. *Biomaterials* 35: 5171-5187.

Li S, Wu W, Xiu K, et al. (2014b) Doxorubicin loaded pH-responsive micelles capable of rapid intracellular drug release for potential tumor therapy. *Journal of biomedical nanotechnology* 10: 1480-1489.

Li X, Liu W, Sun L, et al. (2015a) Effects of physicochemical properties of nanomaterials on their toxicity. *Journal of Biomedical Materials Research Part A* 103: 2499-2507.

Li X, Yang X, Lin Z, et al. (2015b) A folate modified pH sensitive targeted polymeric micelle alleviated systemic toxicity of doxorubicin (DOX) in multi-drug resistant tumor bearing mice. *European Journal of Pharmaceutical Sciences* 76: 95-101.

Li Y, Jin M, Shao S, et al. (2014c) Small-sized polymeric micelles incorporating docetaxel suppress distant metastases in the clinically-relevant 4T1 mouse breast cancer model. *BMC cancer* 14: 329.

Li Y, Tang Y, Narain R, et al. (2005) Biomimetic stimulus-responsive star diblock gelators. *Langmuir* 21: 9946-9954.

Licciardi M, Craparo EF, Giammona G, et al. (2008) in vitro Biological Evaluation of Folate-Functionalized Block Copolymer Micelles for Selective Anti-Cancer Drug Delivery. *Macromolecular bioscience* 8: 615-626.

Licciardi M, Giammona G, Du J, et al. (2006) New folate-functionalized biocompatible block copolymer micelles as potential anti-cancer drug delivery systems. *Polymer* 47: 2946-2955.

Licciardi M, Tang Y, Billingham N, et al. (2005) Synthesis of novel folic acid-functionalized biocompatible block copolymers by atom transfer radical polymerization for gene delivery and encapsulation of hydrophobic drugs. *Biomacromolecules* 6: 1085-1096.

Lim KS. (2003) Corneal endothelial cell damage from glaucoma drainage device materials. *Cornea* 22: 352-354.

Lin J, Zhu J, Chen T, et al. (2009) Drug releasing behavior of hybrid micelles containing polypeptide triblock copolymer. *Biomaterials* 30: 108-117.

Linkov I, Satterstrom FK and Corey LM. (2008) Nanotoxicology and nanomedicine: making hard decisions. *Nanomedicine: Nanotechnology, Biology and Medicine* 4: 167-171.

Liu B, Yang M, Li R, et al. (2008) The antitumor effect of novel docetaxel-loaded thermosensitive micelles. *European journal of pharmaceutics and biopharmaceutics* 69: 527-534.

Liu J, Lee H and Allen C. (2006) Formulation of drugs in block copolymer micelles: drug loading and release. *Current pharmaceutical design* 12: 4685-4701.

Liu X, Miller II AL, Yaszemski MJ, et al. (2015) Biodegradable and crosslinkable PPF–PLGA–PEG self-assembled nanoparticles dual-decorated with folic acid ligands and Rhodamine B fluorescent probes for targeted cancer imaging. *RSC Advances* 5: 33275-33282.

Liu Y, Inoue Y, Mahara A, et al. (2014) Durable modification of segmented polyurethane for elastic blood-contacting devices by graft-type 2-methacryloyloxyethyl phosphorylcholine copolymer. *Journal of Biomaterials Science, Polymer Edition* 25: 1514-1529.

Liu Y, Li K, Pan J, et al. (2010) Folic acid conjugated nanoparticles of mixed lipid monolayer shell and biodegradable polymer core for targeted delivery of Docetaxel. *Biomaterials* 31: 330-338.

Lobb EJ, Ma I, Billingham NC, et al. (2001) Facile Synthesis of Well-Defined, Biocompatible Phosphorylcholine-Based Methacrylate Copolymers via Atom Transfer Radical Polymerization at 20 °C. *Journal of the American Chemical Society* 123: 7913-7914.

Lomas H, Canton I, MacNeil S, et al. (2007) Biomimetic pH sensitive polymersomes for efficient DNA encapsulation and delivery. *Advanced Materials* 19: 4238-4243.

Lomas H, Du J, Canton I, et al. (2010) Efficient Encapsulation of Plasmid DNA in pH-Sensitive PMPC–PDPA Polymersomes: Study of the Effect of PDPA Block Length on Copolymer–DNA Binding Affinity. *Macromolecular bioscience* 10: 513-530.

Lomas H, Massignani M, Abdullah KA, et al. (2008) Non-cytotoxic polymer vesicles for rapid and efficient intracellular delivery. *Faraday discussions* 139: 143-159.

Lu X-Y, Wu D-C, Li Z-J, et al. (2011) Polymer nanoparticles. *Progress in molecular biology and translational science* 104: 299.

Lu Y and Park K. (2013) Polymeric micelles and alternative nanonized delivery vehicles for poorly soluble drugs. *International journal of pharmaceutics* 453: 198-214.

Luo Y, Ling Y, Guo W, et al. (2010) Docetaxel loaded oleic acid-coated hydroxyapatite nanoparticles enhance the docetaxel-induced apoptosis through activation of caspase-2 in androgen independent prostate cancer cells. *Journal of controlled release* 147: 278-288.

Ma IY, Lobb EJ, Billingham NC, et al. (2002) Synthesis of biocompatible polymers. 1. Homopolymerization of 2-methacryloyloxyethyl phosphorylcholine via ATRP in protic solvents: an optimization study. *Macromolecules* 35: 9306-9314.

Ma Y, Tang Y, Billingham NC, et al. (2003) Well-defined biocompatible block copolymers via atom transfer radical polymerization of 2-methacryloyloxyethyl phosphorylcholine in protic media. *Macromolecules* 36: 3475-3484.

Madsen J, Armes SP, Bertal K, et al. (2009) Preparation and aqueous solution properties of thermoresponsive biocompatible AB diblock copolymers. *Biomacromolecules* 10: 1875-1887.

Madsen J, Canton I, Warren NJ, et al. (2013) Nile blue-based nanosized pH sensors for simultaneous far-red and near-infrared live bioimaging. *Journal of the American Chemical Society* 135: 14863-14870.

Maeda H. (2015) Toward a full understanding of the EPR effect in primary and metastatic tumors as well as issues related to its heterogeneity. *Advanced drug delivery reviews* 91: 3-6.

Maeda H, Wu J, Sawa T, et al. (2000) Tumor vascular permeability and the EPR effect in macromolecular therapeutics: a review. *Journal of controlled release* 65: 271-284.

Mahmud A and Lavasanifar A. (2005) The effect of block copolymer structure on the internalization of polymeric micelles by human breast cancer cells. *Colloids and Surfaces B: biointerfaces* 45: 82-89.

Malvern. (2011) Zetasizer Nano ZS90 [Online]. Malvern, Worcestershire: Instruments Ltd. Available: http://www.malvern.com/labeng/products/zetasizer/zetasizer_nano/zetasizer_nano_zs90.htm?gclid=CN_Cl_3Nn6sCFeILtAodZHbokQ. (Accessed 16th December/ 2014).

Mao B, Gan L and Gan Y. (2006) Ultra high molar mass poly [2-(dimethylamino) ethyl methacrylate] via atom transfer radical polymerization. *Polymer* 47: 3017-3020.

Masci G, Bontempo D, Tiso N, et al. (2004) Atom transfer radical polymerization of potassium 3-sulfopropyl methacrylate: Direct synthesis of amphiphilic block copolymers with methyl methacrylate. *Macromolecules* 37: 4464-4473.

Massignani M, Canton I, Sun T, et al. (2010) Enhanced fluorescence imaging of live cells by effective cytosolic delivery of probes. *PloS one* 5: e10459.

Massignani M, LoPresti C, Blanazs A, et al. (2009) Controlling cellular uptake by surface chemistry, size, and surface topology at the nanoscale. *Small* 5: 2424-2432.

Matsumura Y. (2008) Polymeric micellar delivery systems in oncology. *Japanese journal of clinical oncology* 38: 793-802.

Matsumura Y, Hamaguchi T, Ura T, et al. (2004) Phase I clinical trial and pharmacokinetic evaluation of NK911, a micelle-encapsulated doxorubicin. *British journal of cancer* 91: 1775.

Matyjaszewski K. (2012a) Atom transfer radical polymerization (ATRP): current status and future perspectives. *Macromolecules* 45: 4015-4039.

Matyjaszewski K. (2012b) Atom transfer radical polymerization: from mechanisms to applications. *Israel Journal of Chemistry* 52: 206-220.

Matyjaszewski K, Nakagawa Y and Jasieczek CB. (1998) Polymerization of n-butyl acrylate by atom transfer radical polymerization. Remarkable effect of ethylene carbonate and other solvents. *Macromolecules* 31: 1535-1541.

Matyjaszewski K, Pintauer T and Gaynor S. (2000) Removal of copper-based catalyst in atom transfer radical polymerization using ion exchange resins. *Macromolecules* 33: 1476-1478.

Matyjaszewski K and Tsarevsky NV. (2009) Nanostructured functional materials prepared by atom transfer radical polymerization. *Nature chemistry* 1: 276-288.

Matyjaszewski K and Tsarevsky NV. (2014) Macromolecular Engineering by Atom Transfer Radical Polymerization. *Journal of the American Chemical Society* 136: 6513-6533.

Matyjaszewski K, Wei M, Xia J, et al. (1997) Controlled/"Living" Radical Polymerization of Styrene and Methyl Methacrylate Catalyzed by Iron Complexes 1. *Macromolecules* 30: 8161-8164.

Matyjaszewski K and Xia J. (2001) Atom transfer radical polymerization. *Chemical Reviews* 101: 2921-2990.

McDonald S and Rannard SP. (2001) Room temperature waterborne ATRP of n-butyl methacrylate in homogeneous alcoholic media. *Macromolecules* 34: 8600-8602.

Mei L, Zhang Y, Zheng Y, et al. (2009) A novel docetaxel-loaded poly (ε-caprolactone)/pluronic F68 nanoparticle overcoming multidrug resistance for breast cancer treatment. *Nanoscale research letters* 4: 1530.

Messager L, Burns JR, Kim J, et al. (2016) Biomimetic Hybrid Nanocontainers with Selective Permeability. *Angewandte Chemie* 128: 11272-11275.

Mi Y, Liu Y and Feng S-S. (2011) Formulation of docetaxel by folic acid-conjugated d-α-tocopheryl polyethylene glycol succinate 2000 (Vitamin E TPGS 2k) micelles for targeted and synergistic chemotherapy. *Biomaterials* 32: 4058-4066.

Mishra D, Hubenak JR and Mathur AB. (2013) Nanoparticle systems as tools to improve drug delivery and therapeutic efficacy. *Journal of Biomedical Materials Research Part A* 101: 3646-3660.

Misra R, Upadhyay M, Perumal V, et al. (2015) In vitro control release, cytotoxicity assessment and cellular uptake of methotrexate loaded liquid-crystalline folate nanocarrier. *Biomedicine & Pharmacotherapy* 69: 102-110.

Miyata K, Christie RJ and Kataoka K. (2011) Polymeric micelles for nano-scale drug delivery. *Reactive and Functional Polymers* 71: 227-234.

Moghimi SM and Hunter AC. (2000) Poloxamers and poloxamines in nanoparticle engineering and experimental medicine. *Trends in biotechnology* 18: 412-420.

Moghimi SM, Hunter AC and Murray JC. (2001) Long-circulating and target-specific nanoparticles: theory to practice. *Pharmacological reviews* 53: 283-318.

Mohanraj V and Chen Y. (2007) Nanoparticles-a review. *Tropical Journal of Pharmaceutical Research* 5: 561-573.

Moore SL. (1997) The mechanisms of antibacterial action of some nonionic surfactants. University of Brighton.

Morick J, Buback M and Matyjaszewski K. (2011) Activation–Deactivation Equilibrium of Atom Transfer Radical Polymerization of Styrene up to High Pressure. *Macromolecular Chemistry and Physics* 212: 2423-2428.

Morick J, Buback M and Matyjaszewski K. (2012) Effect of pressure on activation–deactivation equilibrium constants for ATRP of methyl methacrylate. *Macromolecular Chemistry and Physics* 213: 2287-2292.

Morikawa Y, Koike H, Sekine Y, et al. (2012) Rapamycin enhances docetaxel-induced cytotoxicity in a androgen-independent prostate cancer xenograft model by survivin downregulation. *Biochemical and biophysical research communications* 419: 584-589.

Morimoto N, Iwasaki Y, Nakabayashi N, et al. (2002) Physical properties and blood compatibility of surface-modified segmented polyurethane by semi-interpenetrating polymer networks with a phospholipid polymer. *Biomaterials* 23: 4881-4887.

Moro T, Kawaguchi H, Ishihara K, et al. (2009) Wear resistance of artificial hip joints with poly (2-methacryloyloxyethyl phosphorylcholine) grafted polyethylene: comparisons with the effect of polyethylene cross-linking and ceramic femoral heads. *Biomaterials* 30: 2995-3001.

Mosmann T. (1983) Rapid colorimetric assay for cellular growth and survival: application to proliferation and cytotoxicity assays. *Journal of immunological methods* 65: 55-63.

Movassaghian S, Merkel OM and Torchilin VP. (2015) Applications of polymer micelles for imaging and drug delivery. *Wiley Interdisciplinary Reviews: Nanomedicine and Nanobiotechnology*.

Munirasu S, Deshpande A and Baskaran D. (2008) Hydrated clay for catalyst removal in copper mediated atom transfer radical polymerization. *Macromolecular rapid communications* 29: 1538-1543.

Muñoz-Bonilla A, León O, Cerrada ML, et al. (2012) Glycopolymers obtained by chemical modification of well-defined block copolymers. *Journal of Polymer Science Part A: Polymer Chemistry* 50: 2565-2577.

Murdoch C, Reeves KJ, Hearnden V, et al. (2010) Internalization and biodistribution of polymersomes into oral squamous cell carcinoma cells in vitro and in vivo. *Nanomedicine* 5: 1025-1036.

Myers GJ, Johnstone D, Swyer WJ, et al. (2003) Evaluation of Mimesys® Phosphorylcholine (PC)-coated oxygenators during cardiopulmonary bypass in adults. *Journal of Extracorporeal Technology* 35: 6-12.

Naahidi S, Jafari M, Edalat F, et al. (2013) Biocompatibility of engineered nanoparticles for drug delivery. *Journal of controlled release* 166: 182-194.

Nachlas MM, Margulies SI, Goldberg JD, et al. (1960) The determination of lactic dehydrogenase with a tetrazolium salt. *Analytical biochemistry* 1: 317-326.

Nagarajan R. (2002) Molecular packing parameter and surfactant self-assembly: the neglected role of the surfactant tail. *Langmuir* 18: 31-38.

Nagarajan R. (2011) Amphiphilic surfactants and amphiphilic polymers: Principles of molecular assembly. *Amphiphiles: Molecular assembly and applications, acs symposium series, American Chemical Society, Washington DC.* 1-22.

Naik S, Patel D, Chuttani K, et al. (2012) In vitro mechanistic study of cell death and in vivo performance evaluation of RGD grafted PEGylated docetaxel liposomes in breast cancer. *Nanomedicine: Nanotechnology, Biology and Medicine* 8: 951-962.

Nakabayashi N and Williams DF. (2003) Preparation of non-thrombogenic materials using 2-methacryloyloxyethyl phosphorylcholine. *Biomaterials* 24: 2431-2435.

Nakai S, Nakaya T and Imoto M. (1977) Polymeric phospholipid analog, 10. Synthesis and polymerization of 2-(methacryloyloxy) ethyl 2-aminoethyl hydrogen phosphate. *Macromolecular Chemistry and Physics* 178: 2963-2967.

Nakayama M, Akimoto J and Okano T. (2014) Polymeric micelles with stimuli-triggering systems for advanced cancer drug targeting. *Journal of drug targeting* 22: 584-599.

Nanda AK and Matyjaszewski K. (2003) Effect of [bpy]/[Cu (I)] ratio, solvent, counterion, and alkyl bromides on the activation rate constants in atom transfer radical polymerization. *Macromolecules* 36: 599-604.

Ng CT, Tang FMA, Li JJe, et al. (2015) Clathrin-Mediated Endocytosis of Gold Nanoparticles In Vitro. *The Anatomical Record* 298: 418-427.

Nicolas J, Mura S, Brambilla D, et al. (2013) Design, functionalization strategies and biomedical applications of targeted biodegradable/biocompatible polymer-based nanocarriers for drug delivery. *Chemical Society Reviews* 42: 1147-1235.

Nishiyama N and Kataoka K. (2006) Current state, achievements, and future prospects of polymeric micelles as nanocarriers for drug and gene delivery. *Pharmacology & therapeutics* 112: 630-648.

Oerlemans C, Bult W, Bos M, et al. (2010) Polymeric micelles in anticancer therapy: targeting, imaging and triggered release. *Pharmaceutical research* 27: 2569-2589.

Oh JK and Matyjaszewski K. (2006) Synthesis of poly (2-hydroxyethyl methacrylate) in protic media through atom transfer radical polymerization using activators generated by electron transfer. *Journal of Polymer Science Part A: Polymer Chemistry* 44: 3787-3796.

Ohno S, Hasegawa S, Liu H, et al. (2015) Aggregation behavior in water of amphiphilic diblock copolymers bearing biocompatible phosphorylcholine and cholesteryl groups. *Polymer Journal* 47: 71-76.

Ostacolo L, Marra M, Ungaro F, et al. (2010) In vitro anticancer activity of docetaxel-loaded micelles based on poly (ethylene oxide)-poly (epsilon-caprolactone) block copolymers: Do nanocarrier properties have a role? *Journal of controlled release* 148: 255-263.

Owen SC, Chan DP and Shoichet MS. (2012) Polymeric micelle stability. *Nano Today* 7: 53-65.

Owens DE and Peppas NA. (2006) Opsonization, biodistribution, and pharmacokinetics of polymeric nanoparticles. *International journal of pharmaceutics* 307: 93-102.

Pan Y, Neuss S, Leifert A, et al. (2007) Size-dependent cytotoxicity of gold nanoparticles. *Small* 3: 1941-1949.

Parveen S, Misra R and Sahoo SK. (2012) Nanoparticles: a boon to drug delivery, therapeutics, diagnostics and imaging. *Nanomedicine: Nanotechnology, Biology and Medicine* 8: 147-166.

Patel HR, Patel RP and Patel M. (2009) Poloxamers: A pharmaceutical excipients with therapeutic behaviors. *International Journal of PharmTech Research* 1: 299-303.

Paterson SM, Brown DH, Chirila TV, et al. (2010) The synthesis of water-soluble PHEMA via ARGET ATRP in protic media. *Journal of Polymer Science Part A: Polymer Chemistry* 48: 4084-4092.

Patten TE and Matyjaszewski K. (1998) Atom transfer radical polymerization and the synthesis of polymeric materials. *Advanced Materials* 10: 901-915.

Patten TE, Xia J, Abernathy T, et al. (1996) Polymers with very low polydispersities from atom transfer radical polymerization. *Science* 272: 866.

Pearson RT, Warren NJ, Lewis AL, et al. (2013) Effect of pH and temperature on PMPC–PDPA copolymer self-assembly. *Macromolecules* 46: 1400-1407.

Pegoraro C, Cecchin D, Gracia LS, et al. (2013) Enhanced drug delivery to melanoma cells using PMPC-PDPA polymersomes. *Cancer letters* 334: 328-337.

Peñaloza JP, Márquez-Miranda V, Cabaña-Brunod M, et al. (2017) Intracellular trafficking and cellular uptake mechanism of PHBV nanoparticles for targeted delivery in epithelial cell lines. *Journal of nanobiotechnology* 15: 1.

Peracchia M, Fattal E, Desmaele D, et al. (1999) Stealth® PEGylated polycyanoacrylate nanoparticles for intravenous administration and splenic targeting. *Journal of controlled release* 60: 121-128.

Piñeiro L, Novo M and Al-Soufi W. (2015) Fluorescence emission of pyrene in surfactant solutions. *Advances in colloid and interface science* 215: 1-12.

Pittella F, Cabral H, Maeda Y, et al. (2014) Systemic siRNA delivery to a spontaneous pancreatic tumor model in transgenic mice by PEGylated calcium phosphate hybrid micelles. *Journal of controlled release* 178: 18-24.

Plummer R, Wilson R, Calvert H, et al. (2011) A Phase I clinical study of cisplatin-incorporated polymeric micelles (NC-6004) in patients with solid tumours. *British journal of cancer* 104: 593.

Porto LC, Aissou K, Giacomelli C, et al. (2011) Nanostructured films made from zwitterionic phosphorylcholine diblock copolymer systems. *Macromolecules* 44: 2240-2244.

Prabhu RH, Patravale VB and Joshi MD. (2015) Polymeric nanoparticles for targeted treatment in oncology: current insights. *International journal of nanomedicine* 10: 1001.

Pratten MK, Lloyd JB, Hörpel G, et al. (1985) Micelle-forming block copolymers: pinocytosis by macrophages and interaction with model membranes. *Macromolecular Chemistry and Physics* 186: 725-733.

Qiu LY and Bae YH. (2006) Polymer architecture and drug delivery. *Pharmaceutical research* 23: 1-30.

Rahman M. (2006) Introduction to flow cytometry. *AbD serotec*.

Rajagopal K, Mahmud A, Christian DA, et al. (2010) Curvature-coupled hydration of semicrystalline polymer amphiphiles yields flexible worm micelles but favors rigid vesicles: polycaprolactone-based block copolymers. *Macromolecules* 43: 9736.

Ran J, Wu L, Zhang Z, et al. (2014) Atom transfer radical polymerization (ATRP): a versatile and forceful tool for functional membranes. *Progress in Polymer Science* 39: 124-144.

Rangel-Yagui CO, Pessoa Jr A and Tavares LC. (2005) Micellar solubilization of drugs. *J Pharm Pharm Sci* 8: 147-163.

Rao JP and Geckeler KE. (2011) Polymer nanoparticles: preparation techniques and size-control parameters. *Progress in Polymer Science* 36: 887-913.

Rapoport N. (1999) Stabilization and activation of Pluronic micelles for tumor-targeted drug delivery. *Colloids and Surfaces B: biointerfaces* 16: 93-111.

Rapoport N. (2007) Physical stimuli-responsive polymeric micelles for anti-cancer drug delivery. *Progress in Polymer Science* 32: 962-990.

Ratoi M, Hoet PH, Crossley A, et al. (2014) Impact of lung surfactant on wettability and cytotoxicity of nanoparticles. *RSC Advances* 4: 20573-20581.

Raveche E, Abbasi F, Yuan Y, et al. (2010) Introduction to flow cytometry. *Flow Cytometry in Drug Discovery and Development*: 3-21.

Redhead H, Davis S and Illum L. (2001) Drug delivery in poly (lactide-co-glycolide) nanoparticles surface modified with poloxamer 407 and poloxamine 908: in vitro characterisation and in vivo evaluation. *Journal of controlled release* 70: 353-363.

Rijcken C, Soga O, Hennink W, et al. (2007) Triggered destabilisation of polymeric micelles and vesicles by changing polymers polarity: an attractive tool for drug delivery. *Journal of controlled release* 120: 131-148.

Riley T, Govender T, Stolnik S, et al. (1999) Colloidal stability and drug incorporation aspects of micellar-like PLA–PEG nanoparticles. *Colloids and Surfaces B: biointerfaces* 16: 147-159.

Robinson K, Khan M, de Paz Banez M, et al. (2001) Controlled polymerization of 2-hydroxyethyl methacrylate by ATRP at ambient temperature. *Macromolecules* 34: 3155-3158.

Robinson KL, Weaver JV, Armes SP, et al. (2002) Synthesis of controlled-structure sulfate-based copolymers via atom transfer radical polymerisation and their use as crystal habit modifiers for BaSO 4. *Journal of Materials Chemistry* 12: 890-896.

Rosen MJ and Kunjappu JT. (2012) *Surfactants and interfacial phenomena*: John Wiley & Sons.

Rowinsky M, Eric K. (1997) The development and clinical utility of the taxane class of antimicrotubule chemotherapy agents. *Annual review of medicine* 48: 353-374.

Ruiz-Pérez L, Madsen J, Themistou E, et al. (2015) Nanoscale detection of metal-labeled copolymers in patchy polymersomes. *Polym. Chem* 6: 2065-2068.

Ruiz-Perez L, Messager L, Gaitzsch J, et al. (2015) Polymersomes confined self-assembly: micellisation in 2D. *arXiv preprint arXiv:1509.02757*.

Sahay G, Alakhova DY and Kabanov AV. (2010) Endocytosis of nanomedicines. *Journal of controlled release* 145: 182-195.

Sahay G, Batrakova EV and Kabanov AV. (2008) Different internalization pathways of polymeric micelles and unimers and their effects on vesicular transport. *Bioconjugate chemistry* 19: 2023-2029.

Salvage JP, Rose SF, Phillips GJ, et al. (2005) Novel biocompatible phosphorylcholine-based self-assembled nanoparticles for drug delivery. *Journal of controlled release* 104: 259-270.

Salvage JP, Smith T, Lu T, et al. (2016) Synthesis, characterisation, and in vitro cellular uptake kinetics of nanoprecipitated poly(2-methacryloyloxyethyl phosphorylcholine)-b-poly(2-(diisopropylamino)ethyl methacrylate) (MPC-DPA) polymeric nanoparticle micelles for nanomedicine applications. *Applied Nanoscience* 6: 1073-1094.

Salvage JP, Thom C, Lewis AL, et al. (2015) Nanoprecipitation of polymeric nanoparticle micelles based on 2-methacryloyloxyethyl phosphorylcholine (MPC) with 2-(diisopropylamino)ethyl methacrylate (DPA), for intracellular delivery applications. *Journal of Materials Science: Materials in Medicine* 26: 150.

Sanna V, Roggio AM, Posadino AM, et al. (2011) Novel docetaxel-loaded nanoparticles based on poly (lactide-co-caprolactone) and poly (lactide-co-glycolide-co-caprolactone) for prostate cancer treatment: formulation, characterization, and cytotoxicity studies. *Nanoscale research letters* 6: 260.

Save M, Weaver J, Armes S, et al. (2002) Atom transfer radical polymerization of hydroxy-functional methacrylates at ambient temperature: comparison of glycerol monomethacrylate with 2-hydroxypropyl methacrylate. *Macromolecules* 35: 1152-1159.

Schmid SL. (1997) Clathrin-coated vesicle formation and protein sorting: an integrated process. *Annual review of biochemistry* 66: 511-548.

Schroeder H, Yalalov D, Buback M, et al. (2012) Activation–Deactivation Equilibrium Associated With Iron-Mediated Atom-Transfer Radical Polymerization up to High Pressure. *Macromolecular Chemistry and Physics* 213: 2019-2026.

Schubert M and Müller-Goymann C. (2003) Solvent injection as a new approach for manufacturing lipid nanoparticles–evaluation of the method and process parameters. *European journal of pharmaceutics and biopharmaceutics* 55: 125-131.

Schubert S, Delaney Jr JT and Schubert US. (2011) Nanoprecipitation and nanoformulation of polymers: from history to powerful possibilities beyond poly (lactic acid). *Soft Matter* 7: 1581-1588.

Seiler HG, Sigel H and Sigel A. (1988) Handbook on toxicity of inorganic compounds.

Sezgin Z, Yüksel N and Baykara T. (2006) Preparation and characterization of polymeric micelles for solubilization of poorly soluble anticancer drugs. *European journal of pharmaceutics and biopharmaceutics* 64: 261-268.

Shang L, Nienhaus K, Jiang X, et al. (2014a) Nanoparticle interactions with live cells: quantitative fluorescence microscopy of nanoparticle size effects. *Beilstein journal of nanotechnology* 5: 2388.

Shang L, Nienhaus K and Nienhaus GU. (2014b) Engineered nanoparticles interacting with cells: size matters. *Journal of nanobiotechnology* 12: 5.

Shaw R. (2014) Dynamic Light Scattering Training. Malvern Instruments: Malvern, UK.

Sheetal M. (2013) A simple ultraviolet spectrophotometric method for the estimation of docetaxel in bulk drug and formulation. *Asian Journal of Pharmaceutical Analysis* 3: 48-52.

Shen L, Du J, Armes SP, et al. (2008) Kinetics of pH-induced formation and dissociation of polymeric vesicles assembled from a water-soluble zwitterionic diblock copolymer. *Langmuir* 24: 10019-10025.

Shen Y, Tang H and Ding S. (2004) Catalyst separation in atom transfer radical polymerization. *Progress in Polymer Science* 29: 1053-1078.

Shi C, Zhang Z, Shi J, et al. (2015a) Co-delivery of docetaxel and chloroquine via PEO–PPO–PCL/TPGS micelles for overcoming multidrug resistance. *International journal of pharmaceutics* 495: 932-939.

Shi C, Zhang Z, Wang F, et al. (2015b) Docetaxel-loaded PEO–PPO–PCL/TPGS mixed micelles for overcoming multidrug resistance and enhancing antitumor efficacy. *Journal of Materials Chemistry B* 3: 4259-4271.

Shigeta M, Tanaka T, Koike N, et al. (2006) Suppression of fibroblast and bacterial adhesion by MPC coating on acrylic intraocular lenses. *Journal of Cataract & Refractive Surgery* 32: 859-866.

Shinoda H and Matyjaszewski K. (2001) Structural control of poly (methyl methacrylate)-g-poly (lactic acid) graft copolymers by atom transfer radical polymerization (ATRP). *Macromolecules* 34: 6243-6248.

Siegwart DJ, Oh JK and Matyjaszewski K. (2012) ATRP in the design of functional materials for biomedical applications. *Progress in Polymer Science* 37: 18-37.

Singh T, Jain C, Sharma S, et al. (1999) Preparation of di s p e rsed s ilica b y hydroly s i s of tetr ae thyl orthosilicate.

Smart T, Lomas H, Massignani M, et al. (2008) Block copolymer nanostructures. *Nano Today* 3: 38-46.

Snipstad S, Hak S, Baghirov H, et al. (2017) Labeling nanoparticles: Dye leakage and altered cellular uptake. *Cytometry Part A* 91: 760-766.

Snipstad S, Westrøm S, Mørch Y, et al. (2014) Contact-mediated intracellular delivery of hydrophobic drugs from polymeric nanoparticles. *Cancer nanotechnology* 5: 8.

Sohaebuddin SK, Thevenot PT, Baker D, et al. (2010) Nanomaterial cytotoxicity is composition, size, and cell type dependent. *Particle and fibre toxicology* 7: 22.

Soletti L, Nieponice A, Hong Y, et al. (2011) In vivo performance of a phospholipid-coated bioerodable elastomeric graft for small-diameter vascular applications. *Journal of Biomedical Materials Research Part A* 96: 436-448.

Son HY, Ryu JH, Lee H, et al. (2013) Bioinspired templating synthesis of metal–polymer hybrid nanostructures within 3D electrospun nanofibers. *ACS applied materials & interfaces* 5: 6381-6390.

Stolnik S, Heald CR, Neal J, et al. (2001) Polylactide-poly(ethylene glycol) micellar-like particles as potential drug carriers: production, colloidal properties and biological performance. *Journal of drug targeting* 9: 361.

Stone V, Johnston H and Schins RP. (2009) Development of in vitro systems for nanotoxicology: methodological considerations. *Critical reviews in toxicology* 39: 613-626.

Strebhardt K and Ullrich A. (2008) Paul Ehrlich's magic bullet concept: 100 years of progress. *Nature Reviews Cancer* 8: 473-480.

Strickley RG. (2004) Solubilizing excipients in oral and injectable formulations. *Pharmaceutical research* 21: 201-230.

Su W-F. (2013) Polymer size and polymer solutions. *Principles of Polymer Design and Synthesis.* Springer, 9-26.

Suk JS, Xu Q, Kim N, et al. (2016) PEGylation as a strategy for improving nanoparticle-based drug and gene delivery. *Advanced drug delivery reviews* 99: 28-51.

Sulheim E, Baghirov H, Haartman E, et al. (2016) Cellular uptake and intracellular degradation of poly (alkyl cyanoacrylate) nanoparticles. *Journal of nanobiotechnology* 14: 1.

Sun Q, Sun X, Ma X, et al. (2014a) Integration of nanoassembly functions for an effective delivery cascade for cancer drugs. *Advanced Materials* 26: 7615-7621.

Sun T, Zhang YS, Pang B, et al. (2014b) Engineered nanoparticles for drug delivery in cancer therapy. *Angewandte Chemie International Edition* 53: 12320-12364.

Sun X-Y, Gan Q-Z and Ouyang J-M. (2017) Size-dependent cellular uptake mechanism and cytotoxicity toward calcium oxalate on Vero cells. *Scientific Reports* 7: 41949.

Tabatabaei Mirakabad FS, Akbarzadeh A, Milani M, et al. (2016) A Comparison between the cytotoxic effects of pure curcumin and curcumin-loaded PLGA-PEG nanoparticles on the MCF-7 human breast cancer cell line. *Artificial cells, nanomedicine, and biotechnology* 44: 423-430.

Takahashi A, Yamamoto Y, Yasunaga M, et al. (2013) NC-6300, an epirubicin-incorporating micelle, extends the antitumor effect and reduces the cardiotoxicity of epirubicin. *Cancer science* 104: 920-925.

Tang W, Kwak Y, Braunecker W, et al. (2008) Understanding atom transfer radical polymerization: effect of ligand and initiator structures on the equilibrium constants. *Journal of the American Chemical Society* 130: 10702-10713.

Tang X, Liang Y, Feng X, et al. (2015) Co-delivery of docetaxel and Poloxamer 235 by PLGA–TPGS nanoparticles for breast cancer treatment. *Materials Science and Engineering: C* 49: 348-355.

Tang Y, Lu J, Lewis A, et al. (2002) Structural effects on swelling of thin phosphorylcholine polymer films. *Macromolecules* 35: 3955-3964.

Teoh RL, Guice KB and Loo Y-L. (2006) Atom transfer radical copolymerization of hydroxyethyl methacrylate and dimethylaminoethyl methacrylate in polar solvents. *Macromolecules* 39: 8609-8615.

Tephly TR. (1991) The toxicity of methanol. *Life sciences* 48: 1031-1041.

Thakur S, Kesharwani P, Tekade RK, et al. (2015) Impact of pegylation on biopharmaceutical properties of dendrimers. *Polymer* 59: 67-92.

Thayer AM. (2005) CHIRAL CATALYSIS. *Chemical & Engineering News Archive* 83: 40-58.

Thomas SC, Sharma H, Rawat P, et al. (2016) Synergistic anticancer efficacy of bendamustine hydrochloride loaded bioactive hydroxyapatite nanoparticles: In-vitro, ex-vivo and in-vivo evaluation. *Colloids and Surfaces B: biointerfaces* 146: 852-860.

Torchilin V. (2004) Targeted polymeric micelles for delivery of poorly soluble drugs. *Cellular and molecular life sciences* 61: 2549-2559.

Torchilin V. (2011) Tumor delivery of macromolecular drugs based on the EPR effect. *Advanced drug delivery reviews* 63: 131-135.

Torchilin V, Levchenko T, Whiteman K, et al. (2001) Amphiphilic poly-N-vinylpyrrolidones:: synthesis, properties and liposome surface modification. *Biomaterials* 22: 3035-3044.

Torchilin VP. (2005) Block copolymer micelles as a solution for drug delivery problems. *Expert opinion on therapeutic patents* 15: 63-75.

Torchilin VP. (2007a) Micellar nanocarriers: pharmaceutical perspectives. *Pharmaceutical research* 24: 1.

Torchilin VP. (2007b) Targeted pharmaceutical nanocarriers for cancer therapy and imaging. *The AAPS journal* 9: E128-E147.

Torchilin VP and Trubetskoy VS. (1995) Which polymers can make nanoparticulate drug carriers long-circulating? *Advanced drug delivery reviews* 16: 141-155.

Tsarevsky NV and Matyjaszewski K. (2007) "Green" Atom Transfer Radical Polymerization: From Process Design to Preparation of Well-Defined Environmentally Friendly Polymeric Materials. *Chemical Reviews* 107: 2270-2299.

Tu S, Chen YW, Qiu YB, et al. (2011) Enhancement of cellular uptake and antitumor efficiencies of micelles with phosphorylcholine. *Macromolecular bioscience* 11: 1416-1425.

Ueda H, Watanabe J, Konno T, et al. (2006) Asymmetrically functional surface properties on biocompatible phospholipid polymer membrane for bioartificial kidney. *Journal of Biomedical Materials Research Part A* 77: 19-27.

Ueda T, Oshida H, Kurita K, et al. (1992) Preparation of 2-methacryloyloxyethyl phosphorylcholine copolymers with alkyl methacrylates and their blood compatibility. *POLYMER JOURNAL-TOKYO-* 24: 1259-1259.

Upadhyay KK, Bhatt AN, Castro E, et al. (2010) In vitro and in vivo evaluation of docetaxel loaded biodegradable polymersomes. *Macromolecular bioscience* 10: 503-512.

Valle JW, Armstrong A, Newman C, et al. (2011) A phase 2 study of SP1049C, doxorubicin in P-glycoprotein-targeting pluronics, in patients with advanced adenocarcinoma of the esophagus and gastroesophageal junction. *Investigational new drugs* 29: 1029-1037.

Van Steenberge PH, D'hooge DR, Wang Y, et al. (2012) Linear gradient quality of ATRP copolymers. *Macromolecules* 45: 8519-8531.

Varela-Moreira A, Shi Y, Fens MH, et al. (2017) Clinical application of polymeric micelles for the treatment of cancer. *Materials Chemistry Frontiers*.

Varela JA, Bexiga MG, Åberg C, et al. (2012) Quantifying size-dependent interactions between fluorescently labeled polystyrene nanoparticles and mammalian cells. *Journal of nanobiotechnology* 10: 39.

Vauthier C and Bouchemal K. (2009) Methods for the preparation and manufacture of polymeric nanoparticles. *Pharmaceutical research* 26: 1025-1058.

Virtanen JA, Cheng KH and Somerharju P. (1998) Phospholipid composition of the mammalian red cell membrane can be rationalized by a superlattice model. *Proceedings of the National Academy of Sciences* 95: 4964-4969.

Wacker WE, Ulmer DD and Vallee BL. (1956) Metalloenzymes and myocardial infarction: Malic and lactic dehydrogenase activities and zinc concentrations in serum. *New England Journal of Medicine* 255: 449-456.

Wang H, Xu F, Li D, et al. (2013) Bioinspired phospholipid polymer prodrug as a pH-responsive drug delivery system for cancer therapy. *Polymer Chemistry* 4: 2004-2010.

Wang J-S and Matyjaszewski K. (1995) Controlled/" living" radical polymerization. Atom transfer radical polymerization in the presence of transition-metal complexes. *Journal of the American Chemical Society* 117: 5614-5615.

Wang J, Jiang P, Han Z, et al. (2012a) Fast self-assembly kinetics of quantum dots and a dendrimeric peptide ligand. *Langmuir* 28: 7962-7966.

Wang J, Ma W and Tu P. (2015a) Synergistically Improved Anti-tumor Efficacy by Co-delivery Doxorubicin and Curcumin Polymeric Micelles. *Macromolecular bioscience* 15: 1252-1261.

Wang J, Mao W, Lock LL, et al. (2015b) The role of micelle size in tumor accumulation, penetration, and treatment. *ACS nano* 9: 7195-7206.

Wang L, Zeng R, Li C, et al. (2009) Self-assembled polypeptide-block-poly (vinylpyrrolidone) as prospective drug-delivery systems. *Colloids and Surfaces B: biointerfaces* 74: 284-292.

Wang M, Han M, Li Y, et al. (2016) Chemosensitization of doxorubicin in multidrug-resistant cells by unimolecular micelles via increased cellular accumulation and apoptosis. *Journal of pharmacy and pharmacology* 68: 333-341.

Wang T, Yang S, Mei LA, et al. (2014) Paclitaxel-loaded PEG-PE–based micellar nanopreparations targeted with tumor-specific landscape phage fusion protein enhance apoptosis and efficiently reduce tumors. *Molecular cancer therapeutics* 13: 2864-2875.

Wang W, Cheng D, Gong F, et al. (2012b) Design of multifunctional micelle for tumor-targeted intracellular drug release and fluorescent imaging. *Advanced Materials* 24: 115-120.

Wani MY, Hashim MA, Nabi F, et al. (2011) Nanotoxicity: dimensional and morphological concerns. *Advances in Physical Chemistry* 2011.

Weiss RB, Donehower R, Wiernik P, et al. (1990) Hypersensitivity reactions from taxol. *Journal of Clinical Oncology* 8: 1263-1268.

Weissig V, Whiteman KR and Torchilin VP. (1998) Accumulation of protein-loaded long-circulating micelles and liposomes in subcutaneous Lewis lung carcinoma in mice. *Pharmaceutical research* 15: 1552-1556.

Wever DAZ, Ramalho G, Picchioni F, et al. (2014) Acrylamide-b-N-isopropylacrylamide block copolymers: Synthesis by atomic transfer radical polymerization in water and the effect of the hydrophilic–hydrophobic ratio on the solution properties. *Journal of Applied Polymer Science* 131.

Wilhelm M, Zhao CL, Wang Y, et al. (1991) Poly (styrene-ethylene oxide) block copolymer micelle formation in water: a fluorescence probe study. *Macromolecules* 24: 1033-1040.

Williams DF. (2008) On the mechanisms of biocompatibility. *Biomaterials* 29: 2941-2953.

Wolf B. (1985) Solubility of polymers. *Pure and Applied Chemistry* 57: 323-336.

Xia J and Matyjaszewski K. (1997) Controlled/"living" radical polymerization. Atom transfer radical polymerization using multidentate amine ligands. *Macromolecules* 30: 7697-7700.

Xia J, Zhang X and Matyjaszewski K. (1999) Atom transfer radical polymerization of 4-vinylpyridine. *Macromolecules* 32: 3531-3533.

Xiang T, Zhang L-S, Wang R, et al. (2014) Blood compatibility comparison for polysulfone membranes modified by grafting block and random zwitterionic copolymers via surface-initiated ATRP. *Journal of colloid and interface science* 432: 47-56.

Xiao L, Xiong X, Sun X, et al. (2011) Role of cellular uptake in the reversal of multidrug resistance by PEG-b-PLA polymeric micelles. *Biomaterials* 32: 5148-5157.

Xie M, Shi H, Li Z, et al. (2013) A multifunctional mesoporous silica nanocomposite for targeted delivery, controlled release of doxorubicin and bioimaging. *Colloids and Surfaces B: biointerfaces* 110: 138-147.

Xu R, Winnik MA, Hallett FR, et al. (1991) Light-scattering study of the association behavior of styrene-ethylene oxide block copolymers in aqueous solution. *Macromolecules* 24: 87-93.

Xu R, Winnik MA, Riess G, et al. (1992) Micellization of polystyrene-poly (ethylene oxide) block copolymers in water. 5. A test of the star and mean-field models. *Macromolecules* 25: 644-652.

Xu X, Ho W, Zhang X, et al. (2015) Cancer nanomedicine: from targeted delivery to combination therapy. *Trends in molecular medicine* 21: 223-232.

Yameen B, Choi WI, Vilos C, et al. (2014) Insight into nanoparticle cellular uptake and intracellular targeting. *Journal of controlled release* 190: 485-499.

Yang H, Liu C, Yang D, et al. (2009a) Comparative study of cytotoxicity, oxidative stress and genotoxicity induced by four typical nanomaterials: the role of particle size, shape and composition. *Journal of applied Toxicology* 29: 69-78.

Yang L, Wu X, Liu F, et al. (2009b) Novel biodegradable polylactide/poly (ethylene glycol) micelles prepared by direct dissolution method for controlled delivery of anticancer drugs. *Pharmaceutical research* 26: 2332-2342.

Ye SH, Watanabe J, Iwasaki Y, et al. (2005) In situ modification on cellulose acetate hollow fiber membrane modified with phospholipid polymer for biomedical application. *Journal of Membrane Science* 249: 133-141.

Yealland G, Battaglia G, Bandmann O, et al. (2016) Rescue of mitochondrial function in parkin-mutant fibroblasts using drug loaded PMPC-PDPA polymersomes and tubular polymersomes. *Neuroscience letters* 630: 23-29.

Yokoyama M. (2010) Polymeric micelles as a new drug carrier system and their required considerations for clinical trials. *Expert opinion on drug delivery* 7: 145-158.

Yokoyama M. (2011) Clinical applications of polymeric micelle carrier systems in chemotherapy and image diagnosis of solid tumors. *Journal of Experimental & Clinical Medicine* 3: 151-158.

Yokoyama M. (2014) Polymeric micelles as drug carriers: their lights and shadows. *Journal of drug targeting* 22: 576-583.

Yokoyama M, Okano T, Sakurai Y, et al. (1996) Introduction of cisplatin into polymeric micelle. *Journal of controlled release* 39: 351-356.

Yoneyama T, Ito M, Sugihara Ki, et al. (2000) Small Diameter Vascular Prosthesis with a Nonthrombogenic Phospholipid Polymer Surface: Preliminary Study of a New Concept for Functioning in the Absence of Pseudo-or Neointima Formation. *Artificial organs* 24: 23-28.

Yoneyama T, Sugihara K-i, Ishihara K, et al. (2002) The vascular prosthesis without pseudointima prepared by antithrombogenic phospholipid polymer. *Biomaterials* 23: 1455-1459.

Yoo HS and Park TG. (2001) Biodegradable polymeric micelles composed of doxorubicin conjugated PLGA–PEG block copolymer. *Journal of controlled release* 70: 63-70.

Ysambertt F, Vejar F, Paredes J, et al. (1998) The absorbance deviation method: a spectrophotometric estimation of the critical micelle concentration (CMC) of ethoxylated alkylphenol surfactants. *Colloids and surfaces A: physicochemical and engineering aspects* 137: 189-196.

Yu H, Gan L, Hu X, et al. (2007) A pH-sensitive double [60] fullerene-end-capped polymers via ATRP: Synthesis and aggregation behavior. *Polymer* 48: 2312-2321.

Yu H, Zou Y, Jiang L, et al. (2013) Induction of apoptosis in non-small cell lung cancer by downregulation of MDM2 using pH-responsive PMPC-b-PDPA/siRNA complex nanoparticles. *Biomaterials* 34: 2738-2747.

Yuan H and Zhang S. (2010) Effects of particle size and ligand density on the kinetics of receptor-mediated endocytosis of nanoparticles. *Applied Physics Letters* 96: 033704.

Yuan J-J, Schmid A, Armes SP, et al. (2006) Facile synthesis of highly biocompatible poly (2-(methacryloyloxy) ethyl phosphorylcholine)-coated gold nanoparticles in aqueous solution. *Langmuir* 22: 11022-11027.

Yuan Y-Y, Du J-Z, Song W-J, et al. (2012) Biocompatible and functionalizable polyphosphate nanogel with a branched structure. *Journal of Materials Chemistry* 22: 9322-9329.

Zbinden G and Flury-Roversi M. (1981) Significance of the LD50-test for the toxicological evaluation of chemical substances. *Archives of toxicology* 47: 77-99.

Zeng X, Tao W, Wang Z, et al. (2015) Docetaxel-Loaded Nanoparticles of Dendritic Amphiphilic Block Copolymer H40-PLA-b-TPGS for Cancer Treatment. *Particle & Particle Systems Characterization* 32: 112-122.

Zhang D, Zhang H, Nie J, et al. (2010a) Synthesis and self-assembly behavior of pH-responsive amphiphilic copolymers containing ketal functional groups. *Polymer International* 59: 967-974.

Zhang H, Zhao L, Chu L, et al. (2014) Preparation, optimization, characterization and cytotoxicity in vitro of Baicalin-loaded mixed micelles. *Journal of colloid and interface science* 434: 40-47.

Zhang L and Eisenberg A. (1996) Multiple morphologies and characteristics of "crew-cut" micelle-like aggregates of polystyrene-b-poly (acrylic acid) diblock copolymers in aqueous solutions. *Journal of the American Chemical Society* 118: 3168-3181.

Zhang L, Hu Y, Jiang X, et al. (2004) Camptothecin derivative-loaded poly (caprolactone-co-lactide)-b-PEG-b-poly (caprolactone-co-lactide) nanoparticles and their biodistribution in mice. *Journal of controlled release* 96: 135-148.

Zhang L, Yu K and Eisenberg A. (1996) Ion-induced Morphological Changes in" Crew-Cut" Aggregates of Amphiphilic Block. *Science* 272: 1777.

Zhang S, Li J, Lykotrafitis G, et al. (2009) Size-dependent endocytosis of nanoparticles. *Advanced Materials* 21: 419-424.

Zhang Y, Tang L, Sun L, et al. (2010b) A novel paclitaxel-loaded poly(ε-caprolactone)/Poloxamer 188 blend nanoparticle overcoming multidrug resistance for cancer treatment. *Acta biomaterialia* 6: 2045-2052.

Zhao B, Wang X-Q, Wang X-Y, et al. (2013) Nanotoxicity comparison of four amphiphilic polymeric micelles with similar hydrophilic or hydrophobic structure. *Part. Fibre Toxicol* 10: 47.

Zhao J, Chai Y-D, Zhang J, et al. (2015) Long circulating micelles of an amphiphilic random copolymer bearing cell outer membrane phosphorylcholine zwitterions. *Acta biomaterialia* 16: 94-102.

Zhao M, Su M, Lin X, et al. (2010) Evaluation of docetaxel-loaded intravenous lipid emulsion: pharmacokinetics, tissue distribution, antitumor activity, safety and toxicity. *Pharmaceutical research* 27: 1687-1702.

Zhao X, Poon Z, Engler AC, et al. (2012) Enhanced stability of polymeric micelles based on postfunctionalized poly (ethylene glycol)-b-poly (γ-propargyl L-glutamate): the substituent effect. *Biomacromolecules* 13: 1315-1322.

Zhiping P, Xinxing L and Zhen T. (2009) EFFECT OF HYDROPHOBIC BLOCKS ON THE AGGREGATE BEHAVIOR OF AMPHIPHILIC TRIBLOCK COPOLYMERS IN AQUEOUS SOLUTION. *Acta Polymerica Sinica*: 936-941.

Zhou L, Tan G-X and Ning C-Y. (2014) Modification of biomaterials surface by mimetic cell membrane to improve biocompatibility. *Frontiers of Materials Science* 8: 325-331.

Zwaal RF and Schroit AJ. (1997) Pathophysiologic implications of membrane phospholipid asymmetry in blood cells. *Blood* 89: 1121-1132.

## APPENDIX (A)

**A 1.0.** Standard calibration curve of DTX. The UV-vis absorbance of DTX in (A) MeOH and (B) EtOH measured at wavelength of 230 nm (Mean ± SD, n=3)

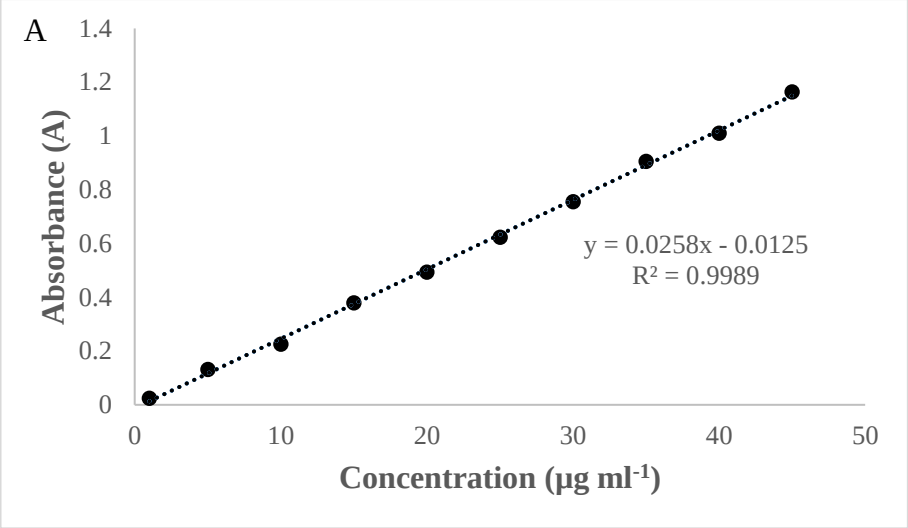


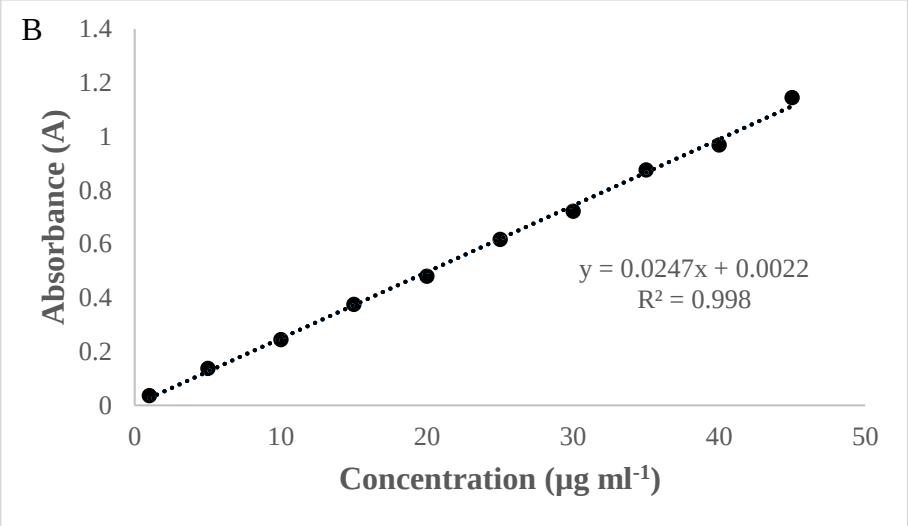

**A2.0** The effect of decreasing solution concentration on nanoparticle diameter of (A) 1:1 and (B) 1:2 ratio MPC-DPA polymeric nano-systems measured with DLS (25°C) formed via nanoprecipitation from methanol in PBS, pH 7.4 (Mean ± SD, n=3)

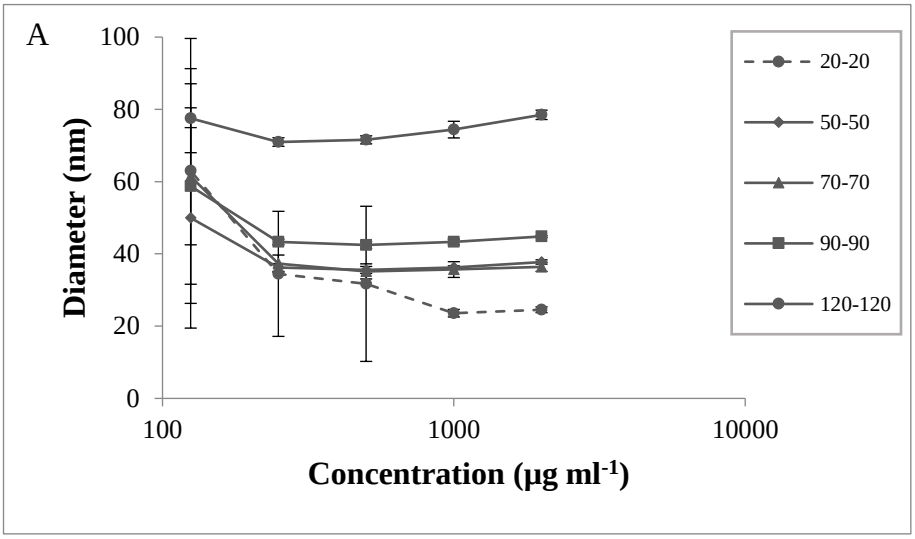


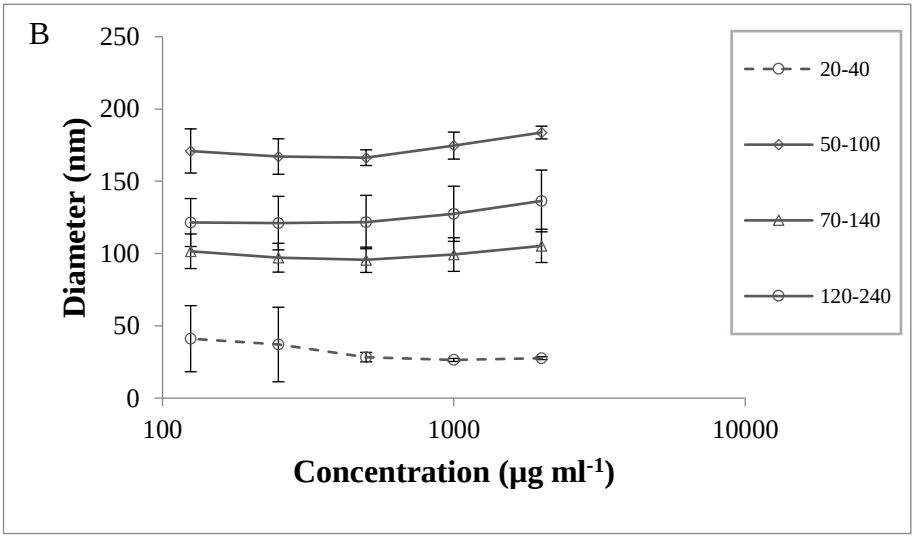

**A3.0** The effect of decreasing solution concentration on nanoparticle polydispersity of (A) 1:1 and (B)1:2 ratio MPC-DPA polymeric nano-systems measured with DLS (25°C) formed via nanoprecipitation from methanol in PBS, pH 7.4 (Mean ± SD, n=3)

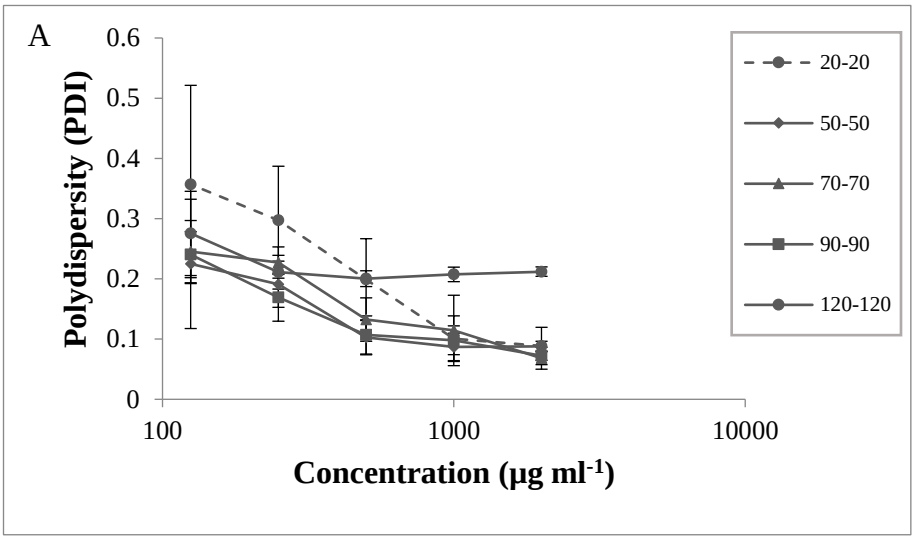


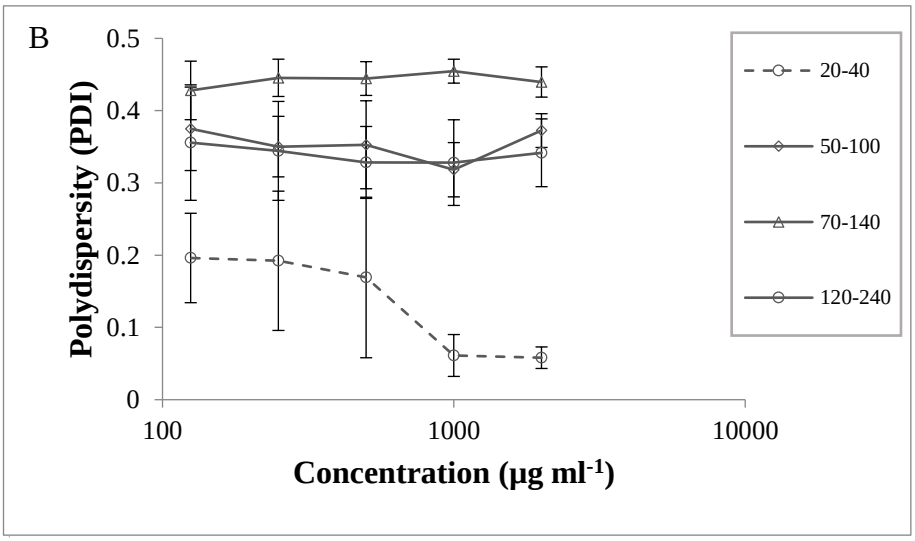

**A4.0.** The effect of decreasing solution concentration on signal intensity (KCps) of (A) 1:1 and (B) 1:2 ratio MPC-DPA polymeric nano-systems measured with DLS (25°C) formed via nanoprecipitation from methanol in PBS, pH 7.4 (Mean ± SD, n=3). The KCps was reduced by half at each dilution

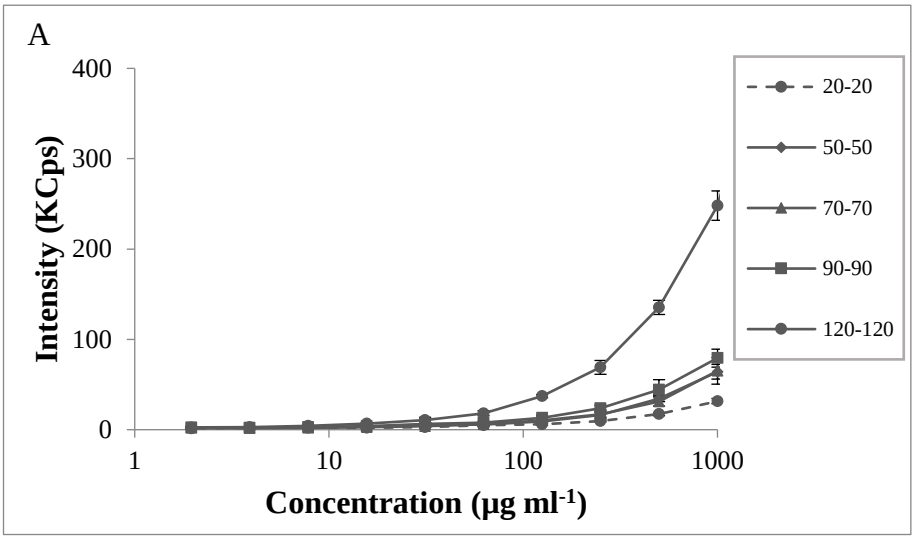


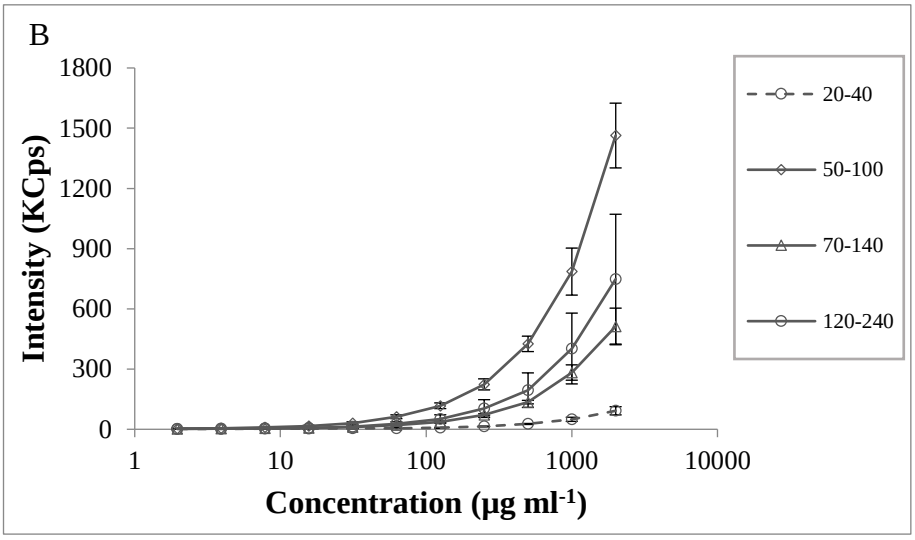

**A5.0.** Effect of varying temperature (5-70°C) on particle polydispersity of (A) 1:1 and (B) 1:2 ratio MPC-DPA polymeric nano-systems formed via nanoprecipitation from methanol in PBS, pH 7.4 measured with DLS (Mean ± SD, n=3)

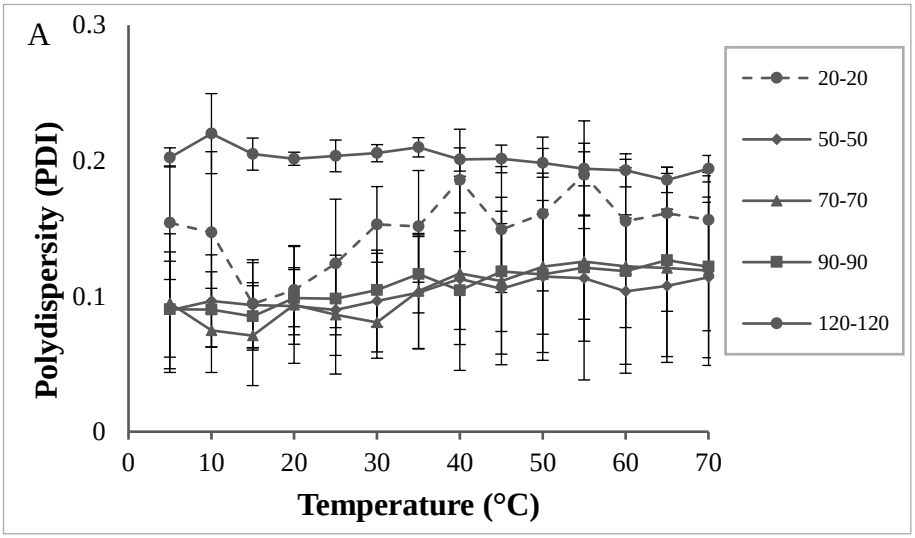


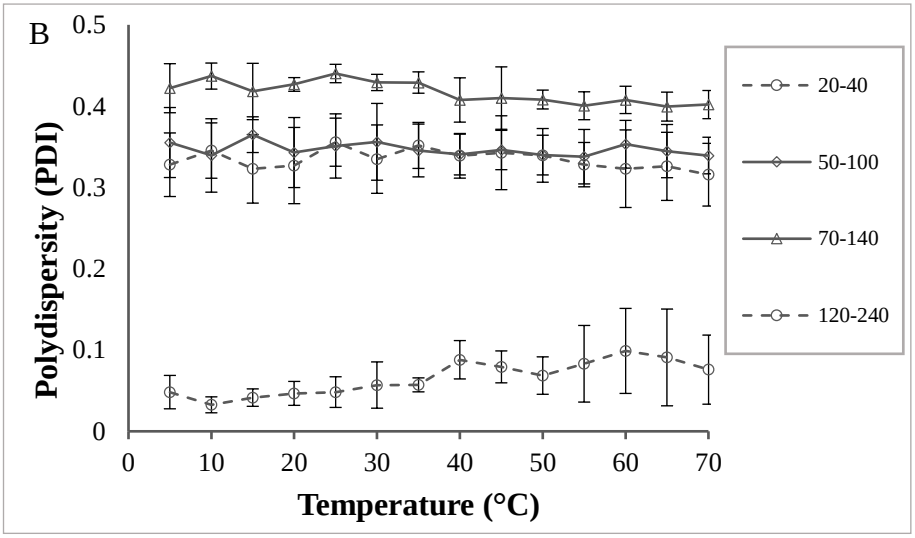

**A6.0.** Effect of varying temperature (5-70°C) on signal intensity (KCps) of (A) 1:1 and (B) 1:2 ratio MPC-DPA polymeric nano-systems formed via nanoprecipitation from methanol in PBS, pH 7.4 measured with DLS (Mean ± SD, n=3)

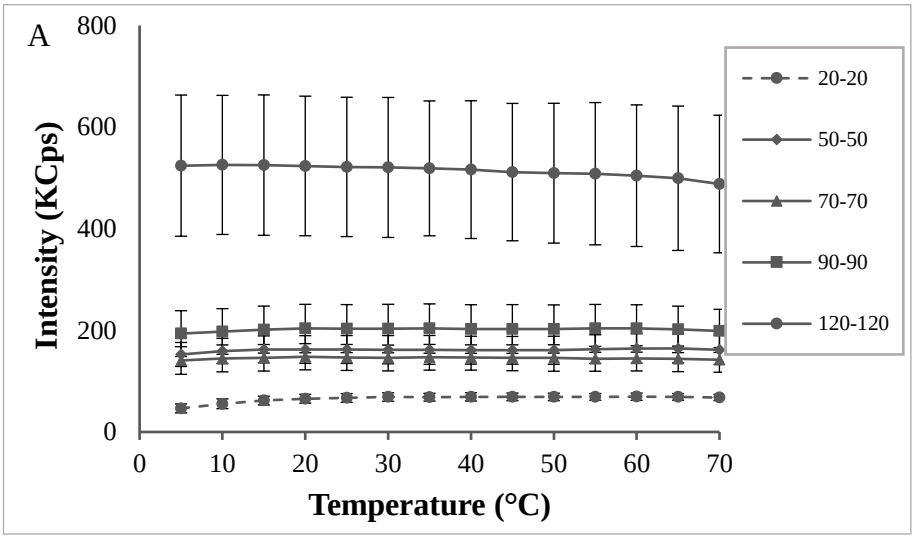


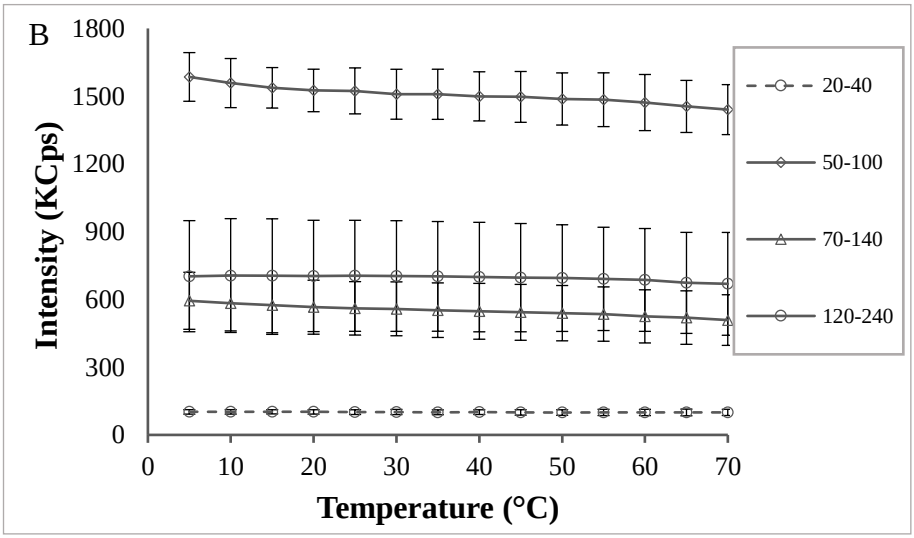

**A7.0.** Particle diameter (nm) at 30- 40 ºC for (A) 1:1 and (B) 1:2 ratio MPC-DPA polymeric nano-systems in pH 7.4, (Mean ± SD, n=3)

| (A) Temperature | MPC-DPA block ratio | | | | |
|---|---|---|---|---|---|
| | **20-20** | **50-50** | **70-70** | **90-90** | **120-120** |
| 30 | 24 ± 0.7 | 36 ± 1.2 | 36 ± 0.5 | 42 ± 0.3 | 72 ± 2 |
| 31 | 24 ± 0.6 | 36 ± 1.1 | 36 ± 0.6 | 42 ± 0.3 | 72± 2 |
| 32 | 24 ± 0.7 | 36 ± 1.2 | 36 ± 0.6 | 42 ± 0.3 | 72 ± 2 |
| 33 | 24 ± 0.7 | 36 ± 1.1 | 36 ± 0.6 | 42 ± 0.2 | 72 ± 2 |
| 34 | 24 ± 0.7 | 36 ± 1 | 36 ± 0.6 | 42 ± 0.3 | 72 ± 2 |
| 35 | 24 ± 0.6 | 36 ± 1.1 | 36 ± 0.5 | 42 ± 0.3 | 72 ± 2 |
| 36 | 24 ± 0.8 | 36 ± 1 | 36 ± 0.5 | 42 ± 0.4 | 72 ± 2 |
| 37 | 25 ± 2.2 | 36 ± 1.2 | 36 ± 0.5 | 42 ± 0.3 | 72 ± 2 |
| 38 | 24 ± 0.8 | 36 ± 1.2 | 36 ± 0.4 | 42 ± 0.3 | 72 ± 2 |
| 39 | 24 ± 0.8 | 36 ± 1 | 36 ± 0.5 | 42 ± 0.3 | 72 ± 2 |
| 40 | 26 ± 5 | 36 ± 1.2 | 36 ± 0.5 | 42 ± 0.4 | 72 ± 2 |

| (B) Temperature | MPC-DPA block ratio | | | |
|---|---|---|---|---|
| | **20-40** | **50-100** | **70-140** | **120-240** |
| 30 | 27 ± 0.3 | 168 ± 4.4 | 96 ± 10 | 126 ± 21 |
| 31 | 27 ± 0.4 | 169 ± 4.4 | 96 ± 10 | 127 ± 23 |
| 32 | 27 ± 0.3 | 169 ± 4 | 96 ± 10 | 127 ± 22 |
| 33 | 27 ± 0.3 | 169 ± 5 | 95 ± 10 | 127 ± 22 |
| 34 | 27 ± 0.3 | 169 ± 4 | 95 ± 10 | 127 ± 21 |
| 35 | 27 ± 0.2 | 168 ± 5 | 96 ± 10 | 127 ± 22 |
| 36 | 27 ± 0.3 | 169 ± 6 | 96 ± 10 | 127 ± 22 |
| 37 | 27 ± 0.2 | 169 ± 3.1 | 96 ± 10 | 127 ± 22 |
| 38 | 27 ± 0.4 | 168 ± 3.3 | 96 ± 10 | 127 ± 22 |
| 39 | 27 ± 0.3 | 170 ± 4.4 | 96 ± 10 | 128± 23 |
| 40 | 27 ± 0.3 | 168 ± 4 | 96 ± 10 | 127 ± 22 |

**A8.0.** Time effect on particle polydispersity of (A) 1:1 and (B) 1:2 ratio MPC-DPA self-assembled polymeric nano-systems formed via nanoprecipitation from methanol in PBS, pH 7.4, stored at room temperature (Mean ± SD, n=3)

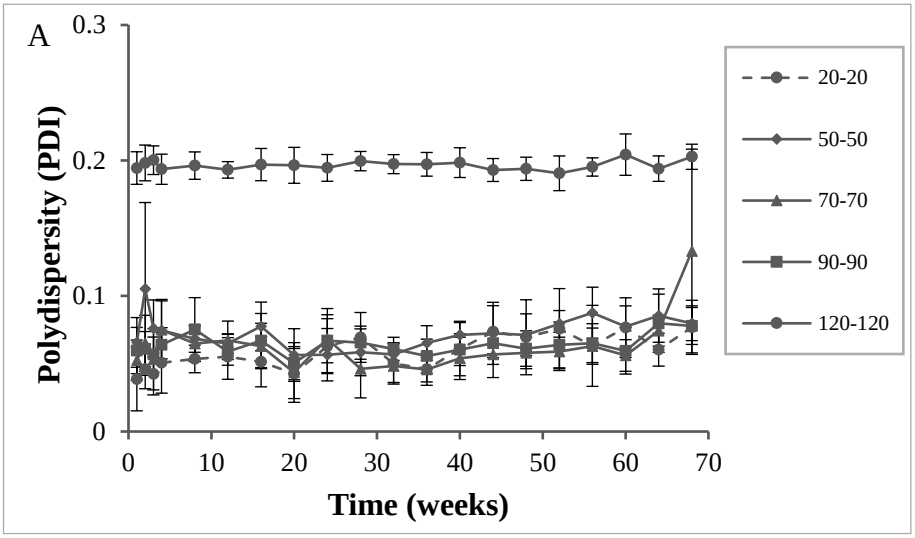


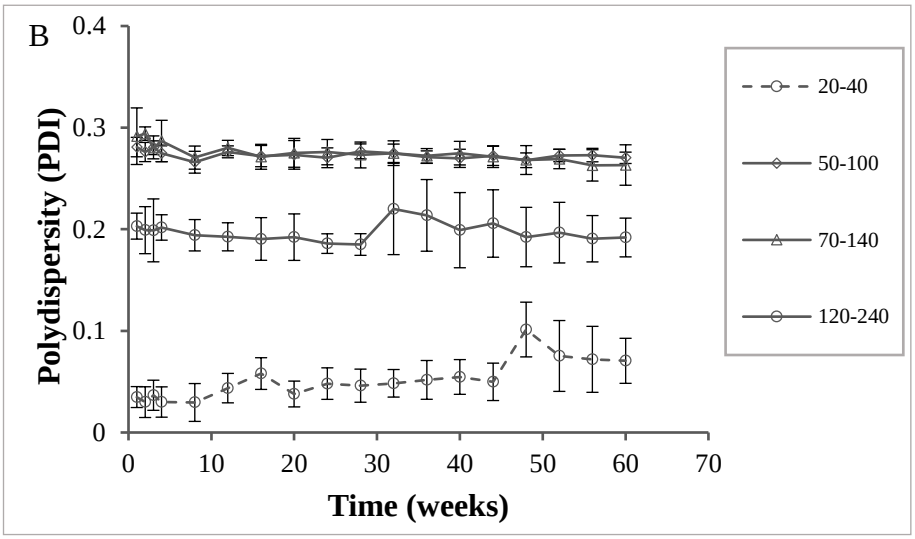

**A9.0.** Time effect on signal intensity (KCps) of (A) 1:1 and (B) 1:2 ratio MPC-DPA self-assembled polymeric nano-systems formed via nanoprecipitation from methanol in PBS, pH 7.4, stored at room temperature (Mean ± SD, n=3)

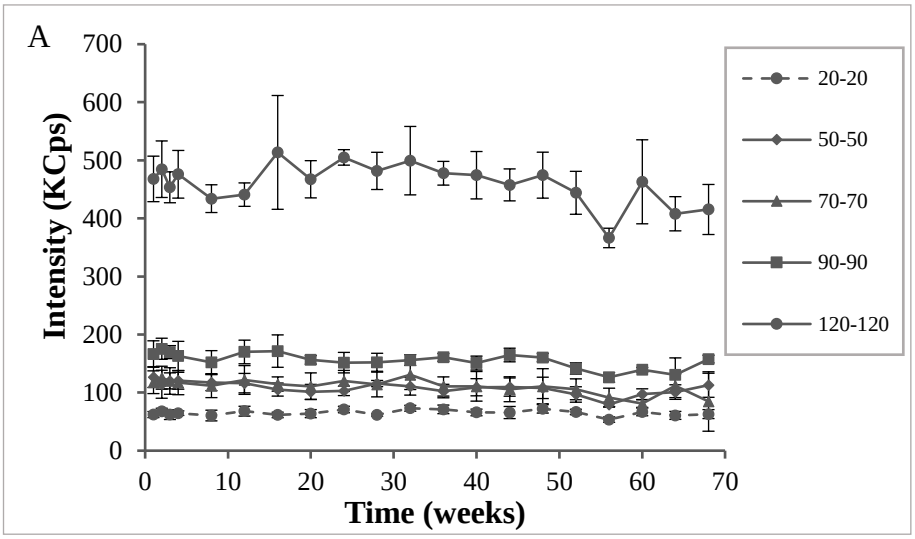


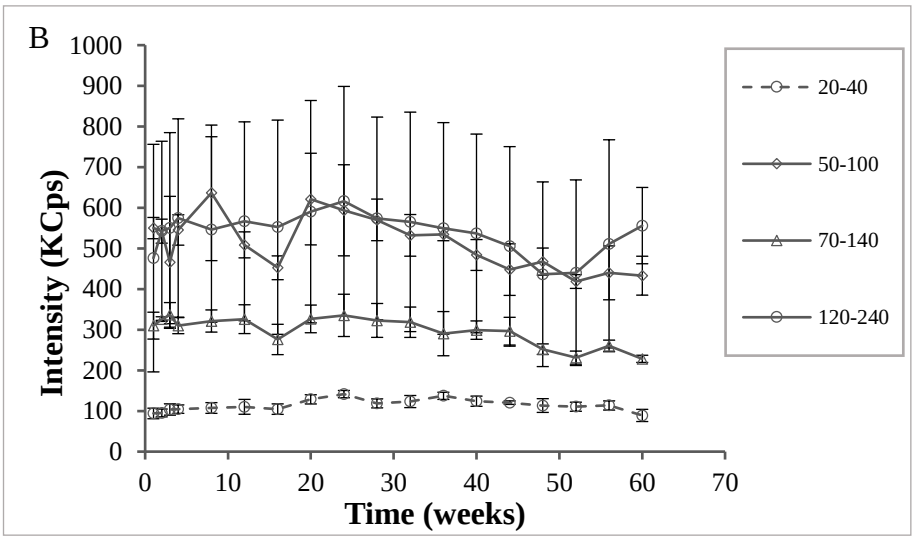

**A10.0.** Time effect on particle polydispersity of (A) 1:1 and (B) 1:2 ratio MPC-DPA self-assembled nanoparticles formed via nanoprecipitation from methanol in PBS, pH 7.4, stored at 4°C (Mean ± SD, n=3)

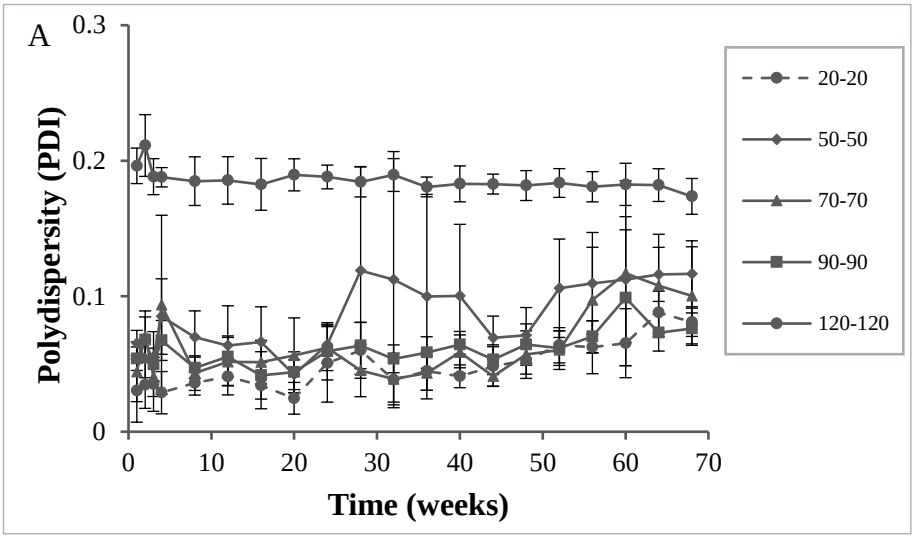


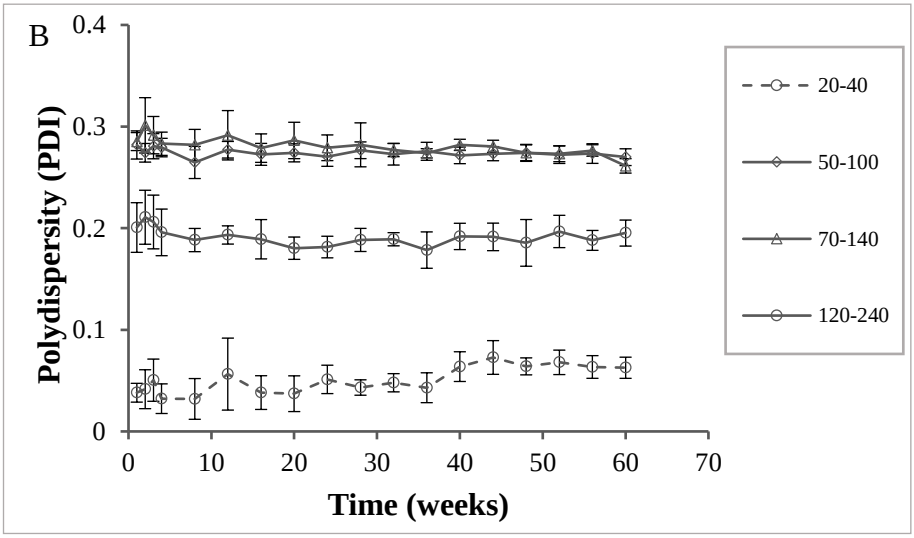

**A11.0** Time effect on signal intensity (KCps) of (A) 1:1 and (B) 1:2 ratio MPC-DPA self-assembled nanoparticles formed via nanoprecipitation from methanol in PBS, pH 7.4, stored at 4°C (Mean ± SD, n=3)

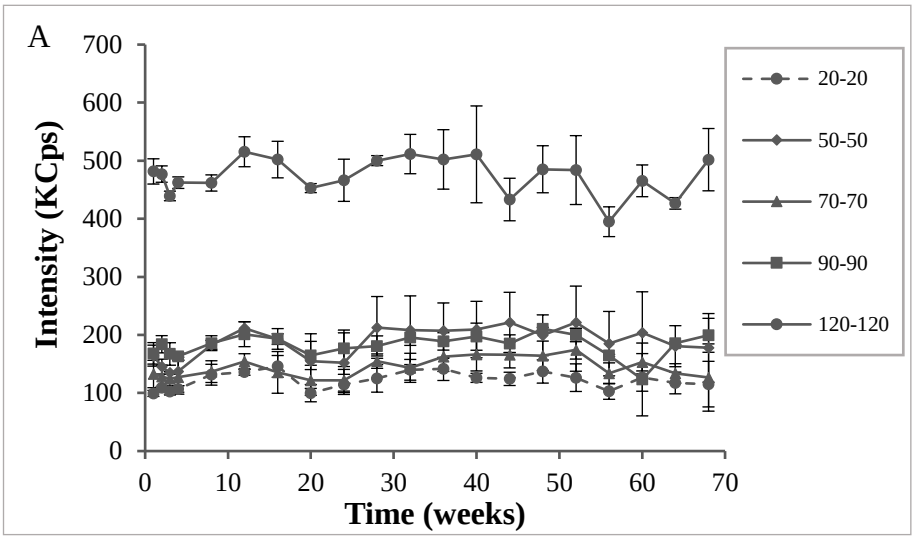


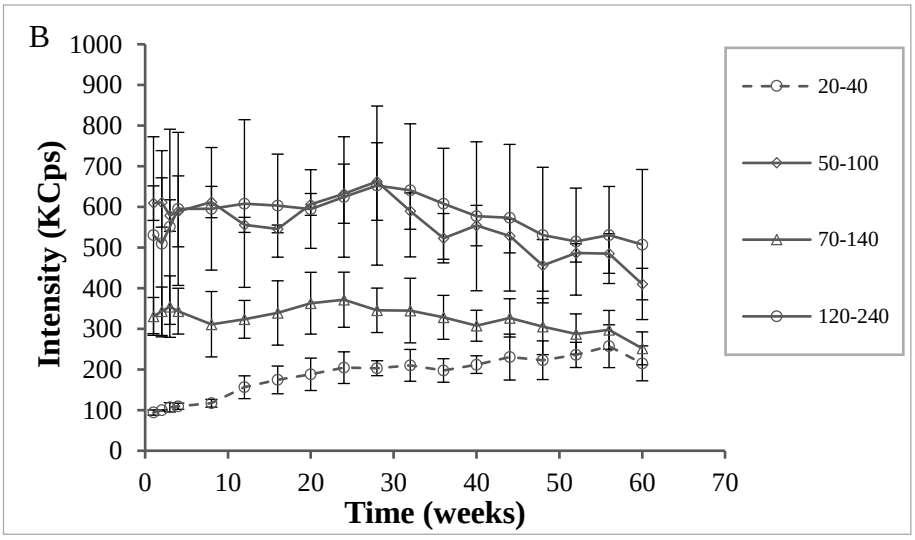

**A12.0** STEM images

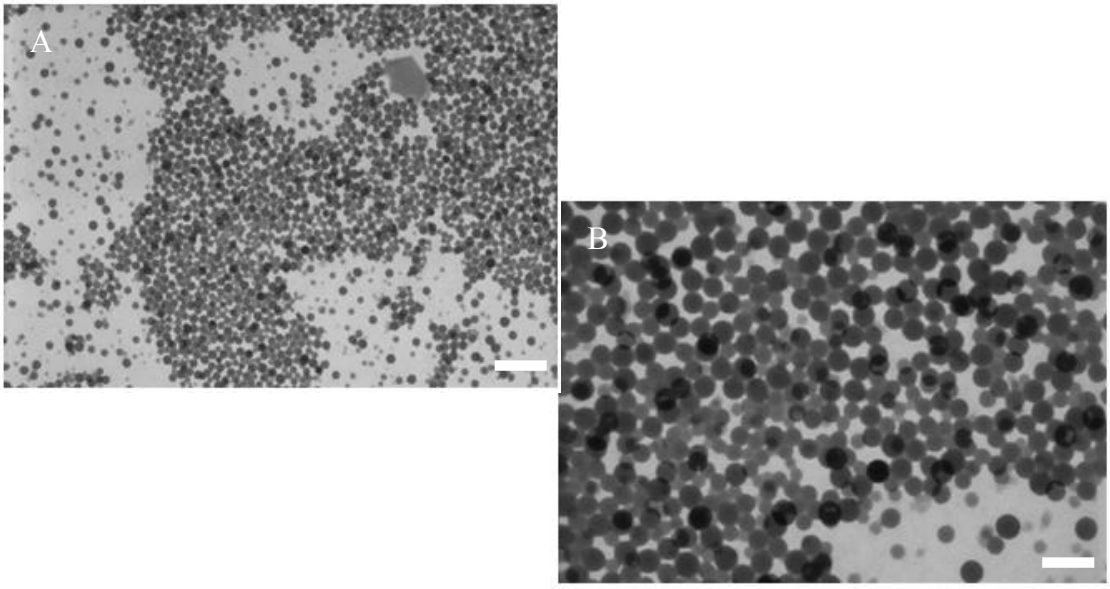


**12.1** STEM images of 50 nm polystyrene standard beads. Scale bars = 200 nm and 20 nm for wide and zoomed areas, respectively

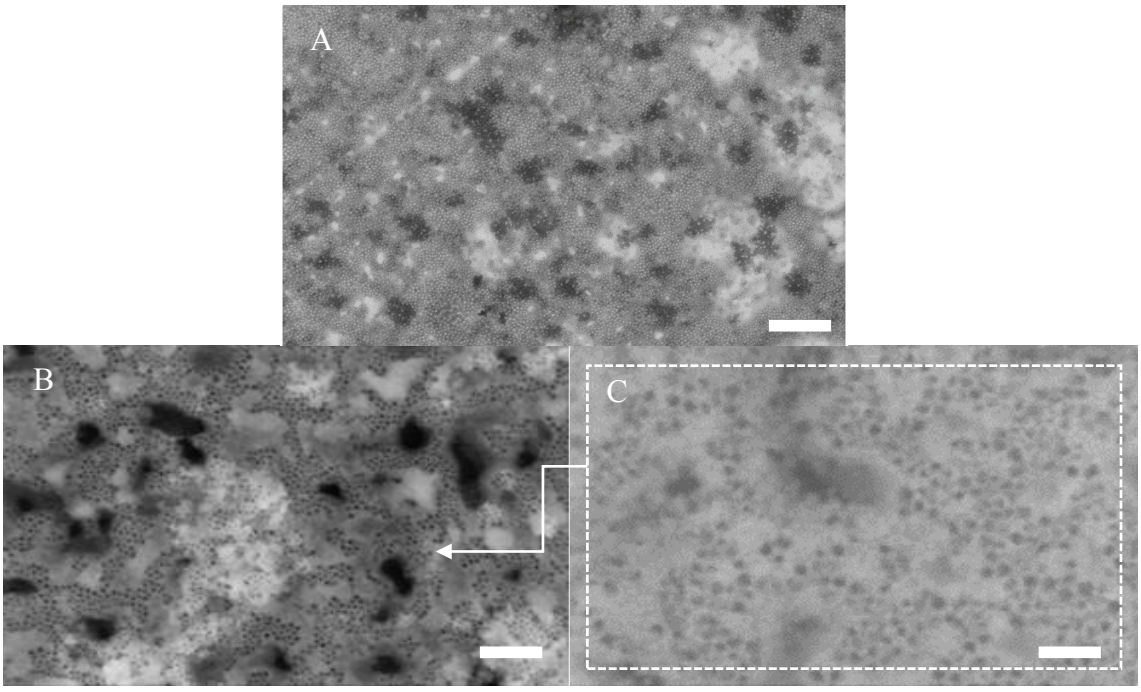


**12.2** STEM images of $MPC_{20}$-$DPA_{20}$ nanoparticles displaying wide and zoomed areas of copolymer nanoparticles. Scale bars = 100 nm, 200 nm and 20 nm for wide and zoomed areas, respectively

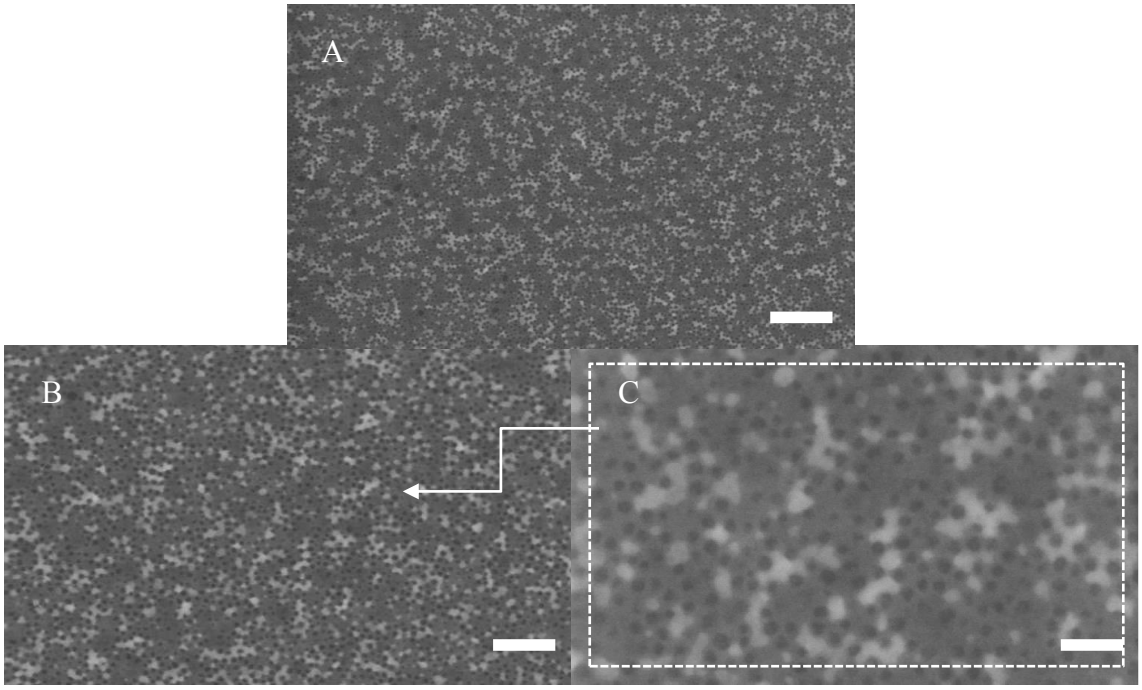


**12.3** STEM images of $MPC_{70}$-$DPA_{70}$ nanoparticles displaying wide and zoomed areas of copolymer nanoparticles. Scale bars = 100 nm, 200 nm and 20 nm for wide and zoomed areas, respectively

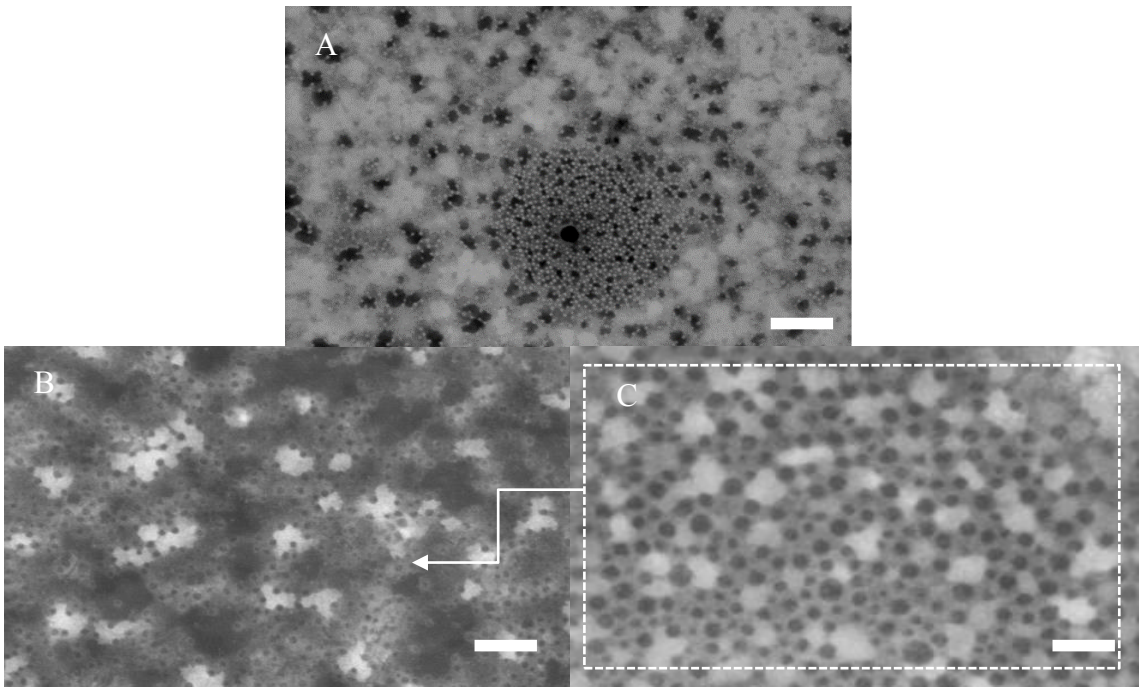


**12.4** STEM images of $MPC_{90}$-$DPA_{90}$ nanoparticles displaying wide and zoomed areas of copolymer nanoparticles. Scale bars 100 nm, 200 nm and 20 nm for wide and zoomed areas, respectively

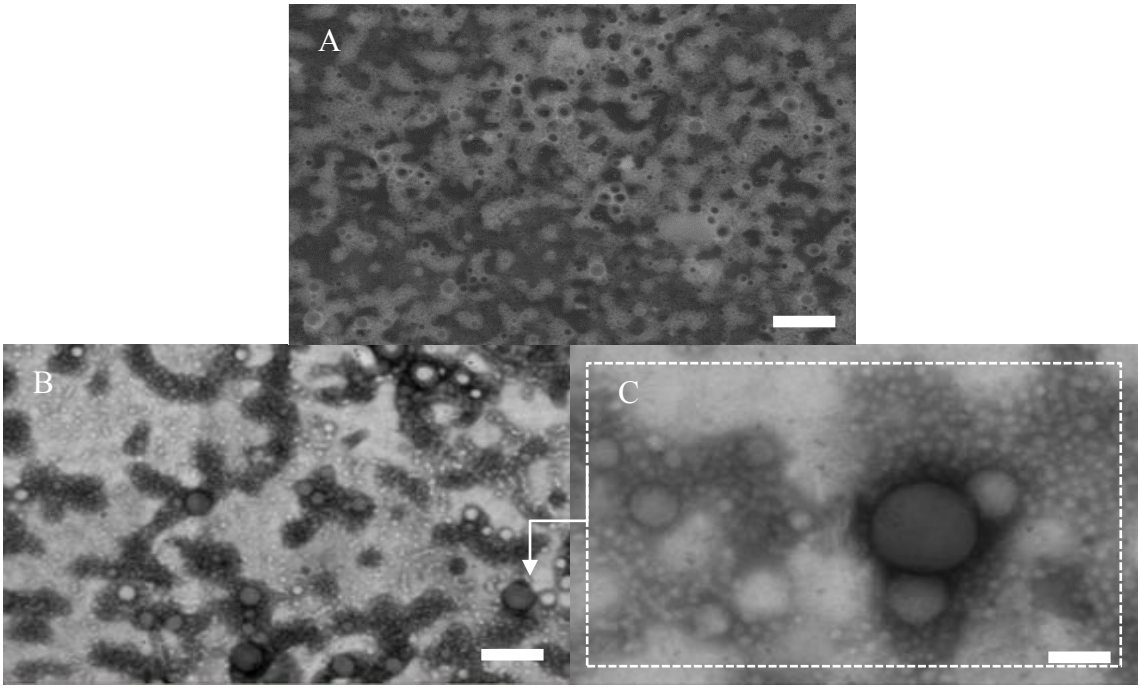


**12.5** STEM images of $MPC_{120}$-$DPA_{120}$ nanoparticles displaying wide and zoomed areas of copolymer nanoparticles. Scale bars = 100 nm, 200 nm and 20 nm for wide and zoomed areas, respectively

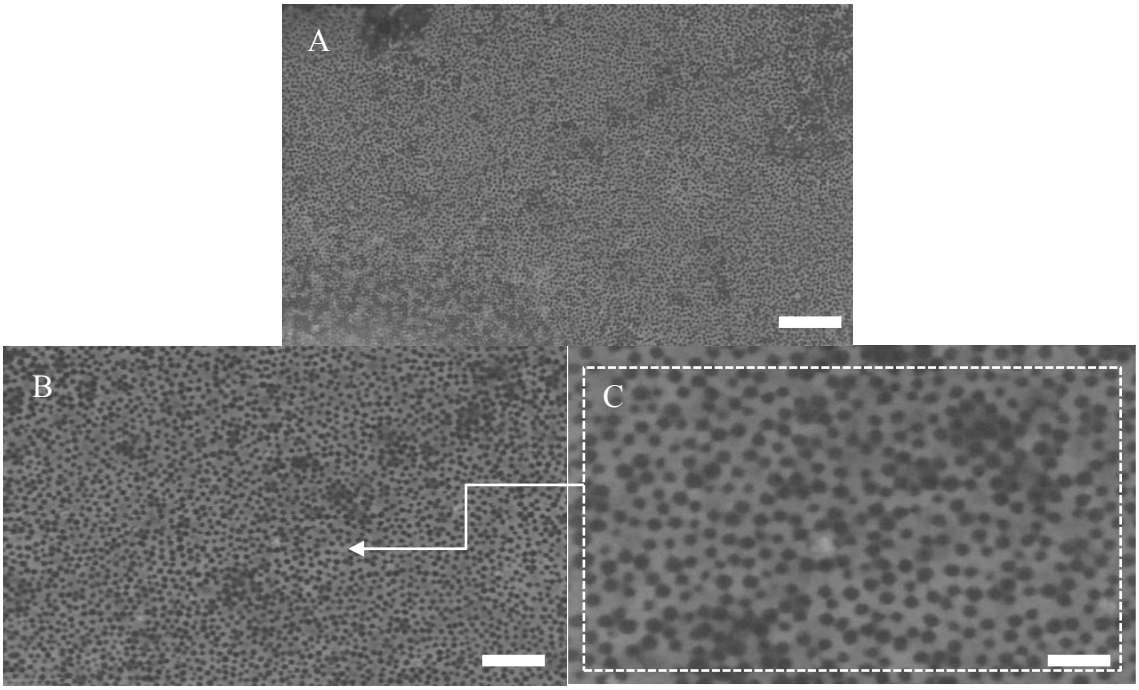


**12.6** STEM images of $MPC_{20}$-$DPA_{40}$ nanoparticles displaying wide and zoomed areas of copolymer nanoparticles. Scale bars = 100 nm, 200 nm and 20 nm for wide and zoomed areas, respectively

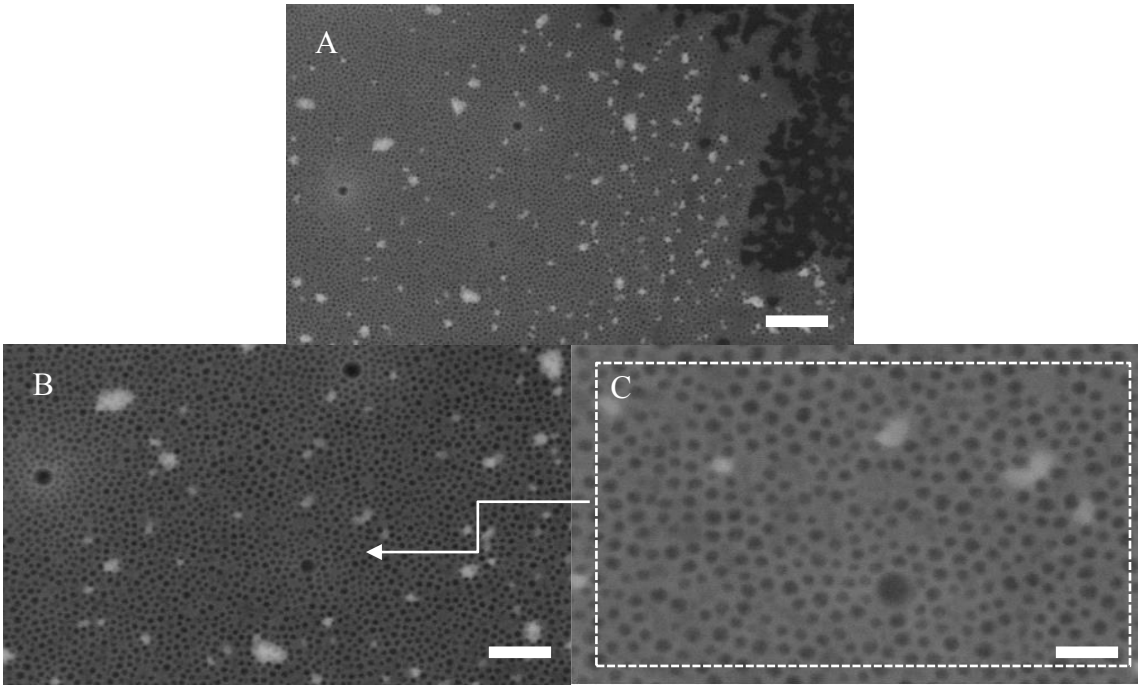


**12.7** STEM images of $MPC_{70}$-$DPA_{140}$ nanoparticles displaying wide and zoomed areas of copolymer nanoparticles. Scale bars = 100 nm, 200 nm and 20 nm for wide and zoomed areas, respectively

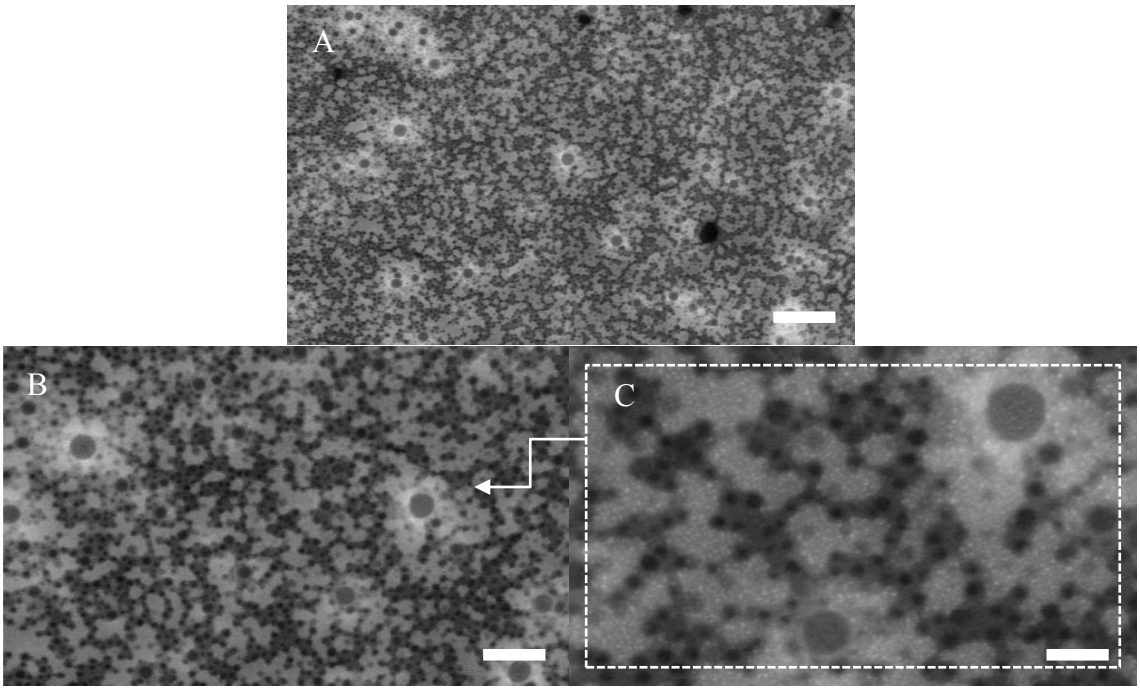


**12.8** STEM images of $MPC_{120}$-$DPA_{240}$ nanoparticles displaying wide and zoomed areas of copolymer nanoparticles. Scale bars = 100 nm, 200 nm and 20 nm for wide and zoomed areas, respectively

## A13.0 Confocal laser scanning microscopy (CLSM) images and flow cytometry histogram profile

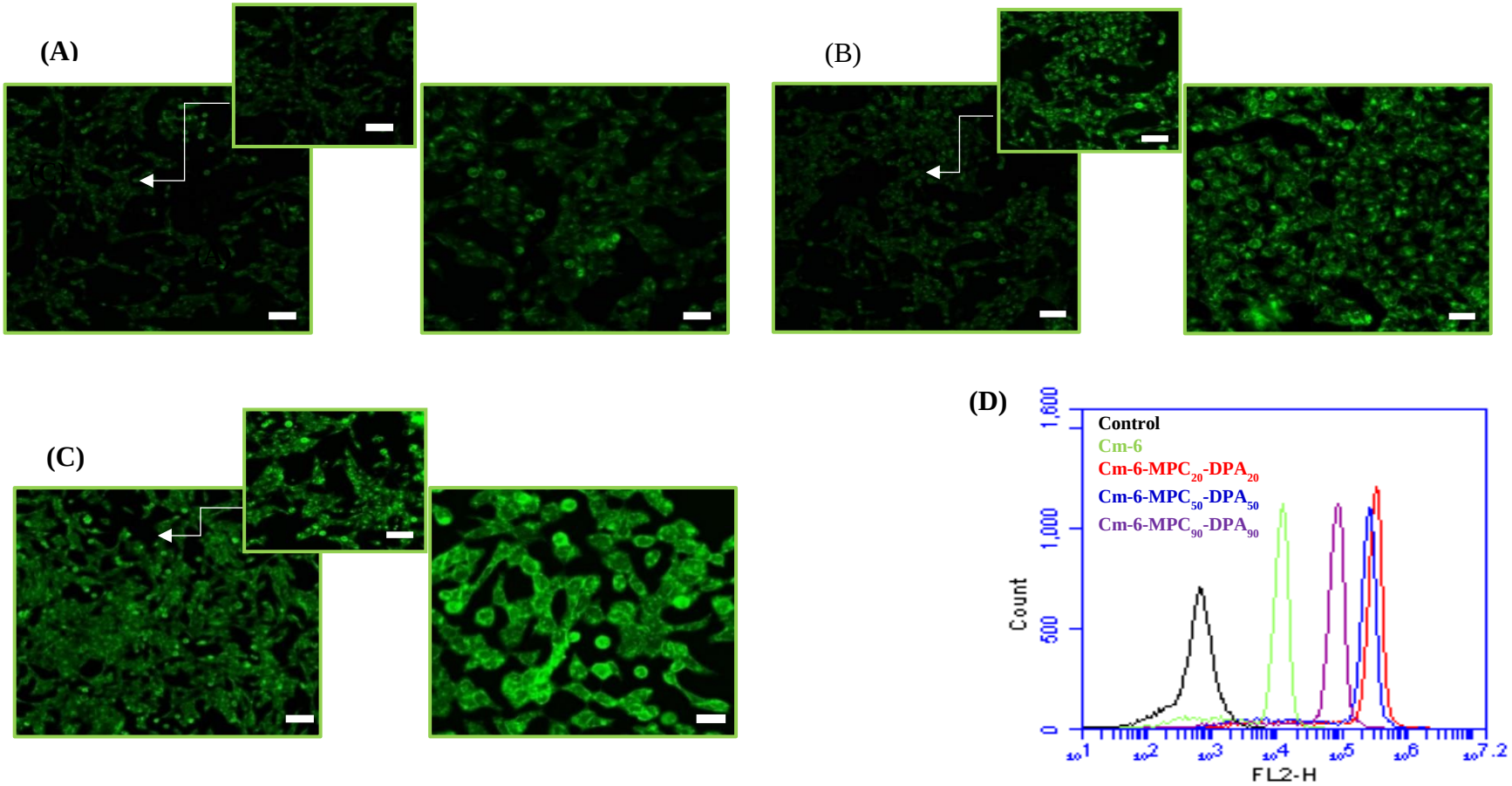


**A 13.1** V79 cells after 5 minutes incubation with Cm-6-loaded MPC-DPA micelles. (A) Cm-6-MPC$_{20}$-DPA$_{20}$, (B) Cm-6-MPC$_{50}$-DPA$_{50}$, (C) Cm-6-MPC$_{90}$-DPA$_{90}$, (D) Flow cytometric profiles. Scale bars = 100, 50, and 25 µm (Original in colour)

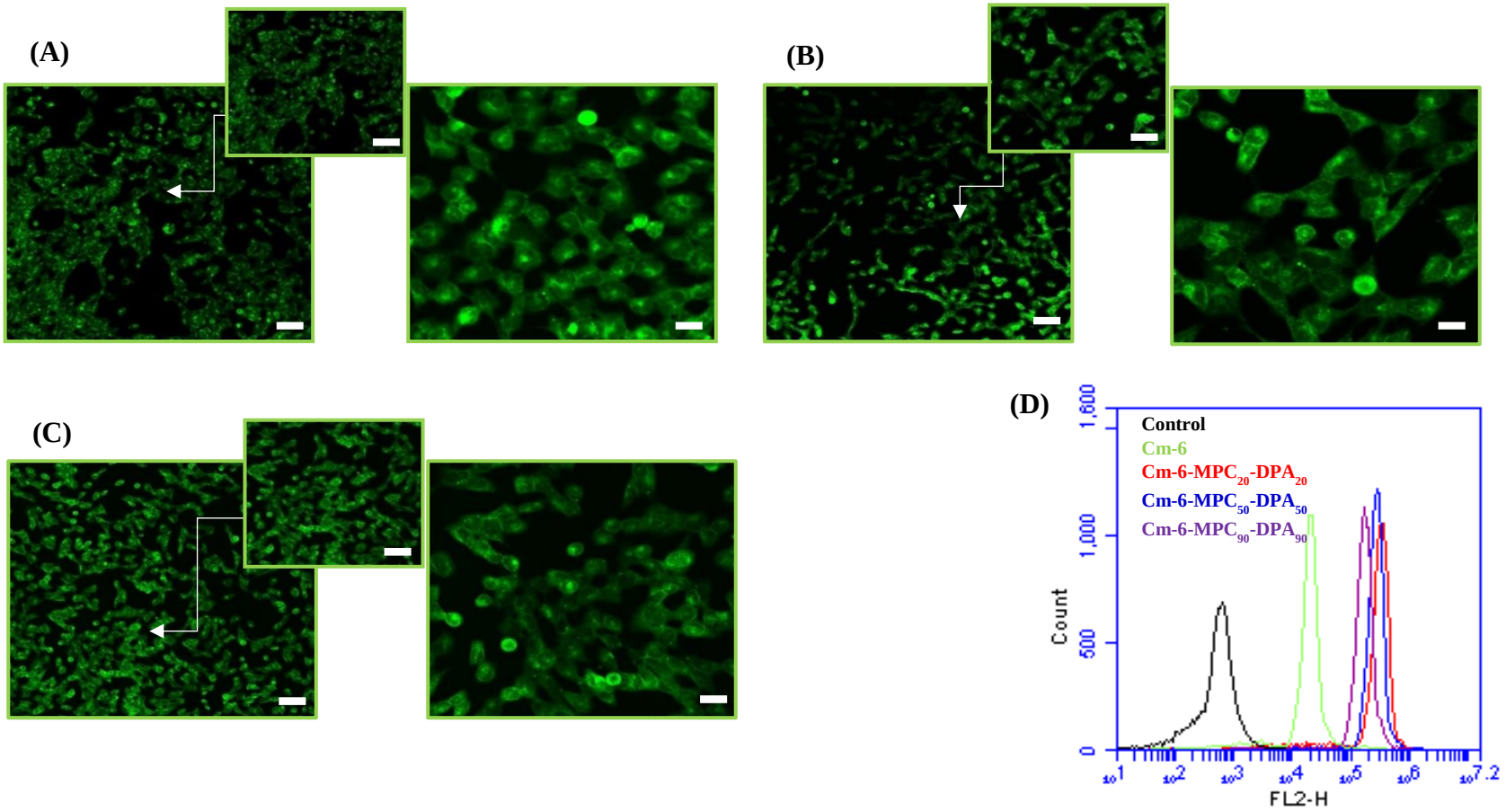


**A13.2** V79 cells after 10 minutes incubation with Cm-6-loaded MPC-DPA micelles. (A) Cm-6-MPC$_{20}$-DPA$_{20}$, (B) Cm-6-MPC$_{50}$-DPA$_{50}$, (C) Cm-6-MPC$_{90}$-DPA$_{90}$, (D) Flow cytometric profiles. Scale bars = 100, 50, and 25 µm (Original in colour)

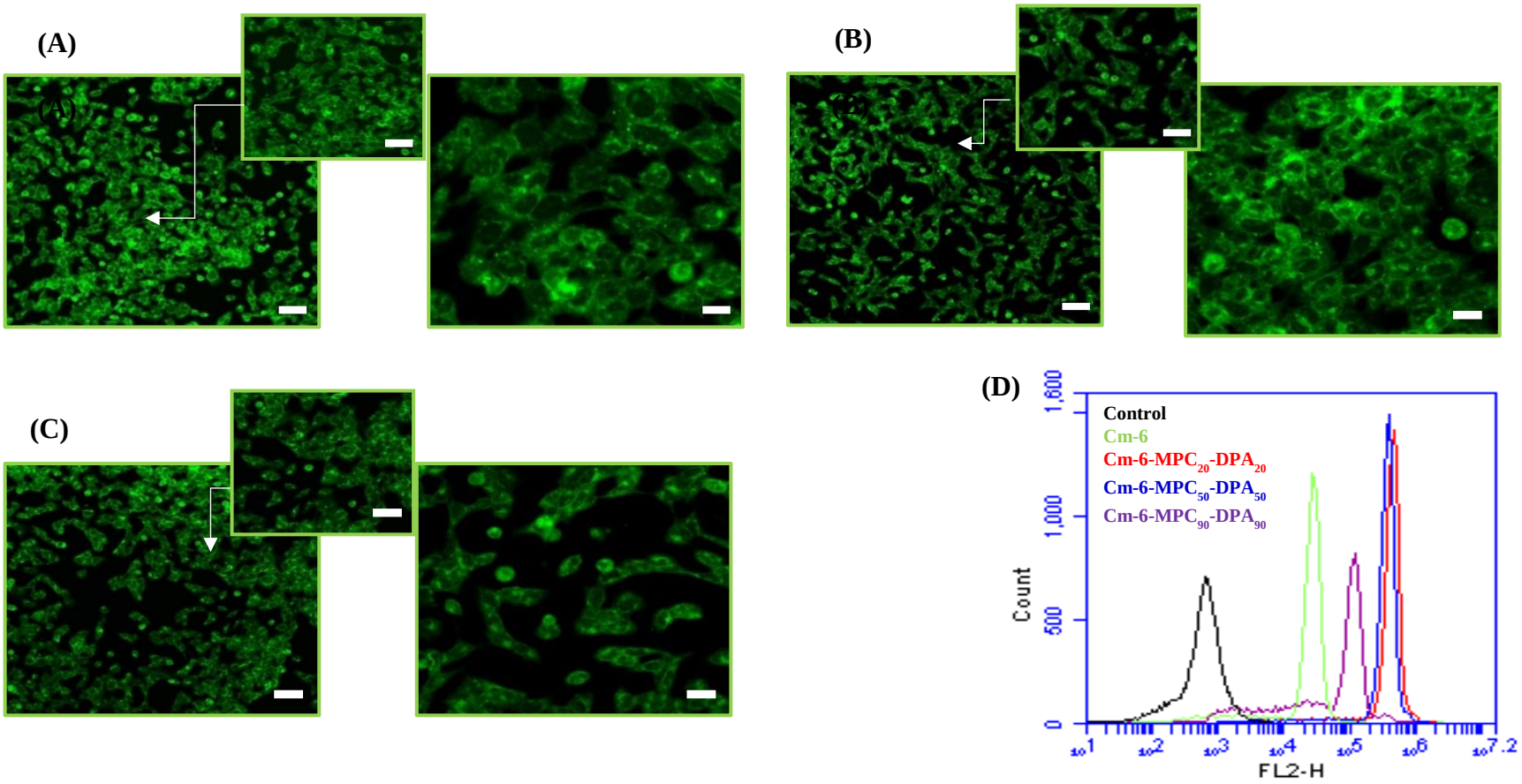


**A13.3** V79 cells after 30 minutes incubation with Cm-6-loaded MPC-DPA micelles. (A) Cm-6-$MPC_{20}$-$DPA_{20}$, (B) Cm-6-$MPC_{50}$-$DPA_{50}$, (C) Cm-6-$MPC_{90}$-$DPA_{90}$, (D) Flow cytometric profiles. Scale bars = 100, 50, and 25 µm (Original in colour)

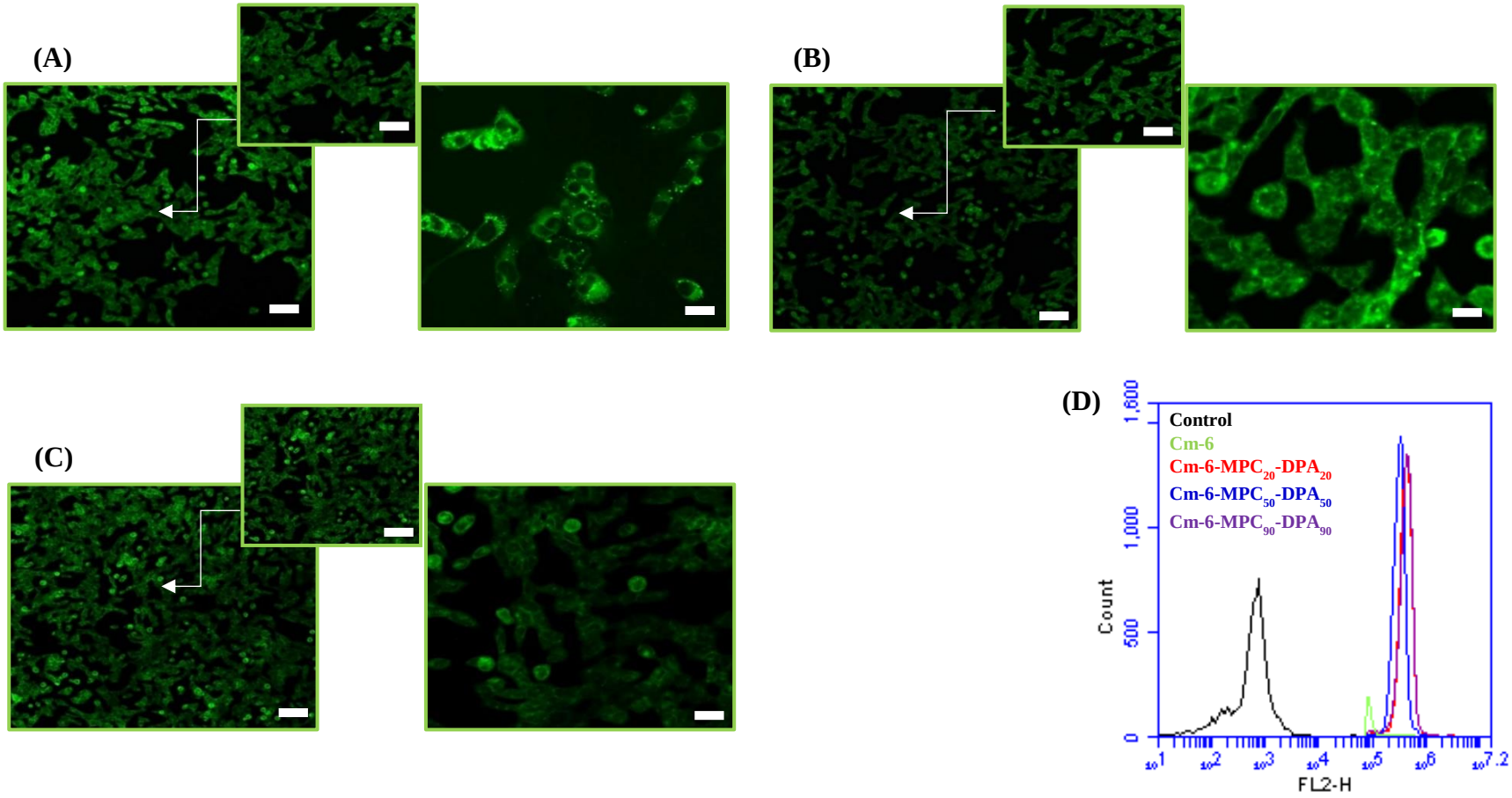


**A13.4** V79 cells after 1 hour incubation with Cm-6-loaded MPC-DPA micelles. (A) Cm-6-$MPC_{20}$-$DPA_{20}$, (B) Cm-6-$MPC_{50}$-$DPA_{50}$, (C) Cm-6-$MPC_{90}$-$DPA_{90}$, (D) Flow cytometric profiles. Scale bars = 100, 50, and 25 µm. (Original in colour)

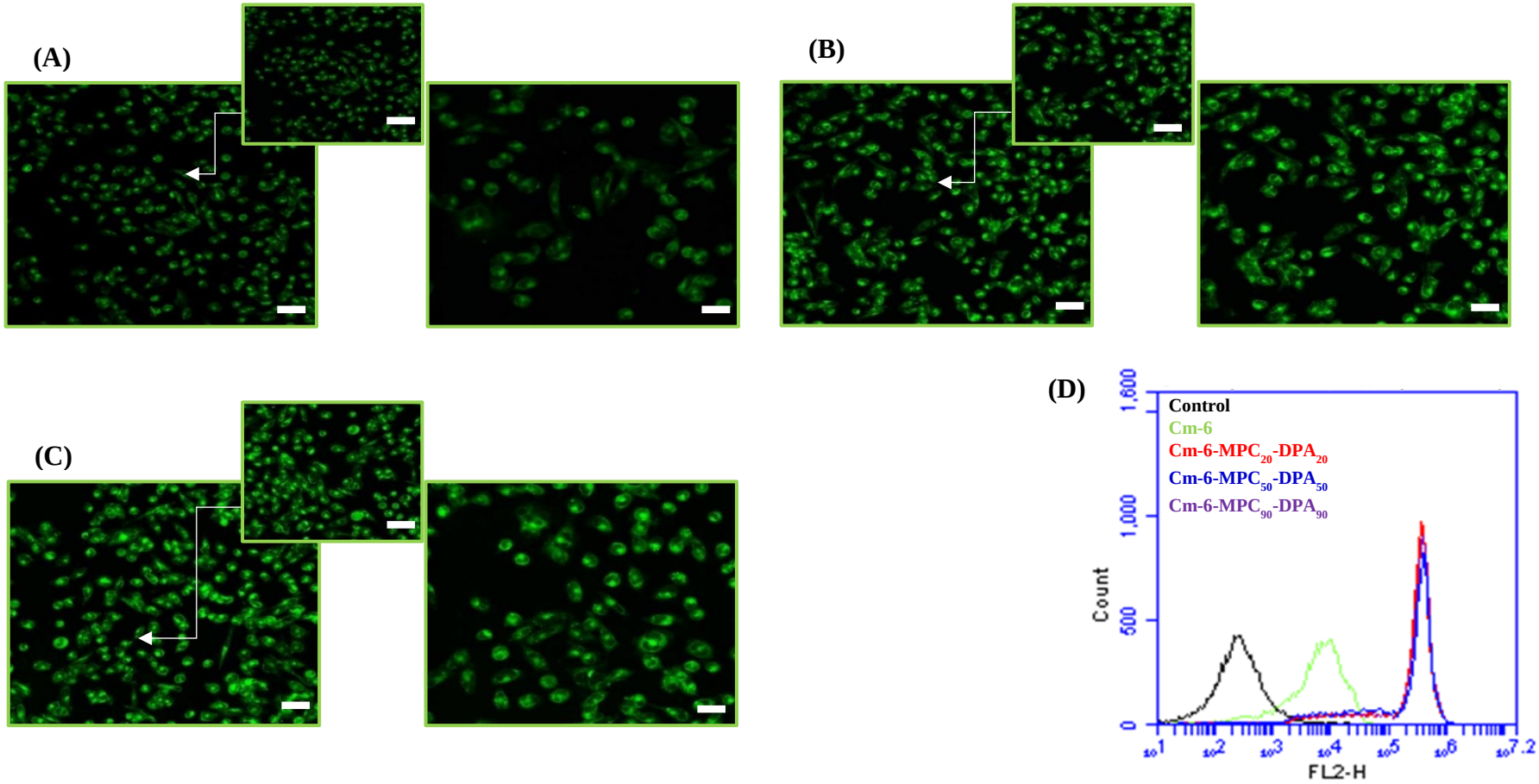


**A13.5** Vero cells after 5 minutes incubation with Cm-6-loaded MPC-DPA micelles. (A) Cm-6-MPC$_{20}$-DPA$_{20}$, (B) Cm-6-MPC$_{50}$-DPA$_{50}$, (C) Cm-6-MPC$_{90}$-DPA$_{90}$, (D) Flow cytometric profiles. Scale bars = 100, 50, and 25 µm (Original in colour)

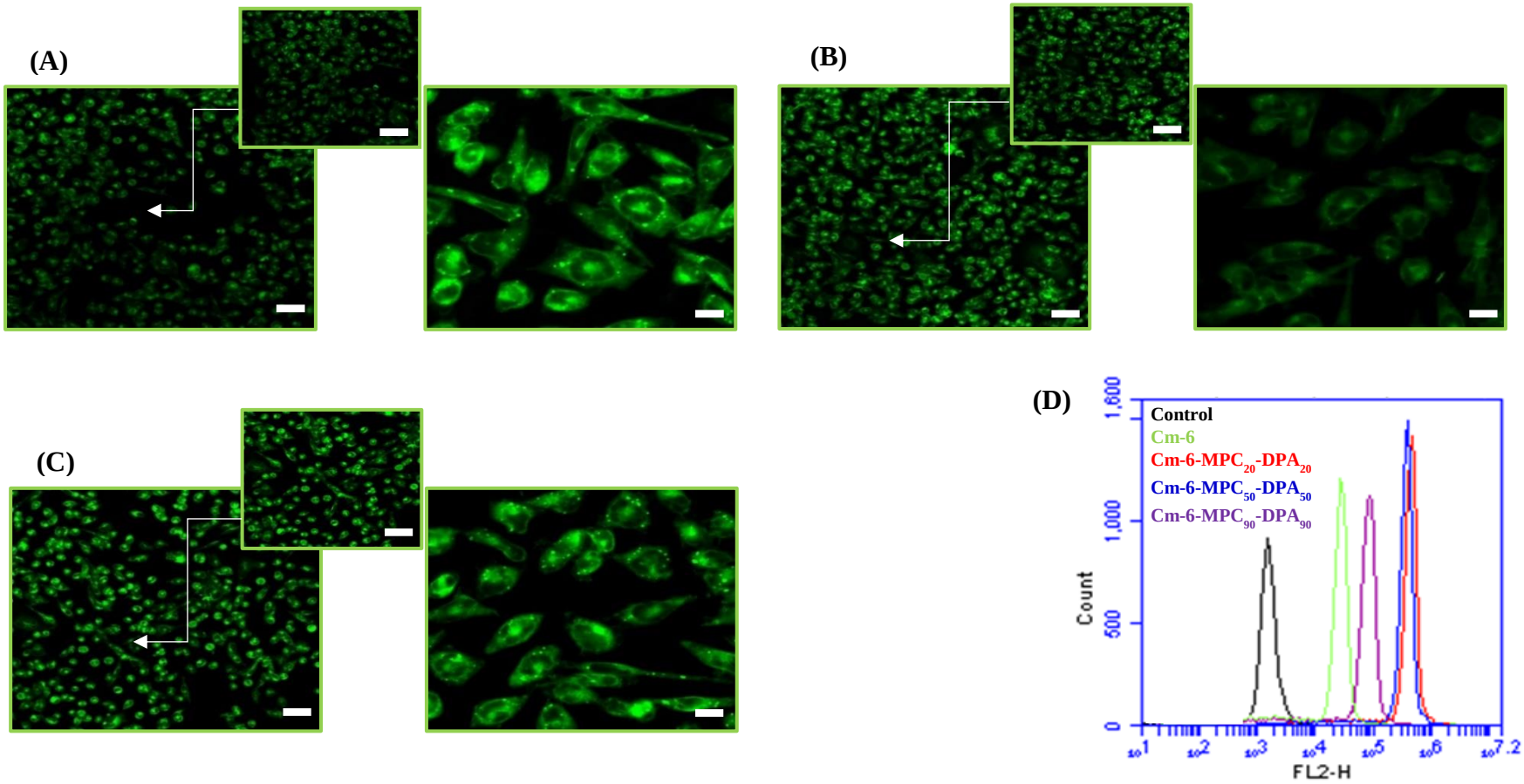


**A13.6** Vero cells after 10 minutes incubation with Cm-6-loaded MPC-DPA micelles. (A) Cm-6-$MPC_{20}$-$DPA_{20}$, (B) Cm-6-$MPC_{50}$-$DPA_{50}$, (C) Cm-6-$MPC_{90}$-$DPA_{90}$, (D) Flow cytometric profiles. Scale bars = 100, 50, and 25 µm (Original in colour)

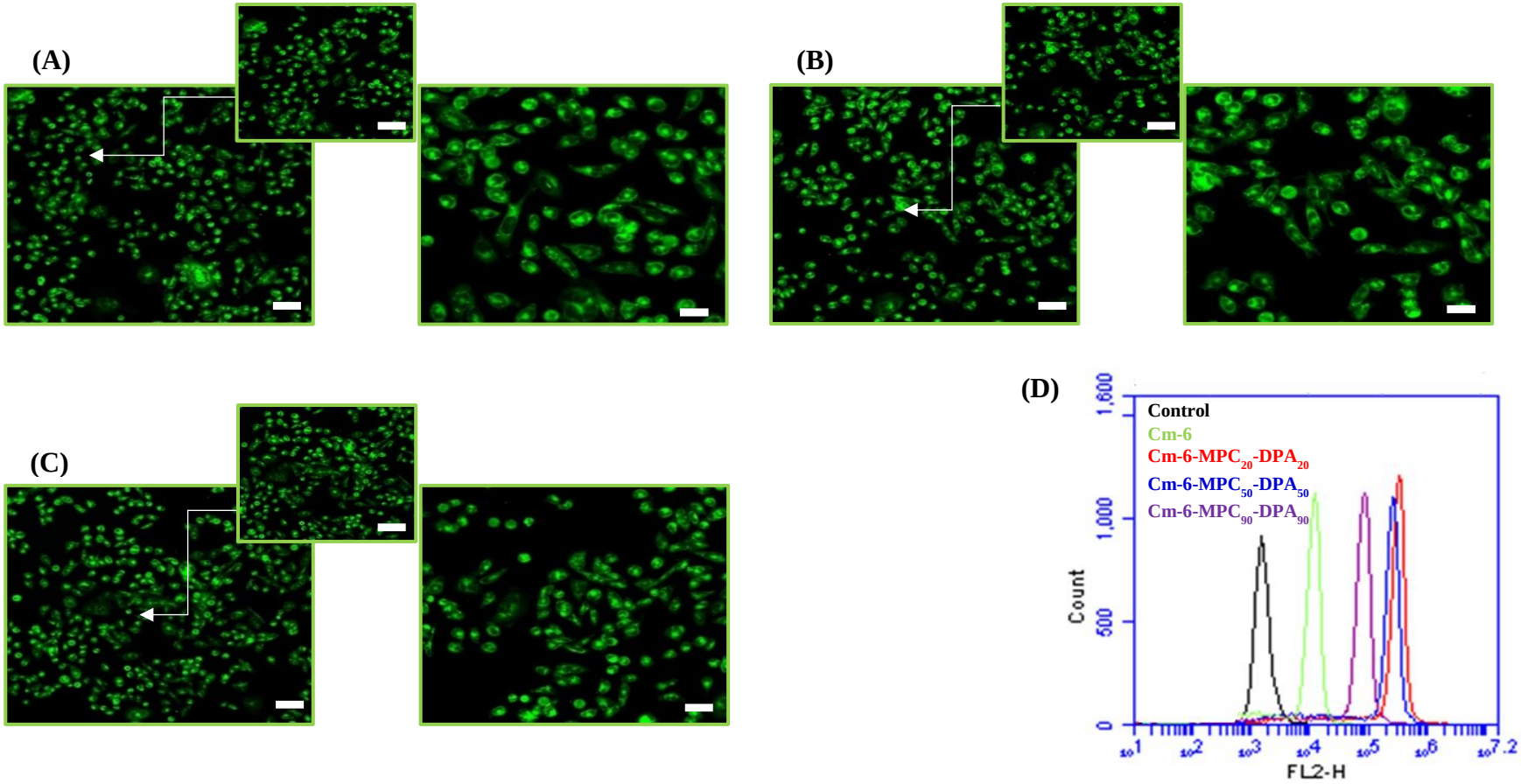


**A13.7** Vero cells after 30 minutes incubation with Cm-6-loaded MPC-DPA micelles. (A) Cm-6-$MPC_{20}$-$DPA_{20}$, (B) Cm-6-$MPC_{50}$-$DPA_{50}$, (C) Cm-6-$MPC_{90}$-$DPA_{90}$, (D) Flow cytometric profiles. Scale bars = 100, 50, and 25 µm (Original in colour)

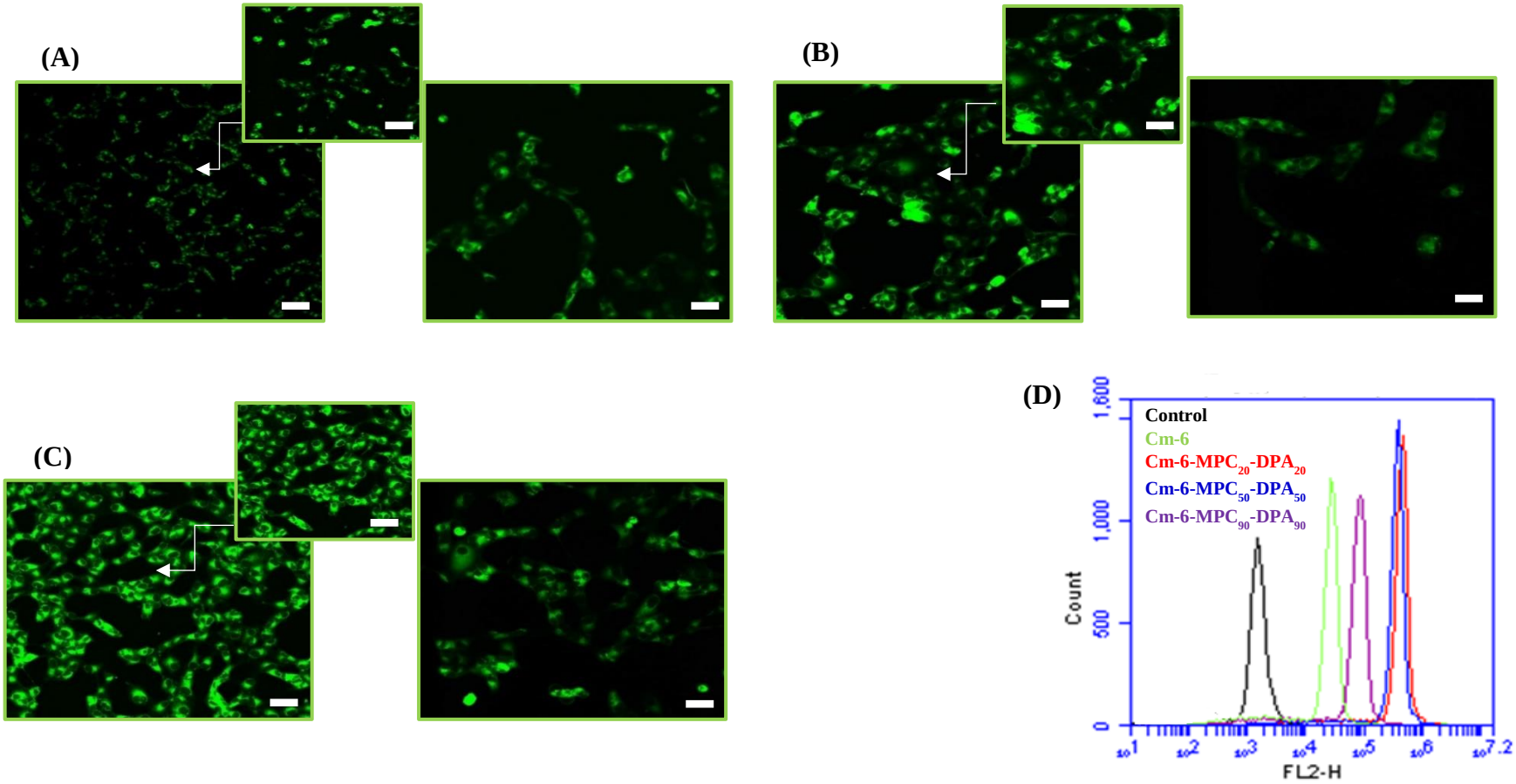


**A13.8** Vero cells after 1 hour incubation with Cm-6-loaded MPC-DPA micelles. (A) Cm-6-$MPC_{20}$-$DPA_{20}$, (B) Cm-6-$MPC_{50}$-$DPA_{50}$, (C) Cm-6-$MPC_{90}$-$DPA_{90}$, (D) Flow cytometric profiles. Scale bars = 100, 50, and 25 µm (Original in colour)

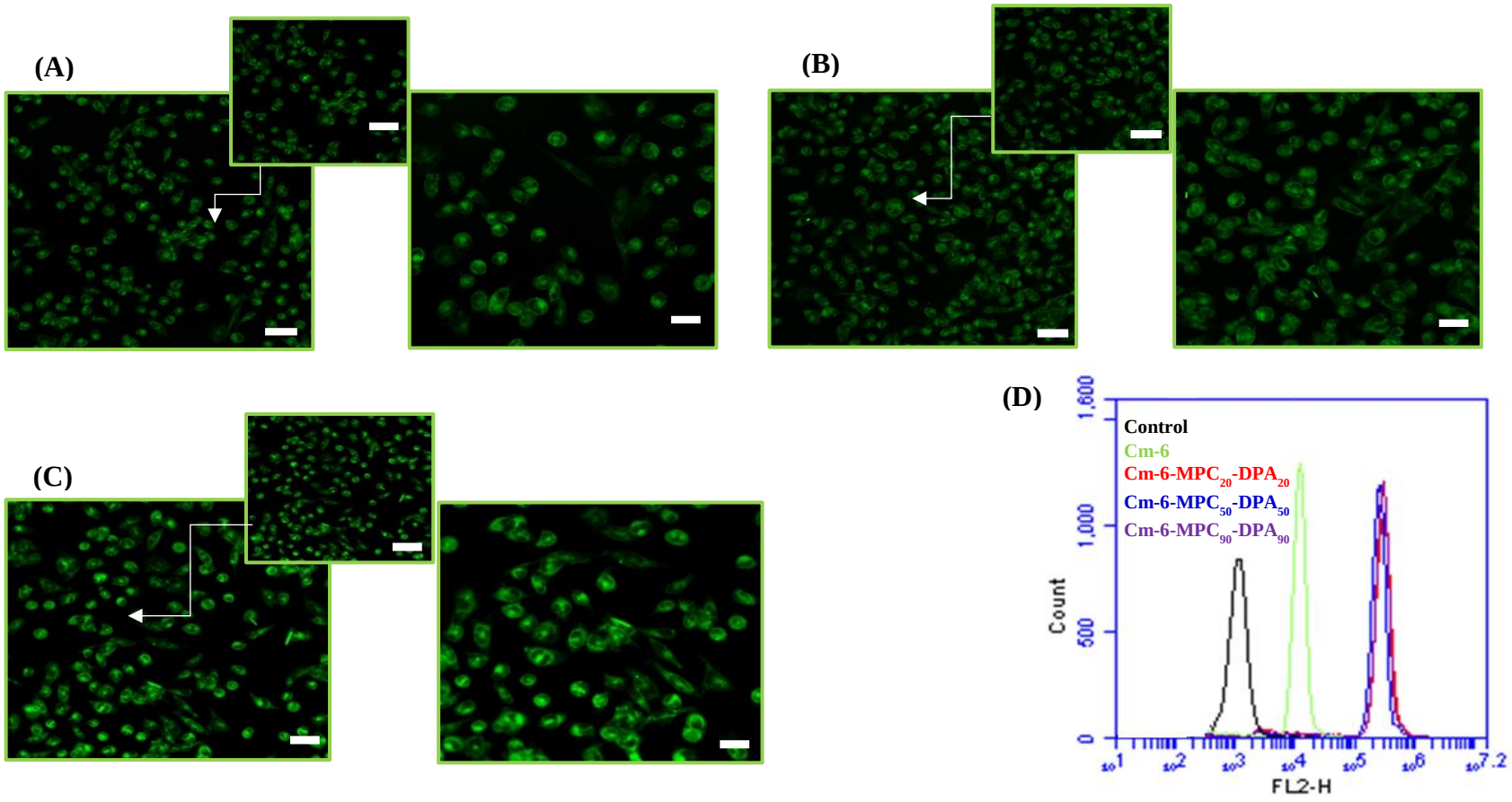


**A13.9** MRC-5 cells after 1 hour incubation with Cm-6-loaded MPC-DPA micelles. (A) Cm-6-$MPC_{20}$-$DPA_{20}$, (B) Cm-6-$MPC_{50}$-$DPA_{50}$, (C) Cm-6-$MPC_{90}$-$DPA_{90}$, (D) Flow cytometric profiles. Scale bars = 100, 50, and 25 µm (Original in colour)

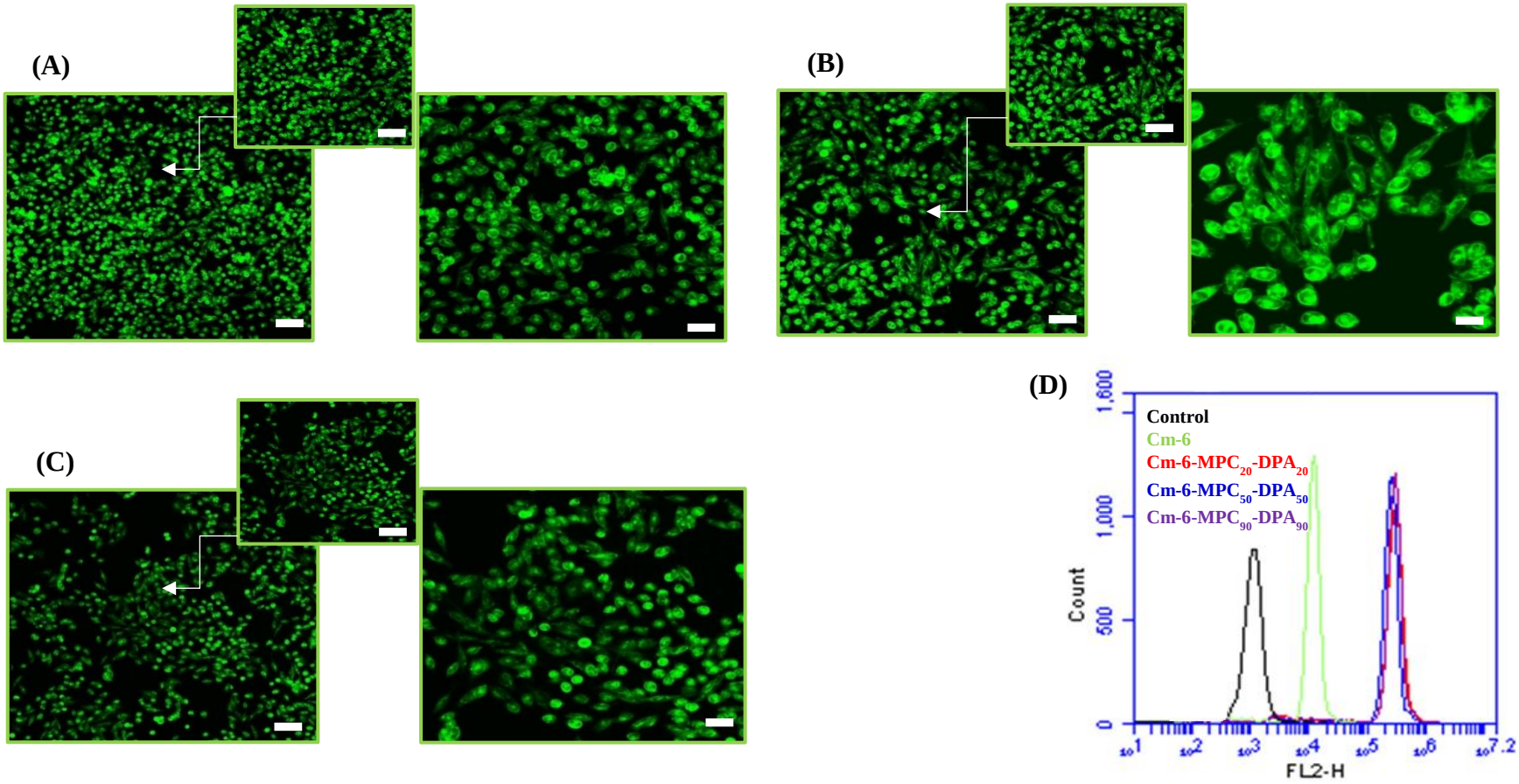


**A13.10.** CHO cells after 1 hour incubation with Cm-6-loaded MPC-DPA micelles. (A) Cm-6-$MPC_{20}$-$DPA_{20}$, (B) Cm-6-$MPC_{50}$-$DPA_{50}$, (C) Cm-6-$MPC_{90}$-$DPA_{90}$, (D) Flow cytometric profiles. Scale bars = 100, 50, and 25 µm (Original in colour)